ABSTRACT

Title of dissertation: PLANNING FOR AUTOMATED OPTICAL MICROMANIPULATION OF BIOLOGICAL CELLS

Sagar Chowdhury, Doctor of Philosophy, 2013

Dissertation directed by: Professor Satyandra K. Gupta
Department of Mechanical Engineering

Optical tweezers (OT) can be viewed as a robot that uses a highly focused laser beam for precise manipulation of biological objects and dielectric beads at micro-scale. Using holographic optical tweezers (HOT) multiple optical traps can be created to allow several operations in parallel. Moreover, due to the non-contact nature of manipulation OT can be potentially integrated with other manipulation techniques (e.g. microfluidics, acoustics, magnetics etc.) to ensure its high throughput. However, biological manipulation using OT suffers from two serious drawbacks: (1) slow manipulation due to manual operation and (2) severe effects on cell viability due to direct exposure of laser. This dissertation explores the problem of autonomous OT based cell manipulation in the light of addressing the two aforementioned limitations. Microfluidic devices are well suited for the study of biological objects because of their high throughput. Integrating microfluidics with OT provides precise position control as well as high throughput. An automated, physics-aware, planning approach is developed for fast transport of cells in OT as-

sisted microfluidic chambers. The heuristic based planner employs a specific cost function for searching over a novel state-action space representation. The effectiveness of the planning algorithm is demonstrated using both simulation and physical experiments in microfluidic-optical tweezers hybrid manipulation setup. An indirect manipulation approach is developed for preventing cells from high intensity laser. Optically trapped inert microspheres are used for manipulating cells indirectly either by gripping or pushing. A novel planning and control approach is devised to automate the indirect manipulation of cells. The planning algorithm takes the motion constraints of the gripper or pushing formation into account to minimize the manipulation time. Two different types of cells (*Saccharomyces cerevisiae* and *Dictyostelium discoideum*) are manipulated to demonstrate the effectiveness of the indirect manipulation approach.

Planning for Automated Optical Micromanipulation of Biological Cells

by

Sagar Chowdhury

Dissertation submitted to the Faculty of the Graduate School of the
University of Maryland, College Park in partial fulfillment
of the requirements for the degree of
Doctor of Philosophy
2013

Advisory Committee:
Professor Satyandra K. Gupta, Chair/Advisor
Professor Hugh Bruck
Professor Jaydev P. Desai
Associate Professor Nikhil Chopra
Associate Professor Wolfgang Losert (Dean's representative)

Dedication

To my wonderful parents and beloved brother

Acknowledgments

First and foremost I would like to thank Dr. Satyandra K. Gupta, my advisor and mentor for giving me the opportunity to conduct research under his guidance. His boundless energy and attitude of accepting nothing-but-the-best helped me refining my skills to become a better researcher every single day. His wonderful analytical skills and motivational power never let me feel short of energy in dealing with difficult research problems.

This dissertation is the result of a collaboration between roboticists and biophysicists. I would like to express my thanks to Dr. Wolfgang Losert for providing me constant support in conducting challenging experiments with biological cells in Biodynamics Laboratory. His close monitoring in conducting experiments and thoughtful insights helped me refining several methods presented in this dissertation.

I would like to thank Dr. Hugh Bruck, Dr. Jaydev P. Desai, and Dr. Nikhil Chopra for serving in my dissertation committee despite of having busy academic and research responsibilities of their own. I would also take this opportunity to thank Dr. John P. Wikswo and Dr. Kevin T. Seale from Vanderbilt University for supplying microfluidic chambers to conduct experiments with optical tweezers.

I also want to thank National Science Foundation for supporting my dissertation research work. Many thanks to the University of Maryland, Department of Mechanical Engineering, and the Institute of Systems Research for providing research facilities and administrative support.

I would also like to thank Ashis Banerjee for his help and advice when I first

started working on optical tweezers. I am grateful to him for being prompt in answering all my questions despite of his busy research commitments at MIT. I would also like to thank Atul Thakur for being such a good friend. I will never forget all the nights and days we spend together in Simulation Based System Design Laboratory in designing new algorithms. His constructive criticism always helped me to improve my technical skills. I was lucky to have Petr Švec as a collaborator throughout my PhD. I would like to thank him for providing me rigorous training in robot motion planning. I am grateful to him for spending hours and hours in front of white board describing novel algorithms that laid out the foundations for my motion planning skills.

I would like to thank former Biophysics Laboratory member Brian Koss for giving me extensive laboratory training on handling sophisticated cell cultures. I would also like to thank another former Biophysics Laboratory member Andrew Pomerance for developing preliminary software to control optical tweezers. I also want to thank current Biophysics Laboratory members - Chenlu Wang, Meghan Driscoll, Can Guven, and Xiaoyu Sun for providing me with cell samples to conduct experiments.

I am thankful to my colleagues Krishnanand Kaipa, Carlos Morato, Michael Joseph Kuhlman, Brual Shah, Joshua Langsfeld, Boxuan Zhao, Wei Shang, Luke J. Roberts, Andrew Vogel, and Gregory Krummel in Simulation Based System Design Laboratory (SBSD) and Advanced Manufacturing Laboratory (AML) for their support and words of encouragement. I would like to thank my past colleagues Arvind Ananthanarayanan, Madan Dabbeeru, Timothy Hall, Adam Montjoy, Alexander

Weissman, Peyman Karimian, and Wojciech Bejgerowski for being great friends. I also want to thank all my dear friends: Saurabh Paul, Subhadeep De, Koushik Pal, Sandip Halder, Rajarshi Roy, Sujal Bista, and many others for making my staying in Maryland a memorable one.

I am also thankful to my brother Shaiket Chowdhury, sister-in-law Nandita Majumder, and nephew Saimantik Chowdhury for all the good wishes that helped me focused throughout my PhD. Finally, I would like to extend my deepest gratitude to my parents, Prohmod Ranjan Chowdhury and Ratna Sree Chowdhury for their emotional support and affection throughout my life.

Table of Contents

List of Tables

List of Figures

List of Abbreviations

OT	Optical tweezers
HOT	Holographic optical tweezers
AFM	Atomic force microscopy
PFM	Photonic force microscopy
AOD	Acousto-optic deflector
DOE	Diffractive optical element
DOF	Degrees of freedom
SLM	Spatial light modulator
PDMS	polydimethylsiloxane
GPU	Graphics processing unit
CPU	Central processing unit
RBC	Red blood cell
RPE	Representative pattern element
CFD	Computational fluid dynamics
SIPLE	Semi implicit method for pressure linked equation
PRM	Probabilistic roadmap
RRT	Rapidly exploring randomized tree
MDP	Markov decision process
POMDP	Partially observable Markov decision process
cAMP	Cyclic adenosine monophosphate
OpenCV	Open source computer vision library
PI	Proportional integral controller

Chapter 1

Introduction

1.1 Background

One of the biggest challenges in biological researches in micro and nano scale is to understand the change of behavior that occurs with the scaling down in size. The effects of forces that are negligible at macroscopic scale may become dominant in micro and nano scale. For example, gravity plays no longer important role, rather forces like electrostatic, van der Waals etc. become dominant at micro and nano scale [ANBN07].

Figure 1.1 illustrates the effects of scaling in attractive forces between a sphere of radius r with a cylinder of height $8r$ and radius $4r$ [ANBN07]. It shows magnetic force dominates over gravitational force as the radius goes below 1 m. The forces like electrostatic and van der Waals that are generally ignored in designing macro-scale manipulators become dominant over gravitational forces as r goes below 10^{-4} m.

Macroscopic techniques that exploit the gravitational forces can no longer be applicable for manipulation of objects in micro and nano scale. This change of behavior due to the scaling down in size encourages the researchers to come up with new manipulation techniques for the biological objects at micro and nanoscale. AFM (Atomic Force Microscope) [RWG$^+$10], electrophoresis [Vol06], magnetic manipulation [SVC$^+$08], optical tweezers (OT) [ADY87], microfluidic techniques [CSW$^+$11],

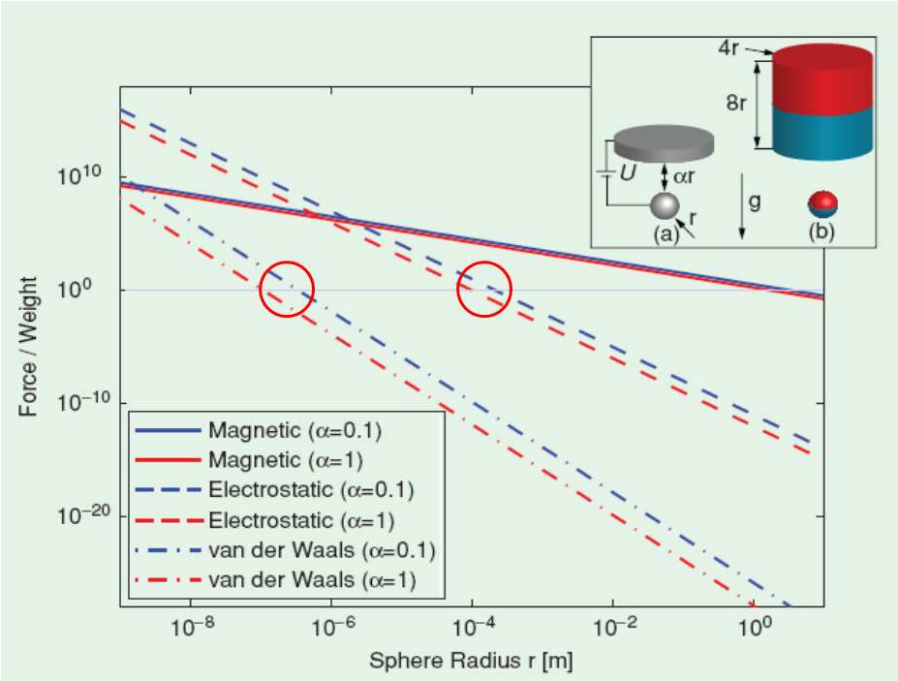

Figure 1.1: *Scaling of attractive forces [ANBN07]: For $r < 1$ m, the magnetic force is sufficient to lift the sphere. Below $r = 10^4$ m, the electrostatic force dominates over gravity, and for $r < 10^7$ m, the van der Waals force is higher than the weight of the sphere*

acoustics [DLK+12], use of microfabricated tools [KDG12a, KYY+12, KDG12b, KDG13, KDG11] etc. are some of the well known manipulation techniques at micro and nano scale. Unlike most of the other manipulation techniques OT provides a non-invasive means of manipulation. OT is particularly suitable for precise manipulation. It can apply a force in order of pN with an accuracy of the order of aN. Hence, it can provide a position accuracy of the order of angstrom.

Targeted cell manipulation is becoming increasingly popular in various cell studies, for example, how cells respond to changes in environment both internally and externally, how do they interact with each other, or how do they undergo complex processes such as differentiation etc. Traditionally the studies listed here are conducted over a large population or ensemble of cells that leave out various

insights mainly due to the difference in behavior in individual cell. Targeted analysis over a small population will provide more insight into the system level properties of signaling pathways and their dependence on in individual cell properties, e.g. cellular age, degree of development, cell cycle progression etc. High position and force accuracy make OT suitable for targeted manipulation of cells. Throughput of targeted OT manipulation can be significantly improved by integrating it with other gross manipulation techniques e.g. microfluidics, acoustics, magnetic etc. [MSD03].

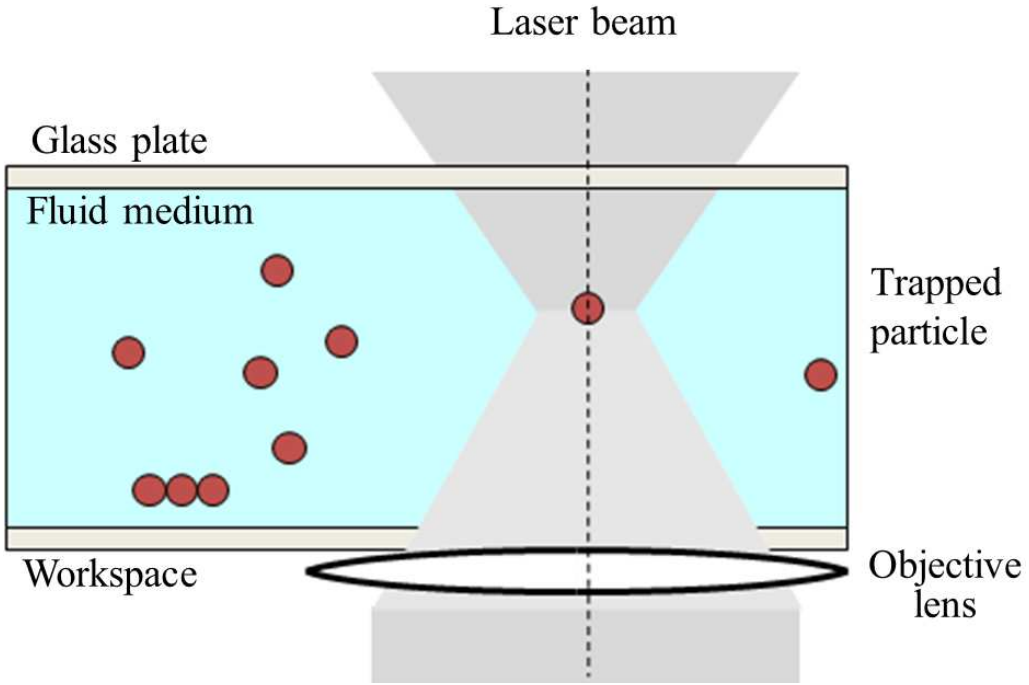

Figure 1.2: *Schematic illustration of optical trapping: the trapped particle is steered by the laser beam*

The interaction of a particle with an optical trap is schematically depicted in Figure 1.2. Particles move randomly due to Brownian motion in a fluid medium. A strongly focused laser beam is used to exert optical gradient and scattering forces on a particle, which results in trapping the particle at the focal point of the laser

[ADBC86, Ash92]. By controlling the laser beam, the trapped particle can be transported precisely to the desired location without any physical contact. Holographic optical tweezers (HOT) uses a spatial light modulator (SLM) that can split the laser to create multiple traps to facilitate manipulation of multiple particles simultaneously. Unfortunately, most of the OT manipulation tasks are conducted manually and hence it is slow. Slow manual manipulation makes OT hard to carry out many systematic biological studies that need to be properly timed to exhibit the desired motility. In order to make OT a useful manipulation tool for sophisticated biological studies real-time and automated planning approaches need to be developed. In the following sections we will discuss OT manipulation in the context of biological studies to identify challenges in developing automated planning algorithms.

1.2 Motivation

As discussed in previous section, OT is an emerging tool to manipulate micro and nonoscale biological objects in fluid medium. Although OT is particularly useful for single cell manipulation, throughput can be significantly improved by integrating it with other gross-manipulation techniques e.g. microfluidics. The hybrid manipulation techniques will provide high throughput as well as precise manipulation control.

An example of such microfluidic device is illustrated in Figure 1.3. This microfluidic device includes around $10,000$ net-like structures to capture cells inside them. However, the number of cells inside the nets cannot be controlled since the manipulation is solely dependent on the fluid flow which subjects to change with

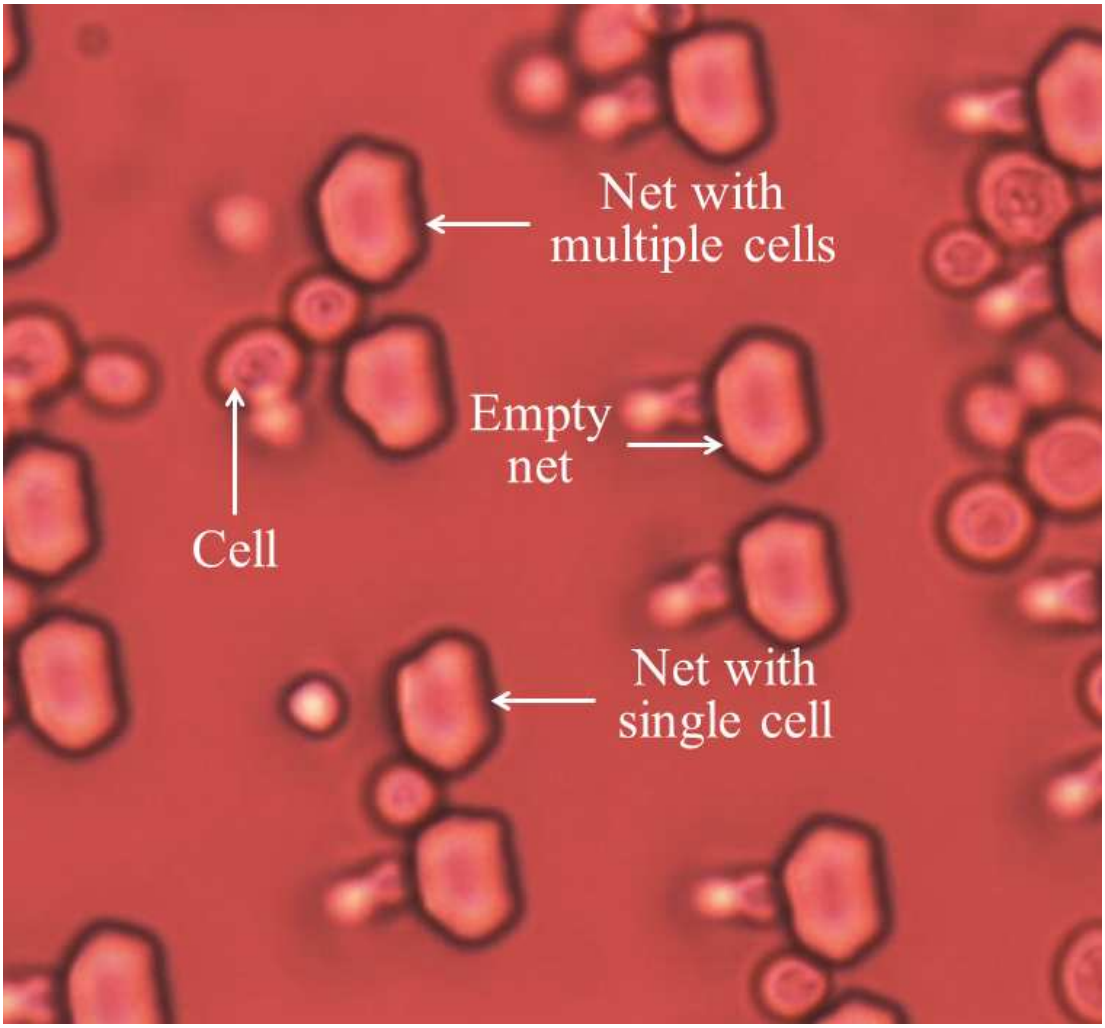

Figure 1.3: *Hybrid manipulation comprising of OT and microfluidics (Courtesy: Dr. John P. Wikswo and Dr. Kevin T. Seale (Vanderbilt University))*

the variation in number of cells at inlet. OT can be integrated with microfluidics to control the equal distribution of cells inside the nets by taking the cells out from crowded nets and placing them in empty nets or to the exits of the chamber. Manual cleaning of large number of nets will require large preparation time for biological experiments that may alter the outcome. The automated approaches need to account for the physics of microfluidic chamber in order to move the cells reliably with the presence of fluid flow. Moreover, the planning environment frequently changes

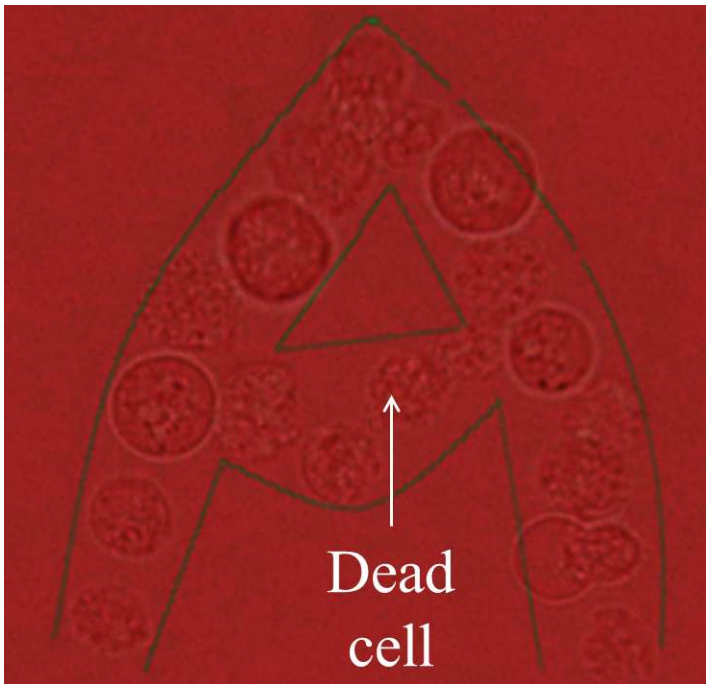

Figure 1.4: *Dictyostelium discoideum cells arranged in a pattern: cells are killed due to direct exposure to laser (Image courtesy: Chenlu Wang and Dr. Wolfgang Losert)*

due to the fluid flow and random Brownian motion of cells in microscale. Planning algorithm needs to have fast replanning capability to cope up with changing environment inside microfluidic chamber.

Another big challenge in integrating OT with microfluidics is the workspace size mismatch. OT can operate in a space of 100 µm × 100 µm whereas microfluidic chamber has a dimension in the range of mm × mm. OT has to be facilitated with long distance transport capability in order to harness the high throughput advantage of microfluidics in a hybrid manipulation setup. The planning strategies have to be developed accordingly to accommodate the long distance transport operation along with fine manipulation using optical trap planning.

Cells need to be arranged in a certain pattern and observed for a reasonable

time length in order to study the evolving behavior due to their interaction with each other. Cells can also be actively nudged during observation to study the underlying mechanism behind their collective behavior. OT can be used to trap different cells and arrange them in pattern. However, direct exposure of laser to the cells may inflict photodamage that can affect their physiological behavior. Vegetative *Dictyostelium discoideum* cells are arranged in a pattern of the alphabet "A" in Figure 1.4 by directly trapping them with OT. Some of the cells are disintegrated while trapping them due to direct exposure to laser. Rather than trapping directly, cells can be manipulated indirectly using inert microspheres as grippers. Each microsphere can be optically trapped to act as a robotic finger to hold and manipulate the biological cell indirectly. Figure 1.5 illustrates a gripper which is made of six inert silica microspheres directly trapped by multiplexed laser traps to manipulate a *Saccharomyces cerevisiae* cell indirectly. The arrangement of microspheres is important to ensure robust gripping as well as minimum laser exposure to the cell. A computational synthesis foundation needs to be developed for designing gripper configurations for the cells that will ensure robust gripping as well as minimum laser exposure while transporting them towards certain goal locations.

Manual control of multiple laser traps for indirect manipulation of cell using gripper formations is nearly impossible. Hence, there is a need for automated planner that can handle multiple lasers simultaneously. The interactions among multiple lasers for indirect manipulation of cell using the gripper formation makes the planning challenging. The planner also needs to be characterized in terms of manipulation speed, laser power, and the resulting exposure of laser intensity to the

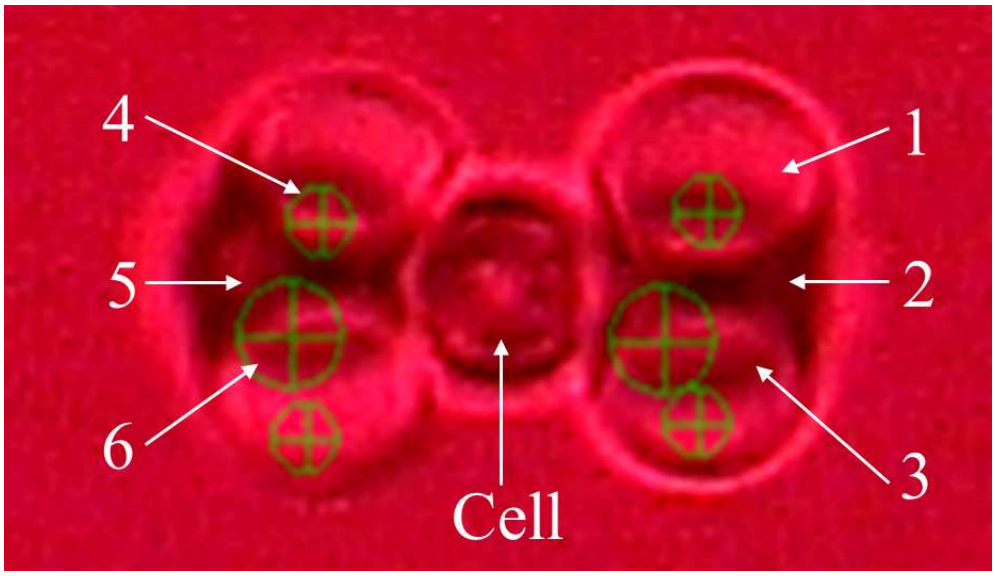

Figure 1.5: *Saccharomyces cerevisiae cell is manipulated indirectly using the gripper made of inert silica beads directly trapped by laser*

manipulated cell.

Polarized *Dictyostelium discoideum* cells are used as model organism to study collective migration of cancer cells. Figure 1.6 shows an example of collective migration of polarized *Dictyostelium discoideum* suspended in water under the influence of chemotaxis cAMP. In order to understand the underlying migration behavior, cells need to be manipulated individually and arranged in some predefined patterns to see different outcomes. However, *Dictyostelium discoideum* are very sensitive to laser and need to be ensured zero laser exposure in case of OT manipulation. While gripper formations can prevent the cell from a large portion of laser, it cannot eliminate entire exposure. Hence, manipulating *Dictyostelium discoideum* cells using gripper formations is not favorable to their viability. A new indirect manipulation approach needs to be developed that ensures zero exposure to the cell. This dissertation describes the development of computational tools that can exploit the physics

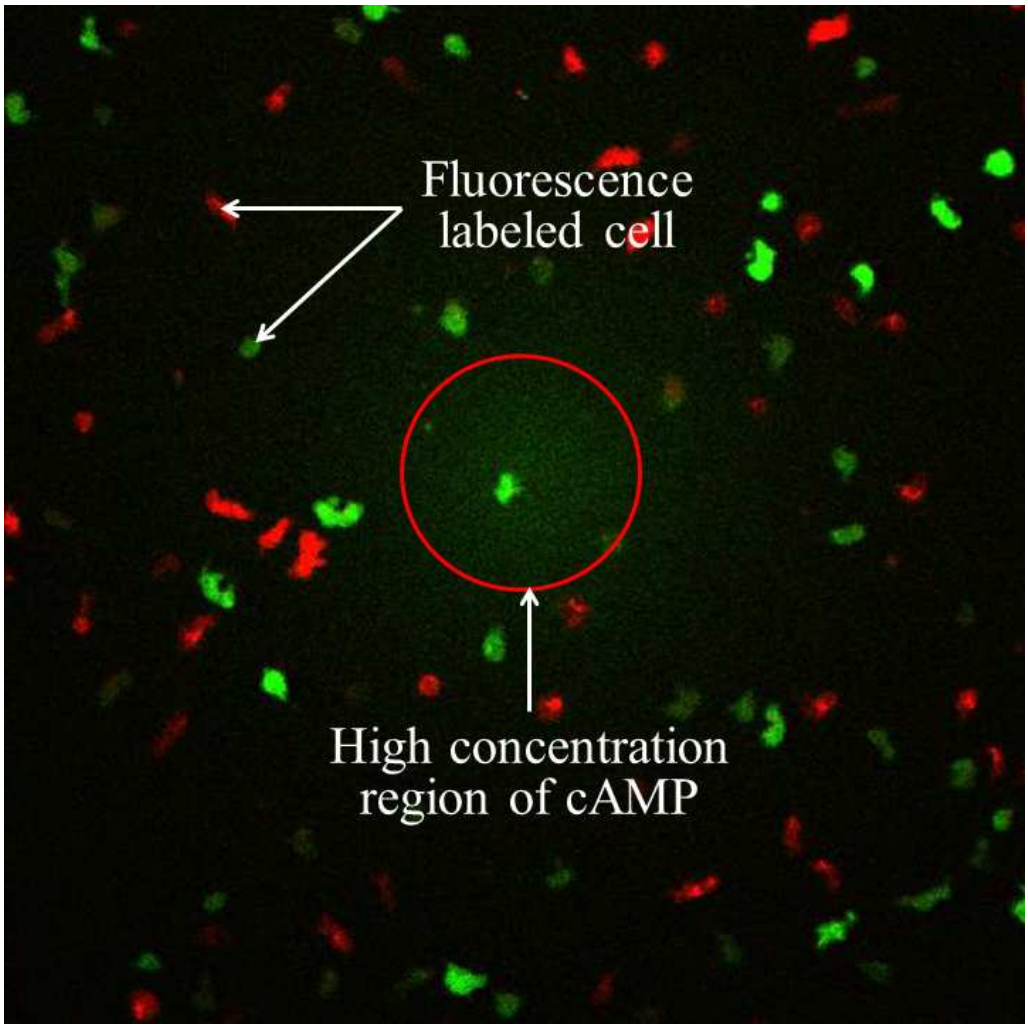

Figure 1.6: *Collective migration of suspended Dictyostelium discoideum cells under the influence of cAMP (Image courtesy: Chenlu Wang and Dr. Wolfgang Losert)*

of the system to automate the cell manipulation using optical tweezers.

1.3 Research Issues

This dissertation identifies three fundamental research issues or challenges in order to perform autonomous manipulation of cells using optical tweezers. Following is the description of the research issues in details.

1. *Utilization of physics of the system for effective planning:* Microparticles im-

mersed in a fluid medium exhibit random stochastic motion due to Brownian motion. Moreover, the presence of external fluid flow in case of microfluidic chamber influences the OT manipulation since particles have a chance to get knocked out of the traps while moving across the fluid streamlines. The plan generated without considering the physics of the system may lead to the path that is risky in terms of successful manipulation or requires more laser power to execute. As mentioned earlier, high laser power will lead to severe photodamage to the trapped cell. In case of microfluidic cleaning operation as mentioned in section 1.2, cells need to be released inside the OT workspace so that fluid flow can take them outside the chamber. The release locations need to be carefully selected so that cells have higher probability of reaching the exits of the chamber. This dissertation explores the use of physically accurate simulations to estimate the probability of success for the cells to reach one of the exists of the microfluidic chamber with the influence of fluid flow. The estimated probability can be used to enhance the performance of realtime planner. However, the simulations need to be performed at very small time intervals (in the order of microseconds). Hence, offline simulations can be used to generate a probability table at discrete points in the OT workspace. The probability table generated by offline simulations can then be used to increase the effectiveness of the real-time planner.

2. *Preventing cells from direct exposure of laser during optical manipulation:* Exposure to laser due to direct trapping during OT manipulation negatively af-

fects physiological activities of cells. Cells can be manipulated indirectly with the gripper formations or pushing formations while preventing them from dangerous laser. The gripping or pushing formations can be created by directly trapped inert microspheres. The arrangement of the microspheres inside the formations need to be carefully designed so that cells can be robustly manipulated as well as the laser exposure remains to be minimum. The interactions of the laser cones among themselves as well as the microspheres need to be considered to be able to generate effective configurations which is impossible to do manually. Hence, this dissertation develops computational synthesis foundations to automatically design the microsphere configurations that facilitates robust manipulation of cell with minimal laser exposure.

3. *Concurrent grasping and planning for indirect manipulation of cells:* Manipulation of cells using gripper or pushing formations requires moving multiple traps simultaneously which is time consuming to perform manually. However, automated manipulation using microsphere formations is challenging for three reasons. Firstly, all the particles which are not directly trapped by laser are constantly moving in the workspace due to Brownian motion. That means the actual position, velocity, and acceleration of any particle are not known in advance. The environment of the OT workspace changes rapidly due to the random motion of the particles. Thus, any planning algorithm needs to have fast replanning capability to handle the dynamic nature of the workspace environment. Secondly, the planning has to deal with noisy images. The po-

sitions of the particles inside the formations are difficult to estimate. Thirdly, the trapping power is not uniform all over the workspace and hence, the trapping effectiveness is not uniform everywhere. The planner has to provide more time for the microparticles to move to the formation where the trapping power is less. The planning algorithm also needs to account for motion constraints specific to a particular formation in order to reliably manipulate cells. This dissertation investigates the use of feedback policy alongside fast planning algorithm to ensure robust manipulation of cells using gripper or pushing formations. The dynamic model of the laser trap can be utilized during planning for better estimation of the positions of microparticles inside the formations.

1.4 Dissertation scope and Outline

Currently, optical tweezers is used for various cell manipulation operation ranging from transport to stretching. However, this dissertation focuses on challenging operations that are challenging for a human operator. Hence, cell localization, rotation, transport, sorting, gripping, pushing, and mechanical probing are termed as cell manipulation. Microfluidics is a widely used cell manipulation tools. Hence, OT assisted microfluidics is demonstrated as an example for hybrid manipulation setup in this dissertation. Similar approaches can be translated to other hybrid setup with Optical tweezers e.g. magnetics, electrophoresis, or acoustics. Automated cell manipulation is demonstrated using two types of cells namely *Saccharomyces cerevisiae* and *Dictyostelium discoideum*. *Saccharomyces cerevisiae* is a Yeast which is a popular model organism for studying eukaryotic cell biology. It can be

easily cultivated in the laboratory. The detection of cells is also easy since they can be approximated with spheres. *Dictyostelium discoideum* is used as an important model organism for studying cancer cell migration. The dynamically changing shapes during migration poses unique challenge during automated manipulation. Amorphous silica microspheres are chosen as material for designing gripper or pusher formations for indirect manipulation of cells.

The rest of the dissertation are organized as follows. The next chapter surveys state-of-the-art literature in the related works in optical manipulation of cells, optical tweezers setups, different hybrid manipulation approaches, robot motion planning under uncertainty, robotic grasping, and robotic pushing based manipulation approaches. Chapter 3 presents the fast real time planning approach for automated manipulation of cell inside OT assisted microfluidic chamber. Chapter 4 extends the automated manipulation approach inside OT assisted microfluidic chamber to enhance the range of transport using automated stage motion. Chapter 5 describes a computational synthesis foundations for designing grippers for indirect manipulation of cells. Chapter 6 describes an automated planning approach with a feedback policy for automated indirect manipulation of cells using gripper formations. Chapter 7 describes a novel automated pushing based manipulation approach to transport irregular shaped cells from its current location to the goal. Finally Chapter 8 summarizes the intellectual contributions of the current work, highlights anticipated benefits of this research in biophysics research community as well as healthcare industry, and outlines for future work.

Chapter 2
Literature Review

In this chapter[1], we survey literature related to the goal and scope we mentioned in Chapter 1. Our work is multidisciplinary in nature and falls in the intersection of Biophysics and Robotics. We present the more relevant research papers in this chapter since it is nearly impossible to review all the papers available in literature.

Section 2.1 deals with different issues related to optical manipulation including instrumentation, effects of direct exposure laser to cells, and different indirect manipulation approaches to encounter the problem of direct exposure. A chronological study on the development of modern optical tweezers system is presented. Direct exposure to high intensity laser affects the cell viability severely. We survey existing literature that characterizes the damage in cell health due to high intensity laser and different indirect manipulation approaches proposed by various research groups to prevent cell from high intensity laser. Indirect manipulation approaches are not only important for preventing photodamage but also for some indirect measurement of physical properties of cell using optical tweezers. Many representative works take the advantage of high precision of OT in indirect measurement of physical properties of the cell.

In section 2.2 we present different hybrid manipulation setups and their potentials to improve biological studies. We have mentioned a list of different techniques

[1] The work in this chapter is partially derived from the published work in [BCLG11].

available for manipulation of biological studies in chapter 1. Every manipulation techniques have their own niche domain of application where it can be the most effective. By combining two or more such manipulation systems, we can add more capabilities into the same system. That will enable more efficient studies that need to be properly synchronized and need different capabilities that cannot be provided with a single system.

Laser traps can be regarded as robots to draw inspiration from robotics in automating the cell manipulation process. We survey existing literature on robot motion planning in section 2.3 that are closely related to our problem. In microscale world, the environment changes randomly due to Brownian motion of particles. Actual position, velocity, and acceleration cannot be known in advance. Hence, we focus mostly into robot motion planning under uncertainty in this section.

In section 2.4 we draw inspiration from robotic grasping literature to develop robust gripper for indirect manipulation of cell. People have developed different metrics to characterize the performance of a gripper in grasping an object robustly. Our problem is unique because of size scale we are operating in.

In section 2.5, we survey another body of literature in the intersection of industrial manufacturing and robotics to derive another mode of indirect manipulation through pushing. Dynamically changing irregular shaped objects cannot be manipulated using grippers. We use pushing based techniques to manipulate those objects. Our problem is interesting because of the dynamical shape of the manipulated cell.

2.1 Optical Manipulation

The idea of optical trapping is based on Newton's particle principle of light. Newton postulated in 1704 that light consists of tiny masses. This postulate contradicts the wave principle proposed by Christian Huygens who believed that light is made up of waves that can vibrate up and down perpendicular to its direction of propagation. Einstein later unified both the principles by describing light as a collection of mass-less particles, photons, which carry momenta proportional to their energy. Any change in the direction of propagation due to reflection or refraction will result in an associated change in momentum of light. As a consequence, the object that causes light to reflect or refract will undergo an equal and opposite momentum change according to the principle of the conservation of momentum. This change in momentum gives rise to a net force acting on the object.

However, we do not feel that force from sunlight in our everyday life because of its ultra low intensity. The intensity of sunlight is about 100 W/m^2. This intensity provides an optical levitation pressure of about 10^{-6} Pa, which is negligible compared with the atmospheric pressure (10^5 Pa approximately). This radiation pressure is much more profound in the space beyond our atmosphere where there is no air resistance. Kepler in 1600 discovered that comet tails always point away from the sun due to the radiation pressure of sunlight. He named the radiation pressure as "Heavenly Breeze". Jules Verne first envisioned the concept of using radiation pressure for the propulsion of sailing ships for traveling in space in his science fiction novel "From the Earth to Moon" which came out in 1865. However, it was not

until 2010, we saw this concept came in live when the scientists of JAXA Space Exploration Center sent the first solar sail IKAROS to monitor the atmosphere of our neighboring planet Venus.

The optical force on our Earth's surface is so small that it did not have any application for a long time until the availability of high intensity laser. Using laser with intensity million times higher than sunlight on the Earth surface, it is possible to generate force in the order of pico-newtons that may be sufficient to manipulate objects in the size scale of micro and nano meters. While scientists were arguing about the design of the future gigantic solar sailing ships that could transport cargoes between the Earth and the Mars, some scientists in Bell Laboratory started asking an even simpler question: can we use the powerful lasers to push objects in the microscale? Ashkin and other colleagues showed that it is, indeed, possible leading to the development of the first optical tweezers in 1986 [ADY87].

Since its inception optical tweezers have become a popular tools for the researchers in physics and biology. Optical tweezes possesses the unique capability of applying force in the order of pN with a sub-pN resolution. Hence, the it provides tremendous position accuracy in the order of micrometers down to angstrom. These unique capabilities make them suitable for variety of nanomechanical measurements, specially in biological applications. Optical tweezers have been successfully used for various cell, DNA, RNA, and motor protein manipulation.

2.1.1 Optical Tweezers Instrumentation

The most fundamental parts of an optical tweezers are a custom-built optical microscope with imaging capabilities, a good objective lens, and a trapping laser source. Over the years, optical tweezers have been equipped with sophisticated technologies including sensitive lens, detection system, beam steering mechanism, calibration methods transforming it to a powerful experimental Instrument.

Earlier optical tweezers were based on one single laser beam capable of creating a single optical trap and hence can manipulate a single object. Soon people realize the necessity for manipulating multiple objects simultaneously. The simplest but expensive solution is to use multiple laser source each of them is responsible for creating a single trap. Visscher *et al.* [VGB96] came up with a new optical tweezers system which is capable of creating two optical traps by splitting a laser into two based on polarization. Their optical tweezers system was equipped with polarizing beam splitters to split the laser beam into two and x-y-z telescopes that can independently in X,Y, and Z axes to provide independent relative positioning of the optical traps. However, it has an inherent disadvantage since the optical traps cannot be independently switched on and off. The authors developed a more flexible method of creating multiple optical traps by time sharing of a single laser beam by fast scanning among multiple locations. The laser dwells on a single trap location briefly before moving to the next location. The fast scanning of laser into the traps gives the capability of manipulating multiple objects simultaneously. The time-sharing optical tweezers system is equipped with acousto-optic deflectors (AOD) for

fast scanning of laser beam which can be computer controlled. The relative positions of the trap locations, the laser power strength, and the scanning rate can be controlled with computer controlled AODs adding to the greater flexibility of the time sharing optical tweezers.

Another method of realizing a optical tweezers system capable of creating multiple optical traps is to use galvanometer scanning mirrors. Balijepalli *et al.* [BLG06] have developed a scanning mirror based optical tweezers system where AODs are replaced with scanning mirrors. The trapping laser passes through an isolator to protect the laser head from beam reflections, a first telescope for beam expansion and two scanning mirrors for increased scan range and a second telescope before reaching the microscopic objective (see Figure 2.1). The telescope is used to provide required magnification and direct the laser to the objective lens which is essential to maximize trapping force. A piezo-electric actuator is attached to the objective to enable scanning in Z-axis. However, all the multiple traps can only be created at the same X-Y plane at a time instant using this optical tweezers system providing only planar manipulation of multiple objects. The scanning mirrors can also be controlled by computers to provide similar flexibility as AOD based optical tweezers systems.

Object detection has become a crucial component of the optical tweezers systems in order to harness the flexibility of computer controlled AOD or scanning mirrors. The users often want to precisely position the optical traps to manipulate the desired objects. The positions and orientations of the objects are very important for accurate manipulation of multiple objects. Depending on manual

detection of objects may lead to slower and error-prone manipulation. Peng *et al.* [PBGL06, PBGL07b, PBGL07a, PBGL09] were motivated to solve the problem of manual detection by its potential application in precise and micro and nano assembly operations. In micro and nano assembly operations, objects need to be brought together with certain position and orientation in order to make a successful manipulation. The authors have utilized the piezo-electric actuator attached to the objective in order to generate a stack of images in different cross-sections in Z-axis for 3D detection of objects. The image processing has three steps to extract regular shaped objects e.g., spheres. In the first step, the image is segmented to isolate the region of interest mainly to reduce the computational overhead of analyzing whole image. In the following step, a suitable gradient based algorithm e.g., Hough transformation is used to identify the locations in x-y plane. From the stack of images generated offline, a set of signature curves have been generated for the regular shaped objects for known z-locations. The current image is compared online with the library of signature curves to identify the z-location of the objects. They later extend the algorithm by improving the feature extraction technique with modified Hough transform in order to find the position, orientation,and geometric identity of irregular shaped object e.g., nanowires.

In order to eliminate the limitation of planar manipulation using scanning based optical tweezers, Dufresne and Grier [DG98] developed an optical tweezers where input laser is split into multiples using a diffractive optical element (DOE) that can create an array of optical traps based on the input pattern (see Figure 2.2). However, it comes with a sacrifice in flexibility since the trap patterns depend on

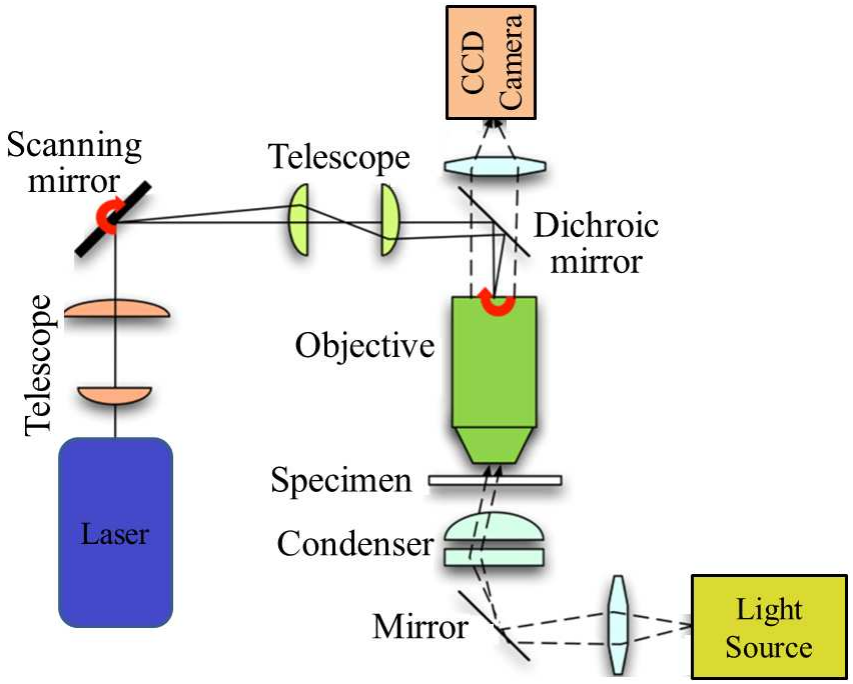

Figure 2.1: *Schematic illustration of scanning mirror based optical tweezers system (Image source:[BLG06])*

the input microfabricated DOE. To create a new trap patterns, a new DOE needs to be fabricated. Later on, Grier and his colleagues [Gri03, CKG02] revolutionized the optical trapping by introducing computer-addressable DOE named as Spatial Light Modulators (SLMs) made from liquid crystals. The new generation of optical tweezers are popularly named as Holographic optical tweezers (HOT). The authors [DSD+01] developed algorithm for inverse Fourier transform in order to compute phase hologram to create dynamically configurable optical traps. However, real time computation of phase hologram has been a major bottle neck for holographic optical tweezers. That is the reason, the trap update frequency of HOT is much lower as compared to scanner based optical tweezers. Over the year numerous algorithms have been proposed for efficient computation of holograms. Recently, Onda and Arai [OA12] used graphics processing unit (GPU) to accelerate the hologram computation

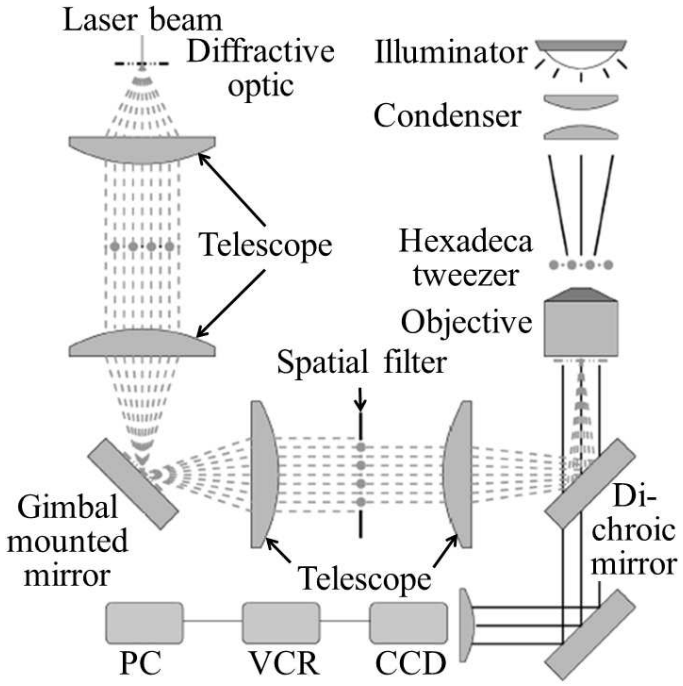

Figure 2.2: *Schematic illustration of Diffractive optical element (DOE) based optical tweezers (Image source:[DG98])*

and managed to improve the update frequency to 250 Hz as compared to 8 Hz using CPU.

2.1.2 Laser exposure using direct trapping

Optical tweezers were initially used to directly manipulate cells. However, soon it was observed that direct trapping can lead to considerable photodamage on trapped cells, including the death of cells as noted by Ashkin [ADY87]. The underlying mechanism for photodamage has been proposed to be due to the creation of reactive chemical species [SB94, LSBT96], local heating [LSBT96], two-photon absorption [KLBT95, KSL$^+$96] and singlet oxygen through the excitation of a photosensitizer [NCL$^+$99].

Many in depth studies that monitored cell health by a variety of methods

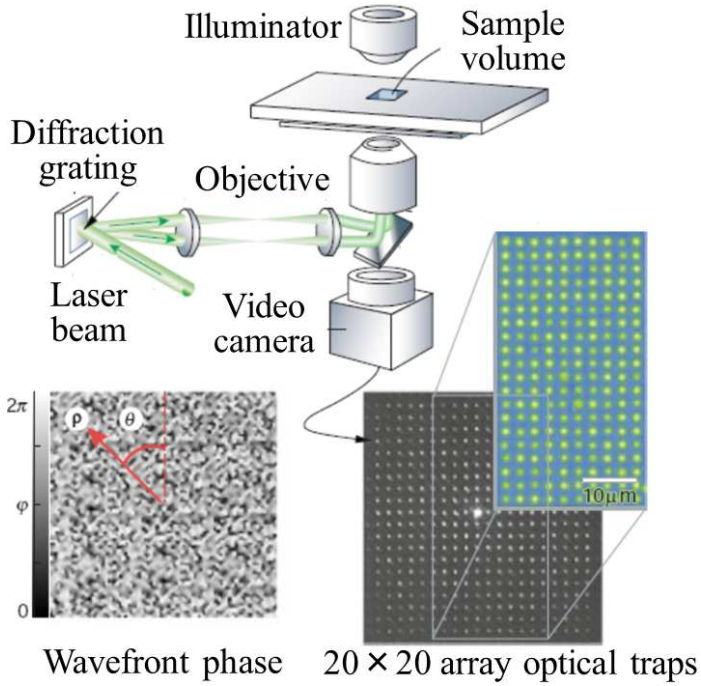

Figure 2.3: *Schematic illustration of Diffractive optical element (DOE) based optical tweezers (Image source:[Gri03])*

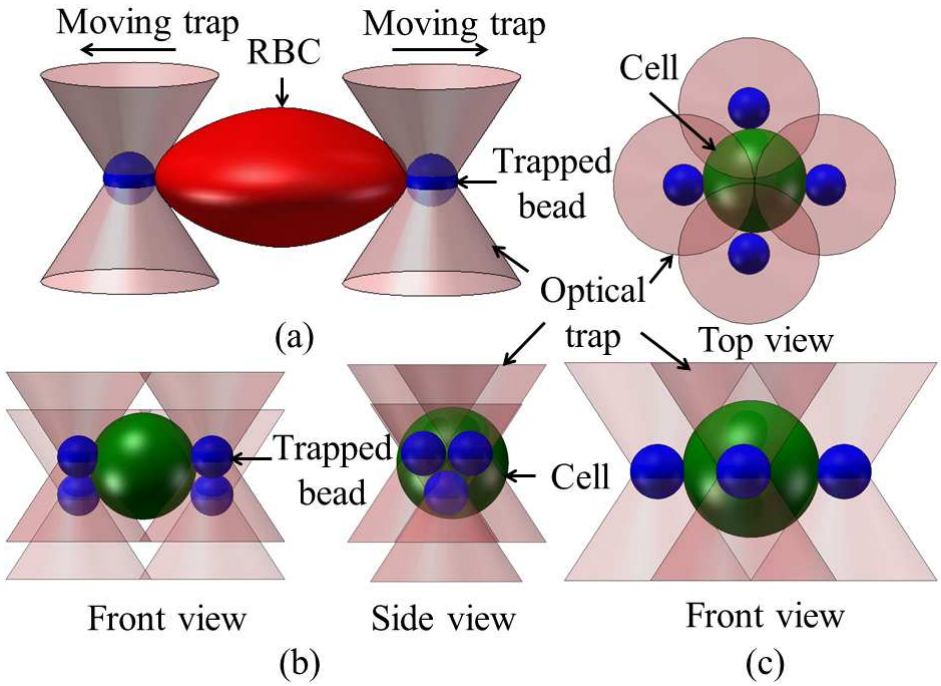

Figure 2.4: *Schematic illustration of two, six, and four bead arrangements to manipulate cells; (a) (adapted from [LLLL08]) is useful for stretching red blood cells, while (b) and (c) (adapted from [KCA+11]) are useful for transporting cells (Note that the figure is not drawn to scale)*

show optical micromanipulation affects cell health to some extent. Using the cloning efficiency of CHO cells [LVK+96], or the rotation rate of the *E.coli* flagella motor [NCL+99], it was found that 830 nm and 970 nm laser wavelengths were significantly less harmful to cells, and that the region from 870 nm to 910 nm was particularly harmful. Using the ability to express genes as a measure of cell health, another group found only a weak dependence of cell viability on wavelength (in the range 840 nm to 930 nm), with the total dose of laser light as dominant parameter determining the ability of cells to express genes [MTT+08].

The low light threshold for cell damage is of great concern for the use of optical micromanipulation: using 1064 nm, Ayano showed that cell damage to E.coli was linearly dependent on the total dose received and found that cell division ability was affected at a dose of 0.35 J [AWYY06]. Rasmussen, using the internal pH as a measure of viability, found that the internal pH of both *E.coli* and Listeria bacteria declined at laser intensities as low as 6 mW [ROS08]. These studies caution that direct cell trapping may not be desirable.

2.1.3 Indirect Manipulation of Cells

Sleep *et al.* [SWSG99] studied the elasticity of red blood cell (RBC) membrane by using two-bead arrangement with optical tweezers. Two aldehyde derivatized polystyrene latex beads, attached to two diametrically opposite ends of the cell, were trapped by optical tweezers. One trap was held stationary while moving the other to induce tension or compression in the cell. The force-extension profile was generated by monitoring the displacement of the bead held in a stationary trap.

To reduce the influence of protein cytoskeleton on the force-extension curve for membrane, the red blood cells were prepared by saponlysis, that interacted with the membrane cholesterol to provide permeability of the membrane.

Henon *et al.* [HLRG99] used optical tweezers to measure the shear modulus of RBC. RBCs were treated with hypotonic buffer to create the spherical or near-spherical shapes. Silica beads were added to RBC solutions to allow them to adhere to the cell surface. For the experiment, RBCs having two silica beads in diametrical position were selected from the solution. The beads were moved away from each other by increasing the relative distance between two traps until one of the beads escaped from the trap. By analyzing the final deformed shape and the associated force determined from optical trapping, the shear modulus was measured as 2.5 $\pm$ 0.4 μN/m which was in an order of magnitude lower than those found in other experiments. The authors addressed that discrepancy by arguing that different experiments examined different elasticity regimes.

More recently, Li *et al.* [LLLL08] studied the deformation of the erythrocyte cells by stretching them using optically trapped beads. The force applied through the bead was calibrated by exposing it to a fluid flow of various speeds. At a certain power level, there existed a maximum flow velocity beyond which the laser could not hold the bead indicating the equilibrium state where trapping force was balanced by viscous drag force. The cells were stretched in a similar way as described in [SWSG99]. The geometry of the deformed shape of the cells was measured with the help of image processing which was later used to calculate the transverse strain and lateral strain. The experimental results were compared by using mechanical model

of liposomes since erythrocytes have very similar phospholipid bilayers. By comparing the experimental and numerical results, the shear stiffness of the phospholipid membrane, a proper shear stiffness was determined to minimize the error between the two. The average estimated shear stiffness agreed with the other published results.

Fontes *et al.* [FFDT$^+$08] recently proposed a new method to measure mechanical (apparent membrane viscosity and adhesion force) and electrical (zeta potential, thickness of the double layer of charges) using double optical tweezers. To measure the adhesion membrane viscosity, an optically trapped silica bead was bound to a RBC of a two cell spontaneously formed rouleaux and moved while the other RBC was directly held by another optical trap. For the adhesion force measurement, two silica beads captured by double optical tweezers were used to manipulate RBCs. One bead was kept stationary while the other was moved in diametrically opposite direction. An special chamber with two electrodes were built to measure the electrical properties . An external electrical field was applied through the electrodes. The double layer thickness was measured by determining the force that the trapped bead bound to a RBC experienced due to the external electrical field. On the other hand, The zeta potential was measured using the velocity of the bead due to the applied electrical field after it was released from trap.

Laurent *et al.* [LHP$^+$02] measured the viscoelestic properties of alveolar epithelial cell and compared the experimental and theoretical measurements using both magnetic twisting cytometry and optical tweezers technique. A silica microbead attached to a cell was trapped and displaced at a low constant speed by moving

the trap parallel to the cover slip. The position of the bead, measured by image processing, was used to calculate the displacement of the bead relative to the trap. The geometric parameters, i.e. cell stiffness, bead immersion angle, were determined from the microscopic images during laser trapping. The two techniques used same size beads and the data was analyzed using the same model. However, The authors reported some discrepancy between the two results that occurred mainly due to the difference in experimental conditions.

Wei *et al.* [WZY+08] most recently used microrheometer based on oscillatory optical tweezers to measure both extracellular and intracellular complex shear modulus with the separate measurement of storage and loss modulus components for alveolar epithelial cell. Protein A coated 1.5 μm silica beads were used as probe for exterior shear modulus experiment whereas internal granule was used as probe for intracellular measurement. To calibrate the system, a trapped bead was forced to oscillate along the x-direction by the application of an oscillatory optical force.

Arai *et al.* [AOF+00] developed a new system for high speed random separation of microbes using optical radiation pressure and dielectrophoretic force in microfluidic chamber. The system was composed of laser scanning manipulator to trap the target microbe, electrophoretic manipulator to create electric field gradient for separating the other objects from the target, and finally capillary flow in the micro channel to extract the isolated target. To avoid the direct exposure of the target microbe to the laser some new microtools were used which could be trapped by laser to manipulate the microbes indirectly. In a similar work, Arai *et al.* [AMS+03] used two types of microtools for indirect manipulation of living objects namely natural

microtool (e.g., microbe such as bacillus) and artificial microtool (e.g., microbead) for separation of target bioorganism. An inner installation method was developed to install the microtools into the manipulation chamber. The target microbes was then transported using the trapped microtool.

In a later work, Arai *et al.* [AYSF04] used synchronized Laser Micromanipulation (SLM) for indirect force measurement of the microbes. SLM facilitated the trajectory control of multiple targets by using single laser. Using SLM two microtools were trapped in a certain distance. When the target microbe was pushed by one of the microtool while keeping the distance among themselves same, the microtool experienced a reaction force which was balanced by the trapping. Measuring the displacement of the microtool from the optical trap, the reaction force was determined.

Fall *et al.* [FSJ+04] also developed an optical force measurement system for the calculation of forces in biological object, for instance, E. Coli. The adhesion force between E. Coli and galabiose functionalized beads was measured using polystyrene beads as handles for optical tweezers. An immobilized large bead was brought into contact with E. Coli. A second galabiose functionalized bead, trapped by optical tweezers, was brought close to E. Coli. The large bead was moved away from the trapped bead at a constant speed (0.05 μm/s) until the bonding collapsed. The maximum displacement of the bead was used to measure the binding force. The microscope was modified to accommodate a probe laser which along with a position detector monitored the position of a bead in the trap.

Sun *et al.* [SHC+01] used irregularly shaped diamond as handles for the con-

trolled rotation and translation of biological object. Diamond microparticles are transparent at visible and infrared wavelength of light and biologically inert. The irregular shape of microparticle induced self rotation in optical trap. The rotation speed and direction of diamond microparticle was controlled by moving the objective in the direction of laser propagation. Mesophyl protoplasts were manipulated by tagging them with diamond microparticles. Controlled rotation as well as pure translation were achieved using diamond microparticles.

Ferrari *et al.* [FEC$^+$05] used two different setups to create multiple traps for indirect manipulation of biological objects. One of the setups used AOD (accousto optics deflectors) to achieve deflection of laser fast enough to maintain multiple traps by sequential sharing of the laser beam. However, AOD could only provide planar trapping configuration. The second setup used DOE (diffractive optical elements) that converts a specified illuminated beam into a beam with desired distribution of amplitude, phase or polarization. 2 μm RGD coated latex beads were trapped in a circular configuration by using AOD based multi-trapping system. By varying the diameter of the circular pattern the trapped beads were moved close enough to the cell such that RGD allowed the bead to adhere to the cell. The cell was shrunk or stretched by varying the circular pattern to investigate the cell reaction to the mechanical stimuli. The same cell was manipulated using an improved 3D multitraping system based on DOE.

Ichikawa *et al.* [IAY$^+$05, IHE$^+$06] proposed a new method for manipulation of biological objects by instant creating and destroying the microtool. The microtool was formed by local thermal gelation using the laser power. After manipulation the

microtool was dissolved by turning off the laser.

Kress *et al.* [KSGR05] investigated the binding mechanism of morphage cell during phagocytosis using fluctuating bead in optical trap as a local probe. By optimizing the numerical aperture of the trap and thereby controlling the trapping position of the bead, a stable 3D position detection was achieved. The trapped bead was moved close to morphage cell. The bead was coated with ligands to trigger the phagocytic binding process. Four different types of ligands were used: Immunoglobulin G(IgG), complement, bacterial lipopolysaccharide (LPS), and avidin. The dynamics of the membrane binding events was monitored using PFM (Photonic force microscopy).

Miyata *et al.* [MRB02] used optical tweezers to study the effect of temperature and opposing force on the gliding speed of *Micoplasma mobile*. 1.1 μ beads were attached to gliding *M. mobile* cells and held into optical trap to apply enough force to stall their forward movement. The authors found that the gliding mechanism is composed of at least two steps. One step generates force while the other allows displacement.

Taka *et al.* [THM03] studied the dynamic behavior of swiss 3T3 fibroblast membrane by using an optically trapped polystyrene bead as a probe. A polystyrene bead coated with BSA was captured with optical trap and brought into contact with cell edge. The image was recorded for 1-2 mins. The experiments were conducted at three trap stiffness (0.024, 0.053, and 0.090 pN/nm). The analysis demonstrated that the protrusion and withdrawal of the cell edge occurred at non-uniform velocities and dependent on stiffness.

Most recently Pozzo *et al.* [PFdT$^+$09] used optical tweezers to study the chemotaxis behavior of flagellated microorganism (*Lashmania amazonensis*) by observing the force response when exposed to a gradient of attractive chemical substance. The propulsion force of the flagellum of *L. amazonensis* was measured by attaching a polystyrene bead using optical tweezers. The displacement of polystyrene bead from the optical trap was used to measure the propulsion force. The protozoan responded to the glucose gradient by circular and tumbling motion whereas swam erratically in the absence of any gradient.

2.1.4 Comparison with Other Approaches for Manipulating Cells

Cell manipulation is an important steps both for medical experiments and making fundamental advances in biological sciences. Hence different techniques have been developed for manipulating cells over the years. In this section, we compare indirect optical manipulation with other well-known techniques for manipulating cells.

Dielectrophoresis involves manipulation of dielectric particles using time-varying electric-fields. This method has been successfully used to manipulate cells [AOM$^+$99, AZ88, WKI$^+$93, NKHM97, DKB99]. Magnetic manipulation involves tagging cells by magnetic particles and then using the time varying magnetic field to move the particles and hence the cells [HJB$^+$03, dVKvDK05, WGB03, LHW04]. Both of these methods place restrictions on the types of cells that can be manipulated by these methods and the environments in which the cells should be manipulated. Moreover, it is very difficult to achieve independent placement control over multiple cells

concurrently.

Recent advances in silicon and polymer based micro-electromechanical systems have been exploited to develop microscale grippers that can hold individual cells and arrays of cells [JIL00, CL05, WUH04, KCL+03, JIP+02]. These methods utilize customized grippers to grasp cell. These grippers are used in conjunction with mechanical micromanipulators to move cells. These grippers are not reconfigurable to allow for changes in the cell shapes. Moreover, only limited field of view is available for imaging while the gripper is holding the cell. Integrating multiple mechanical manipulators together to perform multiple independent operations is challenging due to workspace limitations.

Microfluidics, when combined with e.g. electro-osmotic actuation can be a powerful tool to steer a small number of objects. It has been shown to be a useful technology for cell manipulation [WBC03, ACPS05, YLJY06, OZDF08]. However, fluids are incompressible and thus harder to focus than optical traps. Microfluidics also generally requires a closed system for controlled flows and thus makes further manipulation of the sample (e.g. insertion of a micropipette or a chemoattractant) difficult unless integrated with the microfluidics device. Microfluidics is a promising technology for gross motion and can be combined with the optical manipulation techniques for fine motion control.

The existing research clearly shows that cells can be manipulated by attaching microspheres to them and optically manipulated the microspheres. We anticipate that an increasing level of autonomy in the field of optical tweezers will enable manipulation of cells using multiple different microspheres without a need for the

microspheres to be physically attached to the cells. Such capability will further enhance the field of indirect manipulation of cells using optical tweezers. Moreover, optical tweezers can be combined with gross manipulation techniques e.g. microfluidics, dielectrophoresis etc. to provide high throughput as well as precise control of manipulation.

We have tabulated the different optical tweezer set-ups as well as the type of biological objects, size and type of gripper objects, and the types of manipulation operations being performed, to bring out the common features that can be observed across this research domain. Table 2.1 summarizes the tweezer set-ups, whereas the remaining information is presented in Table 2.2. It may be noted here that we have clustered together all the work published by researchers belonging to the same research group in the same row and used certain abbreviations to represent the tables in a more compact form. NR refers to the fact that the particular data is not reported in the cited paper; PS, Sl, Gl, and Lt stand for polystyrene, silica, glass, and latex respectively, gripper object size refers to the diameter, and the two entries in the objective lens parameters column denote magnification and numerical aperture values respectively.

It can be seen from Table 2.1 that Nd:YAG and Nd:YVO_4 are the two most popular laser types. The lasers are always operated in the infra-red regime, although, the specific wavelengths may vary from (790-1064) nm. Usually, the laser power is kept quite low (mostly below 300 mW), even though in few cases much higher values are used. Typically, very high magnification (100X) and numerical aperture (1.2-1.4) objective lens are used. Only in few cases, lens having 40, 50 or 63X

magnification, and numerical aperture of 1.0 or 0.6 are utilized. Unlike most of the tweezer set-up parameters, lot of variation is observed in case of the gripper object size (shown in Table 2.2). Although in quite a few cases, bead size within the range of (1-2.5)μ-m are selected, in certain cases, beads as small as 75 nm in diameter are used, whereas, in other cases, beads as large as 10 μ-m diameter are utilized. Biotin and streptavidin are commonly used as coating materials to facilitate the binding of beads with the biological objects. It may also be noted here that stretching or pulling is the most prevalent form of manipulation as it enables characterization of biomechanical properties and provides information on the underlying mechanisms behind physiological processes. Moreover, rotation is never performed, although some papers on direct optical manipulation of cells have looked into this.

Table 2.1: *Summary of optical tweezer setups*

Papers	Laser type	Laser power	Wave length	Objective lens parameters
[AYA+99, MYK96, NMY+95, THM03]	Nd:YAG, Nd:YLF	150 mW, 1 W	1064nm, 1053nm	100X, 1.3
[AYA+99, MYK96, NMY+95, THM03]	Nd:YAG, Nd:YLF	150 mW, 1 W	1064nm, 1053nm	100X, 1.3
[BSK+99, BLL+01]	Diode laser	200 mW, 500 mW	829 nm, 1064 nm	100X, 1.2
[BGS90, SSSB93, WYL+97, VSB99]	Nd:YAG, Nd:YVO_4, Nd:YLF	NR	1064 nm	100X, 1.3
[BTER+02, MCB+06]	Nd:YAG, Ti:Sa	1W	1064 nm	100X, 1.25
[CSS05]	NR	NR	NR	NR

continued on next page ...

continued from previous page ...

Papers	Laser type	Laser power	Wave length	Objective lens parameters
[FSS94]	Nd:YLF	NR	1047nm	63X, 1.4
[KB97, DWLB00, LOS+01, LBT07, MWL+07, WML+07]	Nd:YAG	1.5W	835 nm, 1064 nm	NR,1.2
[STNS+05]	Ti:Sa	200 mW	830 nm	NR
[AMS+03, IAY+05, IHE+06]	Nd:YVO_4	4.98 W, 200 mW	1064 nm, 860 nm	100X, 1.3
[LHP+02, HLRG99]	Nd:YAG	600 mW	1064 nm	100X, 1.25
[PFdT+09]	Nd:YAG	NR	NR	100X, 1.25
[KMHY97]	Nd:YAG	300 mW	1064 nm	100X, 1.3
[DGWW97]	Nd:YLF	3W	1047 nm	100X, 1.4
[HBMM02]	Nd:YAG	600 mW	1064 nm	100X, 1.3
[JSGF04]	NR	NR	1064 nm	NR
[PQSC94]	Nd:YAG	100 mW	NR	63X, 1.4
[SWSG99]	Nd:YLF	NR	1047 nm	63X, 1.4
[VBW+98]	Nd: YAG	NR	1064 nm	100X, 1.3
[RHX+04]	Nd:YAG	2.5 W	NR	100X, 1.3
[BVHS09]	Nd:YVO_4	NR	1064 nm	100X, 1.3
[CVJ+05]	Nd: YAG	NR	1064 nm	NR, 1.45
[SL97, SSL98, SHRS02]	Nd:YAG	150 mW	830 nm, 1064 nm	100X, 1.3
[WSY+02]	Nd:YAG	NR	NR	100X, 1.35
[WCMF95]	NR	NR	NR	100X, 1.4
[DLP+07, PPM+05, PPM+07]	Nd:YAG	1 W	1064 nm	60X,NR
[FEC+05]	Nd:YAG	15W	1064 nm	100X, 1.3
[FFDT+08]	Nd:YAG	60 mW; 30 mW; 15 mW	NR	100X, 1.25

continued on next page ...

continued from previous page ...

Papers	Laser type	Laser power	Wave length	Objective lens parameters
[KYI+01]	Nd: YAG	NR	1064 nm	40X, 1.0
[LLLL08]	Nd: YAG	1.5 W	1064 nm	NR
[SHC+01]	Nd: YVO_4	50-500 mW	790 nm	50X, 0.6
[WZY+08]	Nd: YVO_4	NR	1064 nm	100X, 1.3

Table 2.2: *Summary of materials, size, and manipulation type*

Papers	Biological object	Gripper object	Gripper coating	Gripper object size (μm)	Manipulation type
[AYA+99, MYK96, NMY+95, THM03]	α-Actinin, Swiss 3T3 fibroblasts, Actin, HMM, DNA	PS	Galsonin, BSA	1	Translation, Stretching, Tying knot
[BSK+99, BLL+01]	λ-phage DNA	Polystyrene	Streptavidin	2.5	Stretching
[BGS90, SSSB93, WYL+97, VSB99]	Kinesin, DNA	Sl, PS	BSA	0.2-0.6	Tracking
[BTER+02, MCB+06]	DNA, Kinesin	Sl	Streptavidin	1	Translation, Stretching
[CC05]	Kinesin	Sl	NR	1	Keeping bead stationary
[CSS05]	DNA of type A and type B	PS, Au	Streptavidin	1	Forming DNA- DNA linkage
[FSS94]	Actin filament	Sl, PS	NEM	1	Straightening, Pulling
[KB97, DWLB00, LOS+01, LBT07, MWL+07, WML+07]	RNA polymerase, Titin, RBC, P5ab RNA and corresponding DNA	Carboxylated PS, Sl	Streptavidin, T12 antibody, T51 antibody	2 - 3.4	Stretching, Pulling, Relaxing
[STNS+05]	Cell organelle	Lipid granules	NR	0.075	Moving
[SHC+01]	Type 1 Procollagen	PS	Streptavidin, Biotin	2.17 - 6.7	Stretching
[AMS+03, IAY+05, IHE+06]	Yeast, DNA, Viruses	PS	NR	3 - 10	Pushing, Indirect transportation

continued on next page ...

continued from previous page ...

Papers	Biological object	Gripper object	Gripper coating	Gripper object size (μm)	Manipulation type
[LHP+02, HLRG99]	Fibronectin, RBC	Carboxylated Sl	RGD	2.1 - 5	Application of force
[PFdT+09]	P. L. amazonensis	PS	NR	9	Translation
[KMHY97]	Kinesin	Lt	Kinesin	1	Bead is kept stationary
[DGWW97]	Actin	Polybeads amino	Myosin	1	Stretching
[HBMM02]	DNA	Lt	NR	0.2	Stretching
[JSGF04]	Kinesin	Gl	Kinesin	0.430	Allow brownian motion creating weak trap
[PQSC94]	λphage DNA	PS	Streptavidin	1	Stretching
[SWSG99]	RBC membrane	PS	NR	1	Tension
[VBW+98]	Actin, HMM	Lt, Gl	NEM myosin	1.1	Stretching
[BVHS09]	Kip3p(His6-Kip3p-EGFP)	PS	NertrAvidin	0.528	Friction generation
[CVJ+05]	Myosin-V, F-Actin	PS	Myosin-V	1	Moving
[SL97, SSL98, SHRS02]	λ phage DNA	Lt, PS	Streptavidin	3.2	Grafting, Stretching
[WSY+02]	Myosin, G-actin	Polybeads-amino	Myosin	1 - 3.38	Translation
[WCMF95]	Myosin-V, Actin	Sl	Aminoprofyl surface groups	0.3, 0.8	Trapping
[DLP+07, PPM+05, PPM+07]	Blood cells, T-cells, HL 60 cells	Sl	Streptavidin	5	Tagging
[FEC+05]	E. Coli, Eukaryotic cells	Lt, Sl	RGD containing peptide	2	Stretching, Shrinking
[FFDT+08]	RBC	Sl	NR	NR	Pulling
[KYI+01]	DNA	Water droplet in oil	No coating	10	Translation
[LLLL08]	T7 RNA polymerase	Microspheres	Streptavidin, Anti-dioxygenin antibody	NR	Pulling
[WZY+08]	Human lung epithelial type 2 cells	Sl	Protein A	1.5	Oscillating the trapped bead

2.2 Hybrid manipulation systems

There is a growing interest of using hybrid system rather than a single manipulation system for some synchronized biological studies that are not possible otherwise. An example of such capability is combining gross manipulation with targeted single cell studies. Sott *et al.* [SEPG08] show the usefulness of single cell

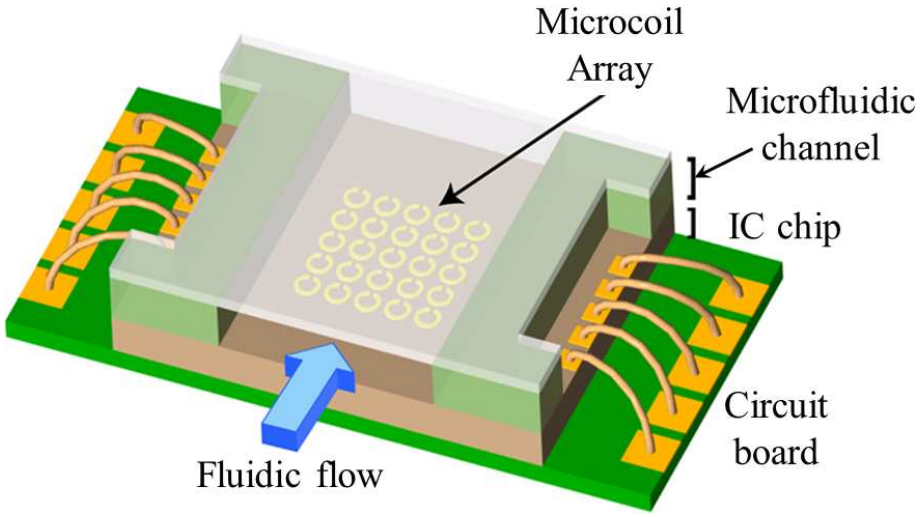

Figure 2.5: *Schematic illustration of a electromagnetic-microfluidics hybrid cell manipulation system (Image source: [Lee05])*

studies in identifying important physiological phenomena which were traditionally studied over a population of biological studies. Experiments by using gross manipulation can only provide the average response over a population of cells. This does not show whether the result is because all the cells respond in the same way or in a all-or-nothing fashion or in a combination of both. To answer the question, a targeted manipulation capability needs to be added with the gross manipulation system. This section presents the literature focused on hybrid manipulation systems.

A hybrid system combining micro-electromagnetic and microfluidics is demonstrated by Lee [Lee05]. The magnetic peaks can be controlled to direct the cell in a predefined path inside a microfluidic channel. A schematic of the hybrid system is shown in Figure 2.5. The author demonstrates its capability by manipulating magnetotactic bacteria and neutral yeast cells tagged with magnetic beads.

Schmidt *et al.* [SYEL07] developed a hybrid optofluidic system to guide the cell transport in a desired direction. A schematic of a optofluidic trapping system is

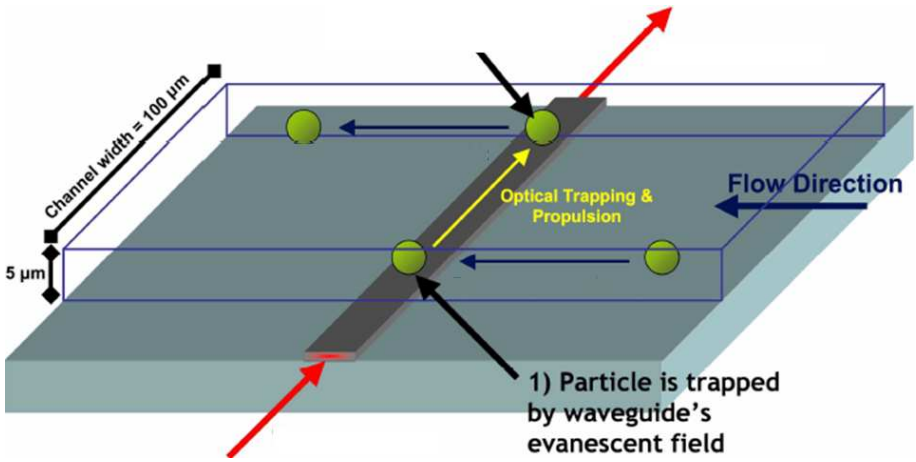

Figure 2.6: *Schematic illustration of a opto-fluidic hybrid cell manipulation system (Image source: [SYEL07])*

shown in Figure 2.6. The solid optical guide provides scattering optical force to push the cell in the direction. The optical force can act in a long range to provide targeted manipulation.

Most of microfluidic devices are built from polydimethylsiloxane (PDMS) which is transparent to laser. That makes it suitable to be combined with optical tweezers. Because of its high precision in manipulation optical tweezers is a popular choice where single cell analysis is a necessary step in biological studies. A schematic of such system is provided in Figure 2.7. Microfluidics provide gross manipulation facility to bring the objects in the workspace where rest of the targeted manipulation is provided by OT. This hybrid system is particularly important to study how individual cells respond to different environment changes in their vicinity. Multiple channels of microfluidics can be used to supply different growth solutions to change the environments in the vicinity [ESL+10]. Umehara *et al.* [UWIY03] developed a similar system to monitor responses of cells in different environment. Cells are trapped and transported by OT in different compartments of microfluidic

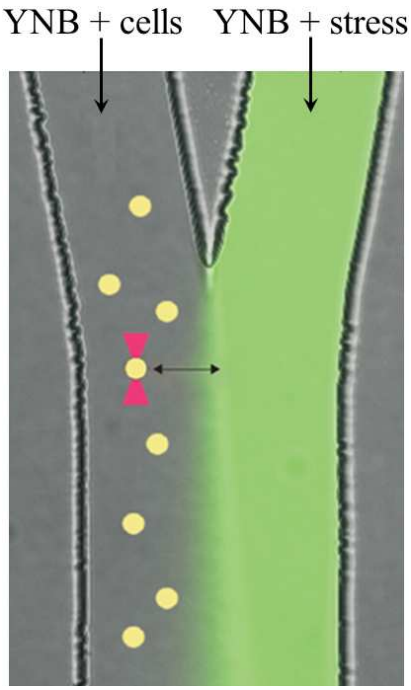

Figure 2.7: *Schematic illustration of a OT-microfluidic hybrid cell manipulation system (Image source: [SEPG08])*

chamber representing different environments.

MacDonald *et al.* [MSD03] use OT-microfluidics hybrid systems to sort rare cells from a large population. OT is used as a complementary device that provides fine manipulation to sort the individual cells in their respective containers, on the other hand, microfluidics provide gross manipulation to bring the population to the workspace of OT. A schematic of a hybrid cell sorting system in shown in Figure 2.8. Wang *et al.* [WWS10] use robotics technologies to automate the cell sorting in such a hybrid system.

2.3 Robot Motion Planning and Control

Planning is an essential part for any autonomous robotic system. There is a huge potential for automated planning and control in the field of micro manipulation

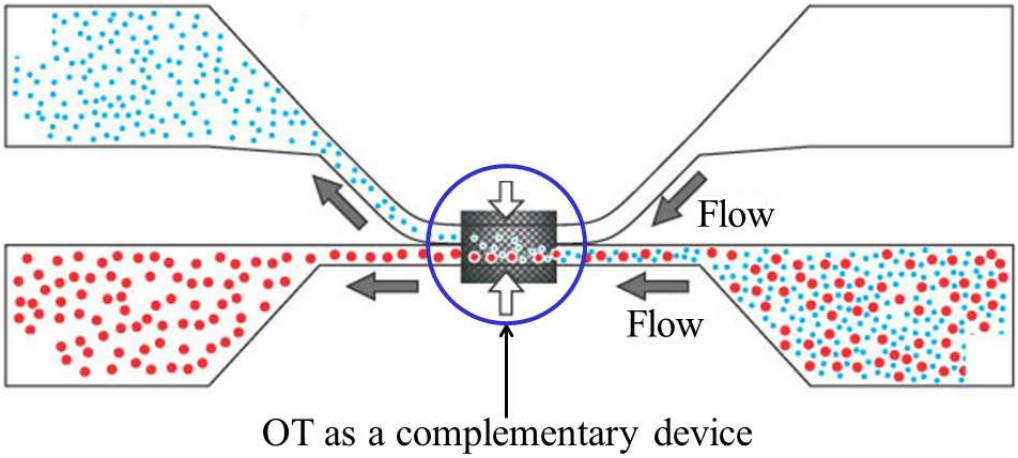

Figure 2.8: *Schematic illustration of a OT-microfluidic hybrid cell sorting system (Image source: [MSD03])*

[BG13]. In most of the autonomous systems planning is used as a high level layer which splits out the desired waypoints for the robot and an underlying control layer is dedicated to ensure that robot is following the path which is known as tracking. Control is a vast research field on its own. This dissertation is only focused on developing novel planning algorithms to facilitate cell manipulation. Hence, the control approaches encountered only in micro-manipulation using optical tweezers are discussed.

Robot motion planning problems can be broadly classified into two categories, namely, deterministic planning and planning under uncertainty. In the first category, the motion planning algorithms assume that the sensor data precisely reflect the current state of the world and the motion of the robot is always deterministic. In the second category, these assumptions are not considered and the planning algorithms explicitly deal with sensor and motion uncertainties. Additional complication for robotic motion planning is the inherent latency between the sensor and motion controller, leading to increased reaction time to new sensory information.

In both the cases, the underlying state space (also known as a configuration space or C-space) is either discretized and then searched using graph search techniques including graph search algorithms [LaV06],decision theoretic approaches [CTS11], or sampled using the sampling-based planning algorithms [LaV06]. The explicit representations of the state space include, e.g., a visibility graph [LP83], road map [LaV06], Voronoi diagram [GL04, LaV06], or lattice-based representations [LaV06].

Some of the most common graph search algorithms include Breadth-first search, Depth-first, Dynamic programming (Dijkstra), and A* [HNR68]. Often time, graph search is equipped with suitable heuristics to direct the search for finding the optimal solution in minimum time. The heuristic function biases the search to the required direction. The heuristics are generally developed by the user based on the objective of the planning. Graph search algorithms have to be provided with a graph representing the workspace of the robot. The workspace or state space is generally created using on-board or remote sensor information. However, in the real world, sensors cannot provide perfect information in most of the cases due to the latency between sensors and controller, highly stochastic nature of the environment, etc. Classical graph search algorithms can be proved to be inefficient in dynamic environment where the state space and hence the resulting graph changes rapidly since the planning has to be started from scratch every time the state space is updated. To address the problem of motion planning under uncertainty, Koenig and Likhachev [KL05] used heuristic based search with the reuse of past information about the environment for fast replanning in unknown terrain. Ferguson *et al.*

[FLS05] modified the same heuristic based search to be able to get a sub-optimal trajectory in a given time interval.

Graph search algorithms were frequently used for automated manipulation using optical tweezers. Wu *et al.* [WTSH10, WSH11] developed a similar A* based approach for automated transport of directly trapped cells using OT. In that approach, the cost function is designed such that smooth paths are computed to ensure reliable transport of cells. Chowdhury *et al.* [CTW+13] developed A* based path planner with a novel cost function for gripper-based automated indirect manipulation of cells using OT.

Decision theoretic approaches have been popular particularly because of their inherent capability to handle both action and sensor uncertainties. Most of problems with uncertainties can be modeled as a Markov decision process which assumes the current state of the robot only depends on its previous state and action. If the uncertainties can be modeled perfectly using the state transition model, decision theoretic approaches can be proved to be much useful since unlike graph search algorithms they do not need to be recomputed every time the graph changes. The solution of a decision theoretic approach is a policy which maps the state into action. For a given state the robot can execute the optimal action from the computed policy. The main criticism of decision theoretic approaches is the dimensional curse. The state space grows exponentially with the increase in dimension. Since, it computes a policy, the cost function (known as value function for decision theoretic approaches) need to be computed all over the state space. Dean *et al.* [DKKN93] developed an algorithm by combining depth first search and MDP. An initial path is computed

using breadth first search and corresponding policy is generated using MDP by creating an envelope of states only along the initial path. As the robot starts executing the plan the planner iteratively update the policy by considering a bigger envelope with more states. Although this reduces the planning time, it provides a sub-optimal solutions since the planner does not consider the whole state space. For instance, if the two consecutive policies define conflicting actions, robot may need to take a much expensive detour to reach the goal. Laroche [Lar00] uses an initial path computed by Dijkstra algorithm and decomposed the path into multiple segments. Each segment is treated as an independent MDP to compute the optimal path in multiple segments. Finally all the paths using multiple MDPs are combined to compute the final path.

A discrete version of the infinite horizon MDP was applied to steer flexible bevel-tip needles inside soft tissues in [ALG+05]. Banerjee *et al.* [BG08, BPLG10] developed a partially observable MDP based planner for automated transport of a particle in an environment with obstacles. They further extended the planner in [BCLG12, BLG09] for automated transport of multiple particles. They introduced a time parameter in the convergence loop to enhance the computational speed and accuracy in deriving the safest paths. In order to incorporate the trapping uncertainty into the MDP framework, they have developed a physically accurate simulation approach incorporating all the forces acting on a freely diffusing particle in a fluid medium [BBGL08, BBGL09, BLGG09]. The output of the simulation framework is a trapping probability table at discrete locations of the OT workspace. However, the timestep of the micro-scale simulation has to be small (in the order of microsec-

onds). Hence, they run the simulations offline and generate a lookup table which is used for the online planning. Later on, Patro *et al.* [PDB+12] used GPU to speed up the computation of trapping probability and showed a 356 times speedup over CPU computation performed by Banerjee et al.. Balijepalli *et al.* [BLG10, Bal11] also showed similar speedup over CPU for nano-scale simulations of freely diffusing particles in a fluid medium. Bista *et al.* [BCGV12, BCGV13] extends the simulation approach for real-time prediction of forces due to interaction of multiple optical traps in a particle ensemble using GPUs. Chowdhury *et al.* [CSW+11] used the MDP framework to compute path for manipulating particles inside OT-assisted microfluidic chamber under the influence of fluid flow.

Sampling based algorithms are particularly useful for planning in higher dimensional space since it does not require to explicitly construct configuration space. Two popular sampling based algorithms are Probabilistic roadmap (PRM) and Rapidly Exploring Randomized Tree (RRT). PRM planner [CLH+05] samples the workspace to construct a roadmap which is equivalent to configuration space and uses a graph search algorithm to compute path on the roadmap. The efficiency of the algorithm is lying on the implementation of an efficient collision detection algorithm and a robust sampling algorithm that can find feasible path. Inefficient sampling sometimes lead to invalid path in case of narrow spaces. On the other hand, RRT based planner [LaV06] creates the map and the optimal path simultaneously, hence does not require an additional graph search.

Missiuro and Roy [MR06] in their Probabilistic Roadmap (PRM) planner made the sampling of the state space biased to specific state space areas by calculating

the collision probability for certain sampled states. The Rapidly Exploring Random Tree (RRT) algorithm was modified by representing the extended nodes by a distribution of states rather than by a single state [MS07] for planning under uncertainty. Another extension of RRT was presented in [FSL09] in which an anytime algorithm was developed that was able to react to changes of the environment and make appropriate re-planning. The nodes were sampled in [GHKR09] according to a suitable probability distribution and thereby an uncertainty roadmap was developed. A sampling RRT based algorithm was developed by Ju *et al.* [JLYS11a, JLYS11b] for automated OT-based transport of cells in 3D.

Trapping force is zero at the focal point of the laser. Hence, particles that are less than 1 m can exhibit Brownian motions inside the traps. Sometimes Brownian motions lead the particles escape the trap. Balijepalli *et al.* [BGGL12] used a feedback controller that can actively control the position and associated laser intensity of the trap to increase the lifetime in trapping nanoparticles. The feedback is achieved by a simple proportional controller to control the laser intensity based on the location of nanoparticles from the center of the traps. The closed loop controller actively changes the laser power and position in order to reduce the escaping of the nanoparticles from the trap. With the controller on, they have seen a 26 and 22 times increase in trap lifetime for 100 nm and 350 nm gold particles respectively without any corresponding increase in laser power. Huang *et al.* [HZM09, HWC$^+$09] used a similar feedback loop based on proportional control law in order to control the Brownian motion of an optically trapped probe. As the probe size goes down to submicrometer or nanometer scale, the diffusion rate due to Brownian forces in-

creases with a rapid decline in stabilizing force from the optical trap. Hence, the probes in submicrometer or nanometer scale used for many biological measurements produce noisy data. Although the stabilizing force can be increased by increasing the laser power that might inflict photodamge to the biological samples. The authors by using their feedback control were able to decrease the variance of their 1.87 m optically trapped probe's Brownian motion. Gorman *et al.* [GBL12] also used feedback control for suppressing Brownian motion of microparticles inside optical trap. Chen *et al.* [CCWS10, CS11, CS12, CWL13] used a potential field based open loop controller to move a collection of optically trapped cells to a desired region while avoiding collisions with each other as well as freely diffusing objects in the workspace. Li *et al.* [LWS13] also used a potential field based controller with vision feedback for reliable positioning of cell to the desired location in the workspace with optical tweezers. In another work on manipulation of a swarm of microparticles Chen *et al.* [CCS11] developed a multi-step approach for assigning goal locations to the individual agent to maintain their formation. A open loop controller is designed to move the microparticles to their assigned goal locations with optical tweezers. Rather than focused on controlling the position of an optical trap, Li and Cheah [LC12] developed a region based controller to automatically transport a cell. The shape and location of the region can be dynamically changed to transport the cell precisely. Wang *et al.* [WYCS12] developed a controller to automatically move the motorized stage while keeping the optical traps stationary to move a group of cells to their desired locations inside a microfluidic chamber. In a separate work Wang *et al.* [WCK$^+$11] used optical tweezers to automatically

move the cell to the desired direction in order to enhance sorting operation inside a microfluidic chamber. Wu *et al.* [WSHX13] integrated a proportional-integral (PI) controller with A* based planner to achieve a stable and precise transport of cells. Hu and Sun [HS11] developed a closed loop controller to precise positioning and transport of multiple cells while maintaining a certain pattern. Li *et al.* [LCHS13] developed closed loop controller based on dynamics of optical trap for simultaneous trapping and manipulation of cells.

A summary of the literature review and the main issues related to this section are the following:

- Heuristic based planning approaches [WTSH10] are efficient. However, the cost function needs to be chosen carefully based on the planning scenario and objectives. Correspondingly, the underlying state-action space representation needs to reflect the requirements of a particular planning domain.

- Decision theoretic approaches can incorporate uncertainty into the planning. However, they are computationally expensive and not suitable when there is a need for fast replanning.

- While sampling based algorithms are suitable for planning in high dimensional space, they are not suitable for planning in randomly changing dynamic environments where the roadmap needs to be constructed again or the planner has to be equipped with a reactive planning component that will take corrective action based on the current scenarios.

- Planning has to be integrated with feedback control in order to reliably trans-

port the particles with optical tweezers.

2.4 Robotic grasping

In this section, we will present literature on robotic grasping closely related to the problem of automated indirect transport of cells.

The overall problem of finding a suitable gripper configuration is closely related to the problem of robotic grasping [Mas01]. One of the basic requirements of robotic grasp is to immobilize the object by preventing its motion due to undesirable external forces, which is characterized by form and force closures. A grasp can be considered as form closured if it immobilizes the object based on frictionless point contact. On the other hand, force closured grasp is able to provide the wrench on the grasped object to balance out any external loads. Hence, the primary distinction between the form and force closures lies in the type of the contact model between the grasped object and the restraining mechanism [Bic00].

Mason [Mas01] divides the robotic grasping into three different issues. The first issue concerns the analysis that determines whether closure applies on an object with a given set of contact points, and possibly other information. Reuleux [Reu76] showed that the minimum contact necessary to achieve the form closure for a rigid body in n dimensional space is $n + 1$. The second issue concerns the existence that determines whether a set of allowable contacts exists to provide closure on an object. Mishra *et al.* [MSS87] proved that any object with any kind of rotational symmetry cannot be fully immobilized with only frictionless point contacts. Hence, only a relative form closure [ZD07] can be achieved. The third issue concerns the

synthesis that determines a suitable set of contacts to achieve closure for an object with a set of allowable contacts. Grasp synthesis is much more challenging problem compared to the other two. Various grasp synthesis algorithms have been proposed [ZW03, ZD07]. Another stream of research deals with the quality of a grasp by developing different metrics [RSC08].

The synthesis problem is cast as a multi-objective optimization problem in [MDS10] where quality metrics are combined with closure properties. Our problem is challenging due to small size scale involved and the uncertainty in placing the beads at the correct locations. Moreover, we want to minimize the intensity of the laser beam experienced by the gripped object resulting from the placement of the configured gripper silica beads. Finally, we want to transport the whole ensemble that consists of a gripper and gripped object, against the drag force resulting from the resistance of surrounding fluid medium. Thus, we need additional validation of robustness that will specify the maximum speed using which the ensemble can be transported without collapsing the gripper configuration.

2.5 Pushing based manipulation

In this section, we will present literature on robotic pushing closely related to the problem of automated indirect transport of cells.

Akella and Mason [AM92] generated open-loop feedback plans to push a polygonal object using a fence. Balorda and Bazd [BB94] reduced motion uncertainty by pushing an object rather than using expensive fixtures arrangements. Lynch and Mason [LM95, LM96] generated a collision-free path for stable pushing of a heavy

object with multiple pusher objects. Abell and Erdmann [AE95] used the idea of stable support to manipulate an object with a known gravitational force and a small uncertainty in its pose. Aiyama *et al.* [AII93] used *pivoting* as a method of automated non-prehensile manipulation. Erdmann [Erd98] implemented a planner that generates a plan for non-prehensile orientation of an object using two palms without the use of fingers to wrap it around. Cappalleri *et al.* [CFM+06] used randomized motion planning techniques for planar micromanipulation tasks based on quasi-static models. Rezzoug and Gorce [RG99] dynamically controlled the multi-finger pushing operation by considering optimal force distribution and center of mass acceleration correction. Goldberg [Gol93] generated a sequence of gripping actions in order to manipulate a part in a sensor-less setup. A similar approach was used by [Qia03, BOvdS02] to orient the part in any arbitrary orientation. Moll *et al.* [MGEF02] used two manipulation primitives: *sequencing* and *rolling* for sensor-less orientation of a micro-scaled asymmetric part. Thakur *et al.* [TCW+12] developed rule-based automated pushing approach for indirectly manipulate a yeast cell with an optically trapped bead. An optically trapped bead is used to push an intermediate bead that is not directly trapped by laser which eventually pushes the cell to the desired location.

In summary, Objects can be transported by pushing rather than grasping. Transporting a cell by pushing requires a feedback control in order to retain the beads in a formation.

2.6 Summary

Optical tweezers is a wonderful instrument for precise manipulation of biological objects. It is very popular to the biologists because of its non-invasive nature of manipulation. However, the slow speed of optical manipulation of cells, confinement to single-cell studies, and lack of widespread usage in cell biology laboratories and clinics indicate that a more systematic approach to design and control this complex system may be valuable for broader implementation. Currently, optical manipulation is limited to a small workspace of 100 µm × 100 µm. The workspace limitation needs to be addressed for comprehensive study on a group of cells using optical tweezers. Another big criticism of optical manipulation is the detrimental effect of laser to the biological objects. Novel manipulation approaches need be developed with tight integration of perception, planning, and control in order to tackle the problem direct exposure of laser to the cell. Hence, we believe that there are many research issues still need be addressed to turn optical tweezers into a promising generalized manipulation technique for objects in micro and nano scale. We list them and briefly discuss how they may help in addressing the current challenges.

- *Automation*: Operation automation is very important since manual intervention and low throughput are major hurdles against wide adaptation of optical tweezers. Although some work has been done on automating transport of colloidal microspheres [CGD06, BCLG12, BPLG10], significant advances in image processing and planning and control are necessary for developing reliable autonomous systems to indirectly manipulate cells. Specifically, automation will

tremendously help in re-adjusting trap and gripper positions by compensating for the constant Brownian motion of the cells, planning optimal trajectories to transport the cells to desired locations in the assays, and selecting appropriate trap intensities and speeds to maximize the operation efficiency.

- *Hybridization*: An alternative to multi-beam tweezer systems for achieving multi-cell manipulation lies in combining optical traps with other forms of manipulation techniques, most notably microfluidic, magnetic, and acoustics. Although many researchers [OPS+03, LLHW07, OCP+07] have already developed hybrid systems to pattern cells or separate them, to the best of our knowledge this has not been done in the context of automated manipulation. We believe that the combination of microfluidic and optical manipulation systems holds the greatest promise in providing high speed of operation and positional accuracy simultaneously. In such systems, the gross motion will be imparted by the fluid flow, whereas the fine and precise positioning of cells at their final locations will be performed by the optical grippers.

- *Manipulation without inflicting photodamage*: Direct exposure of laser to the cell during optical trapping may inflict photodamge. Although a number of indirect manipulation approaches have been reviewed, none of them is particularly useful for transporting and positioning cell to a desired location. Most of the approaches take advantage of adhesive coating to attach cells with optically trapped microparticles to manipulate them indirectly. However, that makes a permanent bonding between cell and microparticle that cannot be de-

tached after manipulation. Hence, these approaches are not useful where cells need be studied for a long time interval after manipulation. A gel microbead is proposed in [MFA09] that can be attached or detached from the cell at will by UV illumination. However, that requires a UV illumination setup along with the optical tweezers. Multiple optically trapped microparticles without any coating can be used as robotic fingers to indirectly grip the cell. However,manual control of multiple particles is nearly impossible. Novel planning and control approaches need to be developed to coordinate the motions of multiple optically trapped particles to manipulate cells indirectly. After manipulation, cells can be released from the optical fingers by simply switching off the laser.

Chapter 3
Automated Cell Transport in Optical Tweezers-Assisted Microfluidic Chambers

In this chapter[2] , we present an automated, physics-aware, planning approach for transporting cells in an optical tweezers assisted microfluidic chamber. We use optical tweezers to achieve efficient manipulation of cells with improved precision inside a microfluidic chamber. The particular application of the developed motion planning approach concerns making a uniform distribution of the cells inside microNets of the chamber to study cell signaling. We use computational fluid dynamics to model fluid forces inside the chamber. The resulting fluid forces are incorporated into the widely used Langevin equation to simulate the motion of cells. The developed simulator is used to build a look-up table for determining probabilities of a cell successfully reaching one of the outlets under the influence of the fluid flow from each location inside the chamber. The developed planner generates collision-free paths that exploit the fluid flow inside the chamber to allow robust cell transport while minimizing the required laser power and operational time. In addition, the planner utilizes the offline generated simulation data to decide a suitable location inside the chamber at which to release the cell to be taken by the fluid flow to one of the outlets. The planner is based on the heuristic D* Lite algorithm that employs a specific cost function for searching over a novel state-action space representation. The effectiveness of the planning algorithm is demonstrated using both simulation

[2] The work in this chapter is derived from the published work in [CSW+11] and accepted work in [CSW+13]

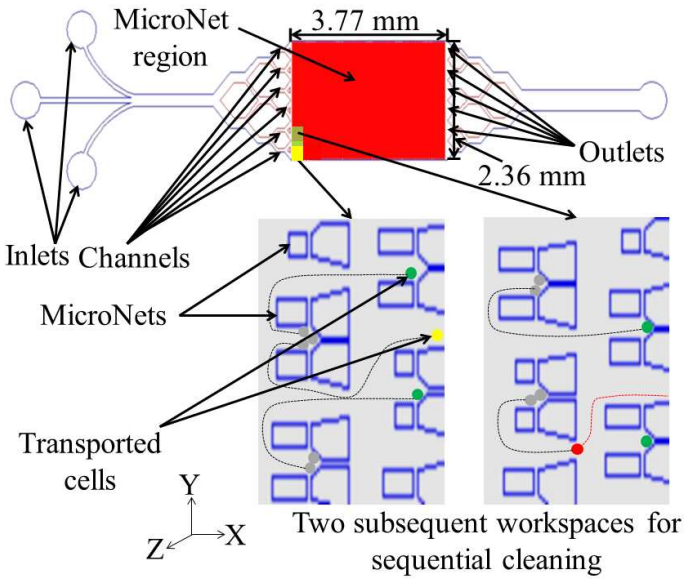

Figure 3.1: *A schematic overview of a microfluidic device and sequential cleaning operation. The cells transported to empty microNets are marked as green, the cells released after moving to the edge of the workspace are marked as yellow, and the cells released inside workspace to allow them to move towards the outlets with the influence of fluid flow are marked as red*

and physical experiments in microfluidic-optical tweezers hybrid manipulation setup.

3.1 Introduction

Cell localization, transport, sorting, and characterization are crucial in many emerging medical and biological applications [CDS09]. We will refer to these types of operations as cell manipulation. In medicine, for example, diagnosis, therapy, and drug delivery can be significantly improved by deploying specialized robotics technologies for manipulating cells. The ability to manipulate individual cells and thereby conduct highly discriminating cell and drug interaction studies will enable development of new drugs and possibly new diagnostic procedures that can detect the onset of lethal diseases at very early stages.

Microfluidics has emerged as a very promising technology to manipulate cells

for high throughput screening [WKC+98], cell signaling analysis [FSH+08] etc. due to its low cost, low power consumption, and ability to handle a large sample population simultaneously. However, careful control strategies must be developed to provide fine position control over the cells in some microfluidic chambers (e.g. see Figure 3.1). Another emerging technique which has become very popular over the last two decades in the field of micro-manipulation is optical tweezers (OT) [ADBC86, Ash92]. OT have been shown to be a very effective technique for transporting cells with high precision; however, throughput significantly depends on the maximum number of traps that can be created.

The advantages of these two manipulation techniques can be exploited by combining them into a single hybrid system. In our hybrid system, we integrated a microfluidic chamber [FSH+08] (see Figure 3.1) into our OT system. The microfluidic chamber contains about $10,000$ microNets [SFCW10] (previously, they have been termed traps, but to avoid confusion with the laser traps, herein we term them MicroNets or nets) that are created intentionally to direct the fluid flow in a certain direction and capture cells in each microNet. However, the number of cells captured in the microNets cannot be controlled by solely regulating the fluid flow. This results in non-uniform distribution of cells inside the chamber which is not desirable for certain biological experiments e.g. cell-cell interaction studies [DMK+12] in which each microNet should contain a desired number of cells to get statistically accurate results.

The optical tweezers can be useful for providing fine control for moving the excess of cells from crowded microNets to the nets with insufficient number of cells

or by releasing the cells in suitable locations to be taken by the fluid flow to one of the outlets of the chamber (we will refer to this operation as cleaning in this chapter). However, the following challenges need to be addressed to utilize OT in providing microfluidics with more efficient and reliable manipulation control.

Presence of fluid flow The microfluidic chamber needs to be provided with continuous fluid flow to keep the cells inside the microNets. Hence, OT needs to take the fluid flow into account during the cleaning operation. Moving the optically trapped cells along the streamlines increases the reliability of the operation. This allows using lower laser power to prevent damaging the cells that are transferred into microNets. On the other hand, in order to reliably transfer the cells to one of the outlets of the chamber by the sole use of the fluid flow, they need to be released by the OT at suitable positions. Although fluid flow is laminar inside the chamber, the streamlines get affected by the fluctuation in flow at the inlet, due to the presence of clogged cells at the entry to the chamber, and laser heating. This noise in streamlines need to be characterized to determine suitable release points for the cells.

Operating space OT operates in a much smaller workspace (102 $\mu m \times 60$ μm in our setup) compared to the microfluidic workspace (see Figure 3.1). This requires sequential cleaning of microNets. A cleaning operation depicted in Figure 3.1 consists of moving the excess of cells from crowded microNets to empty microNets or released at suitable locations. After cleaning all the microNets, the workspace needs to be shifted by using motor-controlled stage. The cleaning operation continues until all the microNets are cleaned. Sometimes, cells (in case of rare cells) need

to be stored in a convanient microNet that can be used to fill empty nets in next cycle rather than releasing them to reach the outlets of the chamber.

Fast operation The cleaning operation needs to be very fast to utilize the high throughput advantage of the microfluidic chamber. Using holographic optical tweezers (HOT) [CKG02], multiple traps can be created to allow cleaning of multiple nets in parallel. However, manual handling of multiple traps in parallel is very challenging due to the presence of randomly moving cells in the workspace as well as fluid flow and hence makes the cleaning process less reliable and thus slower. Exposure to high intensity laser for a longer time due to slow manipulation process may cause photo-damage to the cells [NCL+99].

In this chapter, we have developed an automated, physics-aware, simulation-assisted planning approach for transporting cells in an environment with obstacles and the presence of fluid flow that enables fast cleaning of microNets inside a microfluidic chamber using OT. This involves trapping of desired cells inside microNets, transporting them to other microNets or releasing them at suitable locations from which the cells can be taken by the fluid flow to one of the outlets of the chamber.

In order to maximize the cleaning efficiency, we utilize offline simulation of cells moving with the influence of fluid flow inside the chamber to generate supporting data represented as flow vectors and probabilities of the cells successfully reaching the outlets of the chamber from all its discrete locations. We then use the generated simulation data in online planning as opposed to using manually constructed rules.

The developed planning approach is similar to a physics-aware robot motion planning problem where the traps themselves can be regarded as robots. Our de-

veloped approach is independent of microNet arrangements, hence can be applied to a wide variety of microfluidic designs that focus on immobilizing cells inside the chamber and a secondary manipulation tool (e.g. OT) can be integrated to provide better handle on controlling the cell population.

3.2 Simulations of cell motion in microfluidic chamber

3.2.1 Overview

Given a cell C located in the state $\vec{x} = [x, y]^T$ in a microfluidic chamber under the influence of fluid flow, compute:

- all external forces exerted on the cell C at the state $\vec{x}$.
- the probability p_{reach} and the required time t_{reach} for the cell C to successfully reach one of the outlets $\{\vec{x_{l,exit}} = [x_l, y_l]^T\}_{l=1}^{N}$ of the chamber (see Figure 3.1). Here, N is the total number of outlets.

We adopt following approach to simulate the cell motion

- We use a commercial CFD package FLUENT (ANSYS, Inc. Version 13.0.0) to model the fluid flow inside the microfluidic chamber [KWLT08]. The quality of the fluid flow vectors are tested using experiments.
- We use a open source collision engine Box2D [box] to model the collision force of cells with other cells and microNets inside the chamber.
- We incorporate all the external forces into Langevin dynamics equation and solve the ordinary differential equation using Verlet integration scheme to get the trajectories of the cells.

- We run the simulations for 100 times introducing a random Gaussian noise to the fluid force vectors to calculate the probability p_{reach} and the required time t_{reach} for the cell to reach one of the outlets $x_{l,\vec{exit}}$ from every location inside the microfluidic chamber.

3.2.2 Simulation of cell motion

A cell can be considered as a particle of a spherical shape. A particle moving in a fluid undergoes the effect of a rapidly fluctuating force due to random collisions with the surrounding liquid molecules, as well as a hydrodynamic drag force [BLG10]. These forces are closely related to each other and are modeled using Langevin's equation [Wei89] as follows:

$$\frac{\delta V(t)}{\delta t} = -\frac{\gamma}{m}V(t) + \frac{\zeta}{m}\Gamma(t) \tag{3.1}$$

where $V(t)$ is the velocity of a particle with mass m and radius R_a at time t. This equation assumes a fluid with viscosity η, which is a function of temperature T. The drag coefficient γ for a spherical particle is given by Stokes' law as $6\pi\eta R_a$,where R_a is the radius of the spherical particle. The scaling constant $\zeta = \sqrt{2\gamma k_B T}$ in Equation 3.1 is obtained by applying requirements of the fluctuation-dissipation theorem [AT99], where k_B is the Boltzman's constant. The acceleration of the particle at the end of a uniform time step δt can be written in the finite difference form [PDB+12, BBGL09, BLG10] as shown in Equation 3.2.

$$A(t+\delta t) = -\frac{\gamma}{m}V(t) + \frac{1}{m}\sqrt{\frac{2\gamma k_B T}{\delta t}}N(0,1) + \frac{F_{ext}}{m} \tag{3.2}$$

Here, the stochastic term in Equation 3.1 is replaced by normal distribution $N(0,1)$ and the scaling constant ζ includes the time step δt. The external force term F_{ext} allows us to include the collision force and force due to the influence of fluid flow. Once we calculate the acceleration $A(t+\delta t)$ at the end of the time step δt, we can use the velocity form of the second order Verlet integrator [Ver67] to calculate the position (R) and velocity (V) of the particle at the end of each time [PDB+12, BBGL09, BLG10]. The simulation time step is taken as the closest multiple of 10 smaller than $\frac{m}{\gamma}$ as described in [BLG10]. Before modeling the external forces (collision, and fluid force), we test the Brownian motion behavior of a freely diffusing particle by excluding the F_{ext} term from Equation 3.2. We run the simulation for 300 s without the presence of any external force and recorded the positions of the particle along X axis at different time intervals. Then we plot the distribution of change in positions of the particles at those respective intervals. The distribution resembles the Gaussian distribution with zero mean, which agrees with the Brownian motion model. Then we check the standard deviation of the position-change distribution with the increasing time interval. The standard deviation increases gradually with the increase of time interval, which agrees with the Brownian motion physics. The change in the position of the particle along Y axis at different time intervals follows the same distribution as well.

3.2.3 Modeling of collision forces

We use the open source collision detection library Box2D [box] to check for a collision of the cell with other suspended cells and static nets. Since the simulation

time step is very small, the cell does not move much in a single time step. So we do not need to go through any sophisticated collision force calculations. We use Box2D only for detecting a collision, and if a collision occurred we applied a static force in the normal direction of the collision point. However, checking for collisions for all individual cell-cell pairs and cell-net pairs would be computationally expensive. Therefore, we restrict the collision checking to the vicinity of each individual cell. The collision engine checks for collisions of the cells and nets that lie in $10R_a$ distance of the interested cell.

3.2.4 Modeling of fluid flow

The fluid flow in a microfluidic chamber is laminar since viscosity dominates over inertia in reduced dimension [AB05]. We carried out computational fluid dynamics (CFD) simulations using a commercial package FLUENT (ANSYS, Inc. Version 13.0.0). We used water ($\rho_f = 998.2\ kg/m^3$) as working fluid. Hence, fluid flow fields are Newtonian and incompressible in nature. We used the Design Modeler of ANSYS to create the 2D geometry of the microfluidic chamber. For meshing, we used patch conforming method which is suitable for small features in the geometry. The momentum and continuity equations are solved using the semi implicit method for pressure linked equation (SIMPLE) algorithm. First order upwind scheme is chosen for spatial discretization of momentum. A flat velocity profile is imposed at a uniform flow rate of 1200 nl/min and a constant pressure ($P = P_{atm}$) boundary condition is imposed at the outlet. FLUENT computes the fluid velocity at every node of the mesh element.

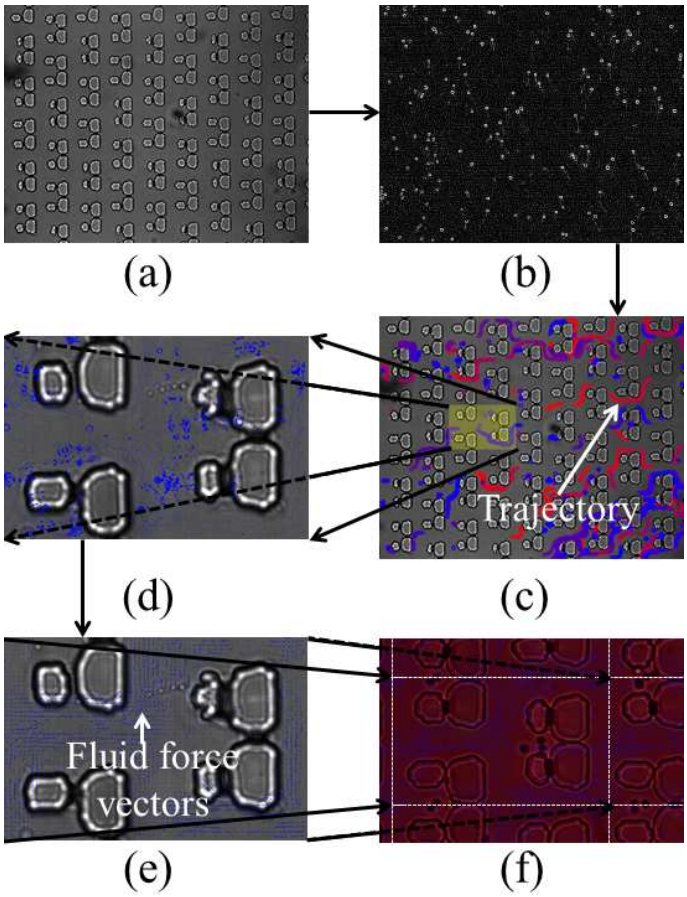

Figure 3.2: *Measurement of flow vectors: (a) Solution of 0.98 µm silica beads is pumped into a microfluidic chamber with a constant flow rate, (b) Detecting the beads from a thresholded image, (c) Tracking the beads to generate streamlines, (d) Confining all the trajectories into the representative pattern element (RPE) of the microfluidic chamber, (e) Calculating the velocity vectors from the streamlines over the RPE, (f) Mapping the flow vectors to the workspace of the OT*

We developed an experimental procedure to qualitatively verify the velocity derived from CFD. We pump 0.98 μm sized silica beads into the microfluidic chamber at a low enough volume rate so that we can track them using a high-speed camera and 40X objective lens. By tracking the positions of the beads we get the streamlines inside the chamber. To measure the velocity vector of the beads in different positions of the chamber we record the images to capture the flowing beads (see Figure 3.2a) using a high-speed camera (at a frame rate of 60 fps). Then we developed a MATLAB script (The MathWorks, Inc. Version 7.10.0.499 (R2010a)) to generate the trajectories followed by individual beads based on the particle tracking algorithm described in [CG96]. The MATLAB script applies a thresholding scheme (see Figure 3.2b) to detect the beads, track them in each frame and generates the trajectories by plotting the positions of the beads in subsequent frames (see Figure 3.2c). We used the generated trajectories to calculate the velocity of the beads in different positions inside the chamber.

However, due to the small size scale, motion of 0.98 μm beads is influenced by a significant Brownian motion while following the trajectories. Hence, we need to filter out the noise due to Brownian motion from the trajectories to retain the monotonic behavior of the streamlines. The appearance of the net structures in our microfluidic chamber is repetitive in nature. We define a representative pattern element (RPE) (see Figure 3.2d) which appears repetitively in the whole chamber. Since fluid flow is dominated by the fluid viscosity (laminar flow), the relative positions of RPEs do not have much effect on the flow. Therefore, the streamlines around the RPEs are assumed to be similar regardless of their relative positions inside the chamber.

We represent all the trajectories found in Figure 3.2c with respect to the RPE coordinates (see Figure 3.2d). In that way, we have enough trajectories that can be averaged to filter out the Brownian motion and retain the monotonic behavior of the streamlines. We apply fine gridlines over the RPE to take the average of all velocities of the beads in each grid to remove the Brownian motion effect from the velocity vectors (see Figure 3.2e). For our automatic cleaning operation we use 60X objective lens with the uEye camera (IDS, Inc., Cambridge, MA) that has a smaller field of view. By applying the concept of repetitive patterns we map the flow vectors to the workspace of the OT (see Figure 3.2f).

The fluid vectors computed experimentally qualitatively match with that computed by FLUENT. Due to their laminar nature, the flow of 0.98 μm beads is caused by only a drag force that can be modeled as Stokes' law given by Equation 3.3.

$$F = \gamma V_f \tag{3.3}$$

This equation assumes the fluid viscosity η as a function of temperature T (η= 1.002×10^{-3} Pa-s and T=293 K for water). The drag coefficient η for a spherical particle is given by Stokes' law as $6\pi\eta R_a$, where R_a is the radius of the spherical particle. The fluid force F causes the beads to flow and V_f is the velocity of the beads. Since we have calculated the force of the fluid at each position in the chamber, we use Equation 3.3 to develop a look-up table for all the forces acting in the corresponding positions. The fluid force acts in the direction of the fluid flow which is computed from the streamlines in Figure 3.2e. The forces at different positions in the chamber are plugged into F_{ext} term in Equation 3.2 for simulation.

Although we use a flat inlet velocity profile for our fluid force computation, the fluid flow velocity is affected by flow fluctuation at inlet, clogged cells at the entrance to the chamber, and the evaporation due to exposed laser. Since there is no suitable way to measure these uncertainties, we apply a Gaussian noise to the fluid force at every discrete location to introduce uncertainty. At every location we change the fluid force from FLUENT by perturbing its direction with a random Gaussian with mean 0 and standard deviation 5 degrees. The standard deviation of 5 degrees is determined by running some initial experiments by releasing a cell at certain location of the chamber and recording its final locations. We ran the simulations for similar location with different standard deviation and chose the one that gives similar distribution of final locations. The standard deviation varies with the inlet fluid flow rate. To maintain the monotonic flow of streamlines we did not change the fluid force at every simulation time step δt rather at every discrete location of the chamber.

3.2.5 Workspace simulator design

In each time step δt, the position, velocity, and acceleration of each cell are advanced in the system. The acceleration of the cell at the next time step $t+\delta t$ is calculated using Equation 3.2. Next, the position of the cell is updated using the previous velocity and acceleration [PDB+12, BBGL09, BLG10]. Finally, we calculate the velocity of the cell at $t+\delta t$ using the average acceleration from the current and previous time steps and the previous velocity. Therefore, the velocity Verlet integration generated a list of positions, velocities, and accelerations in each

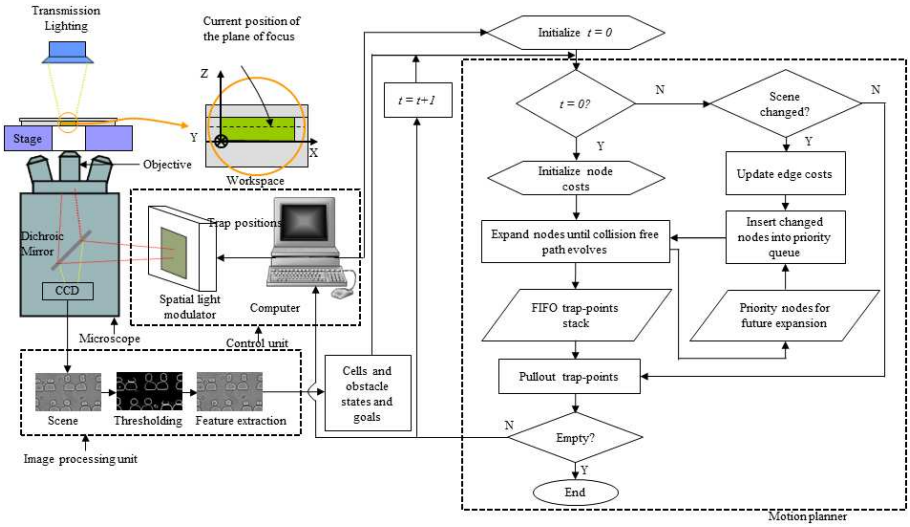

Figure 3.3: *Holographic optical tweezers (HOT) cell transport workstation: the image processing unit returns the positions of cells and obstacles in the workspace from the camera and passes them to the motion planner, the planner then computes the collision-free paths and determines the next trap positions for the control unit that activates the trap positions through the spatial light modulator*

time step. After each time step, the positions of the cells are provided into two force modules (i.e., collision and flow). The force value from the flow force module is perturbed with a random Gaussian noise to model the force fluctuation. Each force module returns a force value depending on the position of the cell. All the force values are then added to F_{ext} to update the external force after each time step.

3.2.6 Building of the probability table

In order to build the look-up tables for probability p_{reach} of cell to reach one of the outlets $(x_{l,\vec{exit}})$ Ψ and time t_{reach} to successfully reach one of the outlets $(x_{l,\vec{exit}})$ Δ, we discretize the whole chamber into rectangular grids of dimension 0.4 μm $\times$ 0.4 μm. We set one of the grid locations as the initial state $\vec{x_{init}} = [x_{init}, y_{init}]^T$ of the cell and run the simulation for 100 times to record the final states $\vec{x_{final}} = [x_{final}, y_{final}]^T$ and required times t_{req}. We use the final states and required times t_{req} to calculate

the probability p_{reach} and average time t_{reach} for the cell to successfully reach one of the outlets $x_{l,\vec{exit}}$ if the cell is released from that particular state. We continue the simulation for all the grid states to build the look-up table Ψ and Δ for whole chamber.

3.3 Motion planning for automated transport of cells

3.3.1 Motion planning problem formulation

Given, (1) the initial states $\{x_{i,\vec{init}} = [x_i, y_i]^T\}_{i=1}^{n}$ of n cells to be transported in the OT workspace $X' \subset X$ of the discretized operating space X of the chamber, (2) their candidate goal states $\{x_{j,\vec{goal}}\}_{j=1}^{m}$ represented either as one of the chamber outlets $x_{l,\vec{exit}}$ or microNets within X', (3) static and dynamic obstacles $\{\Omega_k\}_{k=1}^{l}$ represented either as microNets or other moving cells, (4) a probability look-up table Ψ containing probabilities p_{reach} of a cell successfully reaching $x_{l,\vec{exit}}$ from each possible discretized location $\vec{x} \in X$, (5) a time look-up table Δ containing the average time t_{reach} required for a cell to reach $x_{l,\vec{exit}}$ for each $\vec{x} \in X$, and (5) a fluid force map Φ defining a fluid force vector ϕ for each $\vec{x} \in X$, compute:

- collision-free trajectories $\{\tau_i\}_{i=1}^{n}$ for n laser traps to transport the cells either to their target microNets or release locations within OT operating space X', while following fluid flow streamlines in order to maximize the cleaning reliability as well as operation speed.

3.3.2 Assumptions

We made the following assumptions:

- We approximate cells as perfect spheres of radius R_a.

- We assume the optically trapped cells move with the same velocity as the traps. This is ensured by selecting an operating speed using which the beads can be reliably trapped by the laser traps [BBGL09].

3.3.3 Motion planning approach

Since the microfluidic environment is dynamically changing due to fluid flow and Brownian motion of cells, the required trajectories for the cells must be frequently replanned. The architecture of the cell transport workstation is shown in Figure 3.3. The imaging unit needs δt_g to process the image sequence and the motion planner needs δt_p to generate collision free trajectories. The total time taken by imaging and motion planner unit ($\delta t_g + \delta t_p$) is determined by the control unit update, which is about 66 milliseconds. Hence, we need a fast replanning scheme to be able to compute the trajectory within the planning time interval δt_p.

Our motion planner adopts the fast heuristic search algorithm D* Lite [FLS05] to find an efficient trajectory for a single cell from a given initial $\vec{x_{init}}$ to a goal $\vec{x_{goal}}$ position. The algorithm functions similarly as a backward version of the A* algorithm [HNR68]. It incrementally expands the states from $\vec{x_{goal}}$ to $\vec{x_{init}}$. During computation of a trajectory, all the remaining cells and microNets are considered as obstacles. The heuristic is used to guide the search in order to expand the minimum number of states and thus maximize planning efficiency. During the search, the planner maintains a set of states named as open set $\Theta(\vec{x})$. It contains the states that are more likely to be expanded next based on their cost in a priority queue. For

replanning, the planner reuses the history of the search from previous planning time interval by maintaining the same open set $\Theta(\vec{x})$ throughout the entire planning horizon. When the cost of a node is changed due to the change in OT workspace states X', the planner immediately inserts the node into $\Theta(\vec{x})$ and continues expanding the node with the lowest cost until a new trajectory is evolved. This allows the controller to efficiently launch multiple plans corresponding to multiple traps in order to transport multiple cells simultaneously. The algorithm terminates when each cell reaches its goal position $x_{\vec{goal}}$. The following sections present the state-action space representation, cost function, and planning algorithm itself.

3.3.3.1 State-action space representation for planning

The state space of OT is represented as a 2D rectangular grid since we translate cells only in $x - y$ plane. The discrete state $\vec{x^k} = \left[x_c^k, y_c^k\right]$ of a cell C is thus defined as a vector of its position $\vec{x_c^k}$ at time step k corresponding to a particular grid cell.

An action control set $U = \{\vec{u_{t,1}^k}, \vec{u_{t,2}^k}, \ldots, \vec{u_{t,8}^k}, \vec{u_r^k}\}$ consists of eight *linear* translation actions $\vec{u_{t,i}^k}$ and a single *release* action $\vec{u_r^k}$ available for execution at a given time step k. By executing the *release* action $\vec{u_r^k}$, the cell is immediately released from the trap allowing the fluid flow to transport it to one of the goal states $x_{\vec{j,goal}}$. All *linear* actions can be represented mathematically as follows.

$$\vec{u_t^k}\left(\delta x^k, \delta y^k\right) = \begin{bmatrix} \delta x^k \\ \\ \delta y^k \end{bmatrix} \tag{3.4}$$

where δx and δy are the linear translations along X and Y axis, respectively.

When the optical trap executes an action $\vec{u_t^k}$ at time step k, it transitions from

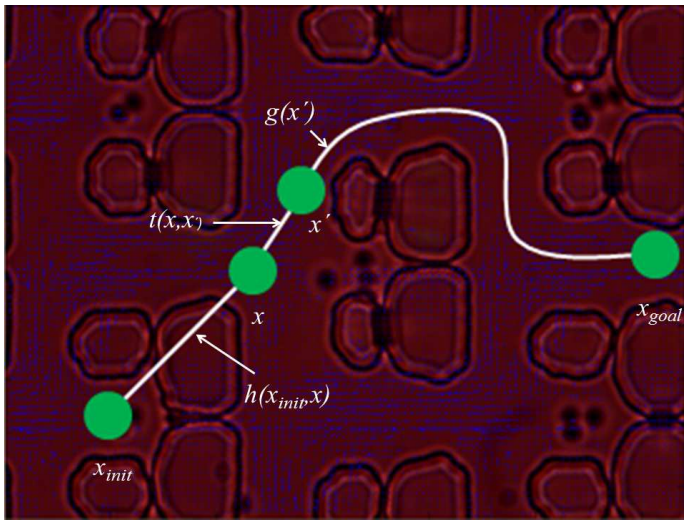

Figure 3.4: *Illustration of cost-to-go* $g(\vec{x'})$*, transition cost* $t(\vec{x}, \vec{x'})$*, and heuristic* $h(\vec{x_{init}}, \vec{x})$

$\vec{x^k}$ to $\vec{x^{k+1}}$ using the following equation.

$$\vec{x^{k+1}} = \begin{cases} \vec{x^k} + \vec{u_t^k} & \text{for the } \textit{linear} \text{ actions,} \\ \\ \vec{x_{j,goal}} & \text{for the } \textit{release} \text{ action} \end{cases} \tag{3.5}$$

3.3.3.2 Cost function

The planning algorithm iteratively expands the states from the priority queue (open set $\Theta(\vec{x})$) with their key values [FLS05] computed as

$$\begin{aligned} key(\vec{x}) &= [key_1(\vec{x}), key_2(\vec{x})], \\ &= [min(g(\vec{x}), rhs(\vec{x})) + h(\vec{x_{init}}, \vec{x}), \\ &\quad min(g(\vec{x}), rhs(\vec{x}))] \end{aligned} \tag{3.6}$$

$g(\vec{x})$ is the optimal cost-to-go from $\vec{x}$ to $\vec{x_{goal}}$, $h(\vec{x_{init}}, \vec{x})$ is the heuristic cost estimate of the trajectory between $\vec{x}$ and $\vec{x_{init}}$, and $rhs(\vec{x})$ is the one-step look-ahead cost

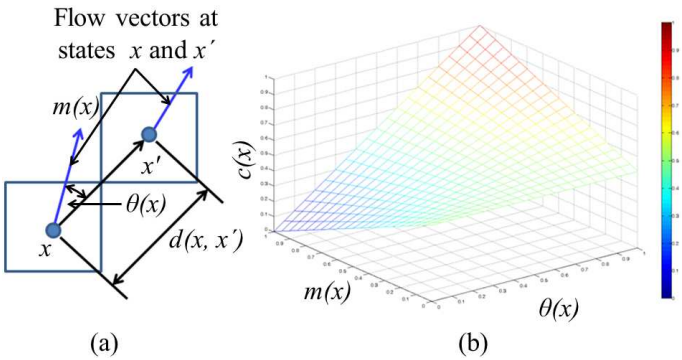

Figure 3.5: *$m-\theta$ coupling cost function: (a) illustration of different components in the cost function: $m(\vec{x})$ is the magnitude of flow vector at state $\vec{x}$, $\theta(\vec{x})$ is the direction of flow vector at state $\vec{x}$ with respect to the direction vector from $\vec{x}$ to $\vec{x'}$, $d(\vec{x}, \vec{x'})$ is the Euclidean distance between states $\vec{x}$ and $\vec{x'}$, (b) characteristics of the $m-\theta$ coupling cost function*

which is calculated according to

$$rhs(\vec{x}) = \begin{cases} 0 & \text{if } \vec{x} = \vec{x_{goal}}, \\ min_{\vec{x'} \in succ(\vec{x}))}(t(\vec{x}, \vec{x'}) & \\ +g(\vec{x'})) & \text{otherwise} \end{cases} \tag{3.7}$$

where $succ(\vec{x})$ denotes a set of possible resulting states after taking an action $\vec{u}$ at state $\vec{x}$ and $t(\vec{x}, \vec{x'})$ denotes the transition cost (see Figure 3.4) of moving from $\vec{x}$ to $\vec{x'}$. In order to ensure optimality, the heuristic function may not overestimate the true cost to $\vec{x_{init}}$. We use the time required for the trap to travel the distance between $\vec{x}$ and $\vec{x_{init}}$ to calculate $h(\vec{x_{init}}, \vec{x})$.

The magnitude $m(\vec{x})$ and direction $\theta(\vec{x})$ (see Figure 3.5a) of the fluid force vector acting at state $\vec{x}$ are combined with the Euclidean distance between $\vec{x}$ and $\vec{x'}$ to calculate the transition cost $t(\vec{x}, \vec{x'})$ for *linear* action. The magnitude and direction of flow vectors are coupled and cannot be separated. Hence, $t(\vec{x}, \vec{x'})$ has

two components as

$$t(\vec{x}, \vec{x'}) = \begin{cases} w\frac{d(\vec{x},\vec{x'})}{v} + (1-w)c(\vec{x}) + e & \text{for } \textit{linear} \text{ actions ,} \\ r(\vec{x}) & \text{for } \textit{release} \text{ action} \end{cases} \tag{3.8}$$

where $d(\vec{x}, \vec{x'})$ is the Euclidean distance (see Figure 3.5a) between $\vec{x}$, $\vec{x'}$ and $c(\vec{x})$ is the m-θ coupling cost defining the contribution of magnitude and direction of flow vectors, and $r(\vec{x})$ is the cost associated with the *release* action. The edge cost e is set to ∞ if either $\vec{x}$ or $\vec{x'}$ lies in obstacle. Otherwise, e is set to 0. v is the constant trap speed and w is a user defined fluid force weight parameter ($0 \leq w \leq 1$). We define the m-θ coupling cost $c(\vec{x})$ using a smooth function stated as follows:

$$c(\vec{x}) = 0.5 + m(\vec{x})(\theta(\vec{x}) - 0.5) \tag{3.9}$$

where $m(\vec{x})$ is the normalized magnitude of the contributing flow vector at $\vec{x}$, and $\theta(\vec{x})$ is the normalized angle between the direction vector from $\vec{x}$ to $\vec{x'}$ and the flow vector. The characteristic of $c(\vec{x})$ is illustrated in Figure 3.5b. $t(\vec{x}, \vec{x'})$ is set to ∞ if $\vec{x}$ lies in an obstacle to prevent it from further expansions.

We want the traps to follow high magnitude flow-lines as long as the angle between the direction vector from $\vec{x}$ to $\vec{x'}$ and the flow vector does not exceed a limit. Beyond that limit, following the high magnitude flow-lines may lead into moving the traps across them. This would require higher laser power to execute the plan in order to prevent the cell being knocked out from the trap by the fluid flow. We define the limiting value of $\theta(\vec{x})$ to be 0.5 for our algorithm to be conservative. The value of $c(\vec{x})$ decreases with the increase of $m(\vec{x})$, preferring the higher magnitude

flow-lines up to the limiting value of $\theta(\vec{x})$. Beyond that, the value of $c(\vec{x})$ increases with the increase of $m(\vec{x})$ to suggest the lower magnitude flow-lines.

We define the cost associated with *release* action $r(\vec{x})$ using the following function.

$$r(\vec{x}) = \begin{cases} (1 - p_{reach})t_{reach} & \text{if } p_{reach} \geq p_{release,T}, \\ \infty & \text{otherwise} \end{cases} \tag{3.10}$$

p_{reach} is the probability of the cell to reach $x_{l,\vec{exit}}$ if released at state $\vec{x}$ and t_{reach} is the corresponding required time according to Ψ and Δ. $p_{release,T}$ is a user-defined release threshold parameter that allows the planner to consider only the states that have higher probability to reach $x_{l,\vec{exit}}$.

3.3.3.3 Planning algorithm

The algorithm for computation of trajectories for the desired cells to transport is given as follows:

Input:

(a.) Finite non-empty state space X.

(b.) Obstacle map Υ where $\Upsilon(\vec{x})$ represents an obstacle state.

(c.) Obstacle cost map Ω such that,

$$\Omega(\vec{x}) = \begin{cases} 1 & \text{if } \vec{x} \text{ lies on obstacle,} \\ 0 & \text{if } \vec{x} \text{ lies on free space.} \end{cases}$$

(d.) Fluid force map Φ, where $\Phi(\vec{x})$ encompasses the magnitude $m(\vec{x})$ and direction $\theta(\vec{x})$ of the fluid force vector at state $\vec{x}$.

(e.) Probability look-up table Ψ, where $\Psi(\vec{x})$ encompasses the probability p_{reach} of the cell to reach one of the outlets $x_{l,\vec{exit}}$ if released at state $\vec{x}$.

(f.) Time look-up table Δ, where $\Delta(\vec{x})$ represents the average time t_{reach} of the cell to reach one of the outlets $x_{l,\vec{exit}}$ if released at state $\vec{x}$.

(g.) Initial states $X_{init} = \{x_{i,\vec{init}}\}_{i=1}^{n} \subseteq X$ of target cells.

(h.) Goal states $X_{goal} = \{x_{j,\vec{goal}}\}_{j=1}^{m} \subseteq X$ of the target cells.

(i.) Planning time interval δt_p, goal deviation threshold w_{th}.

(j.) User defined fluid force weight parameter w and release threshold parameter $p_{release,T}$.

Output:

Trajectories $\{\tau_i\}_{i=1}^{n}$ for the cells to be transported at each planning time interval δt_p

Steps:

(1.) For each target cell go through the following steps:

i. Read the obstacle map Υ and identify the obstacle states $X_{obs} = \{x_{\vec{obs},i}\}_{i=1}^{m} \subseteq X$.

ii. For each obstacle state $x_{\vec{obs},i} \in X_{obs}$, compute a safety zone by determining the adjacent neighboring state set $Neighbor(x_{\vec{obs},i}) \subseteq X$ and setting $\Omega(Neighbor(x_{\vec{obs},i})) = 1$.

iii. Using the cost function described in Section 3.3.3.2 expand the successor states $succ(\vec{x})$ with minimum cost from goal state $\vec{x_{goal}}$ to the initial state $\vec{x_{init}}$ [FLS05] to calculate the initial trajectory τ.

iv. Keep open set $\Theta(\vec{x})$ (priority queue that stores the states that are most likely to be expanded later in the search) for future expansion during re-planning.

(2.) Execute the trajectories. Stop the algorithm if $\parallel X_{init} - X_{goal} \parallel \leq w_{th}$, otherwise update the obstacle cost map at every planning time interval δt_p.

(3.) If there is any change to the cost in any state due to the change in the workspace environment, insert the affected states into the open set.

(4.) Go to Step 1iii to expand nodes from $\Theta(\vec{x})$ based on priority key (see Equation 3.6) until new trajectories are evolved.

3.4 Results and discussions

3.4.1 Experimental setup and methods

A schematic of the microfluidic chamber used in this chapter is shown in Figure 3.1. Cell medium is injected into the chamber through one of the three inlets using a digitally controlled microsyringe pump. The cell medium gets divided into six different channels before entering the rectangular microNet region in order to distribute the cells uniformly. The cells are captured inside different microNets as they flow through the microNet region. The actual dimension of the microNet region is 3.77 mm $\times$ 2.36 mm consisting of 9432 number of nets. The height of the device

is 10 μm to prevent stacking of cells. OT can only operate in a limited space of 74 μm $\times$ 43 μm $\times$ 10 μm that consists of only four microNets. Hence, we have to carry out the cleaning operation in multiple steps to be able to clean the entire chamber. The entire cleaning operation starts from the lower left corner of the rectangular microNet region.

We demonstrate the usefulness of the planner using a BioRyx 200 (Arryx, Inc., Chicago, IL) holographic laser tweezer. It consists of a Nikon Eclipse TE 200 inverted microscope, a Spectra-Physics Nd-YAG laser (wavelength 532 nm), a spatial light modulator (SLM), and proprietary phase mask generation software running on a desktop computer. Nikon Plan Apo 60x/1.4 NA, DIC H oil-immersion objective is used. The maximum rate at which traps can be set is the update rate of the Spatial Light Modulator (SLM), 15 Hz, and the minimum step size is 150 nm. The feedback control is achieved with a second PC equipped with a uEye camera (IDS, Inc., Cambridge, MA) for imaging the cells through transparent microfluidic chamber and running the software for executing the planning algorithm. A digitally controlled microfluidic syringe pump (SP230iW Syringe pump manufactured by World Precision Instruments, Inc., Sarasota, FL) is used to inject cells into the microfluidic chamber through the inlets.

Cells are identified and located by thresholding the image and then calculating the center of mass of all the remaining blobs (see Figure 3.3). Yeast cells used in this experiment are cultivated from fast growing yeast powder. 0.016 gm of yeast powder is mixed with 3% (w/v) glucose solution. The cells are allowed to grow for an hour. After an hour, the concentration of cells is examined under microscope.

The average diameter of cells after an hour is 5-8 μm. For measuring the fluid flow vectors we use 0.98 μm diameter silica beads (density of 2000 kg/m^3 and refractive index of 1.46, purchased from Bangs Laboratories, Inc., Fishers, IN). Initially Yeast solution is pumped into the chamber with a flow-rate of 0.03 μl/m. It takes about 20 minutes to fill the chamber with yeast cells trapped inside the microNets. Once the chamber is filled up, we switch the pump inlet from the Yeast solution to water.

3.4.2 Simulation results

In this section we demonstrate two novel functionalities of the planner using simulations: (1) Utilizing fluid force map Φ to derive collision-free paths based on the user defined fluid force weight parameter w, (2) Using the probability look-up table Ψ and time look-up table Δ based on the user defined release threshold parameter $p_{release,T}$ to decide suitable release points of corresponding laser traps.

The simulation results are obtained on Intel(R) Core(TM)2 Quad processor with 2.83 GHz speed. We scale down the microfluidic chamber for simulation to a region of 195 μm $\times$ 150 μm to avoid computation overhead to build the probability look-up table Ψ and time look-up table Δ. The simulation can be run for whole chamber in the similar fashion described in section 3.2.6 to build the entire look-up table. The dimensions of the OT workspace are chosen as 65 μm $\times$ 50 μm. We discretize the workspace into 7650 number of grids for planning with grid size 0.4 μm $\times$ 0.4 μm. The z dimension of the workspace is ignored since the laser is constrained to move in $x-y$ plane. In each planning time interval δt_p laser can either move only to next neighboring grid or can release the cell to let it move with the influence of

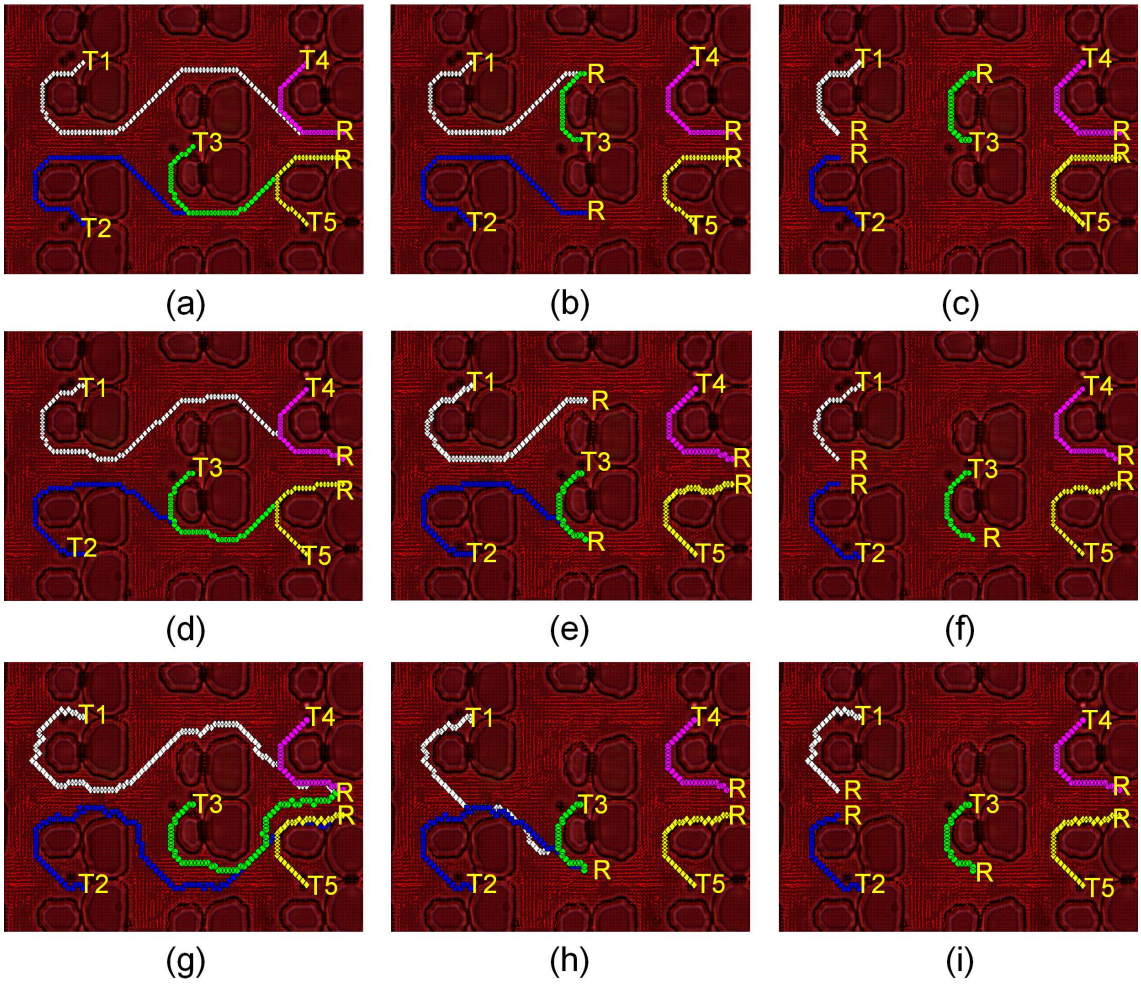

Figure 3.6: *Variations in cell trajectories as well as release locations based on user defined fluid force weight parameter w and release threshold parameter $p_{release,T}$: (a) $w = 1$; $p_{release,T} = 0.85$, (b) $w = 1$; $p_{release,T} = 0.65$, (c) $w = 1$; $p_{release,T} = 0.5$, (d) $w = 0.5$; $p_{release,T} = 0.85$, (e) $w = 0.5$; $p_{release,T} = 0.65$, (f) $w = 0.5$; $p_{release,T} = 0.5$, (g) $w = 0$; $p_{release,T} = 0.85$, (h) $w = 0$; $p_{release,T} = 0.65$, (i) $w = 0$; $p_{release,T} = 0.5$*

fluid flow.

In the workspace, 5 microNets can be accommodated, hence can be cleaned in parallel. The simulation of transporting one cell from each of the 5 microNets to the suitable release location is shown in Figure 3.6. The target cells are labeled as T_i. The goal locations $x_{j,\vec{goal}}$ of all the cells are assigned to the outlets $x_{l,\vec{exit}}$ of the scaled chamber which is outside of the OT workspace. Hence, the planner is forced to release the cell inside the workspace based on $p_{release,T}$ at the locations denoted by R (see Figure 3.6). The suitable release locations vary with the user defined parameters w and $p_{release,T}$.

The computation time for calculating 5 trajectories depends on user defined parameters w and $p_{release,T}$ (see Equations 3.8 and 3.10). Figure 3.6 shows the simulated trajectories for the cells with three different w and $p_{release,T}$. Each trap coordinates with the movements of other traps, while generating the trajectories so that two traps do not move to the same location at the same time.

The planner generates the shortest path between initial and the goal position with the fluid force weight parameter value $w = 1.0$ (see Figures 3.6a, b, c). Since the planner does not account for the fluid flow inside the chamber, the shortest path most often prefers the laser to go across the fluid streamlines. Therefore, the transporting cells have higher risks of being knocked out from the traps. Moreover, the laser power needs to be increased in this case in order to hold the cells against the fluid flow while moving across the streamlines which is susceptible to cell damage.

The planner prefers high magnitude streamlines that are aligned with the direction of motion of traps with the fluid force weight parameter value $w = 0$

(see Figure 3.6c, d, e). Hence, the planner needs to expand more nodes compared to the shortest path search. The resulting path is longer and needs more time to execute. However, the planner can use minimum laser power to execute the path since the laser follows the fluid streamlines making it suitable to retain cell viability. Moreover, it will reduce the chance of cells being knocked out of the traps by the fluid flow.

With the fluid force weight parameter $w = 0.5$ (see Figure 3.6f, g, h), the planner generates a balanced path that can be shorter compared to the path calculated using $w = 0$. The planner prefers the shortest distant grids, where the flow vectors have lower magnitude since the laser can still be able to hold the cell. The user sets the parameters based on the fluid flow conditions and sensitivity of the cells being manipulated by the laser beam.

With the change of $p_{release,T}$, the planner chooses different release points for the cells from respective traps. With a higher $p_{release,T}$ (e.g. 0.85) all the cells are carried to the edge of the workspace before release (see Figure 3.6a, d, e) because of the fact that there is no other locations in the workspace that have higher probability for the cells to reach $x_{l,\vec{exit}}$ if released from the traps. With the decrease of $p_{release,T}$, the planner is able to release the cells much earlier. The release points are also influenced by w (see Figure 3.6e, h) since in addition to reaching probability p_{reach}, the planner uses t_{reach} (see Equation 3.10) to decide the suitable release points.

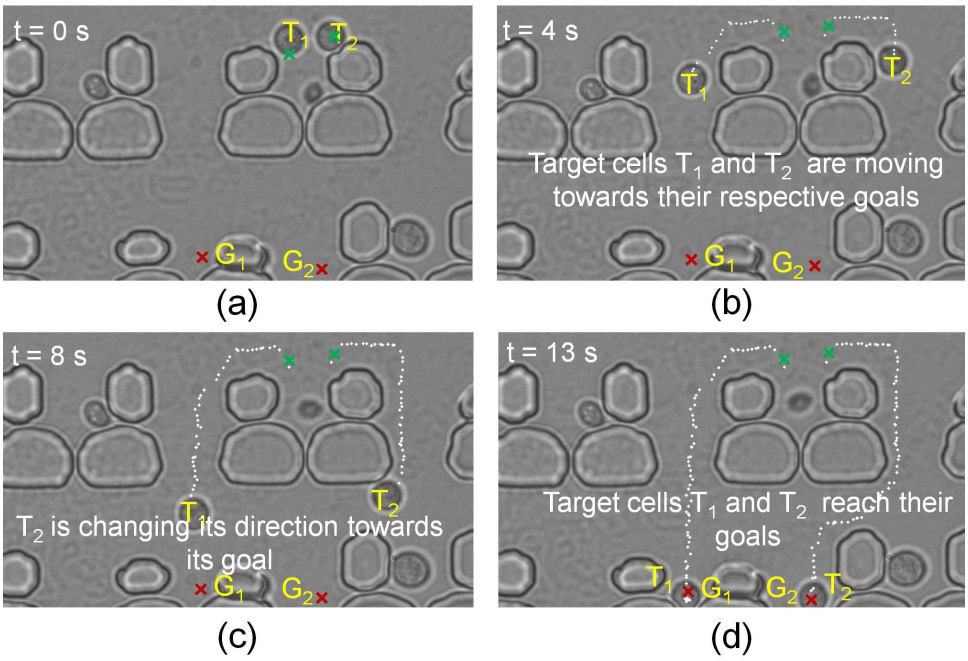

Figure 3.7: *Automated transport of two cells to their respective goals to control cell population: (a) initial scene, (b) target cells T_1 and T_2 are moving towards their respective goals, (c) target cell T_2 is changing direction towards its goal, and (d) target cells reach the respective goal locations*

3.4.3 Experimental results

In this section, we demonstrate the automated cell transport capability of the OT-microfluidic system with some initial experiments with our physical systems. Due to some physical limitations of our customized setup, we restricted the fluid force weight parameter to $w = 1$ and threshold parameter to $p_{release,T} = 0.85$ for this demonstration, i.e. the planner does not utilize the high magnitude streamlines while transporting the cells. Hence, all the cells are transported to the nearest local exits and released while avoiding collisions with the microNets and other transporting cells inside the workspace.

After identifying the cells and microNets using image processing, we select the cells that are in the same optical plane to be transported automatically. The

weight w and threshold $p_{release,T}$ parameters are also provided to the planner. The planner automatically computes collision-free paths to release locations based on the input parameters. The planner transports the cells by creating point traps at every planning time interval δt_p. Since the planner does not generate paths that utilize the fluid flow streamlines, the laser power has to be set to the significant 0.6 watts. However, the laser power at the objective is much smaller due to some losses in the hologram phase calculation. A constant flow of water (0.03 μl/m) is maintained throughout the experiments.

In the designed experiment as illustrated in Figure 3.7, a uniform distribution of a single cell in each microNet has to be maintained. In this figure, the target cells are labeled as T_i, their initial locations are marked using green "$\times$", and their corresponding release locations are marked using red "$\times$" and labeled as G_i, where i represents an index of a target cell. In the experiment, the two cells T_1 and T_2 need to be removed from the microNet (locations are marked using green "$\times$") in order to achieve the required distribution. The cell T_1 is transported automatically to the empty MicroNet location G_1, while the other cell T_2 is transported to the location G_2 and then released. During the transport, the cells avoid other microNets and cells in the workspace. The transport time is shown in the upper left corner of the images in Figure 3.7. The cleaning time of the OT workspace in this experiment is 13 s. After cleaning the microNets, the user can continue in operation at a different location of the microfluidic chamber by manually changing the position of the microfluidic stage.

The effectiveness of the developed system can be expressed in terms of the

expected transport time for a cell to reach the exit of the chamber, which is a function of its maximum transport speed and probability p_{reach} of successfully reaching the exit. In order to measure the successful release rate experimentally, we released the cell for 10 times at a particular region in between two microNets as the planner suggested and let it follow the flow. Each time when the cell went through the chamber without being captured by any other microNet, we marked it as a success, otherwise as a failure. The cell successfully reached the outlet of the chamber 6 times out of 10 test cases. The rate 0.6 of successfully reaching the outlet is lower than $p_{release,T} = 0.85$ suggested by the simulator partly because for the simulation we used a scaled down area which is smaller than the actual microfluidic region. If we hold the cell using the optical trap and move it all the way out of the chamber following the fluid flow lines, p_{reach} will be as high as 0.9 as opposed to releasing it at a suggested location determined by the planner. However, the transport time will increase due to the limited, maximum velocity of the trap which is in the order of 10-20 times less than the speed of fluid flow. Our simulation and physical experiments suggest that there exist release locations inside the OT workspace that have a higher probability of reaching the exit of the chamber. If there does not exist such locations, the planner suggests to hold the cell all the way out of the chamber.

Our approach utilizes a combination of an optical trap and fluid flow for cell transport. There are two options for removing a redundant cell from the chamber. First, the cell can be transported all the way out of the chamber using only an optical trap, making sure the cell does not get stuck inside another microNet. In this case, the transport speed of the cell is limited by the maximum speed of the

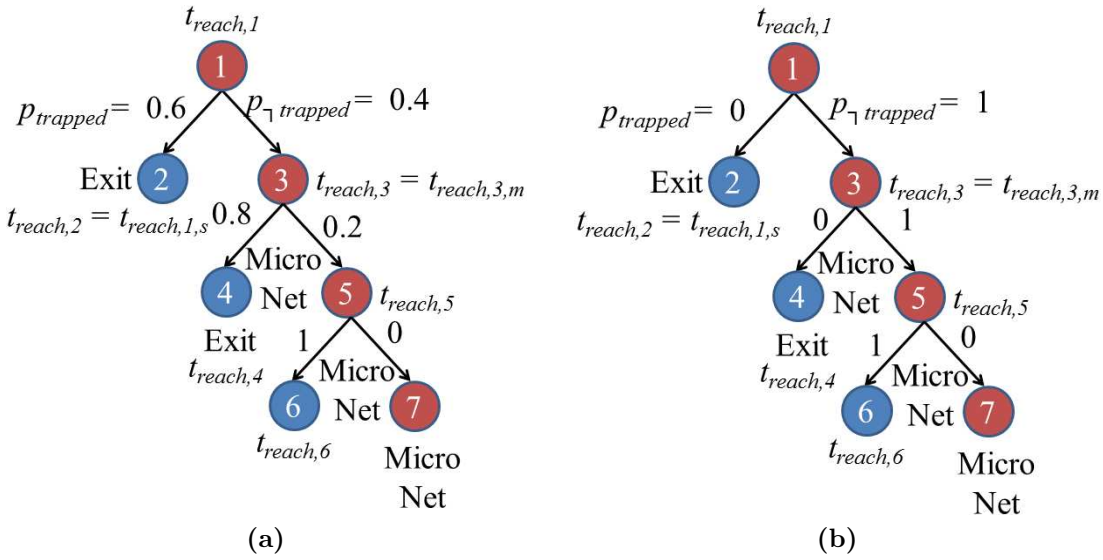

Figure 3.8: *Three-stage probability tree of a cell successfully reaching the exit: (a) an example of a more general scenario with the existence of release positions inside the workspace that have higher probability to reach the cell to one of the exits, (b) an example of a worst case scenario where cell always gets trapped in one of the microNets*

trap which is 10 to 20 times smaller than the speed of the fluid flow. Second, the cell can be transported using a combination of the fluid flow and the optical trap. In this case, the cell is taken out of its current microNet and then released at a suitable location nearby. The location is selected such that it increases the probability of the cell successfully reaching the exit. If the cell gets captured by one of the microNets downstream, it is trapped and released again at a new suitable location.

The probability of the cell successfully reaching the outlet of the chamber increases as the cell gets closer to it. The expected time of the cell reaching the exit can be computed recursively using a probability tree. An example of the tree is shown in Figure 3.8a). The root of the tree represents the current position of the cell. The emanating edges of each node represent two possible outcomes of releasing the cell. The cell either reaches the exit of the chamber or is captured by another

microNet inside the chamber. The edges determine probabilities of the two possible outcomes corresponding to the current state of the cell.

The computation of the expected time starts from the leaves up to the root of the tree. By climbing the tree up to the root, the expected transport time $t_{reach,i}$ for each node i is computed and gradually propagated back to the root. The time $t_{reach,i}$ is computed as the average over the two possible outcomes according to $t_{reach,i} = p_{trapped}t_{reach,s} + (1 - p_{trapped})t_{reach,m}$, where $p_{trapped}$ is the probability of the cell getting trapped in one of the microNets, $t_{reach,s}$ is the expected time of successfully transporting the cell in a single attempt to the exit by the sole use of the fluid flow, and $t_{reach,m}$ is the expected time of multi-step cell transport that combines the use of the optical trap and the fluid flow.

In the worst case (see Figure 3.8b), the cell will be always captured by one of the microNets after it is removed from its current microNet and released from the optical trap to be taken by the fluid flow. Let $t_{reach,t}$ be the time required to transport the cell to the exit by the sole use of the optical trap and the total transport length is $l_{chamber}$. Then, the total time $t_{reach,m}$ required to transport the cell to the exit using a combination of the fluid flow and the optical trap is less or equal to $t_{reach,t}$ since a fraction of $l_{chamber}$ will be transported with the speed of fluid in the former case.

3.5 Summary

Microfluidic devices are becoming widespread tools in cell biology and medicine because of their ability to handle a large volume of cells and non-invasive nature of

manipulation. However, the lack of precise position control makes the tools often inconvenient and highly inefficient. The use of OT as a complementary tool ensures precise position control inside a microfluidic chamber. This chapter describes a fast heuristic based planning approach built on D* Lite algorithm with a novel state-action space representation and a new cost function. That enables efficient and reliable cleaning of multiple nets in parallel inside a microfluidic chamber, while drawing minimum laser power during execution of the cleaning plan. The developed composite cost function incorporates the magnitude and direction of fluid flow vectors in order to compute trajectories that follow the fluid flow. The computed trajectories ensure reliable cell transport since the cells do not need to be transported across the flowlines and need less laser power to execute preventing them from photodamage. Moreover, we utilized our developed physics-based simulator to build a look-up table that contains probabilities of a cell successfully reaching one of the chamber outlets for each discrete location in the chamber. The planner utilized the table to decide suitable release locations for the cells.

Manual control of the microscope stage to move the OT workspace to a different region of the microfluidic chamber slows down the cleaning process. Chapter 4 will focus on planning for synchronized movement of the microscope stage and optical traps that will further expedite the automated cleaning. In this chapter, cells are directly trapped to be transported to their nearby unfilled microNets, which may affect their viability. Hence, another future direction of this research is to use optical grippers [BCLG11, KCA$^+$11] made of optically trapped beads to indirectly trap and transport cells to the desired microNets (See Chapters 5 and 6 for details).

The planner will need to generate trajectories for the entire ensembles, which will require detailed modeling of trap-trap and multiple trap-cell interactions.

Chapter 4
Enhancing Range of Transport in Optical Tweezers Assisted Microfluidic Chambers Using Automated Stage Motion

In this chapter [3], we present a planning approach for automated high-speed transport of cells over large distances inside an Optical Tweezers (OT) assisted microfluidic chamber. The transport is performed in three steps that combine the optical trap and motorized stage motions. This includes optical trapping and transporting the cells to form a desired cell-ensemble that is suitable for a long distance transport, automatically moving the motorized stage to transport the cell-ensemble over a large distance while avoiding static obstacles, and distributing the cells from the ensemble to the desired locations using OT. The speeds of optical traps and the motorized stage are determined by modeling the motion of the particle under the influence of optical trap. The desired cell-ensemble is automatically determined based on the geometry of the microfluidic chamber. We have developed a greedy heuristic method for optimal selection of the initial and the final location of the cell-ensemble to minimize the overall transport time while satisfying the constraints of the OT workspace. We have discussed the computational complexity of the developed method and compared it with exhaustive combinatorial search. The approach is particularly useful in applications where cells are needed to be rapidly distributed inside a microfluidic chamber. We show the capability of our planning approach using physical experiments.

[3] The work in this chapter is derived from the published work in [CATW+13].

4.1 Introduction

Microfluidic chambers are emerging as useful devices for conducting research in biology and biophysics [ZA12]. Common applications include cell sorting [Lan12, MSD03], studying cell response under changing environment [ESL+10, UWIY03], stem cell research [ZA12], etc. However, microfluidic chambers lack the capability of precisely placing individual particles at the desired locations. Integration of optical tweezers with microfluidic chambers has provided fine motion control capabilities [CSW+13, WCK+11, WWS10, EGR+04]. Ma *et al.* [MYP+12] used specially designed dual channel line optical tweezers in Y shaped configuration to separate yeast cells of different sizes within a microfluidic chip. Honarmandi *et al.* [HLLK11] reported an approach combining microfluidics and optical manipulation to locally apply tensile and compressive force on a single target cell. Erikson *et al.* [EEN+07] developed an experimental platform to use epi-fluorescence microscopy and optical tweezers in combination with microfluidic system for the analysis of rapid cytological responses occurring in single cells.

Optical traps enable simultaneous independent manipulation of multiple particles [BCLG11, KCA+11, CSW+12]. However, typically optical tweezers have very limited workspace due to high magnification needed for optical trapping. For example, a microfluidic chamber may have dimension of 3,000 × 2,000 µm (see Figure 4.1), but the optical tweezers might be able to work only in 100 × 100 µm area (with 40× objective lens). So new techniques are needed to expand the workspace in which optical traps can be utilized.

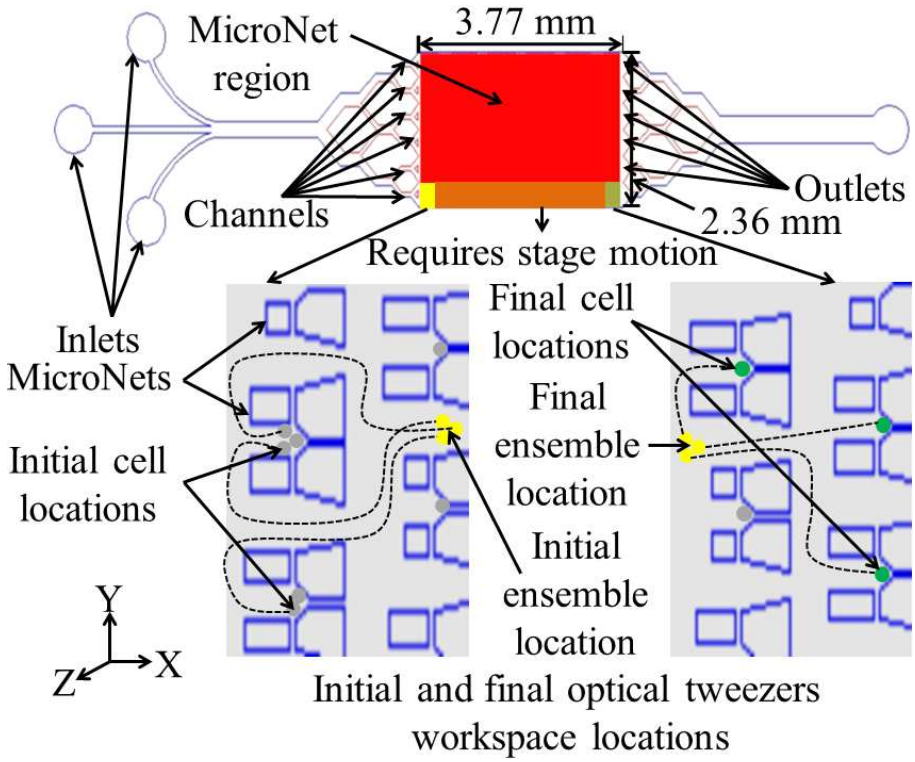

Figure 4.1: *A schematic overview of a microfluidic device with microNets [CSW+13] and long distance cell transport operation*

A typical microscope that is used to realize optical tweezers also has a motion stage driven by electric motors. This stage has large motion ranges in X and Y axes and can move at a very high speed. If a particle is held stationary using an optical trap then the stage motion capability can be used to move the microfluidic chamber and realize relative motion between the particle and the chamber. This capability is easy to realize during manual operation. However, conducting repeated biological experiments requires high level of automation [BPLG10, CTW+12, TCW+12].

The problem addressed in this chapter is motivated by microNet cleaning application described in Chapter 3. In this application, biological cells are injected into a microfluidic chamber containing physical traps defined as microNets (see Figure 4.1) with the objective of placing exactly one cell in each microNet. Due to

the limited control over the flow process, some of the microNets may trap multiple cells, while some other microNets may not trap any cell at all. After the initial cell placement has been completed by the flow, the next step is to redistribute cells by moving them from microNets that contain multiple cells to the empty microNets (not containing any cells). In Chapter 3, we addressed the problem of using optical tweezers for removing extra cells from microNets and getting them out of the microfluidic chamber [CSW+13]. In this chapter, we attempt to redistribute extra cells from overloaded microNets to empty microNets rather than simply removing the extra cells. MicroNets act as obstacles when an ensemble of cells is transported. This type of operation may require long range transport with an obstacle avoidance strategy and is the main motivation behind the problem formulated in this chapter.

In this chapter, we present a new technique for realizing precise, concurrent, and automated transport of multiple cells over large distances. First, cells are moved using optical tweezers into a compact ensemble. During this phase multiple cells can be moved independently and concurrently. The state of the workspace determines the optimal location of ensemble formation and its shape. Once the ensemble is created, multiple optical traps can be used to hold cells in the ensemble in place. Now the stage carrying the chamber can be moved to transport the entire ensemble with respect to the optical traps.

If during the stage motion, a particle dislodges from the ensemble, then the stage motion can be suspended, and an optical trap can be used to move the particle back into the ensemble. Stage motion can be resumed when the ensemble is complete again. The stage motion should move such that the ensemble does not collide

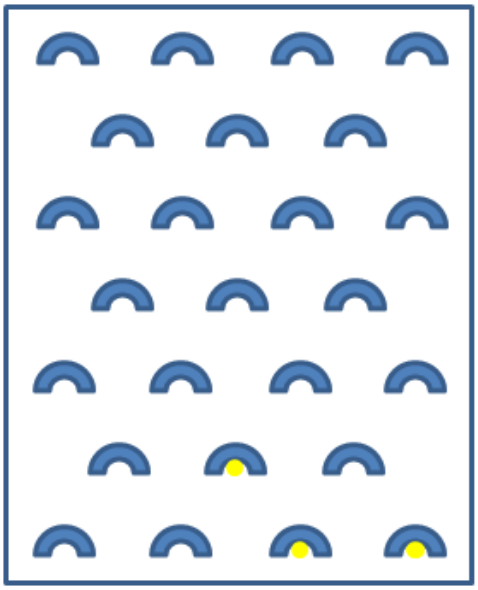

(a) *Chamber with the target microNets filled with cells that need to be transported*

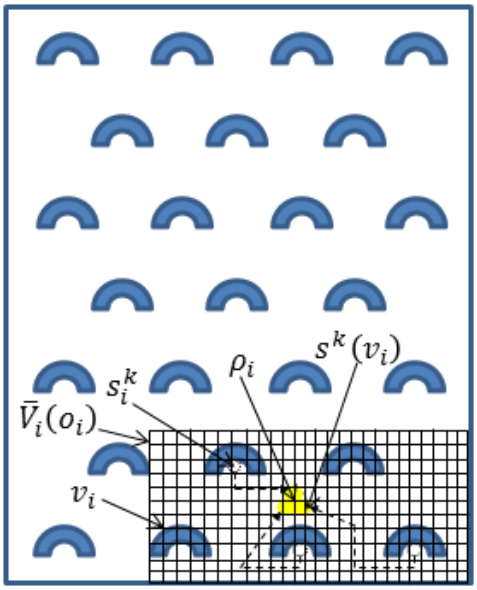

(b) *Cells are transported to form an ensemble using optical traps.*

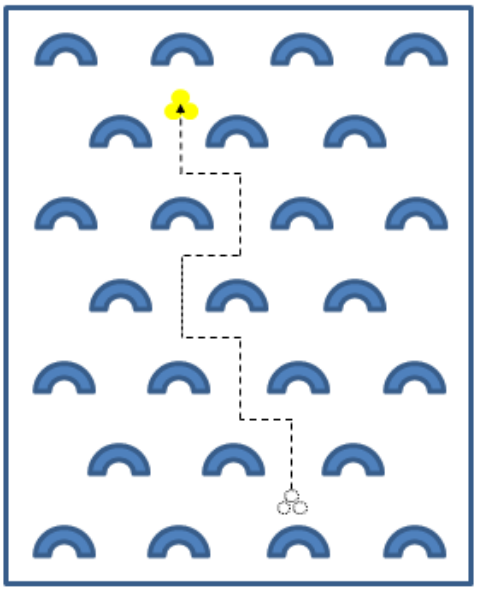

(c) *Cell ensemble is transported to a new location using stage motion.*

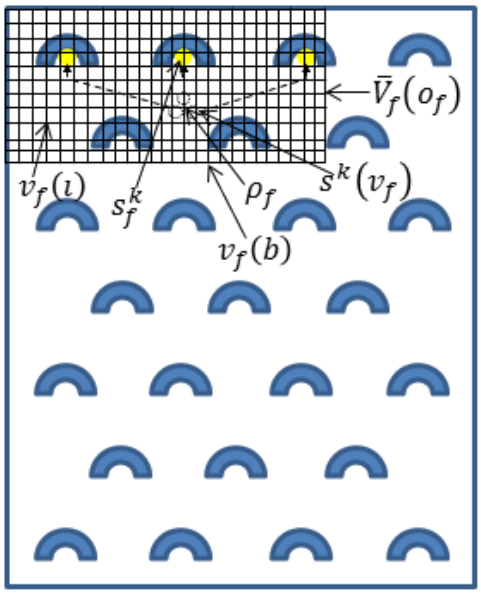

(d) *Cells are distributed to the desired microNets.*

Figure 4.2: *A schematic overview of cell manipulation operation*

with any obstacle in the workspace. Once the ensemble arrives close to the final destinations of cells in the ensemble, the stage motion stops. Now optical traps are used to move all the cells in the ensemble to their final goal locations. Figure 4.2 graphically illustrates this concept.

This chapter describes a planning system for combining motorized stage motion with optical trap motion to realize automated transport of ensemble of cells over large distances. We have enhanced our prior work in the area of optical trap motion planning [CSW+13] by combining it with stage motion planning to realize this capability. Using the combination of both stage and optical trap motion, we are able to automatically transport particles at a fast speed in a larger workspace compared to the limit of optical tweezers workspace.

4.2 Problem formulation and overview of approach

Let $\mathcal{X}$ be the overall workspace of the chamber and $\bar{\mathcal{X}}$ be the corresponding discretized state-space. Let $V(o)$ be the workspace of optical tweezers (OT) when it is located at the location $o \in \mathcal{X}$ in the overall workspace. The location o is selected such that $V(o) \subset \mathcal{X}$. Let $\bar{V}(o)$ be the discretized state-space corresponding to OT workspace $V(o)$ such that $\bar{V}(o) \subset \bar{\mathcal{X}}$. A state in $\bar{\mathcal{X}}$ or $\bar{V}(o)$ is defined as a location of an ensemble or a particle during trap path planning or a stage location during stage path planning (introduced in Section 4.4). If the motion stage is kept stationary, optical traps can only move particles within the OT workspace (a cell can be considered as a particle of certain shape). We apply appropriate safety margins to ensure that particles can be successfully transported between every pair

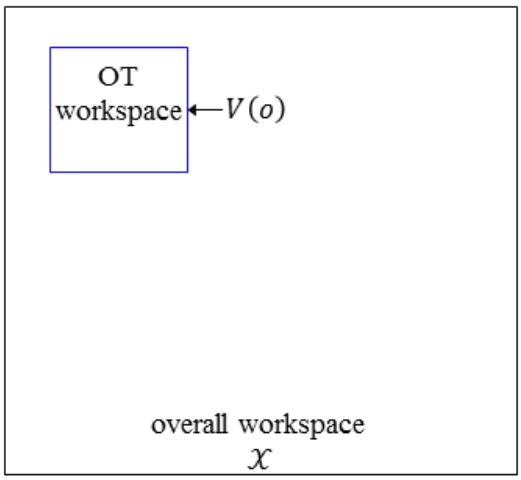

(a) *Dimension of OT workspace with respect to overall workspace.*

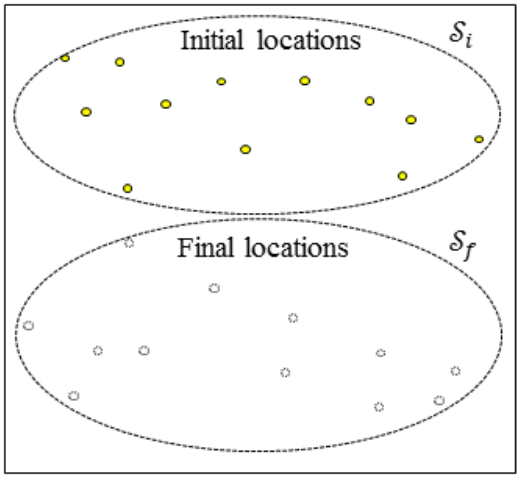

(b) *Initial and final locations of particles.*

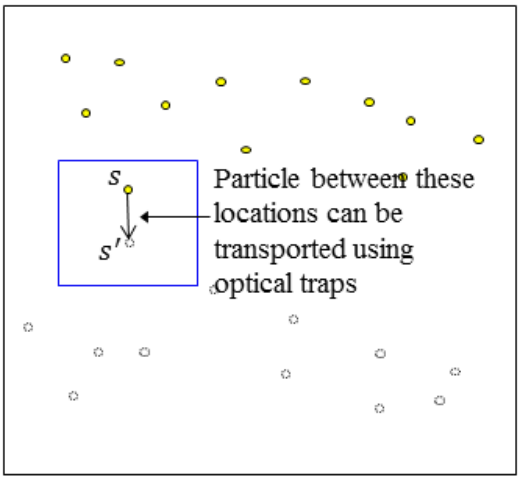

(c) *Particle transportable by only an optical trap.*

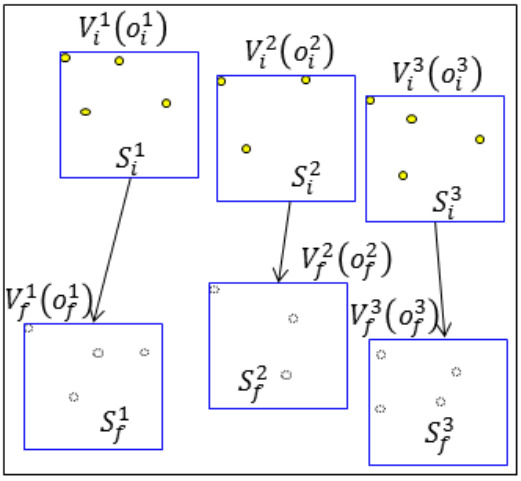

(d) *Matching OT workspaces for transporting particles with a combination of optical motion and stage motion.*

Figure 4.3: *Illustration of problem formulation*

of locations in the OT workspace. By moving the motion stage with respect to OT, the OT workspace can be located at different regions of the overall workspace. In general, the size of the OT workspace is much smaller than the overall workspace (see Figure 4.3a for an illustration).

Let P be the set of particles (assumed to be identical) that need to be transported. Let $\mathcal{S}_i$ and $\mathcal{S}_f$ be the set of initial and final locations of these particles respectively, such that $\mathcal{S}_i$, $\mathcal{S}_f \subset \mathcal{X}$ (see Figure 4.3b for an illustration).

A particle can be moved from a location s in $\mathcal{S}_i$ to location s' in $\mathcal{S}_f$ using *only* an optical trap, if there exists a location o for placing OT such that both s and s' belong to $V(o)$ (i.e., $s \in V(o)$ and $s' \in V(o)$) (see Figure 4.3c for an illustration). In general, we prefer transporting particles using only optical traps because it allows concurrent independent positioning of multiple particles. However, due to having smaller workspace, if an optical trap alone is incapable of transporting particle, then a combination of optical trap and stage motion, i.e., a hybrid strategy is used.

The first step is to find locations in $\mathcal{S}_i$ and $\mathcal{S}_f$ that can be handled by optical traps alone. This is done by finding the closest members of each $s \in \mathcal{S}_f$ in the set $\mathcal{S}_i$. If the closest members are within an OT workspace, then we assign particles at initial locations $\mathcal{S}_i$ to final locations in $\mathcal{S}_f$ using the goal assignment method described in [BCLG12]. All locations that can be handled by only optical traps are removed from $\mathcal{S}_i$ and $\mathcal{S}_f$.

The next step is to find a set of matching OT workspaces $\mathcal{V} = \{(V_i^1(o_i^1), V_f^1(o_f^1)), (V_i^2(o_i^2), V_f^2(o_f^2)), \ldots, (V_i^j(o_i^j), V_f^j(o_f^j)), \ldots\}$ that will use hybrid transport strategy (see Figure 4.3d for an illustration). $V_i^j(o_i^j)$ contains locations S_i^j (i.e., $S_i^j \subset \mathcal{S}_i$).

$V_f^j(o_f^j)$ contains locations S_f^j (i.e., $S_f^j \subset \mathcal{S}_f$). Particles from locations in S_i^j are transported to locations in S_f^j using a combination of optical traps and stage motion.

$\mathcal{V}$ is computed using a greedy heuristic. We start by placing a window of the size of the OT workspace such that the top edge of the window is aligned with the top most location in $\mathcal{S}_f$ and left edge of the window is aligned with the left most location in $\mathcal{S}_f$. If this window contains more than N locations, then we select $N-1$ closest locations of other particles to the particle location in the top-left corner where, N is the maximum number of particles that can be concurrently transported using motion stage. N is set to 4 in the setup used in this chapter. This step leads to computation of $V_f^j(o_f^j)$ and S_f^j for a matching pair j. We then find matching $V_i^j(o_i^j)$ by placing a window that is closest to $V_f^j(o_f^j)$ and contains the same number of locations as in S_f^j. If $V_i^j(o_i^j)$ does not contain enough locations to match the number of locations in S_f^j, we reduce the number of locations from S_f^j so that its cardinality matches S_i^j. Once we compute matching $V_i^j(o_i^j)$, $V_f^j(o_f^j)$, and associated S_i^j and S_f^j, locations in S_f^j and S_i^j are removed from $\mathcal{S}_f$ and $\mathcal{S}_i$, respectively. This process is repeated until $\mathcal{S}_f$ and $\mathcal{S}_i$ are empty.

The following steps are used to transport particles located at locations in S_i^j to locations in S_f^j (we drop reference to index j to simplify the notation).

(i.) Select the shape of the ensemble and its initial and final locations in the overall workspace $\mathcal{X}$.

(ii.) Plan paths for each particle at locations in S_i into the initial ensemble location.

(iii.) Transport particles into the initial ensemble location along the paths computed

in the previous step using optical trap motion.

(iv.) Compute a path for the ensemble from its initial to the final location.

(v.) Transport ensemble along the path generated in the previous step using stage motion. If one or more particles get detached from the ensemble, then stop stage motion. Compute path for the detached particle and bring it back into the ensemble.

(vi.) When the ensemble reaches its final destination, stop stage motion.

(vii.) Plan paths for the particles from their final ensemble locations to their corresponding locations in S_f.

(viii.) Transport particles into their final locations using paths computed in the previous step.

The goal is to minimize overall transport time T, where T can be defined as the following:

$$\begin{aligned} \underset{\rho_i,\rho_f}{\text{minimize}}\ T = \max(t(s_i^k, s^k(\rho_i))) + t(\rho_i, \rho_f) + \max(t(s^k(\rho_f), s_f^k)) \\ s_i^k \in S_i; s_f^k \in S_f \end{aligned} \tag{4.1}$$

Where, $t(s_i^k, s^k(\rho_i))$ is the required time to transport particle k from the initial location s_i^k to its location $s^k(\rho_i)$ in the initial ensemble formation, $t(s^k(\rho_f), s_f^k)$ is the time required to transport the particle k from its location $s^k(\rho_f)$ in the final ensemble formation to the final location s_f^k, ρ_i is the initial ensemble location, ρ_f is

the final ensemble location, S_i is the set of particles at initial locations, and S_f is the set of particles at final locations.

Section 4.3 describes our approach for selecting ensemble shape and the initial and final ensemble location. Section 4.4 describes our approach for computing paths for optical traps as well as motorized stage. This includes computing paths and identifying maximum allowable speeds. Section 4.5 describes the overall system architecture for executing the computed paths.

4.3 Selecting ensemble shape and locations

In order to create and transport ensembles, we need to determine their sizes. The following factors affect the size of an ensemble:

(i.) Ensemble should be able to fit within the available empty space. So the size of the ensemble is restricted by the obstacle region. If a large portion of space is occupied by obstacles, then the ensemble has to be small in size. In other words, the ensemble size is governed by the minimum gap available between obstacles in the workspace.

(ii.) While the stage moves, the ensemble is held together by optical traps. If optical trapping power is insufficient to hold ensemble together at higher speeds, then the stage needs to move slowly to ensure that the drag forces do not exceed the trapping force. This increases the transport time. So the ensemble size is limited by the total available laser power for the optical tweezers.

(iii.) If the number of particles in the ensemble is large, then the probability of

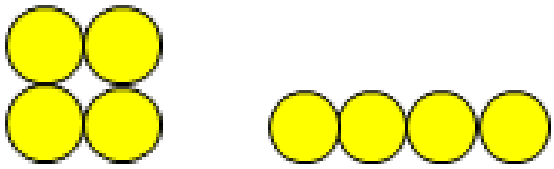

Figure 4.4: *A schematic illustration of ensemble shapes: (a) convex polygonal arrangement and (b) linear arrangement*

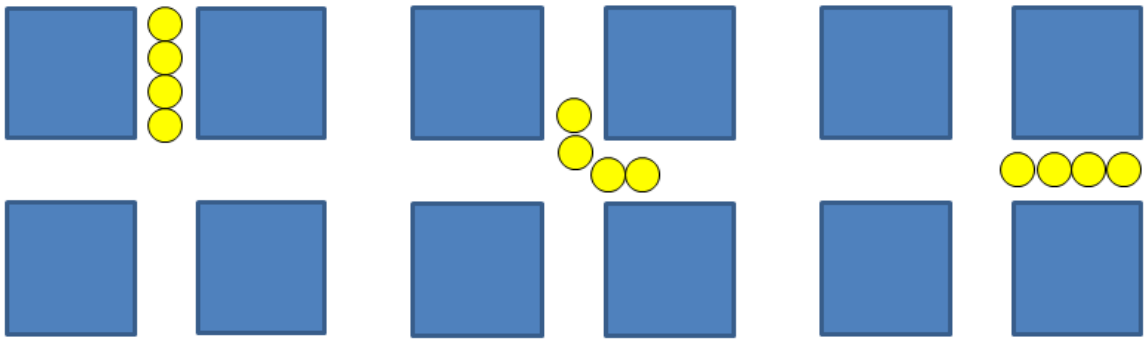

Figure 4.5: *Turning around tight corners may require relative repositioning within linear arrangements*

accidentally loosing a particle increases.

The above described factors determine the optimal ensemble size. In this chapter, we limit maximum ensemble size to 4 particles due to the narrow space available between two consecutive microNets to move it around inside the microfluidic chambers used in the experimental validation.

The next decision to be made in the planning process is about the shape of the ensemble. The following two main shapes are possible: (1) convex compact polygonal arrangement, and (2) linear arrangement. Figure 4.4 shows illustration of these shapes. Linear arrangements can navigate through narrow spaces. However, they require stopping the motion stage and optical trap rearrangements to navigate around tight corners (see Figure 4.5).

Particles in linear arrangement are more likely to dislodge from the ensemble due to drag force and Brownian stochastic forces. In this chapter, we only utilize polygon arrangements for 3 and 4 particle ensembles. For 2 particles we use linear arrangement.

Once the ensemble shape has been decided, we need to determine the ensemble locations ρ_i and ρ_f in the OT workspace. As indicated in the previous section, we select the ensemble locations by minimizing the transport time T. The main steps in our approach for this task are as following:

(i.) Let v_i be a state of the discretized OT workspace $\bar{V}_i(o_i)$ corresponding to $V_i(o_i)$. The initial state ρ_i of the ensemble will lie on this grid (see Figure 4.2b for illustration).

(ii.) For every state v_i in the grid (i.e., the candidate location of the ensemble), compute the time $t_i(v_i)$ to complete the ensemble at v_i using the Equation 4.2:

$$\begin{aligned} t_i(v_i) &= \max(t(s_i^k, s^k(v_i))) \\ s_i^k &\in S_i \end{aligned} \tag{4.2}$$

where $t(s_i^k, s^k(v_i))$ is the required time to transport the particle k from its initial state s_i^k to the state $s^k(v_i)$ in the initial ensemble formation state v_i; S_i is the set of particles at their initial states.

(iii.) Let v_f be a state in the discretized OT workspace $\bar{V}_f(o_f)$ corresponding to $V_f(o_f)$. The final state ρ_f of the ensemble will lie on this grid (see Figure 4.2d for illustration).

(iv.) For every state v_f of the grid, compute the time $t_f(v_f)$ to disassemble the ensemble at v_f using Equation 4.3:

$$t_f(v_f) = \max(t(s^k(v_f), s_f^k)) \quad s_f^k \in S_f \tag{4.3}$$

where $t(s^k(v_f), s_f^k)$ is the required time to transport the particle k from its state $s^k(v_f)$ in the final ensemble formation state v_f to its final state s_f^k; S_f is the set of particles at final states.

(v.) Determine the set of boundary states of the state-space $\bar{V}_f(o_f)$, placed on $V_f(o_f)$. Let $v_f(b)$ be an element of this set. Any path from $V_i(o_i)$ to $V_f(o_f)$ will have to pass through the boundary of $\bar{V}_f(o_f)$. We use this fact to reduce the computational complexity and we first plan a path from the states in $\bar{V}_i(o_i)$ to the boundary states of $\bar{V}_f(o_f)$.

(vi.) Compute a path from every state v_i to every state at boundary $v_f(b)$. Let $t(v_i, v_f(b))$ be the time to transport ensemble from v_i to $v_f(b)$.

(vii.) Compute a path from every boundary state $v_f(b)$ to every interior state $v_f(\iota)$. Let $t(v_f(b), v_f(\iota))$ be the time to transport the ensemble from $v_f(b)$ to $v_f(\iota)$.

(viii.) Select a state ρ_i from the state-space $\bar{V}_i(o_i)$ placed in $V_i(o_i)$ and a state ρ_f from the state-space $\bar{V}_f(o_f)$ placed in $V_f(o_f)$ such that following total time T is minimized:

$$T = t_i(v_i) + t(v_i, v_f(b)) + t(v_f(b), v_f(\iota)) + t_f(v_f) \tag{4.4}$$

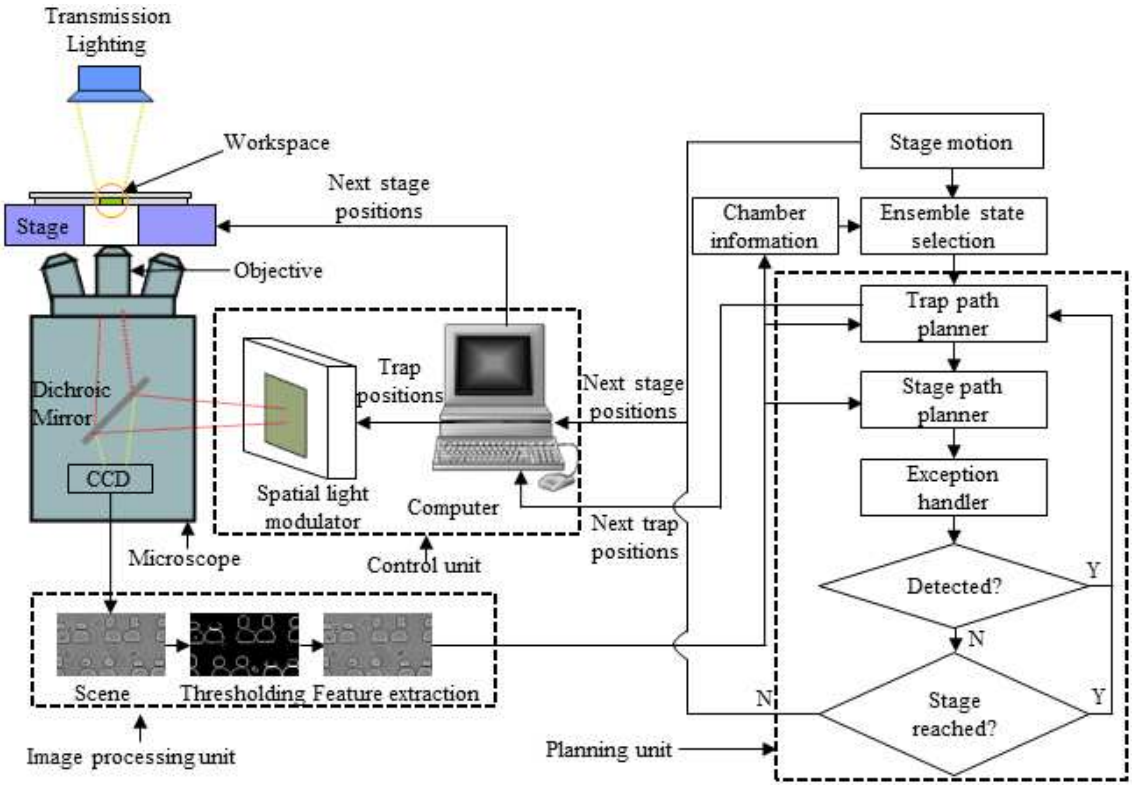

Figure 4.6: *A schematic overview of planning approach*

where ρ_i and ρ_f are selected using dynamic programming. We first compute the optimal time for the ensemble to arrive at every boundary state $v_f(b)$. Then, we compute the optimal arrival time for the ensemble at every interior state $v_f(\iota)$. Finally, by accounting for the disassembly time for the ensemble at every interior state, we find the optimal ensemble final state ρ_f. Tracing the path back, we identify the optimal boundary state, and the optimal ensemble start state ρ_i.

4.4 Path planning

The overall operation envisioned in this chapter (see Figure 4.6) starts with the motorized stage that scans the entire microfluidic chamber and comes back to

the initial location. During the operation, the image processing unit identifies the microNets with unacceptable number of particles. The *ensemble state selection* algorithm (see Sections 4.2 and 4.3) divides the overall task into multiple transport tasks based on the constraints of the OT workspace. The planner is responsible to finish each single transport task. The overall planning is divided into three steps: (a) transporting the individual particle to its desired state in the ensemble using *trap path planning*, (b) transporting the ensemble towards the final ensemble state using *stage path planning*, and (c) transporting the individual particle from its state in the final ensemble formation to the final microNet location using *trap path planning*. Sometimes, the particles may get dislodged from the ensemble while transporting with stage motion. The *exception handler* identifies the breaking ensemble formation, stops passing the stage positions, and passes the control to the *trap path planning* to bring the particles back to the formation. After reaching the final ensemble state, the *trap path planning* is used to move all the particles to the final microNet locations from the final ensemble state. We use discretized OT workspace $\bar{V}(o)$ for *trap path planning* and discretized overall workspace $\bar{\mathcal{X}}$ for *stage path planning*.

A path planning problem can be defined as follows. Given, (1) the initial state $v_{init} = [x_i, y_i]^T$ of a particle represented by the initial particle location in $\bar{V}(o)$ or ensemble location in $\bar{\mathcal{X}}$, (2) its goal state $v_{goal} = [x_g, y_g]^T$ represented by the final location of the particle in $\bar{V}(o)$ or ensemble location in $\bar{\mathcal{X}}$, (3) static and dynamic obstacles $\{\Omega_i\}_{i=1}^{l}$ represented either as microNets or other moving particles, compute a collision-free path τ for the laser trap or the stage to transport the particle or the

Figure 4.7: *Optical tweezers setup with motorized stage*

ensemble to its goal state v_{goal}.

Due to the dynamically changing environment of the microfluidic chamber under the influence of fluid flow and Brownian motion of particles, the required paths for the particles must be frequently replanned. The planning time δt_p is limited by the controller update rate and image processing time δt_g. The controller frequency of the OT system used for this chapter is 15 Hz that limits the allowable processing time $\delta t_c = 66$ ms. The total computation time in combination with δt_g and δt_p must be less than δt_c to maintain continuous operation.

We adopt the D* Lite[KL02] based graph search algorithm as described in [CSW+13] for this chapter. The algorithm incrementally expands the states from the goal state v_{goal} to the initial state v_{init} in a fashion similar to the backward version of A* algorithm [HNR68]. All the remaining particles and the microNets

other than the target particles in the workspace are regarded as obstacles during the computation of the collision-free path τ.

A heuristic function is used that guides the search in order to increase the planning efficiency. The planner maintains an open set Θ containing the states that are more likely to be expanded next based on their cost during the search throughout the planning horizon. Thus, the planner is able to reuse the history of the search from the previous planning time interval during replanning. If the cost of a state node is changed due to the change in workspace, the planner only updates Θ by inserting the state with the changed cost. A new path is computed by expanding the node with the minimum cost from Θ. Hence, the planner does not need to focus on the entire search space that decreases the planning time δt_p significantly. This allows the controller to efficiently launch multiple plans corresponding to multiple traps in order to transport multiple particles simultaneously. The algorithm terminates when each particle reaches its goal state v_{goal}.

4.4.1 Trap Path Planning

We define a state of a particle using $v^{\mathfrak{t}} = [x^{\mathfrak{t}}, y^{\mathfrak{t}}]^T \in \bar{V}(o)$ where $[x^{\mathfrak{t}}, y^{\mathfrak{t}}]^T$ denotes the position of a particle at a discrete time step $\mathfrak{t}$.

We define a control action set $U_{tr} = \{u^{\mathfrak{t}}_{tr,1}, u^{\mathfrak{t}}_{tr,2}, \ldots, u^{\mathfrak{t}}_{tr,8}\}$ that consists of eight linear translation actions $u^{\mathfrak{t}}_{tr,i}$ available for the execution at a given time step $\mathfrak{t}$. All linear actions can be represented as follows.

$$u^{\mathfrak{t}}_{tr}\left(\delta x^{\mathfrak{t}}, \delta y^{\mathfrak{t}}\right) = \begin{bmatrix} \delta x^{\mathfrak{t}} \\ \\ \delta y^{\mathfrak{t}} \end{bmatrix} \tag{4.5}$$

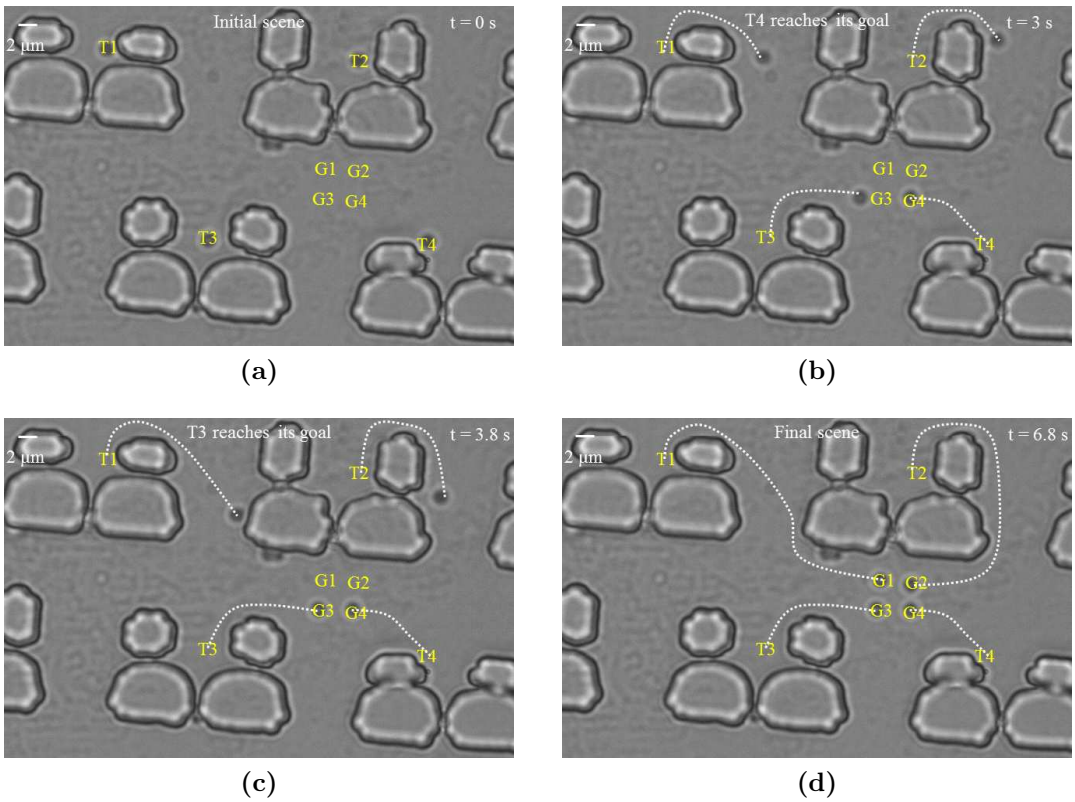

Figure 4.8: *Transport of 2 μm beads to their corresponding goal locations inside the ensemble formation using trap motion: (a) initial scene, (b) particle "T4" reaches to its goal location denoted by "G4", (c) particle "T3" reaches its goal at "G3", and (d) all the particles reach their respective goal locations in the final scene*

where δx and δy are the linear action lengths along X and Y axis, respectively. For trap motion, the action length is selected to be $\delta x = \delta x_{tr}$ and $\delta y = \delta y_{tr}$.

When the optical trap executes an action $u_{tr}^{\mathfrak{t}}$ at the time step $\mathfrak{t}$, it transitions from $v^{\mathfrak{t}}$ to $v^{\mathfrak{t}+1}$ using Equation 4.6.

$$v^{\mathfrak{t}+1} = v^{\mathfrak{t}} + u_{tr}^{\mathfrak{t}} \tag{4.6}$$

We use the cost function defined in [CSW+13] for the planner to consider the fluid flow inside the chamber. This allows to reduce the probability of the particles being dislodged from the traps during the transport operation.

4.4.2 Stage Path Planning

The microNets in the microfluidic chamber are arranged in a rectangular array (see Figure 4.1). We want to compute a path for stage that has minimum turn to avoid continuous readjustment of the particles inside the ensemble (see Figure 4.2c). Hence, we define a control action set consisting of four linear action for the stage. The control action set for the stage $U_s = \{u_N^{\mathfrak{t}}, u_S^{\mathfrak{t}}, u_E^{\mathfrak{t}}, u_W^{\mathfrak{t}}\}$ consists of four linear actions (e.g., north, south, east, and west) that can be represented similarly as in Equation 4.5. The control action length for the stage is selected as $\delta x = \delta x_s$ and $\delta y = \delta y_s$. The state transition is represented by Equation 4.6. We only consider static microNet obstacles for stage planning with the reasonable assumption that the occasionally moving particles will not be able to break the ensemble formation of multiple particles trapped closely using multiple traps. In the worst case, if the formation breaks by sudden fluctuation in the fluid flow the *trap path planning* is invoked to move the particles back into the ensemble formation and continue the

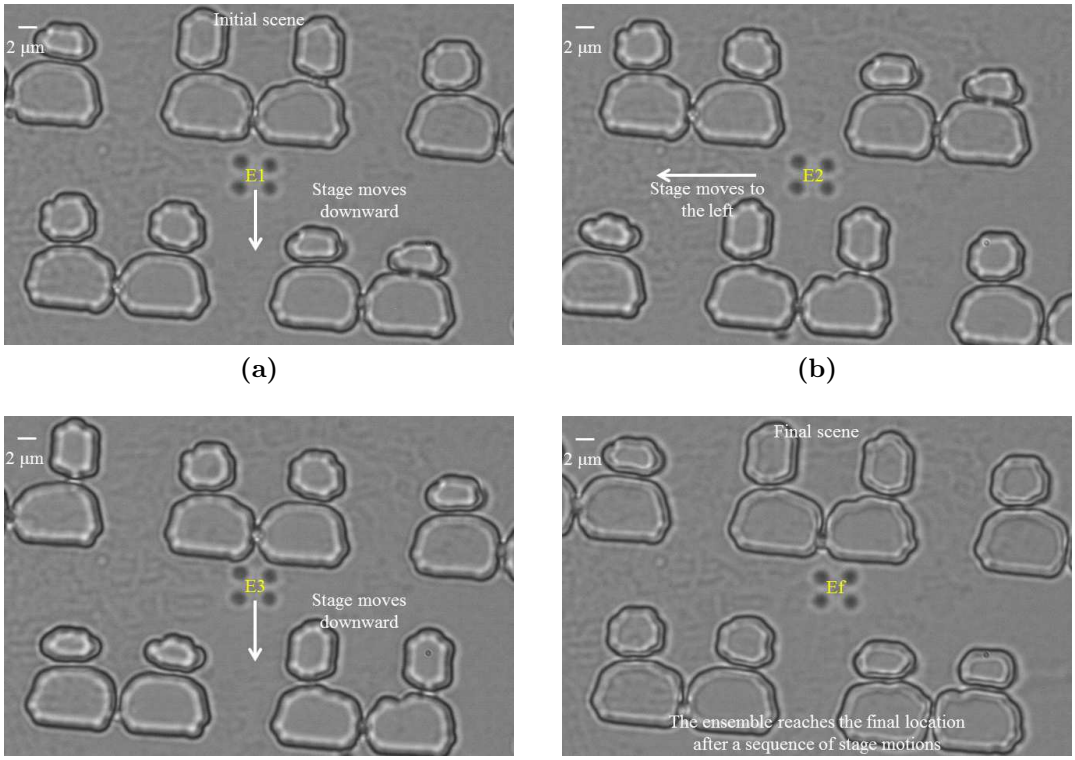

Figure 4.9: *Transport of the ensemble from an initial location to a final location using stage motion: (a) initial scene with the stage position denoted by "E1", (b) the stage moves downward to transport the ensemble to a location at "E2", (c) the stage moves towards left to transport the ensemble to "E3", and (d) the ensemble reaches to its final location at "Ef" after a sequence of stage motions*

stage motion. The cost function $c(v_s)$ for the stage path planner is designed to minimize the transport time as shown in Equation 4.7.

$$c(v_s) = \frac{L}{\mathfrak{v}_s} \tag{4.7}$$

Here, $v_s \in \bar{\mathcal{X}}$ is the state of the stage, L is the linear displacement resulting from the execution of an action u_s, and $\mathfrak{v}_s$ is the operating speed of the stage.

4.4.3 Modeling of Speed Constraints Based on the Trapping Force Considerations

The allowable speeds of the stage and the traps are limited by the corresponding controller frequency (see Section 4.5). The dynamics of a particle moving under the actuation of the optical trap can be described by the following Equation 4.8 [HS11].

$$m\ddot{\mathsf{x}} = F_{tr} - F_d \tag{4.8}$$

Here, m is the mass of the particle, x is the position of the optically trapped particle such that $\mathsf{x} \in \mathcal{X}$, F_{tr} is the trapping force which is a function of incident laser power and index of refraction of the suspending medium, and F_d is the viscous drag force which represents the resistance of surrounding fluid medium. The inertia force $m\ddot{\mathsf{x}}$ can be neglected for low Reynold's number[HS11]. F_{tr} can be modeled as a spring force for trapping a spherical particle lying within a distance less than or equal to its radius from the focal point (see Equation 4.9).

$$F_{tr} = k_{tr}(\mathsf{x}_f - \mathsf{x}), ||\mathsf{x}_f - \mathsf{x}|| < r_0 \tag{4.9}$$

Here, k_{tr} is the trap stiffness and $\mathsf{x}_f \in \mathcal{X}$ is the position of the laser focus. r_0 can be estimated as the radius r of the particle. F_{tr} is the maximum at $r_0 = r$. We compute the stiffness of the trap using ray-tracing approach described in [BCGV12]. Viscous drag force F_d can be calculated using Stoke's law as given by Equation 4.10.

$$F_d = 6\pi\eta r\mathfrak{v}_{tr} \tag{4.10}$$

Here, η is the dynamic viscosity of the surrounding medium and $\mathfrak{v}_{tr}$ is the optical trap speed. The maximum trap speed can be determined corresponding to maximum F_{tr} from Equation 4.8. For a spherical particle of 2 µm diameter trapped in an aqueous medium with a trap stiffness of 1.5×10^{-5} N/m corresponding to 20 mW laser power at the objective lens, the maximum trap speed can be calculated as 795 µm/s. However, the allowable trap speed is dependent on the controller update frequency. For optical trap planner, the trap speed is limited by the SLM update frequency (see Section 4.5). In our calibrated holographic optical tweezers system, the SLM update rate is 15 Hz. Hence, the maximum allowable trap speed is limited to 15 µm/s corresponding to $||\mathsf{x}_f - \mathsf{x}|| = 1$ µm. In case of multiple laser traps, the laser power is significantly reduced due to the formation of stray laser by SLM. Hence, the maximum allowable trap speed is further reduced to around 7 µm/s for our system. On the other hand, in case of stage motion the trap position remains fixed. The transport is executed by the movement of stage which has a resolution of 40 nm (much lower than r_0) and the controller frequency is 6 MHz. Hence, we can safely operate the stage at 795 µm/s without losing the particles from traps.

4.5 System architecture

A schematic of the microfluidic chamber used in this chapter is shown in Figure 4.1. A digitally controlled microfluidic syringe pump (SP230iW syringe pump manufactured by World Precision Instruments, Inc., Sarasota, FL) is used to inject particles into the chamber through one of its three inlets. The particle solution gets divided into six different channels before entering the rectangular microNet

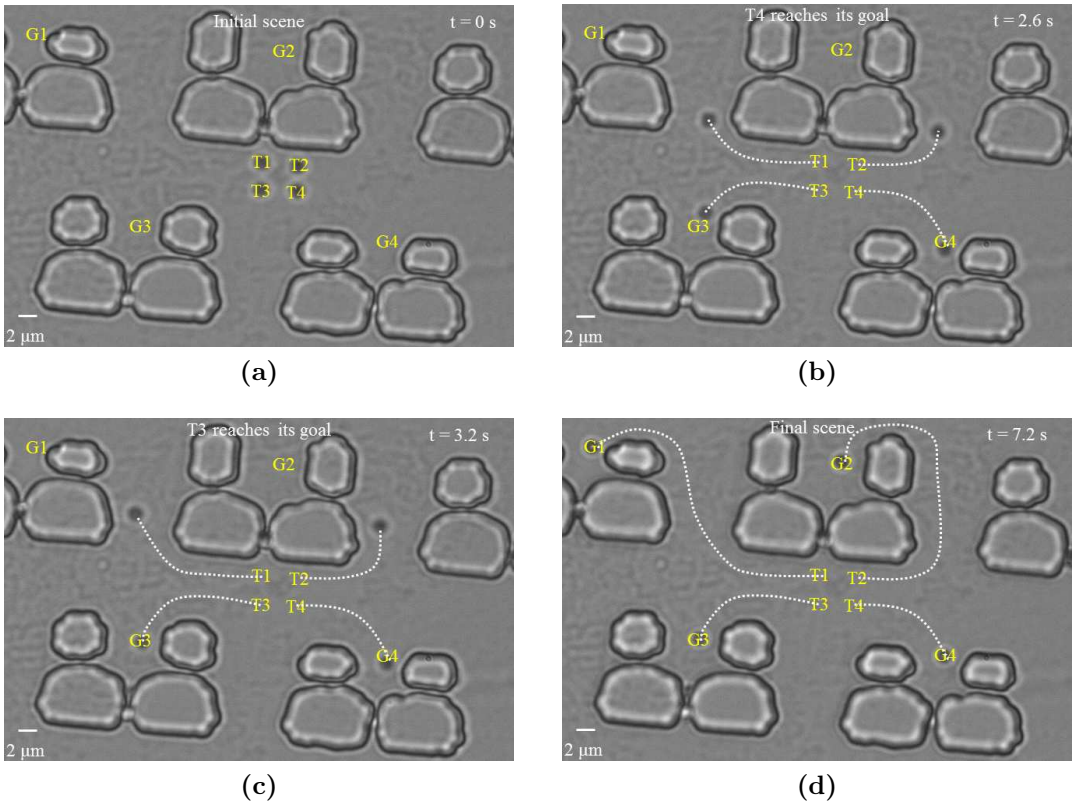

Figure 4.10: *Distribution of particles to their corresponding microNet locations: (a)initial scene with the particles arranged at their final ensemble formation, (b) particle "T4" reaches to its microNet location denoted by "G4", (c) particle "T3" reaches its microNet location at "G3", and (d) all the particles get distributed to their final microNet locations in the final scene*

region in order to uniformly distribute the particles. The particles are captured inside different microNets as they flow through the microNet region. The actual dimension of the microNet region is 3.77 mm × 2.36 mm and consists of 9432 nets. The height of the device is 10 µm to prevent stacking of the particles. OT can only operate in a limited space of 56 µm × 37 µm × 10 µm that consists of only four microNets. Hence, we have to utilize motorized stage to carry out long distance particle transport. The cleaning operation starts from the lower left corner of the rectangular microNet region (see Figure 4.1).

We demonstrate the usefulness of the developed planner using BioRyx 200

(Arryx, Inc., Chicago, IL) holographic laser tweezer as shown in Figure 4.7. The BioRyx 200 consists of a Nikon Eclipse TE 200 inverted microscope, a Spectra-Physics Nd-YAG laser (emitting green light of wavelength of 532 nm with 2 watts at the source), a spatial light modulator (SLM), and proprietary phase mask generation software running on a desktop PC. Nikon Plan Apo $60x/1.4$ NA, DIC H oil-immersion objective is used for laser magnification. The maximum rate at which traps can be set is limited by the update rate of the SLM, which in our case is 15 Hz. The sample holder is placed on a Proscan H107 motorized stage which can move the sample in $X - Y$ with respect to the microscope objective. The stage is equipped with a Proscan H29XYZ controller which can be connected to a PC using a RS 232 serial port connector. The controller can move the stage with the resolution of 40 nm. The stage is capable of moving in a 112 mm $\times$ 70 mm rectangular area. The controller frequency is 6 MHz.

4.6 Results

We performed 20 simulation runs to test the computational complexity of our greedy heuristic approach in determining the initial ρ_i and final state ρ_f of the ensemble. We discretized both the initial and final OT workspace with a 100×100 grids. We chose $N = 4$ to determine the matching OT workspaces for our simulation runs. The simulation was conducted on an Intel(R)Core(TM)i7-2600 CPU. The clock speed is 3.4 GHz with a RAM of 8 GB. We implemented the planning algorithm in MATLAB. Our greedy heuristic method is able to determine the optimal states for initial and final ensemble formations that minimize the overall transport time 23

times faster on an average compared to the time taken by exhaustive combinatorial search.

We demonstrate three different features of our planning approach with physical experiments. We use 10 mW laser power at the objective lens for the experiment. Laser power higher than 10 mW produces bubbles inside microfludic chamber that destabilize the fluid flow. We use a constant trap speed of 5 µm/s and stage speed of 200 µm/s through out the experiment. Hence stage motion provides 40 times faster transport operation compared to the trap motion.

Figure 4.8 shows the trap motion to transport the microparticles to the initial ensemble location. The *trap path planning* unit computes four collision free paths corresponding to four microparticles for transporting them to the locations in the initial cell-ensemble. During the transport the planner continuously replan the paths to avoid other microparticles dynamically moving around. The target particles are denoted by "T" and corresponding goal locations in the ensemble formation are denoted by "G". The paths of the particles are shown by white dotted lines in the figure. The total time taken by the traps is shown upper right corner of the figure. The particles successfully reach their respective goal locations in about 7 s. (corresponding to the associated number in Figure 4.8).

Figure 4.9 demonstrates a sequence of automated stage motions to transport an ensemble from its initial to its final location. Stage locations are denoted by "E" in the figure. The direction of the stage motion is shown using white "→" in the figure. The stage exhibits a zigzag motion due to the action set selection as described in Section 4.4.2. The stage successfully transports the ensemble to its

final location denoted by "Ef" with a high speed of 200 µm/s.

Figure 4.10 shows the transport of 4 microparticles from the locations in the final cell-ensemble to the corresponding microNet locations with trap motions. The particles inside the ensemble are denoted by "T" and final microNet locations are denoted by "G". The total time taken by the traps to transport the particles is shown in upper right corner of the figure. The *trap path planning* is able to compute collision-free paths for the particles in a scene with randomly moving microparticles. All the particles successfully get distributed to their respective microNet locations in about 7 s. It shows the advantage of the trap motion over the stage motion. The trap motion provides total control over the transport by handling all the dynamic and static obstacles in the scene.

4.7 Summary

Microfluidics has gained acceptance as a medium-scale manipulation technique to transport biological objects over larger distances. In order to increase the precision of manipulation, they need to be integrated with other devices such as optical tweezers. However, the limitation of a small workspace makes OT unsuitable for long distance transport operations.

In this chapter, we have utilized a motorized stage for fast shifting of OT workspace to facilitate controlled transport of cells over large distances inside a microfluidic chamber. We have developed an automated manipulation approach that combines the operation of the optical trap and the stage. Our developed planner automatically computes collision-free paths to transport the cells using optical trap

motions to suitable locations to form a cell-ensemble, computes a suitable path to transport the cell-ensemble to a final ensemble location using the stage, and finally computes collision-free paths to disassemble the cell-ensemble by distributing the cells to their final goal locations.

We have developed a greedy heuristic approach for efficient computation of initial and final cell-ensemble locations that will minimize the overall transport time. We have modeled the cell motion within the trap to determine the maximum allowable speeds for the optical trap and the stage.

We have demonstrated the usefulness of the approach using our OT-assisted microfluidic chamber setup by transporting 2 µm particles over a large distance. In the experiments, the shape of the ensemble was determined based on the available space inside the microfluidic chamber. This allowed us to transport the ensemble without any rearrangement of the particles.

The developed approach for fast cell transport is suitable for conducting biological experiments that need to be properly timed to exhibit desired motility. In future, the planner can be improved for concurrent movement of optical trap and stage that will enable us to transport different ensemble configurations in narrow spaces.

Chapter 5
Robust Gripper Synthesis for Indirect Manipulation of Cells using Optical Tweezers

This chapter[4] presents a robust gripper synthesis technique for indirect manipulation of cells using optical tweezers. Optical Tweezers (OT) are used for highly accurate manipulations of cells. However, the direct exposure of cells to focused laser beam may cause significant damage to their structures. In order to ameliorate this problem, we generate multiple optical traps to grab and move $3D$ ensembles of inert particles such as silica microspheres to act as a reconfigurable gripper for a manipulated cell. The relative positions of the microspheres are important in order for the gripper to be robust against external environmental forces and the exposure of high intensity laser on the cell was minimized. In this chapter, we present results of different gripper configurations, experimentally tested using our OT setup, that provide robust gripping as well as minimize laser intensity experienced by the cell. In order to construct the configurations, we developed a preliminary computational approach for gripper arrangement modeling and synthesis. The overall synthesis problem is cast as a multi-objective optimization problem that is solved in order to get a Pareto front of non-dominated solutions.

5.1 Introduction

Cell manipulation (cell localization, transportation, sorting, characterization etc.) is crucial in many emerging medical and biological applications. The ability

[4] The work in this chapter is derived from the published work in [CSW+12].

to efficient and accurate manipulation of individual cells will enable researchers to conduct basic research at the cellular scale. Optical Tweezers (OT) that can grasp and move microscale and nanoscale biological objects using focused light provide a highly accurate and minimally invasive method of micro and nano-manipulation. A strongly focused laser beam is used to exert an optical gradient and scattering forces on an object, which results in creating a stable trap [Ash92] near the focal point. Objects are transported in workspace by moving the laser beam and are released from the trap by simply switching off the laser (see Figure 5.1). Due to the non-contact nature, OT is successfully used in various types of manipulations [SB94] of biological objects, e.g., for orienting, stretching, moving, etc. Holographic Optical Tweezers (HOT) is able to generate a large number of traps allowing simultaneous manipulation of multiple objects in three dimensions.

However, due to the extreme focus of the laser beam to a small region, considerable photodamage can be inflicted on trapped cells, possibly causing death of the cells as noted by Ashkin [ADY87]. The underlying mechanism of photodamage has been proposed to be due to the creation of reactive chemical species [SB94], local heating [LSBT96], two-photon absorption [KLBT95] and singlet oxygen through the excitation of a photosensitizer [NCL$^+$99]. Rasmussen, using the internal pH as a measure of viability, found that the internal pH of both E. coli and Listeria bacteria declined at laser intensities as low as 6 mW [ROS08]. Using the rotation rate of the E. coli flagella motor [NCL$^+$99], it was found that 830 nm and 970 nm laser wavelengths were significantly less harmful to cells, and that the region from 870 nm to 910 nm was particularly harmful.

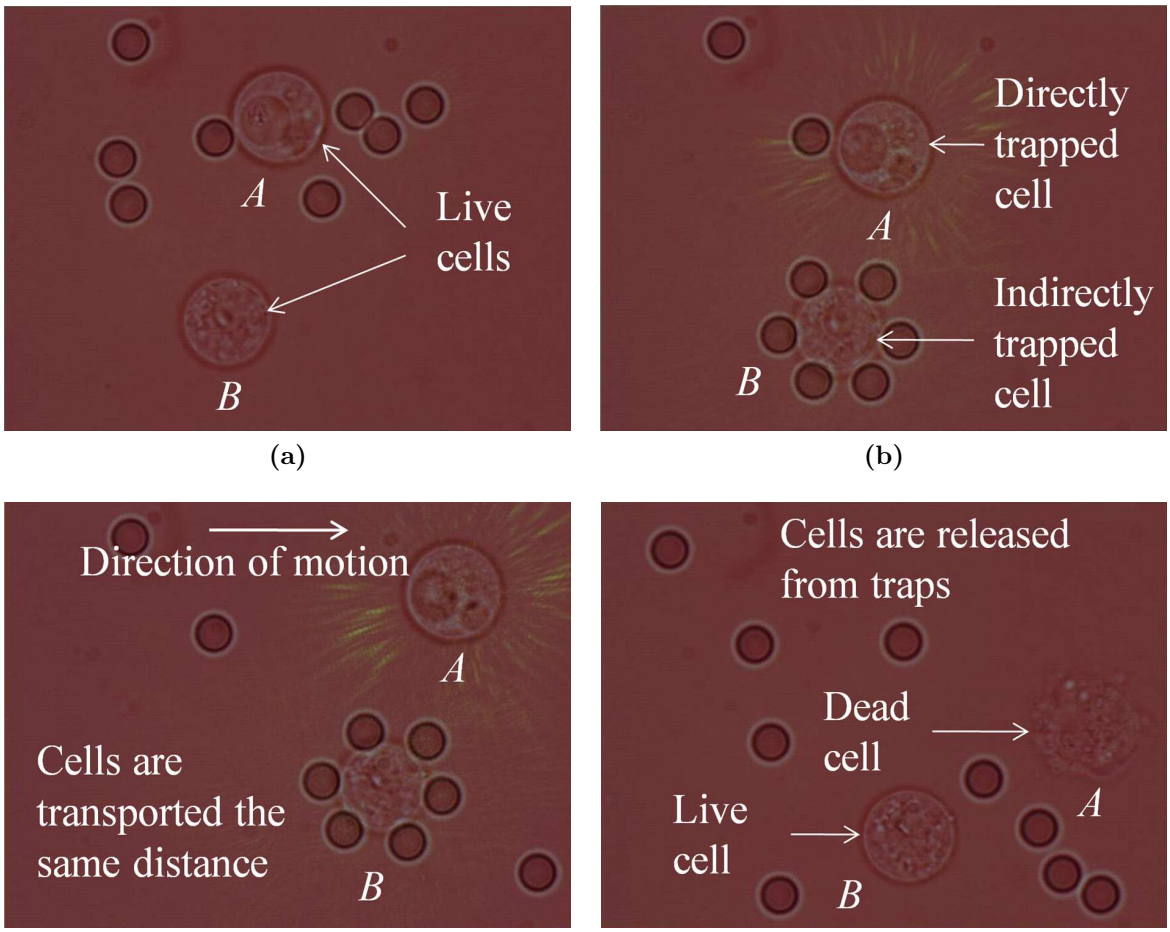

(a) **(b)** **(c)** **(d)**

Figure 5.1: *Direct vs. indirect manipulation using OT: (a) solution of Dictyostelium discoideum cell and inert silica microspheres, (b) the cell A is trapped directly, while the cell B is trapped indirectly using a synthesized gripper ($t = 0$ s), (c) the cells are being transported to their goal locations ($t = 12$ s), and (d) the cells are released at the goal locations; the cell A that was directly trapped is dead, while the indirectly manipulated cell B is still alive ($t = 15$ s)*

Cell damage can be reduced by using less laser power which results in less intensity experienced by the trapped cells. Although, the trap stability of OT can be enhanced by utilizing feedback control [HZM09, WOHT08], this still would not be sufficient for robust manipulation of many sensitive cells. Hence, rather than reducing the damage exerted by optical manipulation on cells by minimizing the intensity of the laser beam (which would weaken manipulation capabilities of OT) or optimizing laser wavelength (which would require intensive calibration due to the need to have a different optimal wavelength for each cell line), in our approach, we indirectly trap [BCLG11] and manipulate cells using grippers composed from inert microspheres (i.e., silica beads; see Figure 5.1).

We utilize HOT device which is capable of generating multiple, independently movable focused optical traps for 3D positioning of silica beads around a biological object. HOT utilizes Gaussian beam that has a maximum intensity at the focal point. The intensity drops exponentially with the increase of distance from the focal point. Thus, by placing the inert beads into safe distances from the manipulated cell, the cell can avoid the maximum intensity of the laser, while still being robustly held by the ensemble of beads.

In this chapter, we present three synthesized gripper configurations that were tested experimentally using our HOT setup. The configurations provide robust gripping as well as impose the least possible intensity of the laser beam on the manipulated cell. We developed a preliminary computational approach for gripper arrangement modeling and synthesis. The overall synthesis problem is cast as a multi-objective optimization problem that is solved in order to get a Pareto front

of non-dominated solutions. The robustness of the gripper is characterized by the maximum velocity using which the ensemble can be moved in XY plane without effecting the stability of cell transfer. To the best of our knowledge, this is the first successful demonstration of a gripper that is able to reliably transport another object using HOT.

5.2 Gripper synthesis problem formulation

We model the biological object that needs to be manipulated as a sphere to resemble the shape of a single yeast cell. Although cells are deformable in nature, we do not want to squeeze them with the gripper. That is why the cell is modeled as a rigid object so that the gripper objects are always placed at a safe distance. The gripper consists of six spherical silica beads of the same size as the cell to be indirectly manipulated. With more than six beads, the gripper might get unstable due to weaker traps (the laser beam needs to be split for creating multiple traps). The contact between a silica bead and the manipulated sphere is modeled as a point contact without friction. Friction is not a dominating force in microscale and thus can be neglected. Even if a small friction force exists, that can only improve gripping. Each bead has three degrees of freedom (DOFs) so that it can be positioned in any location around the object. We are only interested in eliminating undesirable translational motions of the gripped object. Hence, the object can rotate inside the gripper. Therefore, we are looking to achieve 3D relative form closure for the manipulated object by suitable placement of the gripper beads [ZD07].

Every position of a point lying in 3D space can be represented by its spherical

coordinates defined as the radial distance r, azimuthal angle θ, and polar angle ϕ. Hence, a gripper configuration can be defined as $G = [r_1, \theta_1, \phi_1, r_2, \theta_2, \phi_2, r_3, \theta_3, \phi_3, r_4, \theta_4, \phi_4, r_5, \theta_5, \phi_5, r_6, \theta_6, \phi_6]$. Each triplet in the gripper configuration represents the actual position of a silica bead in Cartesian coordinates defined as $P_i = [r_i \cos\theta_i \sin\phi_i, r_i \sin\theta_i \sin\phi_i, r_i \cos\phi_i]$. Here, the radial distance r_i is the distance of the point P_i from the centroid of the object. The overall synthesis problem is to determine the best gripper configuration G_{opt} that will provide robust gripping based on frictionless contacts, as well as minimize the intensity of the laser beam experienced by the object to be manipulated.

5.3 Optimization functions and constraints

Since we are modeling frictionless point contacts between a gripper and the manipulated object, we have to satisfy the form closure properties. Moreover, we want to ensure the best quality of the resulting gripper in terms of its stability and the intensity of the laser beam imposed on the object. Let C_i be a contact point on the object and N_i be the inward normal vector defined at C_i (see Figure 5.2), then the contact wrench at C_i is defined by Equation 5.1

$$g_i = \begin{pmatrix} N_i \\ \\ N_i \times R_i \end{pmatrix} \tag{5.1}$$

Here, R_i is the position vector for C_i in the global coordinate system. The wrench has 6 components for an object in 3D. By placing the origin to the center of the sphere (X', Y', and Z' as shown in Figure 5.2), the wrench space can be

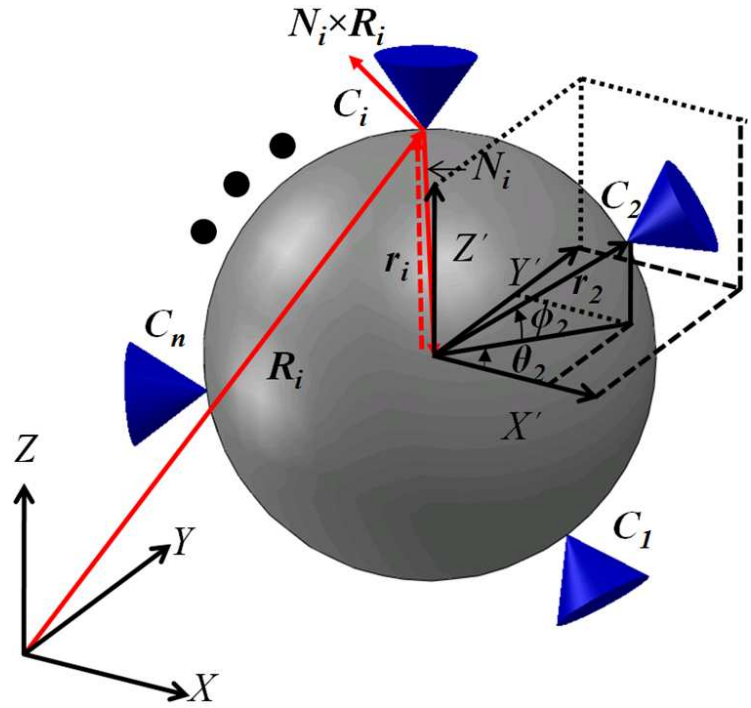

Figure 5.2: *Manipulated object and contact positions of the gripper beads*

reduced to 3. Since we consider only the translational motion, we ignore the torque component in the wrench. All the wrenches can be combined to get grasp matrix $\mathcal{G} = \{g_1, g_2, g_3, \ldots, g_6\} \in \Re^{3\times 6}$ of an 6-point gripper. As stated in [Mas01], a grasp can achieve form closure if the grasp matrix positively span all over the wrench space. The statement comes with the following theorems:

- A set of vectors $\{v_i\}$ positively spans the entire space $\Re^n$ if and only if the origin lies in the interior of the convex hull: $pos(\{v_i\}) = \Re^n \leftrightarrow 0 \in (conv(\{v_i\}))$.

- It takes at least $n + 1$ vectors to positively span $\Re^n$. If the span of $n + 1$ vectors have dimension n, then, there is a set of n coordinates on which they are linearly independent i.e., the rank of the grasp matrix is n.

  The above two theorems necessarily state that the rank of the grasp matrix

must be at least 3 to be able to achieve 3D relative form closure. Furthermore, the number of beads in the gripper must be greater or equal to 4. In our case, the additional two beads help to divide the laser power and thus the maximum intensity of each laser trap will be decreased. Moreover, the additional beads will give more stability to the gripper during transport by covering the periphery of the cell. We used the volume of convex hull of the grasp matrix to measure the quality of the grasp [RSC08]. The more the volume of the convex hull, the more stable the gripping is.

We used the grasp quality measurement as one of the objectives and the form closure properties as one of the constraints for the defined multi-objective optimization problem. Another constraint comes from the geometry of the gripper. The spherical components of the gripper should not intersect each other. Hence, the distance d between two gripper components should be greater than or equal to the diameter of the gripper component i.e., $d \geq 2r_g$, where r_g is the radius of the component. The second objective concerns the intensity experienced by the object due to the gripper configuration. Hence, the objectives can be summarized as follows:

i. maximize the volume of the resulting convex hull of the grasp matrix, and

ii. minimize the intensity of the laser beam imposed on the gripped object,

subjected to the following constraints:

i. the rank of the grasp matrix must be 3 to satisfy the form closure properties, and

ii. the gripper objects must not intersect each other.

To calculate the intensity experienced by the gripped object, the laser beam resulting from positioning the optical trap is modeled as a converging-diverging cone (see Figure 5.3). The half angle α of the cone is calculated using Equation 5.2

$$\alpha = sin^{-1}\left(\frac{NA}{n}\right) \tag{5.2}$$

Here, NA is the numerical aperture of the objective lens and n is the refractive index of the immersion oil. We sample the gripped object uniformly and identify the samples that belong to the region intersected by the optical cones (see Figure 5.3). The intensity of each sample point is calculated using the equations given in [ST01] and summed to get the total intensity of the gripped object.

To optimize the positions of the beads around the object, we utilized multi-objective Genetic Algorithm (GA) [Deb01] as an optimization technique that is robust in respect to local minimums.

5.4 Results

5.4.1 Experimental setup

Figure 5.4 shows our HOT-based cell manipulation system. The HOT used in these experiments was a BioRyx 200 (Arryx,Inc., Chicago, IL) HOT. The BioRyx 200 consists of a Nikon Eclipse TE 200 inverted microscope, a Spectra-Physics Nd-YAG laser (emitting green light of wavelength of 532 nm with 2 watts), a spatial light modulator (SLM), and proprietary phase mask generation software running on a desktop PC. The microscopic field of view is about 71 µm × 53 µm. Nikon Plan

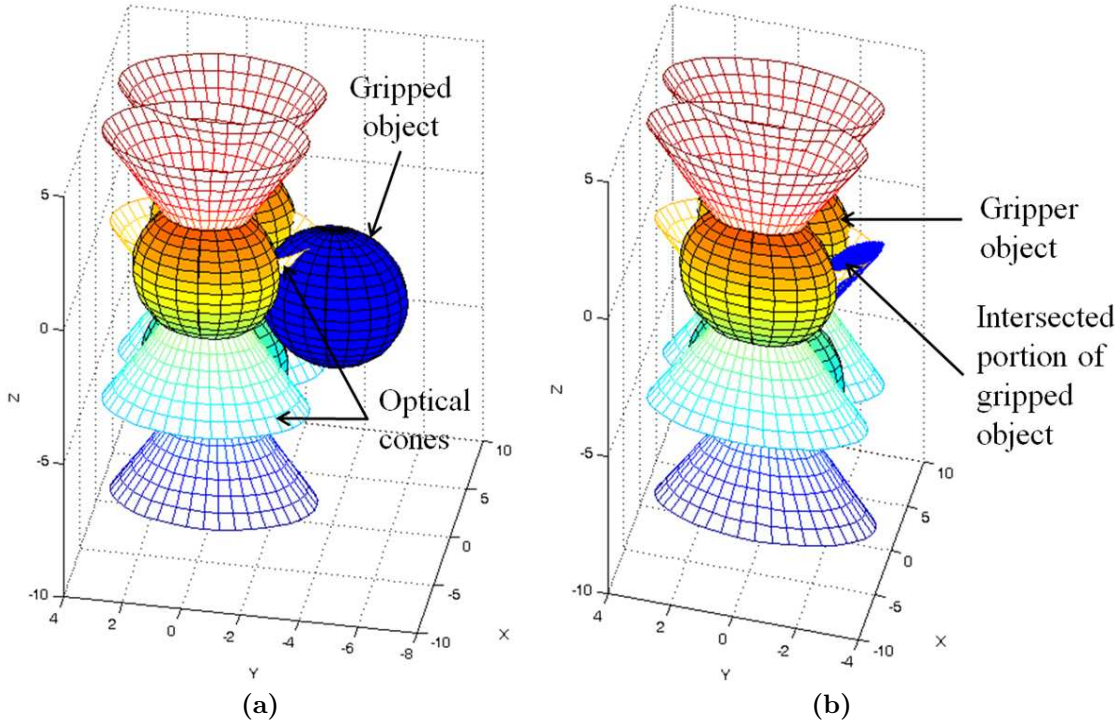

Figure 5.3: *Intensity calculation of the laser beam imposed on the gripped object: (a) partial view of the gripper and the object and (b) partial view of an intersected portion of the target object by optical cones*

Apo $60x/1.4$ NA, DIC H oil-immersion objective is used. Using the Graphical User Interface (GUI), the ensemble is moved along XY plane. The SLM gets the input from the GUI and updates the trap positions to move the ensemble. The maximum rate at which traps can be set is limited by the update rate of the SLM, which in our case is 15 Hz. The gripper is formed by using six point traps through SLM. Each of them traps one 5 µm silica bead and is able to move in the microscopic field of view or up to 10 µm above or below the focal plane of the microscope. Microbead solution is prepared by diluting 5 µl original silica microspheres solution (Microsil) with 1000 µl of distilled water.

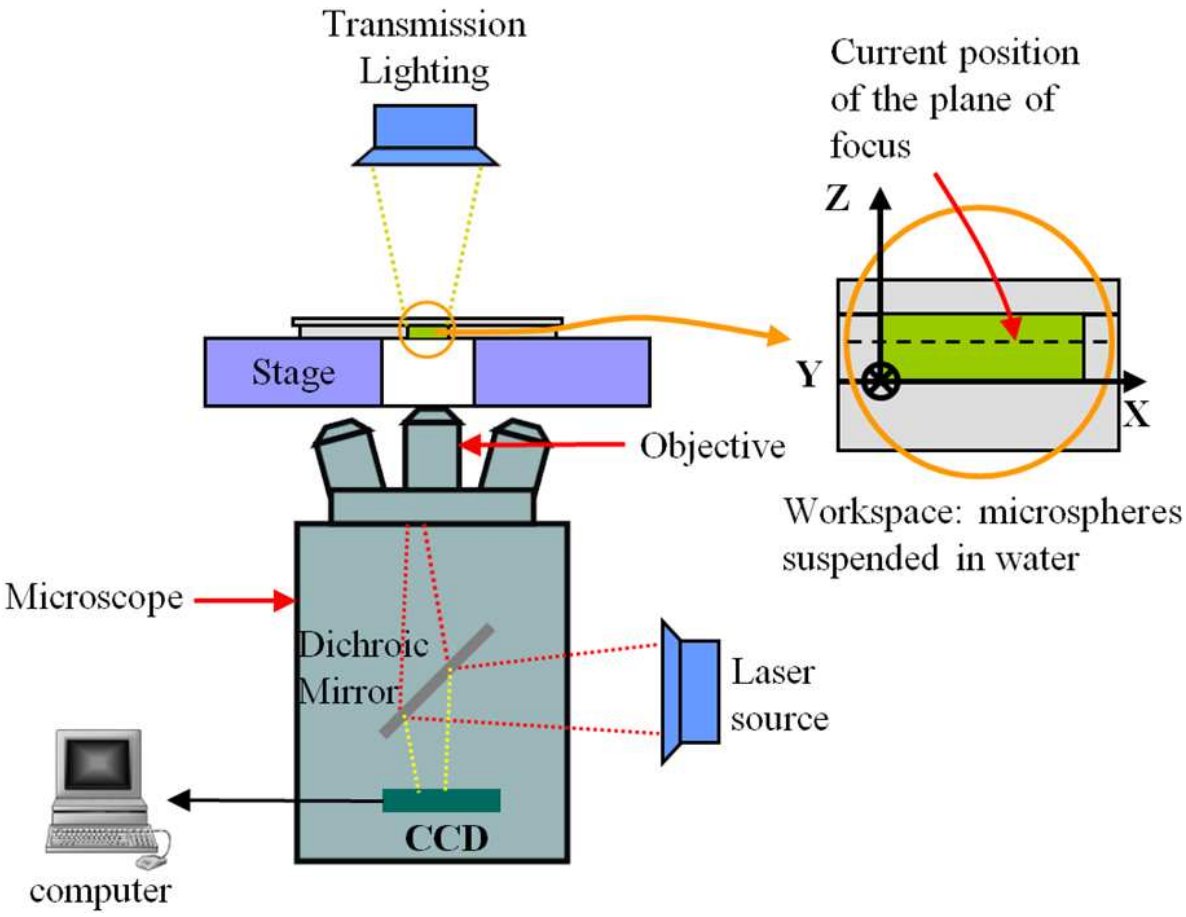

Figure 5.4: *Holographic Optical Tweezers based cell manipulation system*

5.4.2 Gripper synthesis

We used MATLAB implementation of a variant of the multi-objective evolutionary algorithm NSGA-II [Deb01] to solve our multi-objective optimization problem. The population size was set to 200 individuals with the crossover probability of 0.5. The optimization converged after 596 generations. The resulting Pareto front consists of 35 beads configurations. The Pareto front essentially shows that by placing the beads along the 'equator' of the object, we would get the ideal gripper in terms of the imposed minimum laser beam intensity. However, that placements would not satisfy the form closure properties (the convex hull of the grasp matrix does not contain origin). Now, if we start distributing the beads above and below the 'equator', the intensity will increase as well as the convex volume covered by the grasp matrix. Hence, we would start getting non-dominated solutions. From the Pareto front, we selected 5 configurations that significantly differ in terms of positions of the beads and orientation of the gripper. We used the intensity value of the laser beam resulting from the gripper reported in [KCA$^+$11] as a benchmark and further narrowed down the selected set to 3 configurations that result in lesser intensity values. The three selected configurations are characterized based on the maximum transverse velocities in X and Y directions that the grippers can attain without breaking up in the physical setup. For experiments, we used 5 µm yeast cell as a gripped object. In reality, cells are deformable. However, with the velocity (up to 8 µm/s) we want to transport the object, the deformation due to the viscous drag is very small and hence cannot deform the cell significantly. Moreover,

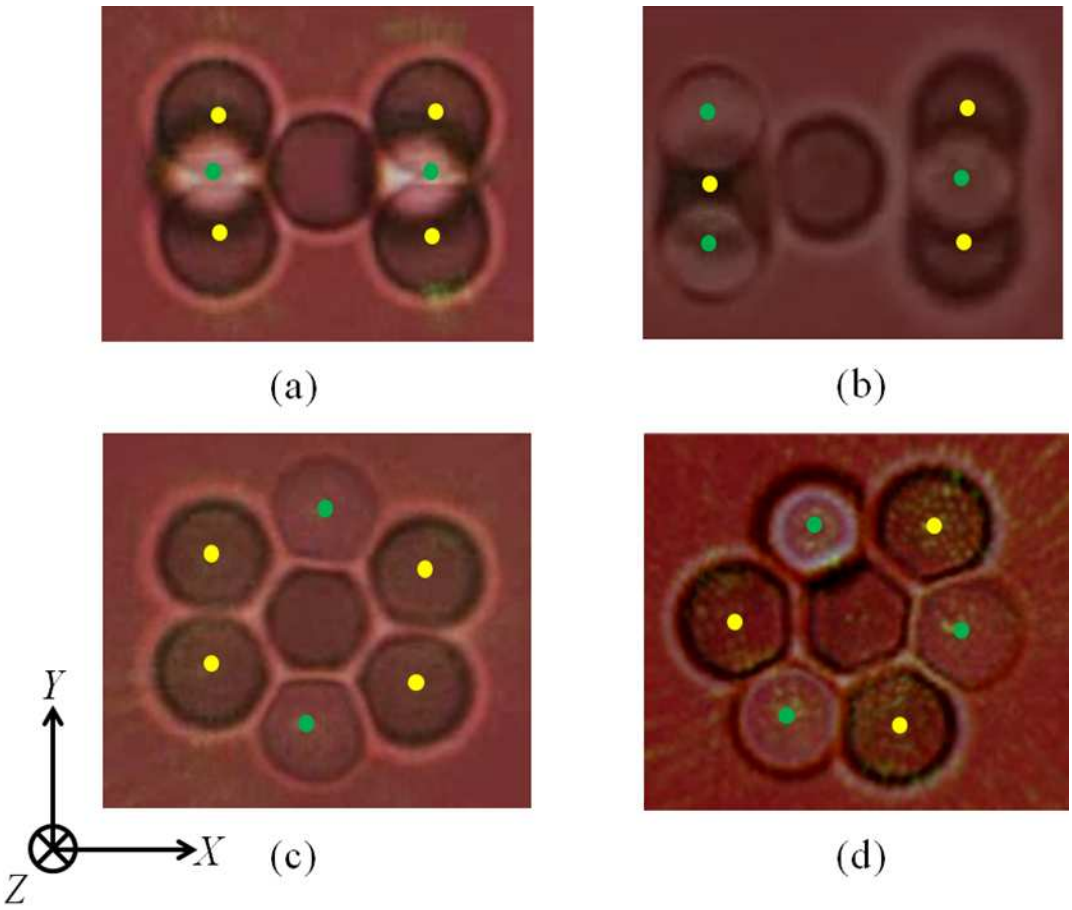

Figure 5.5: *Different gripper configurations (yellow dots indicate the beads lower in Z-axis, while green ones indicate the upper beads): (a) baseline gripper, (b-d) synthesized grippers 1-3. In the baseline gripper, the lower beads are placed approximately* 4.2 *µm lower, while the upper beads are placed* 4.4 *µm above the plane of the gripped object. For the synthesized grippers, the upper beads are* 3.5 *µm,* 1.3 *µm, and* 2.4 *µm above, and the lower beads are* 3.8 *µm,* 1.8 *µm, and* 2.3 *µm below the plane of the gripped object, respectively*

to avoid deformation due to the gripper arrangement, beads have to be placed at a safe distance by considering the cell as a rigid body.

5.4.3 Gripper performance evaluation

Figure 5.6 shows the transportation of a 5 µm yeast cell gripped by the synthesized gripper 1 (see Figure 5.5b). The target cell is successfully transported to the goal location and released from the gripper. The stable transport was also achieved

by the gripper 3 (see Figure 5.5d). In contrast, the gripper 2 (see Figure 5.5c) can become unstable during the movement since the target cell attempts to escape along axial direction (Z axis).

We evaluated the selected grippers by finding out the maximum transverse velocities along X (transverse x) and Y (transverse y) directions v_x and v_y using which the grippers could be transported without breaking down. For each gripper, the velocities in both directions are gradually increased until the ensemble breaks down and the maximum velocity is recorded. However, for moving along a curved path (see Figure 5.6), we had to use a lower speed since the gripped object needs additional time to get the momentum transferred due to change in the direction of motion of the ensemble.

The performance of the baseline and synthesized grippers is summarized in Table 5.1. The performance of the synthesized gripper 1 is comparable to the baseline gripper with an additional advantage that it imposes smaller laser intensity on the transferred object. For both the configurations, there is a significant difference between the maximum achievable transverse x speed v_x and the transverse y speed v_y. The reason is shown in Figure 5.7, where the transverse y component F_y of the maximum trapping force F_{trap}, that provides motion against viscous drag, is smaller than its transverse x component F_x. Synthesized grippers 2 and 3 can achieve similar maximum velocities in both transverse x and transverse y directions since the beads are uniformly placed around the object. In addition, they impose even smaller intensity of the laser beam on the transferred object. On the other hand, the maximum achievable velocity is smaller in the axial direction compared to the

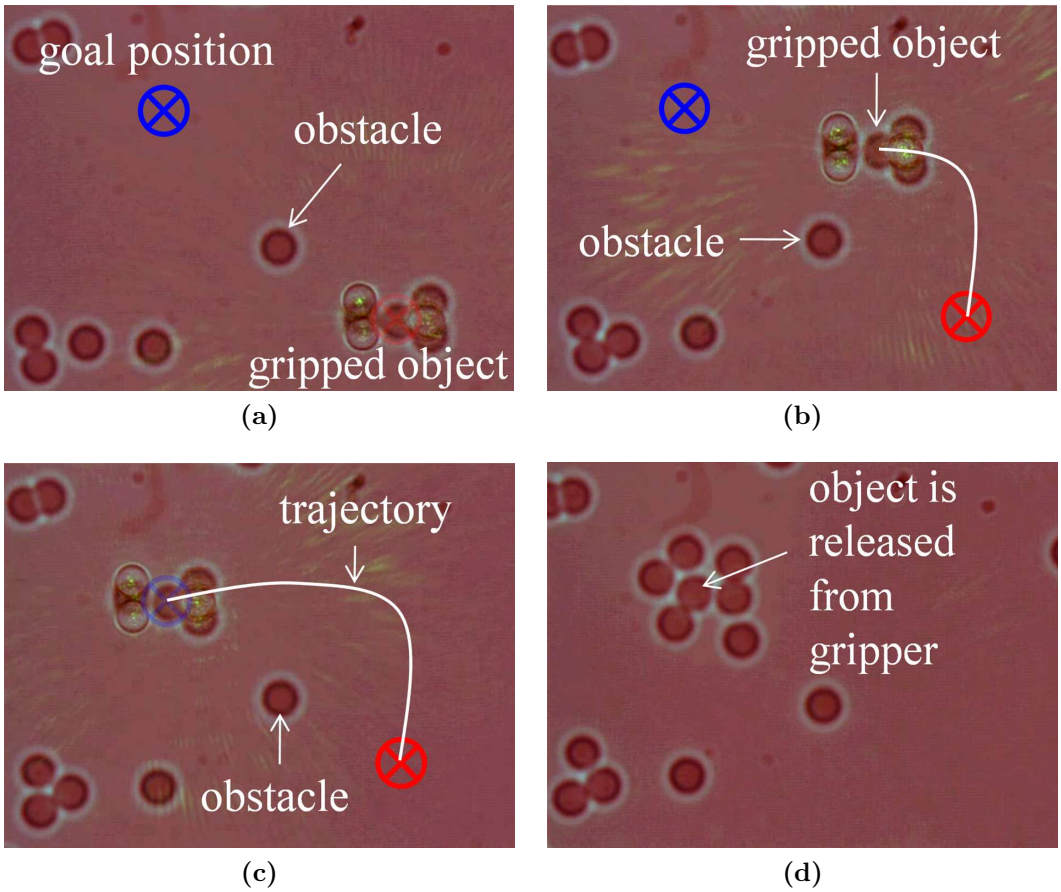

Figure 5.6: *Transportation of a yeast cell using the synthesized gripper 1: (a) at $t = 0$ s, the yeast cell is gripped by the gripper, (b) at $t = 10$ s, the gripper ensemble is avoiding an obstacle by moving in a curved trajectory, while maintaining a safe distance from the obstacle, (c) at $t = 21$ s, the gripper ensemble reached the goal location, and (d) at $t = 29$ s, the yeast cell is released from the gripper by turning off the laser*

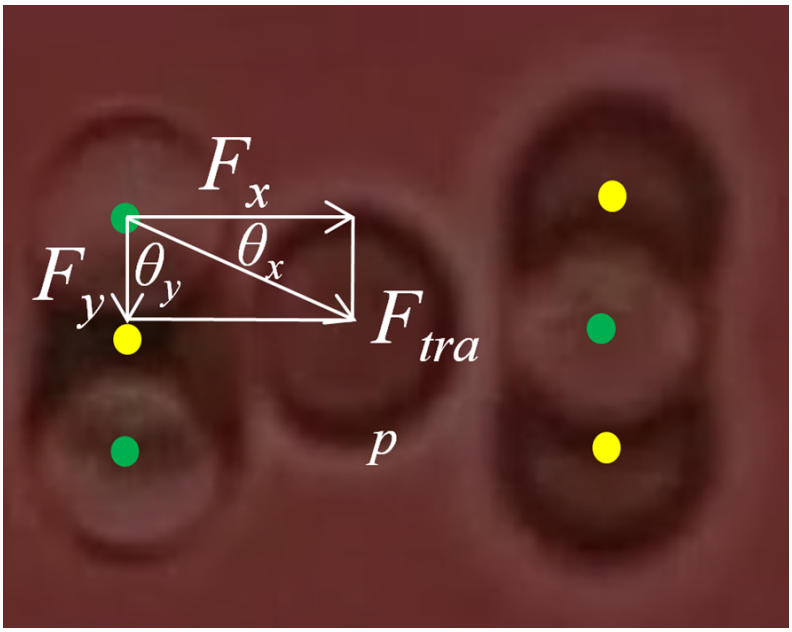

Figure 5.7: *Trapping force components in transverse x and transverse y directions, respectively*

baseline and gripper 1 configurations. Although the gripper 2 can achieve a high speed in both directions, while imposing a very low intensity of the laser beam on the transferred object, it was unstable when moving along a curved path. Because of the less volume covered by the gripper, the transferred object has a tendency to quickly escape in Z direction. However, this gripper can be ideal for arranging sensitive cells (e.g., *Dictyostelium discoideum*) in a line, where the goal is to move them in a straight line for a short distance. Gripper 1 has an additional advantage over the other two due to its double triplet formations. Because of the compact positioning of the beads inside the triplet, the gripper is more robust in terms of resisting the immediate shock exerted by the drag force (of the whole ensemble) as it starts moving from the rest or when it changes a direction of its motion, by creating a composite force field combining all three laser traps. In this way, the beads in the triplet support each other against the immediate drag force.

Table 5.1: *Performance of the synthesized grippers*

Properties	Baseline	Gripper1	Gripper2	Gripper3
Max. v_x (µm/s)	10.02	9.87	8.17	7.62
Max. v_y (µm/s)	5.46	5.68	8.33	7.40
Intensity (watt/µm^2)	3.4e-5	2.87e-6	2.3e-7	1.32e-6
Volume of convex hull (µm^3)	0.77	0.68	0.30	0.46

5.5 Summary

Optical Tweezers are becoming a widespread tool in cell biology and medicine because of its precise and non-contact nature of manipulation. Precise manipulation using OT comes with the cost of exposing a biological cell to higher laser intensity that can be harmful to the biology of the cell.

In this chapter, we successfully demonstrated useful gripper configurations that were evaluated using physical experiments in our HOT setup. The presented grippers can be used for precise manipulation of cells of spherical shape without directly exposing them to dangerous intensity of the laser beam. We developed a computational approach for preliminary modeling and simulations of gripper configurations. This allowed us to synthesize configurations that are optimized for minimizing the laser intensity imposed on the gripped object and maximizing the grasp volume.

We considered a cell of spherical shape in our preliminary modeling. Moreover, we did not model the trapping force during the optimization. Hence, we could not optimize the maximum attainable speed resulting from the gripper configuration. Future work can have two directions. First, an arbitrary shape can be considered to model the cell. That might give more complex gripper configurations. Second,

trapping force can be modeled using [BBGL09] and the developed optimization routine can be utilized to measure the maximum attainable velocity from the resulting configurations.

Chapter 6
Automated Manipulation of Biological Cells Using Gripper Formations Controlled By Optical Tweezers

This chapter[5] presents a planning approach for automated indirect manipulation of cells. The capability of noninvasive, precise micromanipulation of sensitive, living cells is necessary for understanding their underlying biological processes. Optical tweezers (OT) is an effective tool that uses a highly focused laser beam for precise manipulation of cells and dielectric beads at micro-scale. However, direct exposure of the laser beam on the cells can negatively influence their behavior or even cause a photo-damage. In this chapter, we introduce a planning and control approach for automated, indirect manipulation of cells using silica beads arranged into gripper formations. The developed approach employs path planning and feedback control for collision-free, efficient transport of a cell between two specified locations. The planning component of the approach computes a path that explicitly respects the motion constraints of the gripper formations. The feedback control component ensures stable tracking of the path by manipulating the cell using a set of predefined maneuvers. We demonstrate the effectiveness of the approach in transporting a yeast cell using different gripper formations along collision-free paths on our OT setup. We analyzed the performance of the proposed gripper formations with respect to their maximum transport speeds and the laser intensity experienced by the cell that depends on the laser power used.

[5] The work in this chapter is derived from the published work in [CTW+12] and accepted work in [CTS+13].

6.1 Introduction

Many experiments in biology and biophysics concerning (1) cell-based screening [WWS10], (2) studying environmental effects on cell behavior [UWIY03], (3) studying mechanical properties of cells [BSG+95], (4) cell diagnosis for therapy [CQZ+06], etc. require manipulation of cells at different population scales to form cell assays. For example, the experiments pertaining to cell diagnosis involve sorting large groups of cells. Similarly, studying a behavior of a medium-sized group of cells exposed to environmental influences requires arranging the cells in specific patterns. On the other hand, single-cell manipulation is needed when studying mechanical properties of individual cells. Hence, there is no single manipulation technique that would be usable at all scales. Rather each technique has its own operating niche.

Microfluidics [CSW+11], electrophoresis [Vol06], gradient based centrifugation [SA08, TDANE12], magnetically activated manipulation [AKS08], acoustics [DLK+12], magnetically actuated manipulation [TZQ+12], AFM [RWG+10], and Optical Tweezers (OT) are among some of the common techniques used for cell manipulation. Among these techniques, the gradient based centrifugation, acoustics, magnetically activated manipulation, and electrophoresis operate on a large scale. Microfluidics together with OT operate on a medium scale, and AFM, OT, and magnetically actuated manipulation techniques can also be used for single-cell manipulation.

In OT, a highly focused laser beam is used to exert gradient and scattering forces (of the order of few pN) on a dielectric particle (size scale ranging from few

nanometers to few tens of micrometers) which results in the particle being stably trapped at the focal point. The trapped particle can then be transported by simply moving the laser beam or released by switching off the beam. Due to the precise position control and non-contact nature of manipulation, OT is successfully used in different single-cell manipulation operations (e.g., such as rotation, stretching, and transportation). Holographic Optical Tweezers (HOT) enable generation of multiple traps allowing simultaneous manipulation of multiple objects in 3D.

One of the main challenges in OT based manipulation of biological cells is *photodamage* resulting in impaired functionality or even death of cells [ADY87]. Laser photodamage can occur due to the creation of reactive chemical species [SB94], local heating [LSBT96], two photon absorption [KLBT95], and singlet oxygen through the excitation of a photosensitizer [NCL$^+$99]. The intensity of the laser can be reduced by decreasing the operating laser power leading to generation of weaker traps. By using the rotation rate of the *E. coli* flagella motor, Neuman *et al.* [NCL$^+$99] found that the laser wavelengths between 830 nm and 970 nm were significantly less harmful to the cells. Optimization of laser wavelengths require extensive recalibration of OT setup for each type of the cell to be manipulated. Although the trapping stability can be enhanced by utilizing a feedback control of trap positions while using less laser power [HZM09, WOHT08], that may not provide effective manipulation of a large number of sensitive cells.

Rather than trapping directly, cells can be entrapped indirectly with thermosensitive hydrogel that can be transformed from sol-to-gel or gel-to sol through local heating or cooling by microheater [ANM$^+$05]. However, thermosensitive hydro-

gel can only be used to immobilize the cells. The cells still need to be directly trapped to bring them close to the microheater. In another mode of indirect manipulation, cells can be attached with optically trapped functional gel microbeads, thereby can be manipulated without a direct exposure to the laser [AEM+07]. Functional microbeads make permanent bond with the cells and thus they cannot be separated after manipulation. Arai *et al.* [AOIM09] used microtools that can be fabricated from an optically trappable material to indirectly manipulate cells. However, microtool based manipulation requires special microfabrication facility along with optical tweezers.

We propose indirect manipulation of cells using gripper formations made up of dielectric beads [CSW+12, KCA+11, BCLG11, TCW+12] directly trapped by laser beams. Figure 5.1 shows the transport operation of two *Dictyostelium discoideum* cells. One is directly held by a laser trap while the other is indirectly gripped using six optically trapped silica beads. The wavelength of the laser is 532 nm and the laser power is set to 2 watts. After 15 s both the cells are released from the laser traps. The directly gripped cell has been disintegrated due to the high intensity laser, while the indirectly gripped cell is still alive. This is because the silica beads allow to indirectly grip the cell and thus protect it from the direct exposure to the laser. Similar experiments with polarized *Dictyostelium discoideum* cells [WCGL13] shows the advantage of gripper based manipulation over direct trapping.

Transport of gripper formations requires to deal with multiple optical traps simultaneously which is time consuming and in some cases impossible to do manually. In this chapter, we develop an approach [CTW+12] for automated transport

of grippers for indirect manipulation of cells. The sequence of operations during manipulation are as follows: 1) trapping the target gripper beads, 2) automatically transporting the trapped beads to their desired locations around the target cell [BCLG12, CSW+13] to form a gripper formation, 3) automatically transporting the gripper formation to the desired goal location, and 4) releasing the cell at the goal location. The desired locations in the step 2 are determined using a gripper formation generator (see Section 6.2). Automated manipulation in microscale is difficult because of the challenges including Brownian motion, dynamical interactions among fluid, beads, and cells, and image processing based measurement uncertainty. We use A* based heuristic approach for fast planning in order to deal with the changing nature of the environment due to Brownian motion. For this planner, we derived a cost function that allows to compute a path for a particular gripper formation to transport a cell in minimum time. We use Kalman filtering to filter out the noise introduced during image processing.

6.2 Problem overview and terminology

6.2.1 Terminology

Gripper Formation We define a gripper formation as $G_n = \{\vec{X_{B,i}} : \vec{X_{B,i}} \in \Re^2, i = 1, 2, \ldots, n\}$, where $\vec{X_{B,i}}$ represents the position of the bead i in the global coordinate system (X, Y) and n specifies the number of beads in the formation. Figure 6.1 depict the examples of 2, 3, 4, and 6-bead formations G_2, G_3, G_4, and G_6, respectively. During the manipulation operation, all the beads $B_i, i = 1, 2 \ldots, n$ are held by their corresponding optical traps $T_i, i = 1, 2 \ldots, n$. We classify the

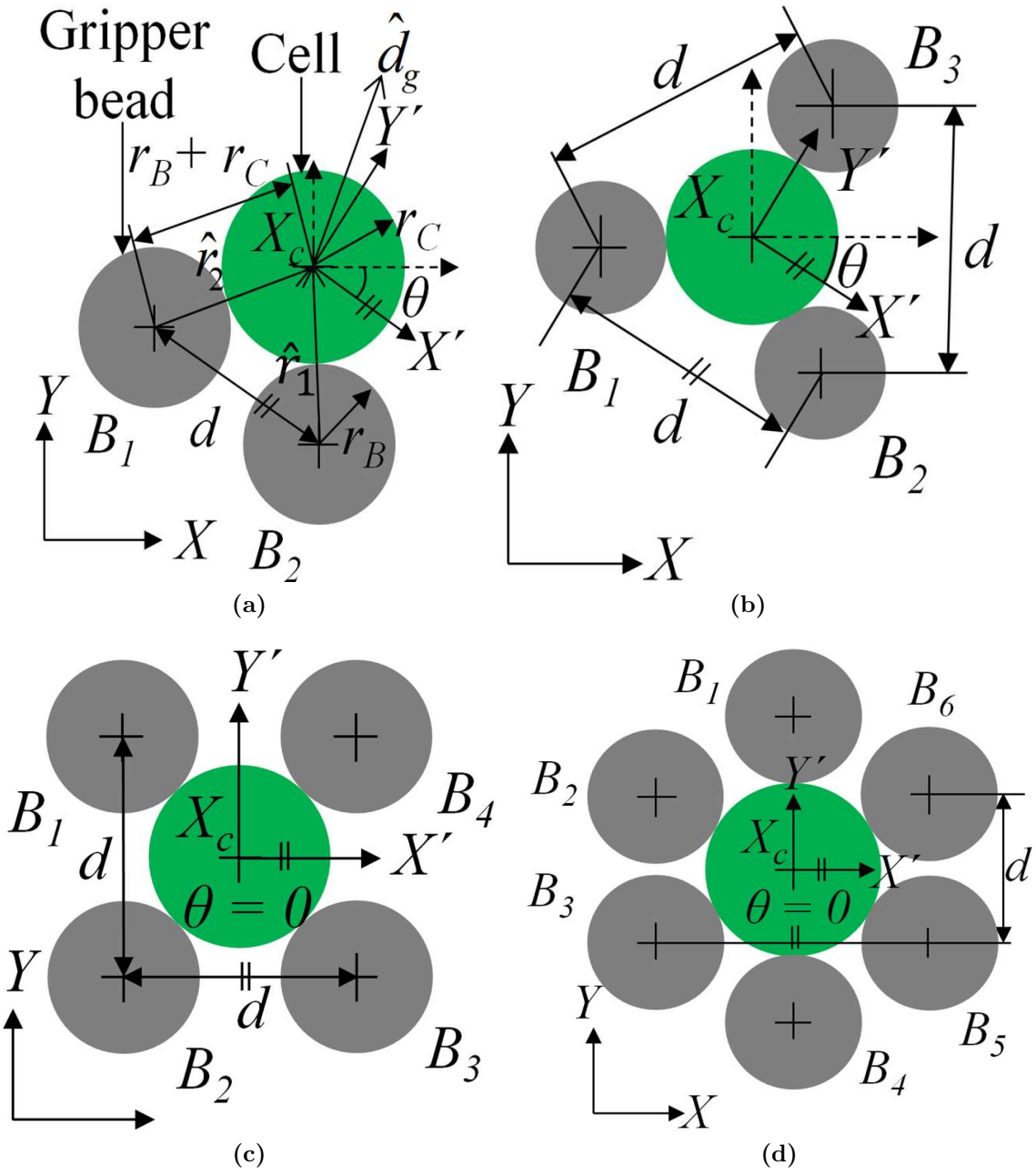

Figure 6.1: *Gripper formations: (a) 2-bead formation, (b) 3-bead formation, (c) 4-bead formation, and (d) 6-bead formation*

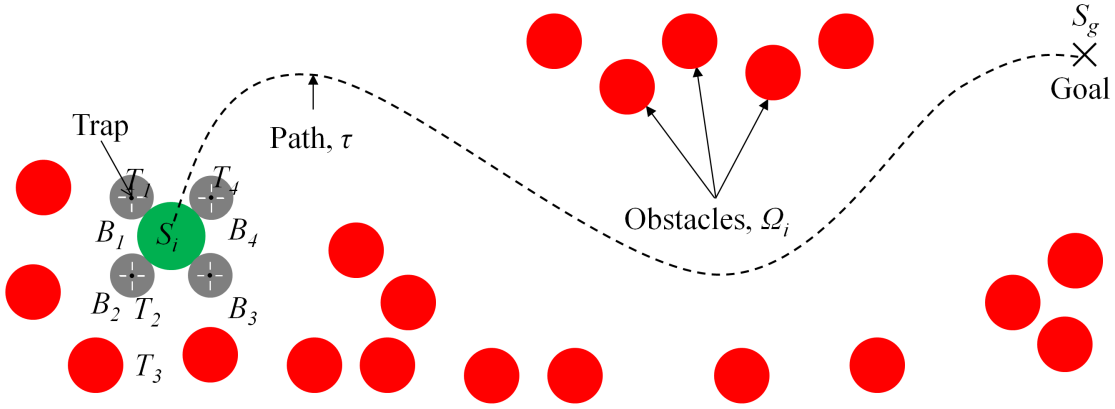

Figure 6.2: *Problem statement: the cell inside the gripper formation needs to be transported indirectly from the initial state S_i to the goal state S_g while avoiding collisions with the obstacles*

gripper formations into two classes based on their permitted mode of transport. G_2 and G_3 form one class where the gripper formations with less than or equal to 3 gripper beads need to be rotated to ensure there are enough beads to push the gripped object towards the desired direction. The gripper formations with more than 3 beads (G_4 and G_6) do not need to be rotated to change their direction of transport. Hence, they form the second class of grippers.

Gripper Formation Generator The beads in the gripper formation G_n are not specified manually. Instead, we designed a gripper formation generator $g : f_n \rightarrow G_n$, where the tuple $f_n = (\vec{X_C}, \theta, d, n)$ includes $\vec{X_C}$ as the position of the cell C expressed in (X, Y), θ as the angular difference between (X, Y) and the local coordinate system (X', Y') attached to the center of the cell (see Figure 6.1), d as the distance between any two beads in G_n (assuming a regular configuration), and n as the number of the beads in G_n. For example, a tuple $f_2 = ([10\ 10], \pi/6, 7, 2)$ with both the gripper beads and cell of 5 µm diameter will produce a two-bead gripper formation $G_2 = \{[11.25\ 5.16], [5.18\ 8.66]\}$ (see Figure 6.1a). Here, the distances

are expressed in µm. The generator thus allows us to automatically construct the entire gripper configuration using fewer number of parameters which is suitable for optimization [CSW+12]. It should be noted that gripper generator can be designed by the user of the planning system to create grippers of various shapes to handle cells of different shapes.

Gripper Formation State We define a state of the gripper formation G_n as $\vec{x} = [\vec{X_c}, \theta]^T$ in which $\vec{X_c} \in \Re^2$ is the position of the gripper (identical to the position of the manipulated cell) and θ is the orientation of the formation in (X, Y).

Manipulation Maneuvers We define a finite maneuver space $M(\vec{x})$ of the gripper formation for each state $\vec{x} \in \vec{X}$. The maneuver space includes *rotate*, *translate*, and *retain* atomic maneuvers that determine possible modes of locomotion of the gripper in the state $\vec{x}$. The *rotate* maneuver represents a function $m_R(x\delta\theta) = \vec{x'}$, where $\vec{x'} = [\vec{X_c}, \theta + \delta\theta]^T$, that rotates the formation by a constant angle $\delta\theta$. The *translate* maneuver represents a function $m_T(\vec{x}, \vec{\delta d}) = \vec{x'}$, where $\vec{x'} = [\vec{X_c} + \vec{\delta d}, \theta]^T$ that causes a linear translation for a constant distance $\vec{\delta d} = [\delta x, \delta y]^T$. The *retain* maneuver $m_{RET}(\vec{x}) = \vec{x}$ enforces the original formation G_n around the cell if one or more beads get displaced from their required positions. The generator g takes the desired formation states $\vec{x'}$ or $\vec{x}$ to determine the desired bead positions $\vec{X_{B,i}}$ and thereby the next trap positions T_i as shown in Table 6.1.

Obstacles We define a set of obstacles $\Omega_i = \{\vec{X_{\Omega,i}} : \vec{X_{\Omega,i}} \in \Re^2, i = 1, 2, \ldots, m\}$, where $\vec{X_{\Omega,i}}$ represents the position of an obstacle Ω_i in (X, Y). The set of obstacles includes all the cells and beads in the workspace besides the beads that are part of G_n and the cell C being manipulated.

6.2.2 Problem statement

Given a gripper formation G_n along with a formation tuple f_n optically held by traps T_is, where $i = 1, 2, \ldots, n$, and randomly moving obstacles Ω_js, where $j = 1, 2, 3, \ldots, N$, compute the following:

- A collision-free global path τ which consists of discrete waypoints $W_p : p = 1, 2, 3, \ldots, N_\tau$ to indirectly transport the cell using G_n. N_τ is the total number of waypoints in τ.

- A complete feedback control that selects appropriate maneuvers for any given gripper formation state so that the cell can reliably follow the path τ or return an *exception* if the current path is no longer valid due to randomly moving obstacles. In case of the *exception*, the global path is recomputed.

6.2.3 Assumptions

We made the following assumptions:

- We approximate yeast cells and gripper beads as perfect spheres of radius r_C and r_B, respectively. (see Figure 6.3).

- We assume that optically trapped beads can move with the same velocity as the traps. This is ensured by choosing an operating speed using which the beads can be reliably trapped and moved by the laser traps [BBGL09].

6.2.4 Solution approach

We have adopted the following approach (see Figure 6.4) to solve the problem:

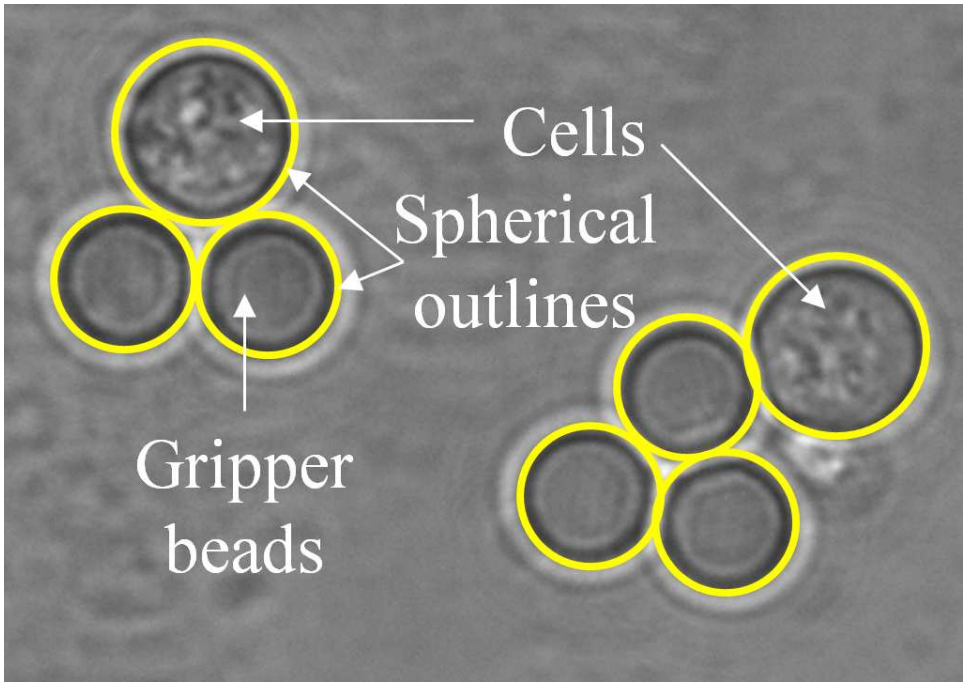

Figure 6.3: *Workspace with a spherical cell and beads*

- We have developed A* based global path planner to generate a collision free path that minimizes the transport time of a gripper formation between two given locations, while satisfying its motion constraints. We derive two cost functions compliant with the specific class of gripper formations.

- We have developed a feedback controller based on inverse kinematics to generate paths for individual traps so that the formation can follow the global path.

- We used Kalman filtering to handle measurement uncertainties.

6.3 Path planning for gripper formation

We used A* based global path planner to find a collision-free path for a gripper formation to transport a cell between two given locations. The planner recomputes

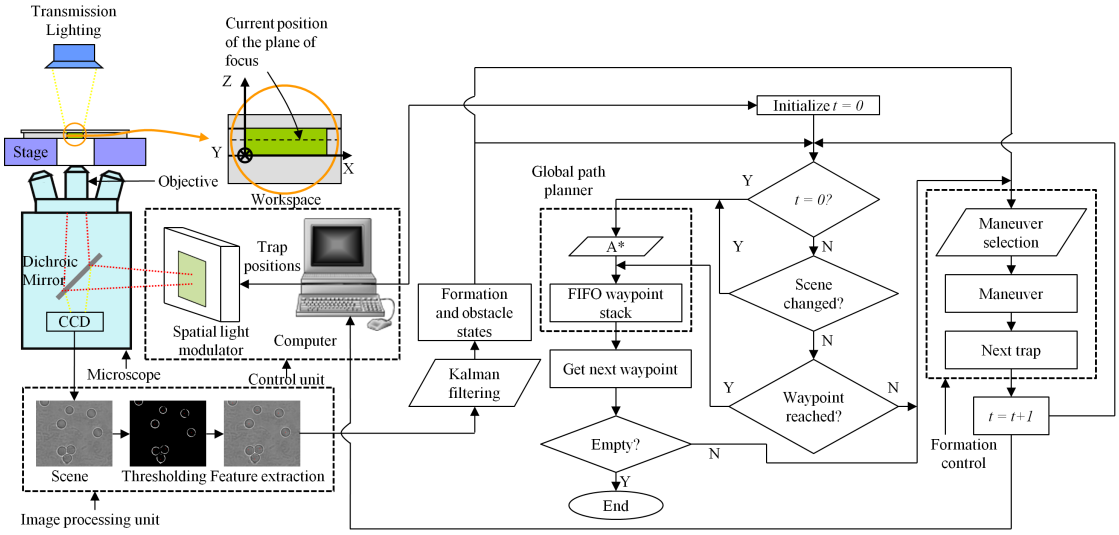

Figure 6.4: *Optical Tweezers setup and manipulation approach*

the path if the workspace is changed significantly due to random motion of freely diffusing beads and cells (see Figure 6.4).

In order to make search for the path τ feasible, we discretize the state space $\vec{X}$ into the discrete state $\vec{S}$ consisting of grid cells of constant sizes. In this way, the planner can make only constant advancements during the search for τ between the initial $\vec{S}_i$ and goal $\vec{S}_g$ state. The following sections present the state-action space representation and cost function for the planner.

6.3.1 State-action space representation for planning

The discrete state $\vec{S}^k$ of a gripper formation is defined as a vector of position $\vec{X}_c^{\,k}$ of the cell C and the orientation θ^k of the formation at a given time step k (see Equation 6.1).

$$\vec{S}^k = \left[\vec{X}_c^{\,k}, \theta^k\right] \tag{6.1}$$

The state space is a 3D grid with each grid cell representing a state of the formation G_n. A control action is represented as a vector consisting of velocity of

individual traps at a given time step k (see Equation 6.2).

$$\vec{u}^k = [\vec{v_1}^k, \vec{v_2}^k, \ldots, \vec{v_n}^k] \tag{6.2}$$

Here $\vec{v_i}^k$ represents the velocity of i'th trap at time step k and n is the total number of traps corresponding to each gripper beads. The dynamics of formation G_n is described by Equations 6.3 and 6.4

$$\dot{\vec{X}}^k = \sum_{i=1}^{n} max(0, \vec{v_i}^k.\hat{\vec{r}_i})\hat{\vec{r}_i} \tag{6.3}$$

$$\dot{\theta}^k = \sum_{i=1}^{n} \left(\frac{\vec{v_i}^k}{(r_B + r_C)} \times \hat{r}_i \right) \alpha_{contact} \tag{6.4}$$

$$\alpha_{contact} = \begin{cases} 0 & \text{if } d_{B_i,C} > (r_B + r_C)\,, \\ 1 & \text{otherwise.} \end{cases}$$

Here, $\hat{\vec{r}_i}$ (see Figure 6.5) is the unit direction vector towards the cell C from the gripper bead B_i and $d_{B_i,C}$ is the distance between them. The momentum is transferred to the cell only when the beads are in contact to the cell. Hence, $\dot{\theta}$ is set to 0 when cell and bead are not in contact. We imposed some constraints on the action u when executing different types of maneuvers depending on the formation type to satisfy its motion constraints. For G_4 and G_6 gripper formations, the velocities of all the traps are constrained to be the same as given by Equation 6.5

$$\vec{v_i}^k = \vec{v_j}^k : \forall i, j, \text{where } i, j = 1, 2, 3, \ldots, n \tag{6.5}$$

In case of G_2 and G_3 gripper formations, the speed of all the traps is constrained to be the same (see Equation 6.6). The trap motions are constrained only

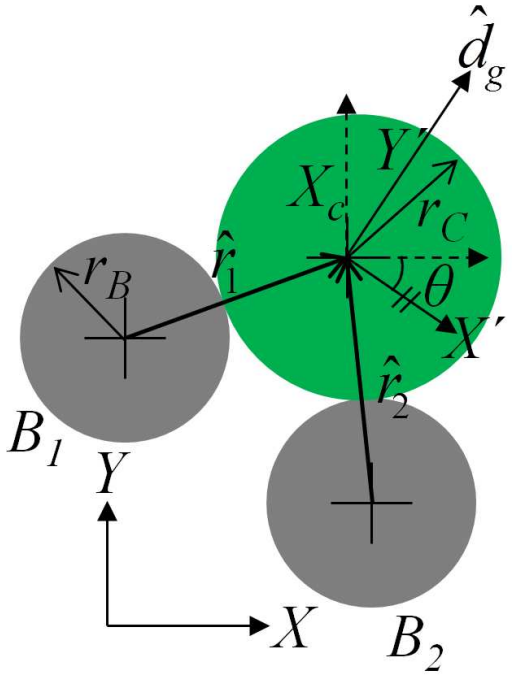

Figure 6.5: *Gripper formation with all the direction vectors*

parallel to the desired direction of the cell C in case of *translate* maneuver to prevent the formation from falling apart (see Equation 6.7). Similarly, the traps are restricted to move only towards the tangential direction of the cell in case of *rotate* maneuver (see Equation 6.8).

$$|\vec{v_i}^k| = |\vec{v_j}^k| : \forall i, j, \text{where } i, j = 1, 2, 3, \ldots, n \tag{6.6}$$

$$\vec{v_i}^k . \hat{\vec{d}}_g = 1 \tag{6.7}$$

$$\vec{v_i}^k . \hat{\vec{r}}_i = 0 \tag{6.8}$$

Here, $\hat{\vec{d}}_g$ (see Figure 6.5) is the unit direction vector from the cell towards the desired waypoint that can be derived from the orientation of the gripper formation (see Equation 6.9).

$$\hat{\vec{d}}_g = [cos\theta, sin\theta]^T \tag{6.9}$$

When the gripper formation takes an action $\vec{u}^k$ at time step k, it transitions from $\vec{S}^k$ to $\vec{S}^{k+1}$ using Equations 6.10 and 6.11.

$$\vec{X}^{k+1} = \vec{X}^k + \dot{\vec{X}}^k \triangle t \tag{6.10}$$

$$\vec{\theta}^{k+1} = \theta^k + \dot{\theta}^k \triangle t \tag{6.11}$$

Here, $\triangle t$ is the time spent between two subsequent time steps.

6.3.2 Cost function

The planner iteratively expands the nodes of candidate paths in the state-space from the initial state $\vec{S_i}$ to the goal state $\vec{S_g}$ according to the cost function $f(\vec{S})$.

$$f(\vec{S}) = g(\vec{S}) + h(\vec{S}) \tag{6.12}$$

Here, f is the total cost estimation of a path starting from $\vec{S_i}$ to $\vec{S_g}$ through the state $\vec{S}$, $g(\vec{S})$ is the optimal cost-to-come from $\vec{S_i}$ to $\vec{S}$, and $h(\vec{S})$ is the heuristic cost estimate from $\vec{S}$ to $\vec{S_g}$. The formation is transported with a constant speed and thus we use the transport time as the cost estimate. The cost of a newly encountered state $\vec{S'}$ is computed as follows:

$$f(\vec{S'}) = g(\vec{S}) + l(\vec{S}, \vec{u}) + h(\vec{S'}) \tag{6.13}$$

Here, $l(\vec{S}, \vec{u})$ is the transition cost from the state $\vec{S}$ to $\vec{S'}$. We use a general transition cost function $c(\vec{S})$ to calculate the transition $l(\vec{S}, \vec{u})$ and heuristic $h(\vec{S})$ costs as described by Equation 6.14:

$$c(\vec{S}) = \begin{cases} \frac{L}{v} + \frac{\Delta\theta}{\omega} & \text{if } n < 4, \\ \frac{L}{v} & \text{otherwise,} \end{cases} \tag{6.14}$$

where v and ω are the constant linear and angular speeds of the trap ensemble, respectively. In order to calculate $l(\vec{S}, \vec{u})$, L and $\Delta\theta$ are taken as the linear and angular displacements resulting from the execution of an action $\vec{u}$ (see Figure 6.6). For the calculation of $h(\vec{S})$, we take the Euclidean distance between the states $\vec{S}$ and $\vec{S_g}$ as the linear displacement L, and the total angular displacement required to move from $\vec{S}$ to $\vec{S_g}$ as $\Delta\theta$. During the transport along a given direction, some of the beads in the formation exert a pushing force (actuator beads) on the cell, whereas other beads prevent the cell from drifting out of the ensemble. For the gripper formations G_4 and G_6, there are enough actuator beads to be able to push the cell in any direction. Hence, they do not need to be rotated to change the transport direction of the formations, while they need to be rotated for gripper formations G_2 and G_3 to be able to orient the actuator beads along the transport direction. Therefore, we do not consider the rotation for $n \geq 4$ in Equation 6.14.

In this dissertation, we will use the controllable degrees of freedom and the total degrees of freedom to characterize whether a gripper ensemble is *holonomic* or *nonholonomic* systems [NF72]. In robotics, a system is considered *holonomic* if the controllable degrees of freedom are equal to the total degrees of freedom. On the other hand, a system is considered *nonholonomic* if the controllable degrees of freedom are less than the total degrees of freedom. In our case, we are manipulating cells in a plane with the gripper formations. Hence, the total number of degrees of freedom for the gripper ensemble is three (two for position and one for orientation). In case of G_4 and G_6, gripper ensemble can be translated in arbitrary directions and rotated. Hence, the number of total degrees of freedom for G_4 and G_6 is equal to

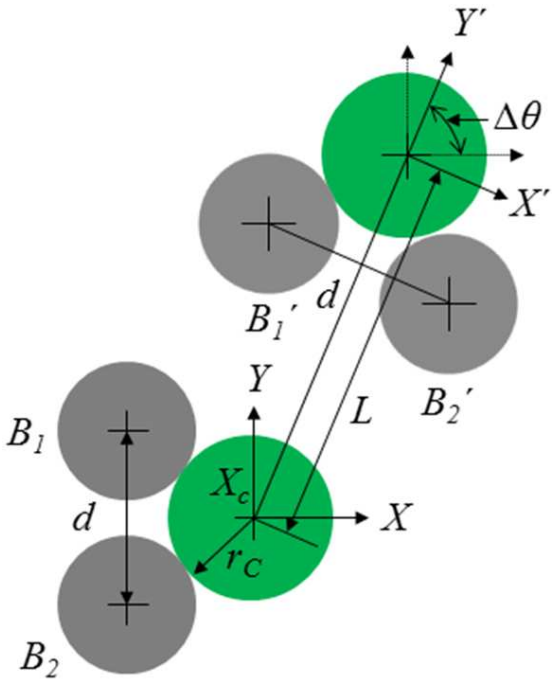

Figure 6.6: *Cost function for $n < 4$*

the controllable degrees of freedom. However, in case of G_2 and G_3, grippers cannot translate in arbitrary direction because moving in certain direction may result in the cell coming out of the formation.

The resulting cost function can then be divided into two classes: *holonomic* cost function for G_4 and G_6 and *nonholonomic* cost function for G_2 and G_3. *Holonomic* cost functions do not account for changes in orientations and are only based on translations. *Nonholonomic* cost functions account for both translations and rotations.

6.4 Feedback control for gripper formation

The maximum operating speed of a particular gripper formation to transport a cell to a given goal location needs to be determined. With the increase in the speed, the formation tends to break down gradually due to Brownian motion and

Table 6.1: *Rules used by the formation generator g to determine the positions of beads inside the gripper*

Formation type	Bead positions
G_2	$\vec{X_{B,1}} = \vec{X_c} - \vec{D_1} - \vec{D_2}$; $\vec{X_{B,2}} = \vec{X_c} - \vec{D_1} + \vec{D_2}$
G_3	$\vec{X_{B,1}} = \vec{X_c} - \vec{D_1} - \vec{D_2}$; $\vec{X_{B,2}} = \vec{X_c} - \vec{D_1} + \vec{D_2}$; $\vec{X_{B,2}} = \vec{X_c} - \vec{D_1} + \vec{D_3}$
G_4	$\vec{X_{B,i}} = \vec{X_c} + d[cos(\pi/4 + i\pi/2), sin(\pi/4 + i\pi/2)]^T$
G_6	$\vec{X_{B,j}} = \vec{X_c} + d[cos(\pi/6 + j\pi/3), sin(\pi/6 + j\pi/3)]^T$
$\vec{D_1} = \sqrt{(r_B + r_C)^2 - d^2/4}[cos\theta, sin\theta]^T$; $\vec{D_2} = d/2[sin\theta, -cos\theta]^T$, $\vec{D_3} = \sqrt{3}d/2[sin\theta, -cos\theta]^T$, $i = 1, 2, \ldots, 4$; $j = 1, 2, \ldots, 6$	

drag force. Hence, we need a feedback controller that retains gripper beads in the formation if they get deviated for more than the maximum specified distance. In each planning interval, the planner executes one of the three maneuvers: *translate*, *rotate*, and *retain* (see Figure 6.4). The positions of the gripper beads expressed using the formation tuple f_n, that is computed using inverse kinematics, are shown in Table 6.1. not rotate in order to reach a particular waypoint. Hence, they need only two maneuvers to follow a path. In each planning time interval, the next trap positions are selected using the following algorithm:

Formation control algorithm: (see Figure 6.4)

Input: A finite nonempty maneuver library, formation tuple f_n, waypoint library Λ, bead deviation threshold l_{th}, waypoint deviation threshold w_{th}, and time step t.

Output: The next positions of the traps $\{T_i\}_{i=1}^n$.

Steps:

(i.) If $t = 0$, select the first waypoint W_p from the library Λ, where $p = 1$.

(ii.) If $\| \vec{X_c} - \vec{W_p} \| \leq w_{th}$, set $p = p + 1$.

(iii.) Measure the positions of beads $\{\vec{Z_{B,i}} : \vec{Z_{B,i}} \in \Re^2, i = 1, 2, \ldots, n\}$. If $\|$

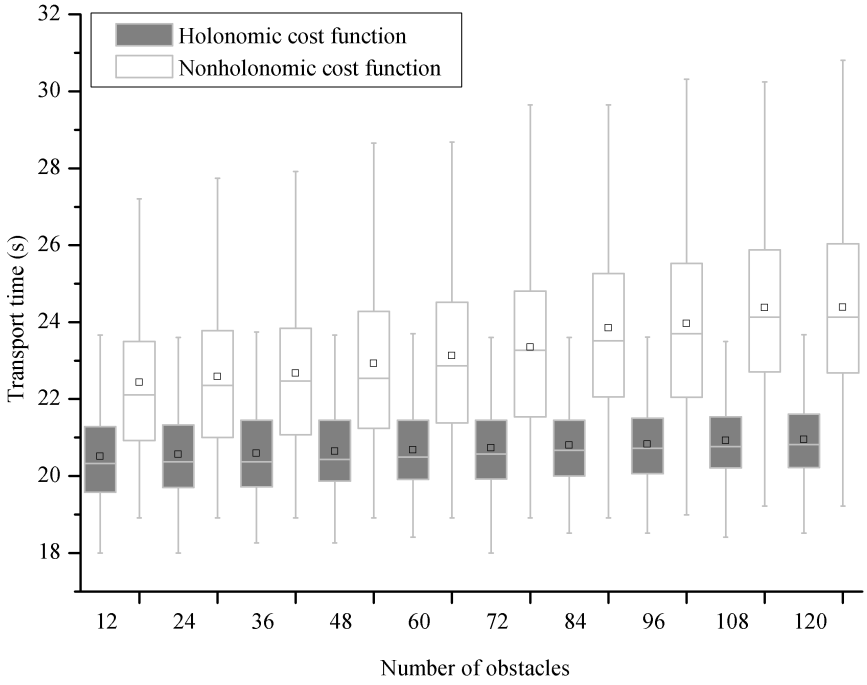

Figure 6.7: *Transport time required for G_4 and G_6 gripper formations to follow trajectories in various obstacle fields computed using two different cost functions*

$\vec{X_{B,i}}^{t-1} - \vec{Z_{B,i}} \| \leq l_{th}$ go to step v.

(iv.) Select the *retain* maneuver. Use the formation generator g to calculate $\{\vec{X_{B,i}}\}_{i=1}^{n}$ based on the formation state $\vec{x}$ (see Table 6.1). Set $T_i = \vec{X_{B,i}}$, $\forall\ T_i \in T$ and return T.

(v.) Based on the waypoint $\vec{W_p}$ and the formation state $\vec{x}$, calculate the desired action $\vec{u}$. If the action requires both *rotate* and *translate* maneuvers, first select the *rotate* maneuver. Calculate the desired formation state $\vec{x}$ and the corresponding $\{\vec{X_{B,i}}\}_{i=1}^{n}$ using the rules in Table 6.1. Set $T_i = \vec{X_{B,i}}$, $\forall\ T_i \in T$ and return T.

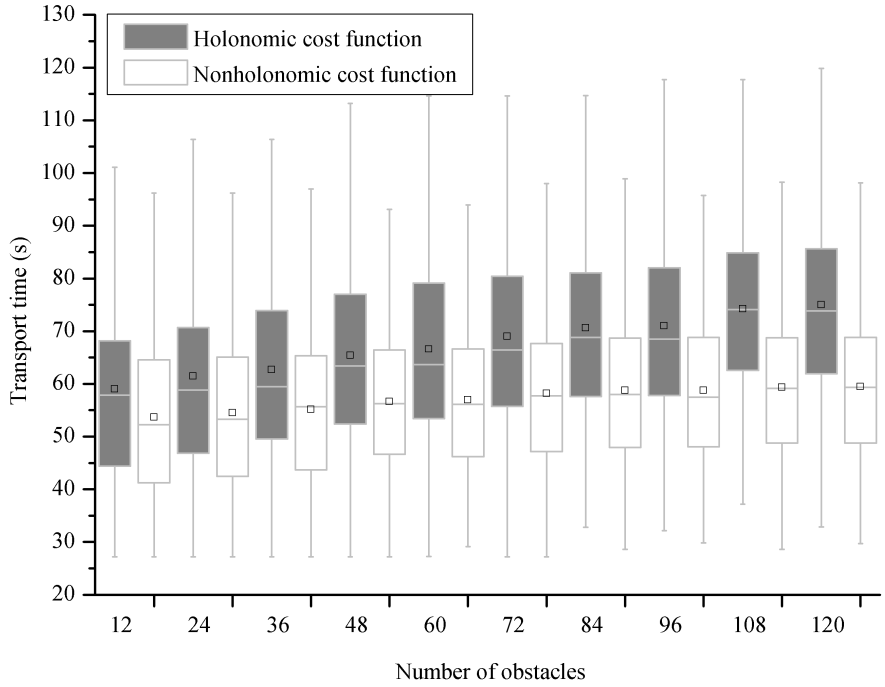

Figure 6.8: *Transport time required for G_2 and G_3 gripper formations to follow trajectories in various obstacle fields computed using two different cost functions*

6.5 Results and discussions

6.5.1 Experimental setup and method

We demonstrate the effectiveness of the planner using a BioRyx 200 (Arryx, Inc., Chicago, IL) holographic laser tweezer platform. The platform consists of a Nikon Eclipse TE 200 inverted microscope, a Spectra-Physics Nd-YAG laser (wavelength of 532 nm), a spatial light modulator (SLM), and a proprietary phase mask generation software running on a desktop computer. The objective used is the oil-immersion Nikon Plan Apo 60x/1.4 NA, DIC H. The maximum rate at which traps can be set is the update rate of the Spatial Light Modulator (SLM), 15 Hz, and the minimum step size of 150 nm. The feedback control is achieved with a second PC equipped with a uEye camera (IDS, Inc., Cambridge, MA) for imaging the cells and

beads in the workspace.

We use 5.0 µm diameter silica beads (with the density of 2000 kg/m^3 and a refractive index of 1.46 purchased from Bangs Laboratories, Inc., Fishers, IN) as the gripper beads. Yeast cells used in this experiment are cultivated from a fast growing yeast powder. 0.016 mg of yeast powder is mixed with 3% (w/v) glucose solution. The cells are allowed to grow for an hour. After an hour, the concentration of cells is examined under a microscope. The average diameter of the cells after an hour is 5-8 µm.

Beads and cells are identified by thresholding the image and calculating the center of mass of all the remaining blobs (see Figure 6.4). The measurement noise in the particle positions is suppressed through the use of Kalman filtering. The objects at microscale undergo Brownian motion. In order to construct the covariance matrix for the Kalman filter, we hold the object (a bead or cell) using a laser trap and log the measured positions for 1000 time steps. The actual position of the object is determined from the position of the trap since the object gets hopped into the focal point of the laser. The update rate of SLM is about 66 ms. Since the Brownian motion of the object is suppressed by the optical trap, the covariance of the measured positions can be regarded as a metric for the measurement noise. We have calculated the measurement noise covariance matrix from the recorded positions and used Kalman filter to estimate the actual positions.

6.5.2 Simulation results of path planning

In this section, we present a comparison of the required average transport time for two classes of gripper formations executing two different paths computed using *holonomic* and *nonholonomic* cost functions as presented in Equation 6.14 in scenes with different obstacle densities.

We use 10 different levels of obstacle densities to generate the scenes. For each obstacle density level, we create 20 different scenes by randomly distributing the obstacles. For each scene, we randomly choose 100 different initial S_i and goal states S_g to compute trajectories. The trajectories are computed using two different cost functions as shown in Equation 6.14. We record the transport time required by each formation type for execution of trajectories computed using the two cost functions. The transport time is averaged over 2000 test cases for each obstacle density. The gripper formations are transported with the maximum constant linear velocity of 10 µm/s and maximum angular velocity of 0.25 rad/sec.

Figure 6.7 shows the box plots of transport time of G_4 and G_6 gripper formations executing paths computed using two different cost functions in scenes with different obstacle densities. The average transport time (indicated using $\Box$ sign) gradually increases with the increase of obstacles in the scene for both cost functions. This increase is not significant for *holonomic* cost function since the planner does not consider the time for rotation which is a dominant component in calculation of the total transport time. The transport time required for execution of a path computed using the *holonomic* cost function is less than that of the *nonholonomic*

Table 6.2: *Performance of designed grippers*

Gripper type	Properties	Transport speed µm/s		
		7	8.5	10
G_2	Laser power (w) Intensity (w/µm^2)	0.2 6.03e-7	0.3 9.05e-7	0.5 1.51e-6
G_3	Laser power (w) Intensity (w/µm^2)	0.4 8.02e-7	0.5 1.00e-6	0.8 1.60e-6
G_4	Laser power (w) Intensity (w/µm^2)	0.6 9.06e-7	0.8 1.21e-6	1.2 1.81e-6
G_6	Laser power (w) Intensity (w/µm^2)	1.0 1.00e-6	1.5 1.50e-7	2.0 2.00e-6

cost function. The *nonholonomic* cost function leads to computation of a path that has less number of turns since it explicitly takes the angular transport time into account. It thus does not necessarily need to be the shortest path between S_i and S_g in terms of Euclidean distance in the position space. On the other hand, the *holonomic* cost function leads to computation of the shortest path in the position space, not taking the orientation of the gripper into account. The G_4 and G_6 gripper formations do not need to rotate to change the direction of their transport. Hence, the shortest path computed using the *holonomic* cost function requires the least transport time for G_4 and G_6 gripper formations.

On the contrary, the actual transport time of G_2 and G_3 gripper formations following a path computed using the *nonholonomic* cost function is less than that of the *holonomic* cost function (see the plot in Figure 6.8). The formations need to rotate to change the direction of their transport. Hence, it is preferable to choose a path that has less number of turns, rather than choosing the shortest path in the position space to minimize the total transport time as well as to maintain stability.

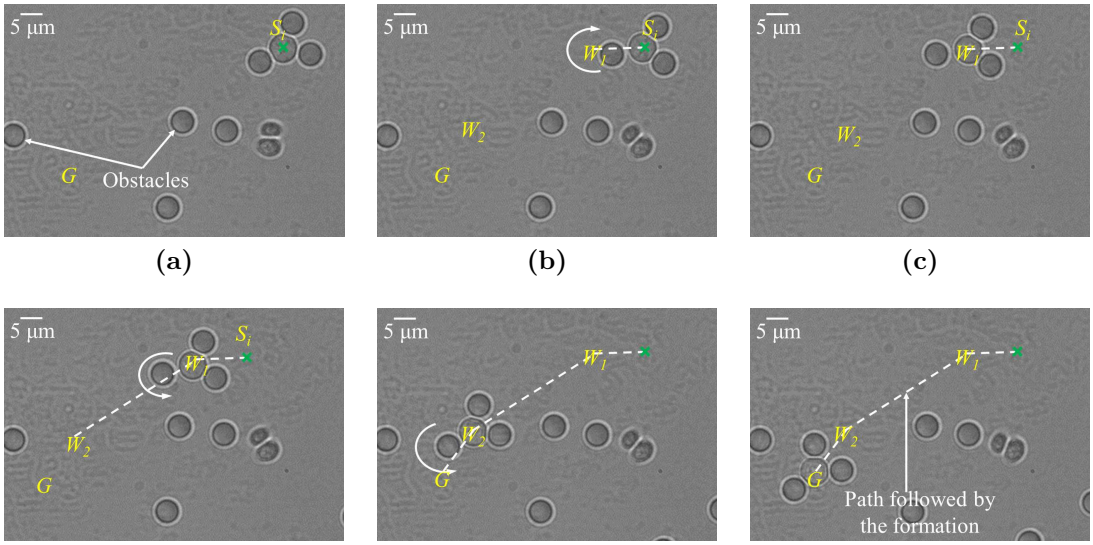

Figure 6.9: *Indirect transport of a bead using the 3-bead gripper formation: (a) gripper in the initial state S_i, (b) the gripper applies the rotate maneuver to align itself towards the waypoint W_1, (c) the gripper applies the translate maneuver to reach the first waypoint W_1, and (d) the gripper applies the rotate maneuver to align itself towards W_2, (e) the gripper applies the translate maneuver to reach W_2, and (f) the gripper reaches the final goal G with the use of rotate and translate maneuvers respectively*

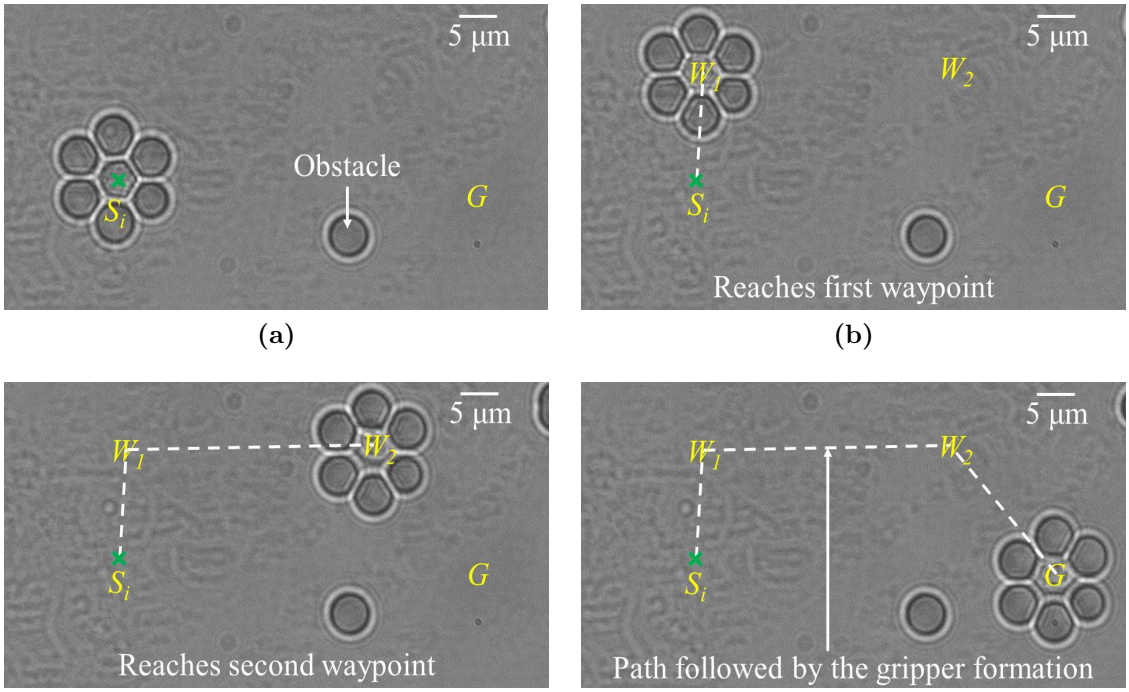

Figure 6.10: *Indirect transport of a bead using the 6-bead gripper formation: (a) the gripper in the initial state S_i, (b) the gripper applies the translate maneuver to reach the first waypoint W_1, (c) the gripper applies the translate maneuver to reach the second waypoint W_2, and (d) the gripper reaches the final goal G by applying the translate maneuver*

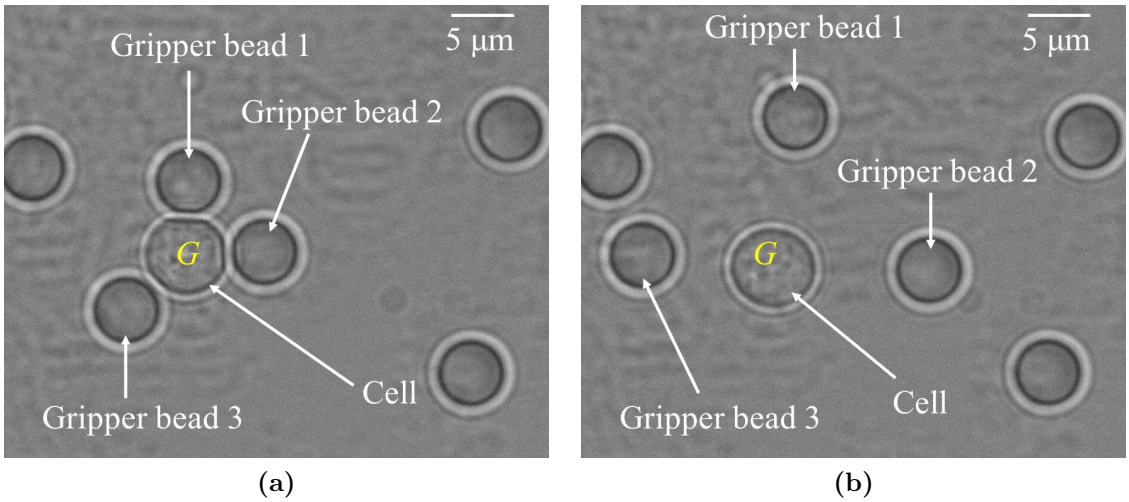

Figure 6.11: *Releasing a cell from the gripper: (a) the cell is transported to the goal G using the gripper formation, and (b) the cell is released from the formation by transporting the beads away from the cell*

6.5.3 Experimental results

We demonstrate the effectiveness of the planner in transporting a yeast cell with different types of gripper formations (see Section 6.4) towards a specified sequence of waypoints by running experiments on our OT setup. The waypoints are generated by the A* based path planning algorithm presented in Section 6.3. The waypoints are denoted as W and the initial and final location of the gripper is denoted as S_i and G, respectively. Each formation successfully follows the waypoints, while transporting the gripped cell. Figure 6.9 shows the selection of different maneuvers by G_3 to follow three waypoints including the goal G in a challenging scene with obstacles. In these experiments, the complexity of the obstacle scene is limited by the allowable dimension of our OT workspace as well as the size of the gripper formation.

The formations with two and three beads use the same set of maneuvers to follow similar waypoints. The formation G_3 is more stable than its G_2 counterpart because the extra bead prevents the gripped object from drifting out of the gripper. The planner has to invoke the *retain* maneuver intermittently to keep the cell inside the gripper formation.

Figure 6.10 shows a target cell being transported with G_6 through three waypoints using the *retain* and *translate* maneuvers. Due to the larger size of the formation, we can only demonstrate automated transport of the cell in a space with a single obstacle. Hence, G_6 formation is not suitable for a relatively cluttered environment. It does not require the *rotate* maneuver since it does not need to rotate

itself to change the direction of transport. As soon as some of the gripper beads get deviated from their desired locations beyond the user defined bead deviation threshold l_{th} (see section 6.4), the gripper uses the *retain* maneuver to keep the traps stationary for a specified time interval so that the beads can get back to their original formation. The formation G_4 utilizes the same set of maneuvers to transport the gripped bead.

Both of the beads in G_2 act as actuators (see Figure 6.1a). Hence, there is a risk that the cell will get deviated from its desired location inside the gripper when moving along a curved path. This formation is suitable for transporting the cell in a relatively cluttered environment since it requires low clearance space for navigation due to its smaller diameter. The formation G_3 (see Figure 6.1b) has one extra bead which always holds the cell inside the gripper. Both G_2 and G_3 need to stop and then rotate to change their direction of motion. The formation gets destabilized in case of a drastic change in the direction of transport since it has only one bead to restrict the cell from drifting out of the formation. The formations G_4 and G_6 (see Figure 6.1c and Figure 6.1d) are much more robust to destabilization for transporting along a curved path since they do not need to rotate to change the direction of their motion. Hence, the required transport time will also be less compared to the transport time of G_2 and G_3. However, G_4 is more prone to get destabilized when moving along a diagonal direction since it can utilize only one actuator bead.

Figure 6.11 shows how the cell is released from the gripper formation after it reaches the desired destination. The gripper beads are transported by moving

the traps away from the cell to safe locations. Once the gripper beads move away from the cell, they are released from the corresponding traps by switching off the laser. We did not observe any tendency for the gripper beads to stick to cells due to surface tension in our experiments involving yeast cells and silica beads. Hence, simply moving the beads away from the cell was adequate to release the cell. We also observed that once beads were not trapped, Brownian motion alone was adequate to keep the beads and the cells apart from each other. For manipulating sticky cells, gripper beads may need to be functionalized with appropriate coatings to reduce the adhesion to the cell.

A formation with a higher number of beads, although more stable, requires higher laser power and hence causes the target cell to be exposed to more intense laser beam compared to a formation with fewer number of beads. Moreover, it requires larger clearance space in the workspace for safe navigation. We have analyzed the performance of each gripper formations in terms of the minimum laser power required to transport a cell at a given speed without the formation falling apart. We also measured the corresponding average laser intensity experienced by the cell using the method described in [CSW$^+$12, KCA$^+$11]. We record the minimum laser power required and corresponding average laser intensity experienced by the cell for a particular transport speed setting. For each setting we run 10 experiments to be statistically accurate. The results of the analysis are summarized in Table 6.2. Depending on the sensitivity of a cell to the laser (in terms of allowable average laser intensity) and required transport speed, an appropriate gripper can be chosen based in Table 6.2.

To provide a direct comparison between G_3 and G_6, we have experimentally determined the maximum allowable speeds of the traps during rotation without the formation getting destabilized. We determined the maximum speed for G_3 as 3.3 µm/s. Transport speeds higher than the allowable limit will position the traps closer to the cell, which results in trapping the cell before the gripper beads can move towards them even at higher laser power. To navigate through a path with the curvature of 90 degrees, G_3 will require approximately 4 s more time than G_6. However, G_3 will use about 40% of the laser power used by G_6. Moreover, the formation can be utilized in denser obstacle field compared to G_6. The formation G_6 can be useful for highly targeted experiments with less sensitive cells in a small population where reliability of transport is more important.

6.6 Summary

In this chapter, we have presented an approach for automated, indirect transport of cells using planar gripper formations consisting of 2, 3, 4, and 6 beads. We used A* based path planning algorithm to generate collision-free paths for the formations. We designed a cost function for the developed planner to be able to find executable paths that minimize the transport time. We have also developed a feedback controller for the gripper to select and execute appropriate maneuvers when following the path. The maneuvers are used for determining the required trap positions for the formation and maintaining its stability.

The main contributions of this chapter include the following:

(i.) We present an approach for automated indirect manipulation, including ro-

tation and linear displacement, of biological cells using planar gripper formations.

(ii.) We present a global path planner based on the A* algorithm [HNR68] to automatically transport cells using cell-based gripper formations along collision-free paths.

(iii.) We demonstrate experimental results of the developed automated indirect cell transport and path planning.

(iv.) We present detailed experimental evaluation results of gripper formations in terms of their stability, transport speed, and required laser power.

In future, dynamical interactions between a cell and gripper beads can be considered to develop a model predictive control for robust transport of cells. The gripper formations reported in this chapter are tested only for transporting spherical cells. In general, cells can be of arbitrary shapes. Gripper formations can be synthesized to transport cells of irregular shapes as introduced in Chapter 5 for spherical cells.

Chapter 7
Automated Indirect Manipulation of Irregular Shaped Cells With Optical Tweezers for Studying Collective Cell Migration

This chapter[7], presents a planning approach for automated indirect manipulation of irregular shaped cells in order to study collective cell migration. Studying collective migration of cells is currently of considerable interest in biology and medicine leading to possibility of novel diagnosis and treatments, for example, in cancer research. We propose optical tweezers as a useful tool for dynamically positioning of cells in certain geometrical patterns to allow new discoveries on how cell-signaling influences their collective behaviors. Some cells are highly sensitive to direct laser exposure, which may influence their behavior or even cause photodamage. In addition, manual manipulation of cells is time consuming making it hard to carry out systematic studies that are properly timed to exhibit the desired motility. We have developed an automated planning approach for precise, collision-free, indirect manipulation of cells with irregular, dynamically changing shapes using Optical Tweezers (OT). We use a triangular triplet formation for indirect pushing of a cell. This particular formation has the advantage of preventing laser exposure on the cell and is highly stable and thus suitable for automated indirect manipulation. We have carried out an experimental study to demonstrate the effect of indirect pushing using the triplet formation on cell-viability. We find that the triplet formation does not influence the boundary protrusions of *Dictyostelium discoideum*

[7] The work in this chapter is partially derived from the published work in [CTW+13].

cells and generation of blebs in contrast to direct trapping or gripping approaches. We have evaluated the effectiveness of our manipulation approach using physical experiments.

7.1 Introduction

Collective cell migration [IF09] plays a prominent role in various highly regulated processes and physiological conditions during animal development such as embryogenesis, wound healing, or cancer. Gaining insights into the behavior of the cell migration may help in effective diagnosis and therapy for cancer treatment. *Dictyostelium discoideum* cells [AF09] are used as model organisms for studying cell-signaling and collective migration. When polarized, they migrate using protrusions. The protrusions start at the front of the cells and then propagate along their boundaries at speeds of tens of micrometers per minute [DFL11]. In order to study how the cells behave collectively, they need to be positioned in certain geometrical patterns. Figure 7.1 shows the collective migration of polarized *Dictyostelium* cells towards the highest concentration gradient of the chemoattractant cAMP. Cells formed chain by extending the protrusions towards the trailing end of the leading cell. Now, in order to understand how the cells can track the concentration gradient, a new sets of experiments can be designed, for example, cells can be constantly rearranged in a stack with their leading and trailing protrusion ends being flipped and observe how they behave under the new scenarios. This requires an automated tool for fast and precise, simultaneous micromanipulation of the cells. Various tools for micromanipulation of cells have been developed (e.g., microfluidics, electrophoresis,

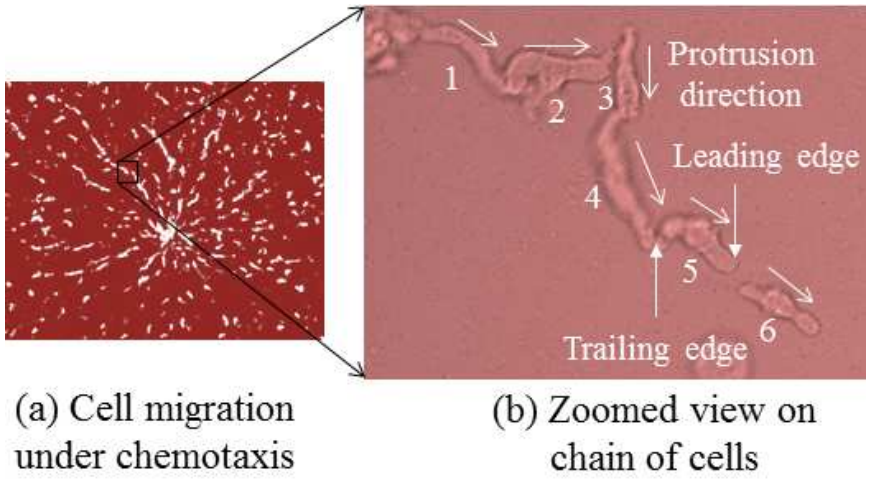

Figure 7.1: *Collective cell migration during chemotaxis (Courtesy: Chenlu Wang and Dr. Wolfgang Losert): (a) cells migrate towards the highest concentration of the chemoattractant cAMP, and (b) cells form chains by tracking the back of other cells*

magnetic manipulation, AFM, acoustic tweezers, and Optical Tweezers) [CPPM08]. Optical Tweezers (OT) has recently become a popular tool [BCLG11] that uses a highly focused laser beam exerting gradient and scattering forces to stably trap a particle at the focal point [Ash92]. However, direct manipulation by a laser beam can cause significant photodamage to the cells.

In order to reduce the laser exposure, several approaches have been proposed, namely (1) the use of a laser beam with lesser intensity, (2) the use of feedback control during manipulation to increase the trap effectiveness [HZM09], (3) the use of optimum laser wavelength [NCL$^+$99], and (4) indirect manipulation using grippers made of silica beads (we term it as direct gripping in this chapter) [CTW$^+$12], functionalized microbeads [AEM$^+$07], or microtools [AOIM09], or pushing using 2-bead chains [TCW$^+$12]. Indirect gripping of a cell (i.e., the cell is partially exposed to a laser beam) even with lower laser power is not suitable for sensitive cells such as

Dictyostelium. Similarly, using optimal laser wavelength may influence the behavior of the cell, and in general has to be specifically tuned for a particular type and size of the cell. Pushing using 2-bead chains is highly unstable, slowing down the manipulation process.

In this chapter, we use triangular pushing triplet formations consisting of an intermediate bead that is not directly trapped, and is positioned between two optically trapped beads and a target cell (see Figure 7.2a). The formation has the advantage of preventing laser exposure to the cell and is highly stable which makes it particularly suitable for automation. We have carried out an experimental study to demonstrate the effect of indirect pushing using the triplet formation on cell-viability. We specifically compare it with direct trapping and gripping approaches.

Since cells constantly change, divide, and migrate, many biological experiments are constrained by the available time to set up cells in a desired configuration. Manual manipulation of optically trapped beads to push the intermediate bead and thereby the cell towards its desired pose may be time consuming, and at times even infeasible when pushing more than one cell is needed. We have developed an automated manipulation approach for dynamic positioning of an irregular shaped cell using triangular triplet formations. The developed approach is able to handle dynamically changing shape of the cell.

7.2 Problem overview and terminology

We used the following terminology throughout the chapter.

Gripper Formation is defined as $\Gamma_n = \{\{\vec{P}_{B,i}, \vec{P}_I\}, |\vec{P}_{B,i}, \vec{P}_I \in \mathbb{R}^2, i = 1, 2, \ldots, n\}$,

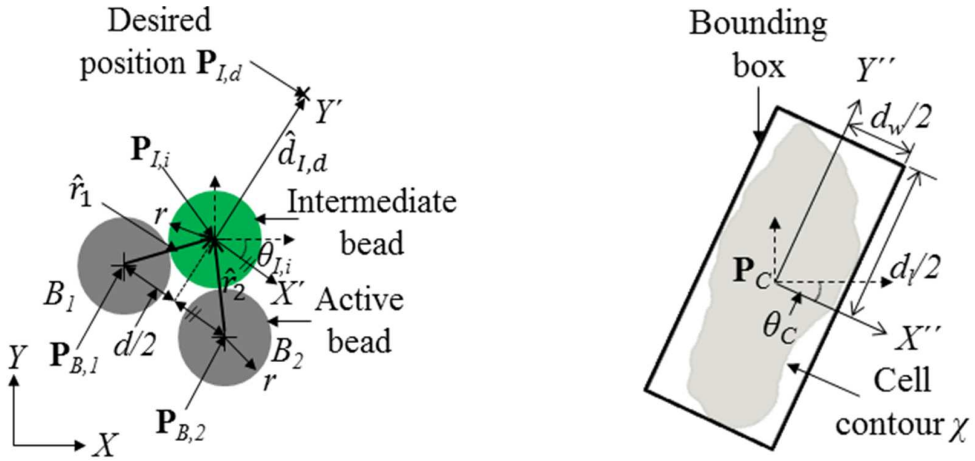

Figure 7.2: *Gripper formation state and cell state: (a) two bead gripper formation, and (b)cell state with irregular shaped contour*

that consists of n active beads, where each bead B_i has a position $P_{B,i}$ in the local coordinate system (X', Y') of the formation. The origin of the formation is defined by P_I that represents a position of the intermediate bead I in the global coordinate system (X, Y). The intermediate bead is not directly trapped by the laser during the manipulation of the cell. Figure 7.2a shows an example of Γ_2 where two active beads are separated by a distance d. During the manipulation operation, $\{B_i\}_{i=1}^{n}$ are held with their corresponding optical traps $T_i, i = 1, 2, \ldots, n$ by setting the status of the laser beam λ to 1. The intermediate bead is not trapped and thus indirectly manipulated by the laser.

Gripper Formation State is defined as $\vec{x}_\gamma = [\vec{P}_I, \theta_I]^T$, $\vec{P}_I \in \mathbb{R}^2$ is the position (identical to the position of I) and θ_I is the orientation of the formation in (X, Y) (see Figure 7.2a).

Cell State is defined as $\vec{x}_\psi = [\vec{P}_C, \theta_C]^T$ in which $\vec{P}_C \in \mathbb{R}^2$ is the position, θ_C is the orientation of the cell C which is the angular difference between X-Y and

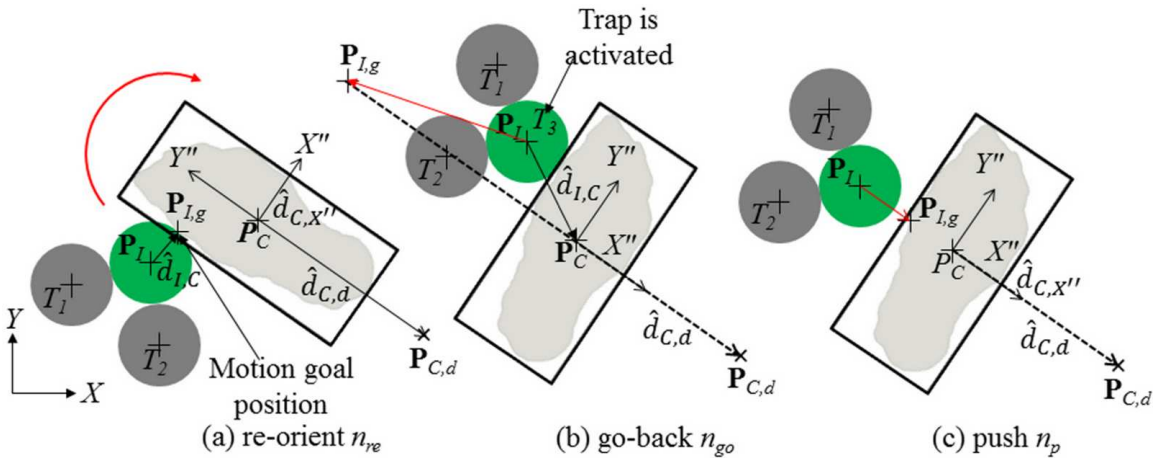

Figure 7.3: *Gripper formation-cell ensemble maneuvers: (a) re-orient r_{re}, (b) go-back r_{go}, and (c) push r_p*

the local coordinate system X''-Y''. $\vec{x}_\psi$ is determined from the bounding box of cell computed from contour information χ (see Figure 7.2b).

Obstacles is defined as $\{\Omega_i | \vec{P}_{\Omega,i} \in \mathbb{R}^2, i = 1, 2, \ldots, m\}$, where $\vec{P}_{\Omega,i}$ represents the position of an obstacle Ω_i in (X, Y). The set of obstacles includes all the cells and beads in the workspace besides the beads that are not part of Γ_n and the cell C being manipulated.

Gripper Formation Maneuver We define a maneuver set $\mathcal{M} = \{m_r, m_t, m_{re}\}$ that consists of rotate m_r, translate m_t, and re-arrange m_{re} maneuvers used by active beads $\{B_i\}_{i=1}^n$ to transport the intermediate bead I that eventually pushes the target cell C. m_r rotates the formation by a constant angle $\delta\theta_I$, m_t causes a linear translation for a constant constant distance $\delta d = [\delta x_I, \delta y_I]^T$ (δx_I and δy_I are the translations in X and Y directions respectively), while m_{re} arranges back the active beads in the formation if I is displaced from Γ_n.

Ensemble Maneuver We define a similar maneuver set $\mathcal{N} = \{n_{re}, n_p, n_{go}\}$ that consists of re-orient n_{re}, push n_p, and go-back n_{go} used by Γ_n to push the

target cell C (see Figure 7.3. Only n_{re} and n_p are used to manipulate the cell and we call them primary maneuvers. n_{go} is only invoked during switching between the primary maneuvers since the motion goal $\vec{x}_{\gamma,g} = [\vec{P}_{I,g}, \theta_{I,g}]^T$ of Γ_n also needs to be changed. It will allow the formation enough space to turn before moving towards the new motion goal without affecting the cell state. In case of n_{go} we have to trap the intermediate bead since the gripper formation cannot execute backup action (see Equation 7.4) by setting the corresponding laser status to be 1. That does not affect the cell viability since n_{go} leads the gripper formation away from the cell.

7.2.1 Problem formulation

Given,

(i.) a continuous, bounded, non-empty state space $X \in \mathbb{R}^2 \times \mathbb{S}^1$ in which each state $\vec{x}$ consists of position in (X, Y) and orientation about the Z axis,

(ii.) the current state $\vec{x}_{\psi,i} = [\vec{P}_{C,i}, \theta_{C,i}]^T$ and the goal state $\vec{x}_{\psi,g} = [\vec{P}_{C,g}, \theta_{C,g}]^T$ of the cell,

(iii.) the current state $\vec{x}_{\gamma,i}$ of the gripper formation Γ_n,

(iv.) an obstacle map Ω such that $\Omega(\vec{x}) = 1$ if $\vec{x} \in X_{obs} \subset X$, otherwise $\Omega(\vec{x}) = 0$, and

(v.) the goal region X_G represented as a permitted distance range (r_{min}, r_{max}) of the cell C from it's state $\vec{x}_{\psi,g}$.

Compute,

(i.) a collision-free global path τ_ψ between $\vec{x}_{\psi,i}$ and $\vec{x}_{\psi,g}$, where $X_{free} = X \setminus X_{obs}$,

(ii.) a motion goal $\vec{x}_{\gamma,g} = [\vec{P}_{I,g}, \theta_{I,g}]^T$ for the gripper formation Γ_n based on the desired state $\vec{x}_{\psi,d}$ of the cell and its current state $\vec{x}_{\gamma,i}$,

(iii.) a feasible path τ_γ between $\vec{x}_{\gamma,u}$ and $\vec{x}_{\gamma,g}$ for the gripper formation Γ_n, and

(iv.) a complete feedback control to select formation maneuvers $\mathcal{M}_d$ to determine the trap positions T_i and corresponding status of the laser λ for the formation Γ_n so that it can reliably follow the path τ_γ.

7.2.2 Assumptions

We approximate both the gripper beads and the intermediate bead as perfect spheres of radius r. The beads trapped by laser are assumed to move with the same velocity as the traps. This is ensured by choosing an operating speed using which the beads can be reliably trapped by the laser traps [CTW+12].

7.3 Approach

7.3.1 Solution approach

The outline of the technical approach used in this chapter can be divided into four high level tasks namely (see Figure 7.4): (1) Development of an image based feature recognition and tracking system to estimate contours of cells and positions of beads, (2) Development of a global path planner based on A* algorithm that computes the desired waypoints for the cell based on its desired initial state $\vec{x}_{\psi,i}$ and goal state $\vec{x}_{\psi,g}$, (3) Development of an algorithm to determine motion goal $\vec{x}_{\gamma,g}$ for the gripper formation based upon $\vec{x}_{\psi,i}$ and $\vec{x}_{\psi,g}$, and (4) Development of a formation

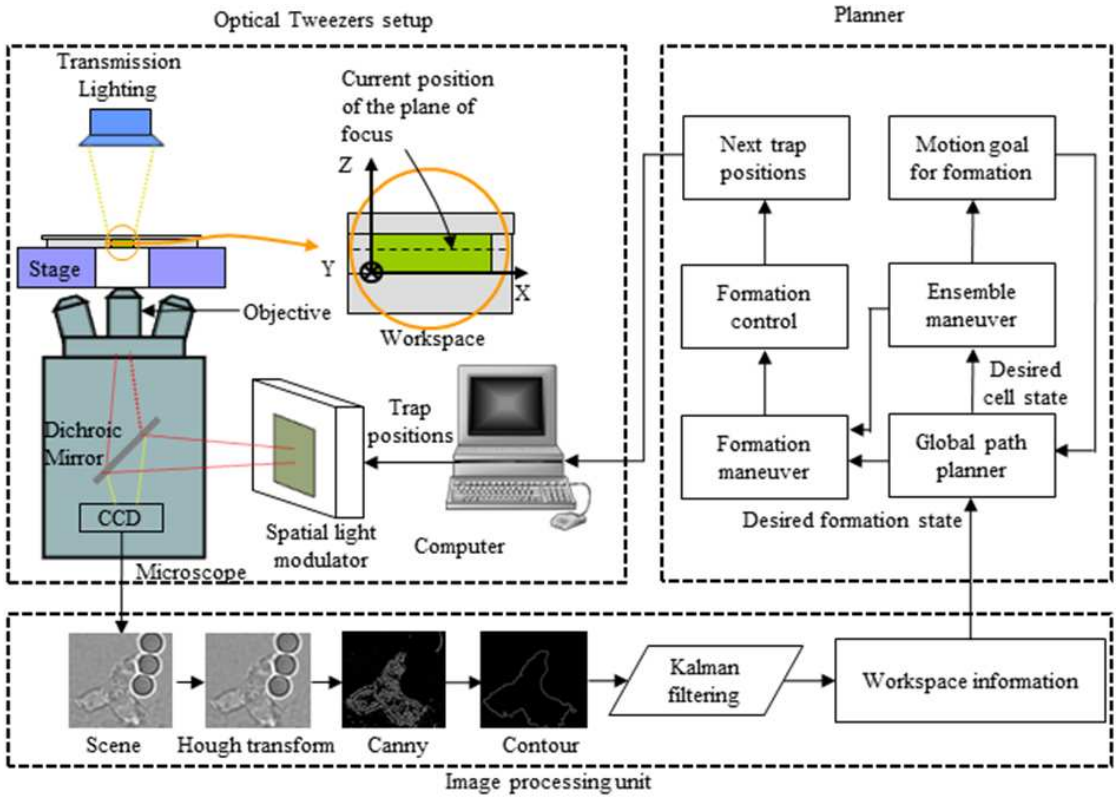

Figure 7.4: *Solution approach and OT setup*

control algorithm that determines desired maneuver $\mathcal{M}_d$ and the corresponding trap positions T_i for the gripper formation to reliably follow the desired state $\vec{x}_{\gamma,d}$.

7.3.2 State-action space representation

We discretize the continuous state space $X \in \mathbb{R}^2 \times \mathbb{S}^1$ into a finite discrete space $X_d \subset X$. $\vec{x}_{\psi}^{k}$ and $\vec{x}_{\gamma}^{k} \in X_d$ are the cell state and formation state at time step k respectively. The state space is a 3D grid with each grid cell representing a state of the formation Γ_n or the cell C.

A control action u^k is represented by a vector of velocities of individual traps and corresponding status of the laser at a given time step k (see Equation 7.1).

$$\vec{u}^k = [[\vec{v_1}^k, \lambda_1], [\vec{v_2}^k, \lambda_2], \ldots, [\vec{v_{n+1}}^k, \lambda_{n+1}]] \tag{7.1}$$

Here $\vec{v_i}^k$ represents the velocity of ith trap at time step k and n is the total number of gripper beads. (n+1)th trap corresponds to the intermediate bead I. It gets activated by setting the status λ_{n+1} of (n+1)th laser trap to be 1 whenever required based on the selected ensemble maneuver $\mathcal{N}_d$. The dynamics of formation Γ_n is described by Equations 7.2 and 7.3

$$\dot{\vec{P}}_I^k = \sum_{i=1}^{n} max(0, \vec{v_i}^k \hat{\vec{r}}_i)\hat{\vec{r}}_i \tag{7.2}$$

$$\dot{\theta}_I^k = \sum_{i=1}^{n} \left(\frac{\vec{v_i}^k}{2r} \times \hat{r}_i \right) \alpha_{contact} \tag{7.3}$$

$$\alpha_{contact} = \begin{cases} 0 & \text{if } d_{B_i,I} > 2r, \\ 1 & \text{otherwise.} \end{cases}$$

Here, $\hat{\vec{r}}_i$ (see Figure 7.2a) is the unit direction vector towards the intermediate bead from the active bead B_i and $d_{B_i,I}$ is the distance between them. The momentum is transferred to the intermediate bead only when it is in contact with the gripper beads. Hence, $\dot{\theta}_I$ is set to 0 when there is no contact.

The speed of all traps are constrained to be same (see Equation 7.4). The trap motions are constrained only parallel to the desired direction of the intermediate bead in case of formation maneuver n_t to prevent the formation from falling apart (see Equation 7.5). Similarly, the traps are restricted to move only towards the tangential direction of the intermediate bead in case of n_r (see Equation 7.6).

$$|\vec{v_i}^k| = |\vec{v_j}^k| \forall i, j, \text{where } i, j = 1, 2, 3, \ldots, n \tag{7.4}$$

$$\vec{v_i}^k \times \hat{\vec{d}}_{I,g} = 0 \tag{7.5}$$

$$\vec{v_i}^k . \hat{\vec{r}}_i = 0 \tag{7.6}$$

Here, $\hat{\vec{d}}_{I,g} = [c_{\theta_I}, s_{\theta_I}]^T$ (see Figure 7.2a) is the unit direction vector from the current position $\vec{P_{I,u}}$ towards the desired waypoint of Γ_n that is derived from it's orientation θ_I.

When Γ_n takes an action $\vec{u}^k$ at time step k, it transitions from $\vec{x}_\gamma^k$ to $\vec{x}_\gamma^{k+1}$ using Equation 7.7.

$$\vec{x}_\gamma^{k+1} = \vec{x}_\gamma^k + \dot{\vec{x}}_\gamma^k \triangle t \tag{7.7}$$

Here, $\triangle t$ is the time spent between two subsequent time steps. As the intermediate bead I comes in contact with the cell the momentum will be transferred to the cell C. We assume that Γ_n can only cause either pure rotation or pure translation to the cell. That is ensured by careful selection of it's motion goal $\vec{x}_{\gamma,g}$. The dynamics of the cell C is described using Equations 7.8 and 7.9

$$\dot{\vec{P}}_C^k = (max(\langle \dot{\vec{P}}_I^k, \hat{\vec{d}}_{I,C} \rangle, 0) \hat{\vec{d}}_{I,C}) \beta_{contact} \tag{7.8}$$

$$\dot{\theta}_C^k = (\frac{\dot{\vec{P}}_I^k}{|d_{C,I}|} \times \hat{\vec{d}}_{I,C}) \beta_{contact} \tag{7.9}$$

$$\beta_{contact} = \begin{cases} 1 & \text{if in contact,} \\ 0 & \text{otherwise.} \end{cases}$$

Here $\hat{d}_{I,C}$ is the unit vector from Γ_n towards the cell and $|d_{C,I}|$ is the perpendicular distance from $\vec{P}_C$ to the velocity vector of the gripper formation. The cell transition to time step $k+1$ is given by Equation 7.10

$$\vec{x}_{\psi}^{k+1} = \vec{x}_{\psi}^{k} + \dot{\vec{x}}_{\psi}^{k} \triangle t \tag{7.10}$$

7.3.3 Image processing

In OT setup, beads and cells are identified by processing gray-scale video (see Figure 7.5a) stream captured by a CCD camera. We used Open Source Computer Vision library (OpenCV) to detect the beads and the contour of the cells. We applied Hough transform to the input gray-scale image to identify spherical gripper beads (see Figure 7.5b). The center of the identified gripper beads are calculated before replacing them with the background (see Figure 7.5c) to isolate them from the image. We applied Canny Edge Detector [Can86] on the image containing only cell to detect the fine edges of the cell (see Figure 7.5d). We dilated the canny image to make the edges more prominent and decrease the linear gaps between them (see Figure 7.5e). The resulting image contains some disconnected black pixels inside the cell boundary. To remove the disconnected black pixels we filled all the reachable black pixels with white pixels using a flood filling algorithm (see Figure 7.5f). The while image after flood filling contains the black patches left after dilation. We took a complimentary of the image that turns the black pixels inside the cell into white (see Figure 7.5g) while makes the rest of the image black. We got a well-defined boundary of the cell by adding the dilated image with the complementary image (see Figure 7.5h). We refined all the noises by retaining the boundary with the largest

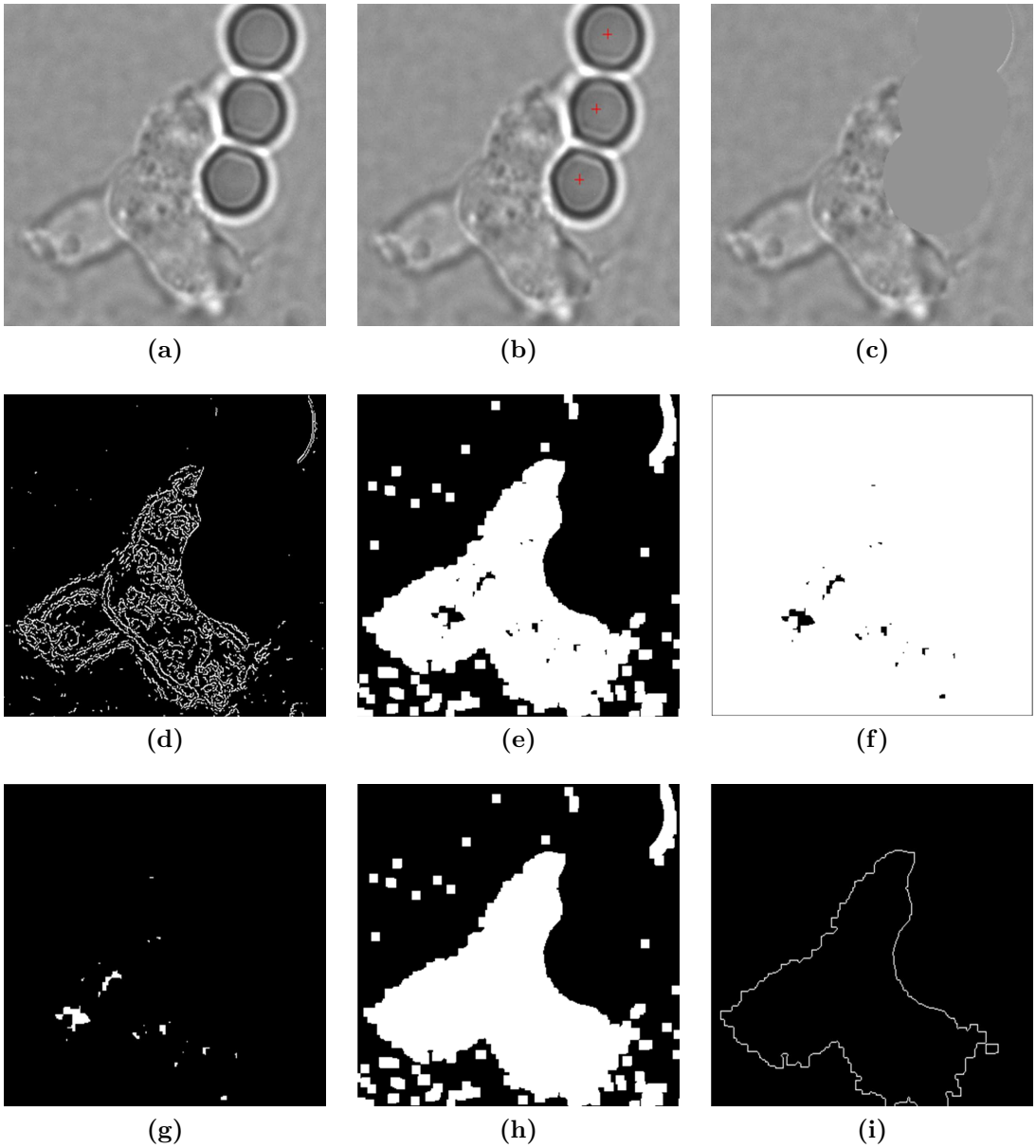

Figure 7.5: *Image processing steps: (a) input image, (b) Hough transformation to identify the beads, (c) replacing beads with background of the image to isolate the bead information, (d) identify edges using Canny Edge Detector, (e) dilate the image, (f) flood fill the image, (g) complement of the image, (h) addition of dilated image and complement image to detect the boundary, and (i) identify the contour of the image*

area since the cell represents most of the images. Finally, we determined the contour points χ of the boundary to identify the detailed shape of the cell (see Figure 7.5i). We computed the oriented bounding box and calculate it's side lengths d_l and d_w (see Figure 7.2b). The side lengths are used to compute the state $\vec{x}_\psi$ of the cell.

Before starting the planning, the planner records the contour points for 100 frames. Subtracting the contour points χ^{i-1} of (i-1)'th frame from χ^i of i'th frame gives the direction of protrusion where $i = 1, 2, 3, \ldots, 100$. The protrusion direction provides the knowledge about the leading and trailing edge of the cell that can be used by the user to select the goal state $\vec{x}_{\psi,g}$ of the cell.

7.3.4 Motion goal for gripper formation

The planner takes the current and desired state of the cell as inputs to select the desired maneuver $\mathcal{N}_d$ for the formation Γ_n. Based on the desired maneuver $\mathcal{N}_d$ the planner computes the next motion goal $\vec{x}_{\gamma,g}$ for Γ_n. Let us assume the current and next desired states for the cell are $\vec{x}_{\psi,i} = [\vec{P}_{C,i}, \theta_{C,i}]^T$ and $\vec{x}_{\psi,d} = [\vec{P}_{C,d}, \theta_{C,d}]^T$ respectively. The planner first reorient the cell such that $\langle \hat{d}_{C,X''}, \hat{d}_{C,d} \rangle = 1$ (see Figure 7.3) by calling ensemble maneuver n_{re} to align its axis perpendicular to the desired state direction. Here, $\hat{d}_{C,X''}$ is the unit vector defining the axis of the cell C and $\hat{d}_{C,d}$ is the direction vector from C towards the desired state $\vec{x}_{\psi,d}$. Then it switches to n_p to translate the cell to the desired location. Finally it again switches back to n_p to re-orient the cell to the desired orientation. Before switching to the n_p from n_{re} or vice-versa, it has to invoke n_{go} maneuver to move the gripper formation in a safe location. We have to change the motion goal to switch the ensemble

maneuver. Γ_n has to move away from the cell to provide itself enough space to move to the new motion goal $\vec{x}_{\gamma,g}$ without affecting the cell orientation. We define a reference position $\vec{P}_{I',g}$ as shown in Equation 7.11 to define the motion goal position for Γ_n.

$$\vec{P}_{I',g} = \begin{cases} \vec{P}_{C,i} + c_{\theta_{C,i}}/4[d_l, -d_w] & \text{if } \delta\theta_C\text{is positive,} \\ \vec{P}_{C,i} + c_{\theta_{C,i}}/4[-d_l, -d_w] & \text{if negative} \\ \vec{P}_{C,i} + c_{\theta_{C,i}}/4[0, -d_w] & \text{if 0} \end{cases} \tag{7.11}$$

Here $\delta\theta_C = \theta_{C,d} - \theta_{C,i}$. We now compute the nearest contour point from the contour data χ of the cell to compute the motion goal position $\vec{P}_{I,g}$. The orientation $\theta_{\gamma,g}$ is set to the desired orientation of the cell. For n_{go} maneuver we project the cell state to a new state as shown in Equation 7.12

$$\vec{x}_{\gamma,g} = [\vec{P}_{C,i} + 4rc_{\theta_{C,i}}[0, -d_w], \theta_{\gamma,u}]^T \tag{7.12}$$

The desired maneuver $\mathcal{N}_d$ is computed using Algorithm 1.

7.3.5 Global path planner

We use the A* based global path planner for computing the intermediate states for both Γ_n and C that iteratively expands nodes from the initial state $\vec{x}_i$ to goal state $\vec{x}_g$ using a cost function $f(\vec{x})$. We use a similar cost function as described in [CTW+12] that takes transport time for both re-orientation and translation into account to compute the collision-free path with minimum time.

Input: Ensemble maneuver library $\mathcal{N}$, planning time t_p, previously executed maneuver $\mathcal{N}_p$, current state of gripper $\vec{x}_{\gamma,i}$, current state $\vec{x}_{\psi,i}$ and desired state $\vec{x}_{\psi,d}$ of the cell, a user defined threshold difference between current and desired orientation of cell $\theta_{C,th}$, a binary variable *go-back-reach* that indicates whether the motion goal for *go-back* maneuver is reached or not .

Output: Desired maneuver $\mathcal{N}_d$ for the gripper formation-cell ensemble.

1: Compute $\delta\theta_C = \theta_{C,i}$ - $\theta_{C,d}$.
2: Compute $\delta d_{C,I} = \vec{P}_{C,i}$ - $\vec{P}_{I,i}$
3: Compute $align = \langle \hat{d}_{C,X''}, \hat{d}_{C,d} \rangle$ (see Figure 7.3)
4: **if** $\parallel \delta\theta_C \parallel < \theta_{C,th} \parallel align < 1$ **then**
5: **if** $t_p = 0 \parallel \mathcal{N}_p = n_p \parallel (\mathcal{N}_p = n_{go}$ && *go-back-reach* $= TRUE) \parallel \parallel \delta d_{C,I} \parallel > 4r$ **then**
6: set $\mathcal{N}_d \leftarrow n_p$
7: **else**
8: set $\mathcal{N}_d \leftarrow n_{go}$
9: **end if**
10: **else**
11: **if** $t_p = 0 \parallel \mathcal{N}_p = n_{re} \parallel (\mathcal{N}_p = n_{go}$ && *go-back-reach* $= TRUE) \parallel \parallel \delta d_{C,I} \parallel \geq 4r$ **then**
12: set $\mathcal{N}_d \leftarrow n_{re}$
13: **else**
14: set $\mathcal{N}_d \leftarrow n_{go}$
15: **end if**
16: **end if**
17: **return** $\mathcal{N}_d$.

Algorithm 1: GRIPPER-CELLMANUEVERSELECTION(): Compute the desired maneuver for the gripper formation Γ_n to determine it's the motion goal.

7.3.6 Formation control

In this section we describe a feed-back policy to determine the trap positions T_i in order to transport the cell towards the desired state $x_{\psi,d}$. The trap positions are determined by the choice of ensemble maneuver $\mathcal{N}_d$. We use the global path planner to compute the desired next state $\vec{x}_{\gamma,d}$ of the formation based on its motion goal state $\vec{x}_{\gamma,g}$ computed in section 7.3.4. Based on $\vec{x}_{\gamma,d}$ the required formation maneuver $\mathcal{M}_d$ is selected as shown in Algorithm 2. m_t transports the formation linearly, m_r changes the orientation of the formation, and m_{re} keeps the traps stationary to allow

the active beads to move into the formation [CTW+12]. The desired trap positions associated with the active beads B_i in our triple formation Γ_2 can be determined from the desired formation state $\vec{x}_{\psi,d}$ as shown in Equation 7.13

$$\begin{aligned} T_1 &= \vec{P}_I - D_1 - D_2 \\ T_2 &= \vec{P}_I - D_1 + D_2 \\ T_3 &= \vec{P}_I \end{aligned} \tag{7.13}$$

Here, $D_1 = \sqrt{4r^2 - \frac{d^2}{4}}[c_{\theta_{I,d}}, s_{\theta_{I,d}}]^T$ and $D_2 = \frac{d}{2}[s_{\theta_{I,d}}, -c_{\theta_{I,d}}]^T$. The algorithm for selecting the desired trap positions T_i is shown in Algorithm 2

7.4 Results and discussions

7.4.1 Cell preparation and experimental setup

AX3 *D. discoideum* were grown in HL-5 media at the concentration below 4×10^6 cells/mL at 21℃, starved at the concentration of 1×10^7 cell/mL in develop buffer (5 mM Na_2HPO_4, pH 6.2, 2 mM $MgSO_4$, and 0.2 mM $CaCl_2$) with pulses of 80 μM of cAMP every 6 minutes for 5 hours, shaking at 140 rpm [SLB+10]. Cell pellets were gathered by centrifuging at 500 g in 1 mL micro-centrifuge tube and aspirating the supernatant. Cell pellets were washed twice with DI water afterwards for washing out ions containing in the develop buffer. 1×10^5 cells were added into a chamber (0.8 cm^2 surface area) that containing 400 μL DI water and were allowed to settle down for 15 minutes. 10 μL of silica beads (5 μm) solution (0.01% solid, from Microsil) were added into the same chamber and were allowed to settle down for 10 mins. Cells and silica beads remained suspending in DI water during manipulation experiments because of the electronic repulsion between cover-glass surface (negative

Input: Planning time t_p, current state of gripper $\vec{x}_{\gamma,i}$, current state $\vec{x}_{\psi,i}$ and desired state $\vec{x}_{\psi,d}$ of the cell, a binary variable *go-back-reach*, goal region X_G, a user defined threshold difference between current and desired orientation of gripper formation $\theta_{I,th}$, formation deviation threshold l_{th} .

Output: trap positions T_i along with corresponding laser status λ_i .

Initialize $t_p \leftarrow 0$.
while $\parallel \vec{P}_{C,d} - \vec{P}_{C,i} \parallel < X_g$ **do**
  if $t_p = 0$ **then**
    set *go-back-reach* $\leftarrow TRUE$
  end if
  compute desired ensemble maneuver $\mathcal{N}_d$ using Algorithm 1
  compute the desired motion goal $\vec{x}_{\gamma,g}$ for the formation Γ_n (see Equations 7.11 and 7.12)
  compute the desired next state $\vec{x}_{\gamma,d}$ for Γ_n using global path planner
  if $\mathcal{N}_d = n_{go}$ **then**
    if $\parallel \vec{P}_{I,i} - \vec{P}_{I,d} \parallel < X_g$ **then**
      set $\lambda_{n+1} \leftarrow 1$
      set *go-back-reach* $\leftarrow FALSE$
    else
      set $\lambda_{n+1} \leftarrow 0$
      set *go-back-reach* $\leftarrow TRUE$
    end if
  end if
  if $\parallel \vec{P}_{B,i} - T_i \parallel < l_{th}$ **then**
    set $\mathcal{M}_d \leftarrow m_{re}$
  else
    if $\parallel \theta_{I,i} - \theta_{I,d} \parallel < \theta_{I,th}$ **then**
      set $\mathcal{M}_d \leftarrow m_r$
    else
      set $\mathcal{M}_d \leftarrow m_t$
    end if
  end if
  compute the desired bead locations corresponding to $\mathcal{M}_d$
  compute the corresponding trap positions T_i along with laser status λ_i using Equation 7.13
  set $t_p \leftarrow t_p + 1$
end while
return T_i.

Algorithm 2: COMPUTETRAPPOSITIONS(): Compute the desired laser trap positions based on the selection of formation maneuvers

charged) and cell membrane/surface of silica beads (negative charged). We used the same OT setup described in [CTW+12].

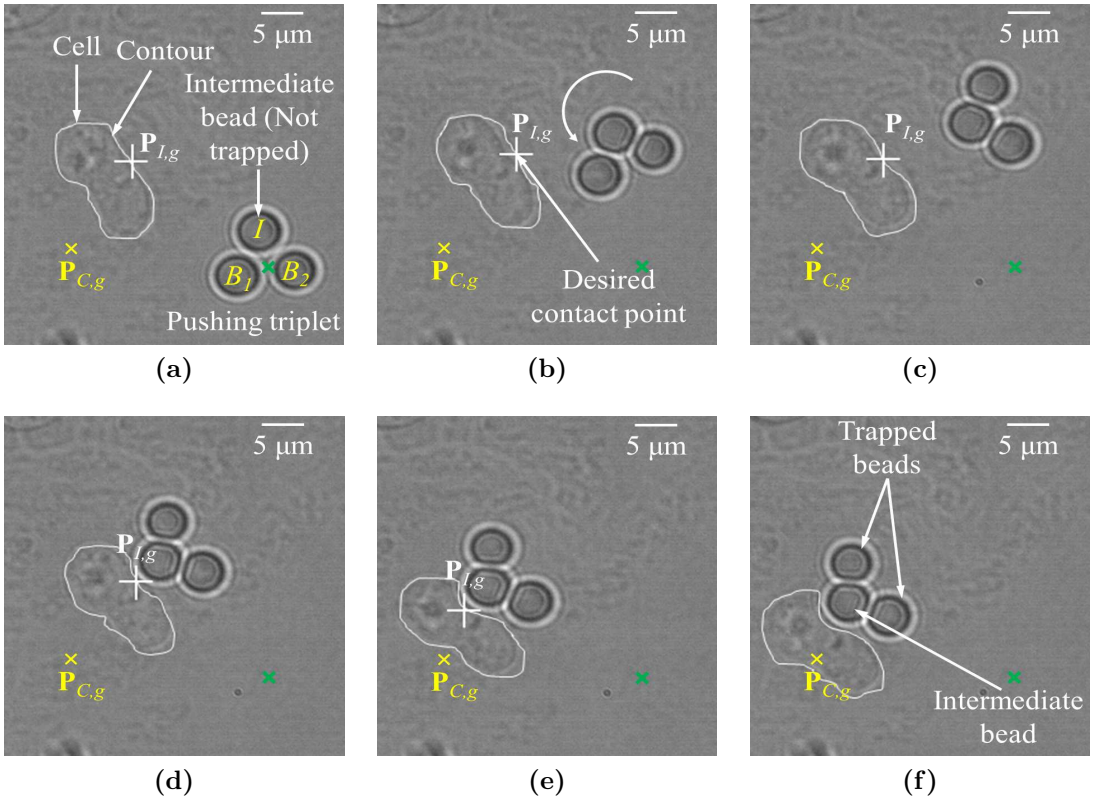

Figure 7.6: *Pushing a Dictyostelium cell: (a) initial scene (initial and goal locations are marked by green and yellow × signs respectively), (b) gripper Γ_2 rotates to change the direction to align itself with the direction of push, (c) Γ_2 aligns itself, (d) Γ_2 reaches the first motion goal, (e) Γ_2 starts pushing the the cell towards the goal G, and (f) cell reaches the goal*

7.4.2 Experimental results

We showed the automatic execution of two ensemble maneuvers, i.e., n_p and n_{re} with experiments to show the effectiveness of the planner. We also assessed the viability of the cell while manipulating with our triplet formation Γ_2 and compare with it with direct trapping and direct gripping approach.

Figure 7.6 shows the pushing operation of a *Dictyostelium* cell with Γ_2. The goal position $\vec{P}_{C,g}$ of cell is marked using yellow "×" sign. The planner selects the motion goal $\vec{x}_{\gamma,g}$ for Γ_2 accordingly. The motion goal position $\vec{P}_{I,g}$ is marked by

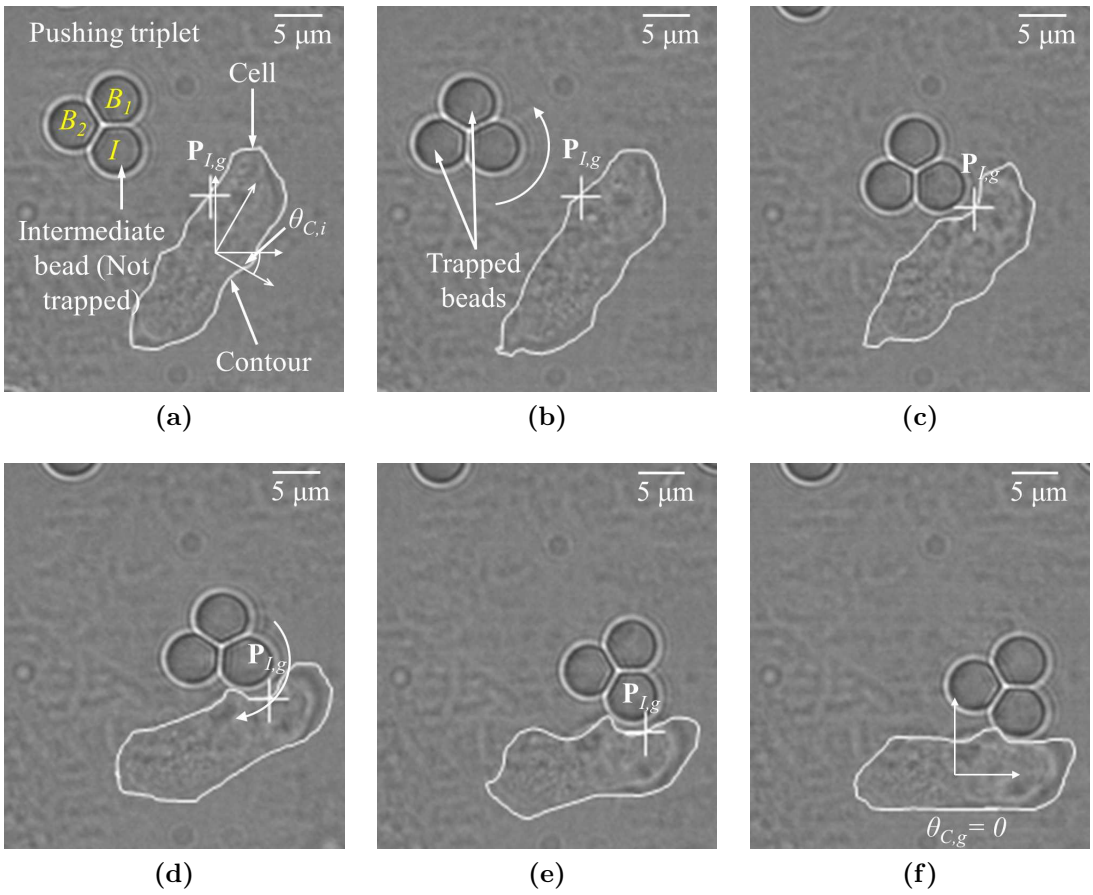

Figure 7.7: *Re-orientation of a Dictyostelium cell: (a) initial scene with the cell with orientation $\theta_{C,i}$, (b) gripper Γ_2 rotates to change the direction towards the motion goal, (c) Γ_2 reaches the first motion goal, (d) Γ_2 pushes the cell to gets re-oriented, (e) Γ_2 changes the motion goal to move the cell to the desired orientation $\theta_{C,g}$, and (f) cell reaches the final orientation $\theta_{C,g}$*

using white "+" sign. However, the dynamic behavior of the cell constantly changes it's state. The planner eventually changes $\vec{x}_{\gamma,g}$ by changing the final orientation of Γ_2 to be able to push the cell towards the goal location. The laser power is set to the minimum (0.2 watt) that is enough to trap two beads. The intermediate bead is not trapped by the laser. Γ_2 first executes m_t formation maneuver in order to reach the first desired state (see Figure 7.6b) that is computed based on the motion goal $\vec{x}_{\gamma,g}$. It then uses m_r maneuver to change the direction of transport (see Figure 7.6b). Cell gets deviated from its current position due to it's dynamic nature. Hence the motion goal $\vec{x}_{\gamma,g}$ also dynamically changes. Γ_2 reaches its motion goal (section 7.3.4) with the execution of m_t maneuver (see Figure 7.6). The motion goal gets updated towards the course of pushing until the cell reaches its desired state. Triplet formation is much more stable because the momentum transfer from trapped beads to the intermediate bead is more efficient and directional compared to single bead unstable pushing shown by Thakur *et al.* [TCW$^+$12]. Moreover, the minimum laser power (0.2 watt) is divided into two beads that further decreases the detrimental effect of laser on the cell.

Γ_2 uses a similar set of maneuvers to re-orient the cell from an initial orientation $\theta_{C,i}$ to a final orientation $\theta_{C,g}$ of 0.0. Γ_2 changes the motion goal state $\vec{x}_{\gamma,g}$ by changing the orientation in order to maneuver the cell to its final orientation $\theta_{C,g}$. Based on the motion goal state $\vec{x}_{\gamma,g}$, the formation Γ_2 chooses appropriate maneuvers $\mathcal{M}_d$ until the cell achieves it's final orientation (see Figure 7.7).

We studied the viability of the cell while indirect gripping using triplet formation. We used the cell's ability to extend protrusion during and after manipulation

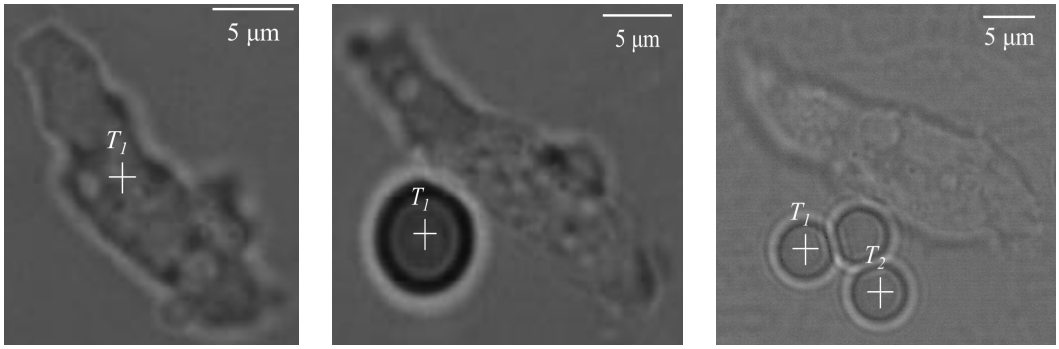

(a) **(b)** **(c)**

Figure 7.8: *Three different approaches (T_i indicates the position of laser traps): (a) direct trapping, (b) direct gripping, and (c) indirect pushing using triple formation* Γ_2

Table 7.1: *Experiments of cell viability for direct trapping, direct gripping and indirect gripping (Courtesy: Chenlu Wang and Dr. Wolfgang Losert)*

Manipulation type	generate protrusion during manipulation(%)	generate protrusion after manipulation(%)	generate blab(%)
Direct trapping	8.3	0	75
Direct gripping	50	0	40
Indirect gripping	100	100	0

and the generation of bleb after manipulation to assess the viability of cell. The generation of bleb is considered as a deteriorating cell health condition. We used three manipulation modes to compare the cell viability namely: direct trapping, direct gripping using gripper formations [CTW+12], and using our triplet formation (see Figure 7.8). The results of 10 experiments are summarized in Table 7.1. It shows cells are able to extend protrusion both during and after manipulation in case of triplet formation. Moreover, cells do not produce bleb in case of indirect manipulation with triplet formation.

7.5 Summary

In this chapter, we have proposed a comprehensive approach capable of automated Optical Tweezers-based micromanipulation of cells with irregular, dynamically changing shapes. We have demonstrated the effectiveness of the developed approach by automatically manipulating a *Dictyostelium discoideum* cell using *push* and *re-orient* ensemble maneuvers. The developed approach can manipulate the cell with high precision and speed, while maintaining a high stability of the triplet formation. In addition, we have carried out an experiment to study the effect the indirect pushing has on viability of the cell. We specifically compared the indirect pushing versus direct trapping and gripping approaches. We found that the indirect pushing does not influence the creation of boundary protrusions of *Dictyostelium discoideum* cells and generation of blebs.

The workspace of OT is very small compared to the dimension of polarized *Dictyostelium discoideum* cells. Hence, in future automated control of the stage can be integrated for dynamically changing the workspace. In addition, the developed approach can be applied for dynamical evaluation and improvement of a mathematical model of the cell behavior. This will require complex planning strategies.

Chapter 8
Conclusions

This chapter presents the intellectual contributions and anticipated benefits from the work proposed in this dissertation.

8.1 Intellectual Contributions

The research issues listed in chapter 1 broadly aims toward building experimental framework and development of algorithms to automate cell manipulation using holographic optical tweezers. Some of the key expected contributions are described as follows:

1. *Physically accurate simulation under the influence of external force field to enhance the performance of real time planner*: A simulator is developed for simulating the motion of particles under the influence of external fluid flow inside a microfluidic chamber. The fluid velocity at a discrete location inside the microfluidic chamber is computed using computational fluid dynamic simulations. An experimental approach is developed by using high speed camera to validate simulated fluid velocity. Intensive offline simulation is performed to estimate the probability of a particle to reach one of the exits of the chamber if released at a location inside. Conventional planning algorithms do not take the physics of the environment account. Hence, the resulting strategies are sometimes not feasible or cannot generate successful actions based on the surrounding scenarios. For example, moving a particle across the fluid flow

may result in the particle getting knocked out of the optical trap. This dissertation demonstrates how offline simulations can be utilized to increase the performance of online planning.

2. *Novel planner with fast replanning capability for automated transport of particles inside microfluidics* : This dissertation develops a novel heuristic planning algorithm for automated transport of multiple cells inside a microfluidic chamber. The planner utilizes the offline simulations for determining an optimized released location for a cell from the optical trap. It uses a novel state-action space representation that can provide fast search capability in determining the release locations for the cells that have higher probabilities to reach one of the exits. The effectiveness of search is increased with a novel heuristic cost function that takes the fluid velocity as well as the reaching probability of the particle to the exit into account. The fluid velocity component of the cost function helps the planner taking actions that have higher success rates in transporting cell. On the other hand, reaching probability component helps the planner to decide the release location for the cell. The planner with a composite heuristic cost functions limits the probability of cells being knocked out the traps by the fluid flow and the laser power drawn during manipulation. The use of low laser power reduces the chance of cells getting damaged during manipulation.

3. *Highly precise long distance transport operation in hybrid setup*: This dissertation realizes a hybrid manipulation approach by integrating microfluidics

with optical tweezers. Microfluidics is particularly good for high throughput operation whereas optical tweezers is well-known for it's highly precise manipulation. Combining these two in a single manipulation setup provides the opportunity for high throughput manipulation with superb precision. Integrating microfluidics with optical tweezers requires a long distance transport capability by optical tweezers. This dissertation introduces an automated stage planning approach to realize the long distance transport capability using optical tweezers. The long distance transport is achieved by moving the motorized stage while keeping the optical traps stationary. After long distance gross transport, the high precision of optical trap motion is utilized for fine positioning of particles at the desired goal locations. The trap update rate is limited by the frequency of SLM which is about 15 Hz whereas the frequency of motorized stage controller is about 6 MHz. High frequency of motorized stage controller enables fast transport of particles over a long distance. Both the stage and trap motions are synchronized for transporting particles automatically to the desired locations inside the microfluidic chamber.

4. *Gripper synthesis for indirect manipulation of cells*: This dissertation introduces a novel approach for keeping the cell out of the reach of detrimental laser during manipulation using OT. Multiple inert silica microspheres are optically trapped by laser to form a gripper to grip the cell indirectly. Since the cell is not directly trapped by laser, the exposed intensity is reduced. The positions of the microparticles inside the gripper need to be carefully selected for effec-

tive gripping as well as to minimize the exposure of the laser. A constrained multi-objective optimization framework is developed which can automatically derive the best configuration based on the geometry of the cell. A sampling based approach is developed by considering the geometry of the cells and the laser cones to compute the average intensity experienced by the cell inside the gripper. The robustness of the gripping is measured by computing the volume of the convex hull of the configuration. However, every configuration is not suitable for gripping. The configurations need to satisfy the closure properties for stable gripping. The optimization framework models all the constraints to synthesize the optimized gripper configurations.

5. *Planning with feedback policy for reliable manipulation of cells using gripper formations*: This dissertation develops a novel approach for automated manipulation of cells using gripper formations. This requires moving multiple laser beams to move microparticles while keeping the cell inside the gripper formation. The planner has to deal with multiplexed laser traps to control the inert micropartilces in a gripper that manipulate the cell indirectly. The interaction of multiple laser traps among themselves as well as with the microparticles are considered while deriving the planning strategies. A kinematic model of the particle motion is used to develop the state-transition model that is utilized by the planner to compute the desired actions. The motion constraints specific to a certain gripper configuration are considered to design a novel heuristic cost function that can derive path with minimum transport time. The plan-

ner not only derives collision-free path but also gives low level decision on how to move the gripper along a trajectory. It utilizes three different maneuvers to move the gripper along a path. Based on a desired waypoint planner can decide which maneuver needs to be executed for reliable transport. Because of non-uniform trapping force distribution in the workspace, the planner has to provide more time at certain locations to move the particles in order to retain the formation of the gripper. The planner uses a dedicated maneuver for allowing more time to move the microparticles when it detects lower trapping force. A feedback policy is developed based on inverse kinematics to compute the desired maneuver for reliable transport of cell. The performance of the different gripper formations is also characterized based on the dexterity of manipulation and required laser power for execution.

6. *Automated pushing based approach for manipulating sensitive cells* : This dissertation demonstrates a pushing based manipulation approach for automated manipulation of irregular shaped sensitive cells e.g. *Dictyostelium discoideum*. Gripper formations are not suitable for manipulating sensitive cells because they cannot prevent all the laser exposed to the cell rather a maximum portion of it. This dissertation develops a new pushing formation which is suitable for manipulating irregular shaped sensitive cells. It can provide zero exposure of laser to the cell. The pushing formation is composed of two optically trapped beads and an intermediate bead which is not directly controlled by laser. The intermediate bead acts as an insulator between the

cell and the optically trapped active beads. The trapped beads push the intermediate bead which eventually pushes the cell to the desired direction. An image processing algorithm is developed for computing the contour of the cell online that is utilized by the planner. A four-layered planning algorithm is developed for pushing the cell autonomously. Based on the initial and final state of the cell, the top layer computes a collision free path for the cell. The second layer takes the current and desired next state of the cell as input and determines the desired goal state for the pushing formation. The third layer computes the path for the pushing formation. Finally the lowest layer determines the desired maneuver to reliably transport the pushing formation to its goal state. Multi-layered features of the planner ensure reliable transport of sensitive cell. The viability experiment on cell demonstrates the effectiveness of the pushing based manipulation.

8.2 Anticipated Benefits

This dissertation work addresses the key issue of optical manipulation of biological objects. As discussed in chapter 2 the main limitation of OT manipulation is lack of automation that limits its manipulation speed and throughput significantly. Despite being one of the most precise manipulation techniques, the biologists are still skeptical about its usefulness because of its slow manipulation which is very important for biological studies that needs to be properly timed to exhibit desired motility. Cancer studies in particular will be highly benefited from our developed automated planning approaches. Precise manipulation of cells to arrange them in

certain pattern will help us understand how the cancer cells send signals to their neighbors during collective migration towards a certain direction. The long distance manipulation capability of optical tweezers discussed in chapter 4 will help in manipulating a large number of cells simultaneously. A group of cells can be monitored and actively manipulated to derive the underlying mechanism of their migration behavior.

Hybrid manipulation approaches combining OT and microfluidics can be utilized for enhanced cell sorting which is a fundamental step in stem cell research. The fine manipulation using optical tweezers can be utilized for arranging stem cells in a uniform concentrated density inside the microfluidic device to mimic biological tissue. All these automated manipulation approaches will help the biologists monitoring a large number of cells inside microfluidic chamber.

The health care industry will be greatly benefited from this dissertation. The manipulation of cell is a necessary primary task in studying the effects of drugs on a group of cells. These automated manipulation algorithms can be heavily used in studying how a particular pathogen invades to its host cell. Precise manipulation of both pathogen and host cell will enable close monitoring of invading events. This will open up the possibility of developing new drugs that can prevent the pathogen to invade the host cell. OT assisted microfluidic chamber can be transformed into a modern cell diagnosis tool with the integration of all the automated approaches developed in this dissertation. Cells can be arranged uniformly inside the chamber with the use of optical tweezers before applying a certain drug. The drug is collected from the exit of the chamber after it interacts with the cell. The effectiveness of the

drug can be determined by analyzing the drug collected at the exit of the chamber. The uniform of distribution of the cell will ensure statistically accurate results in analyzing the drug.

8.3 Future Directions

This dissertation provides a solid foundation for automated cell manipulation using optical tweezers. The approaches discussed here can be extended in the following directions to provide better maneuverability of optical tweezers in cell manipulation.

1. *Simultaneous gross and fine manipulation*: In chapter 4 we have introduced a gross manipulation capability of OT. Gross manipulation along with fine manipulation by moving the traps can be a powerful capability in doing useful biological experiments. However, the planning algorithm developed in chapter 4 is capable of doing gross and fine manipulation independently. Gross manipulation using motorized stage motion was synchronized with fine manipulation using optical trap motion to realize long distance transport of biological objects. The ability of achieving both gross manipulation and fine manipulation simultaneously will enable many difficult manipulation which is otherwise impossible. For example, cells were needed to be transported to form an ensemble for long distance transport. With simultaneous gross and fine manipulation this step will not be necessary. Hence, the manipulation time can be further reduced. Moreover, the fluid flow can also be utilized to assist in manipulation with this capability. For example, cells need not to be

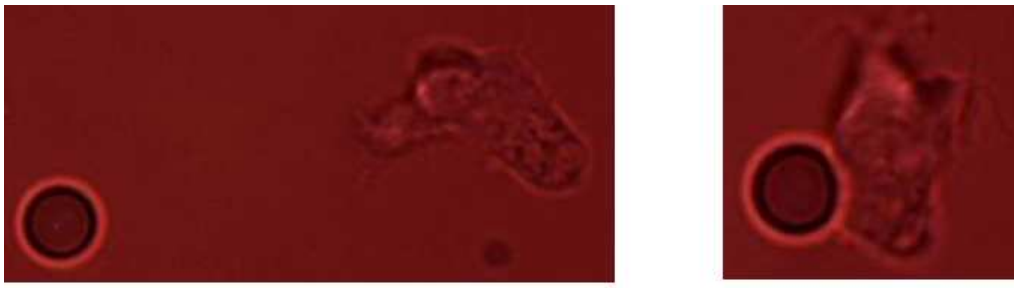

Figure 8.1: *Changing in cell motion due to the presence of a bead: (a) cell motion before the cell comes in contact with bead, and (b) cell motion changes after it comes in contact with the bead (Image courtesy: Chenlu Wang and Dr. Wolfgang Losert)*

trapped for entire manipulation time rather optical traps can be used to guide the cells to follow the fluid streamlines. Thus more objects can be manipulated with less laser power which will reduce the possibility of photodamage of cells.

2. *Automated measurement of sensitivity of cells*: In chapter 7 we have developed an automated framework to push polarized *Dictyostelium discoideum* cells. However, the manipulation should not affect the dynamics of the cells to study their signaling without any bias. The body of a *Dictyostelium discoideum* cell which guides the locomotion direction is very sensitive to the presence of any foreign element, e.g. pushing formation in our case. Cell may change its course of locomotion in the occurrence of such disturbance. Figure 8.1 shows a polarized cell changes its direction of motion due to the presence of a bead on its way. If the presence of pushing formation changes the natural locomotion of a cell, the final result of the experiment will no longer close to the natural outcome. Hence, a method to automatically measure the sensitivity of the cell needs to be developed that will help the planner to decide how it will

manipulate the cell.

Dictyostelium discoideum cells move by extending the active protrusions from front to back. The protrusions can be tracked through frame-by-frame analysis of images. The cell curvature changes with the extension of protrusions. The changes in curvature of cell can be tracked in different frames to plot their distribution. The standard deviation of changes in curvatures will be higher on the sensitive side of cell compared to the other side. The images can be analyzed for couple of seconds before manipulation to find out the sensitive side of the cell.

Another indirect way of determining sensitivity is by measuring the forces exerted in different portions of a cell on a pushing formation. Active protrusions exert more forces compared to other parts of the body. One or several pushing formation can be used as active probes in different locations on the cell surface for a short period of time so that its natural motion is not affected. The beads in the traps will get displaced from the traps with the force exerted by active protrusions. The displacements of the beads can be recorded to measure the exerted force indirectly. Using the high precision capability of OT, forces as low as 1 pN can be measured. Hence, the sensitivity of cell can be determined accurately by experiment.

3. *Integration of fluorescence microscopy with optical tweezers* : fluorescence intensity is used as a label to study the signaling pathway of single cells. Integration of fluorescence microscopy with OT will provide useful sensor information

that can be utilized for automated manipulation of cells. Cells can be actively monitored based on their signaling pathway that can be fed to the planner to derive optimal strategies that will be useful for certain biological experiments. However, the beads in the gripper or pushing formation cannot be detected with the fluorescence microscopy unless they are also labeled. Fluorescence labeled microparticles are expensive. In order to get away with labeled microparticles phase contrast images can be utilized along with fluorescence images. The fluorescence channel can be used to detect the signaling pathway of cell whereas phase contrast channel can be utilized to detect the beads in the gripper or pushing formation. Unfortunately, both the channels cannot be opened at the same time. The open and closing of both the channels have to be efficiently controlled to maximize the information about the cells and microparticles in the workspace. The planning algorithm has to deal with the partial blackout of information about the cells or the microparticles in deriving optimal control actions.

4. *Developing sensing for 3D workspace*: Right now the capability of HOT cannot be properly utilized in automated manipulation due to the lack of proper sensing information in measuring the depth in Z-axis. Although the fast heuristic based planning introduced in this dissertation can be easily extended in 3D, it was not possible to demonstrate the effectiveness since depth information was not available. It is possible to obtain a stack of images of the workspace at various horizontal cross-sections by simply changing the focus of the mi-

croscope. Peng et al. [PBGL06, PBGL07b, PBGL07a, PBGL09] have devised new algorithms for detecting some regular shaped objects (e.g. spherical microspheres, cylindrical nano-wires etc.) by utilizing the stack of images taken in different layers of Z-axis. However, there is still lot more to be done to transform the techniques for extracting 3D shapes of biological objects considering their translucency and irregular shaped boundaries. A generalized image processing algorithm needs to be developed that can detect 3D shapes of objects of arbitrary shapes. The reconstruction of 3D workspace needs to be real time to make it useful of online planning. Machine learning might be useful in 3D reconstruction of workspace with multiple objects of arbitrary shapes.

Bibliography

[AB05] J. Atencia and D. J. Beebe. Controlled microfluidic interfaces. *Nature*, 437(7059):648–655, Sep 2005.

[ACPS05] M. Armani, S. Chaudhary, R. Probst, and B. Shapiro. Using feedback control and micro-fluidics to steer individual particles. In *Proceedings of the 18th IEEE International Conference on Micro Electro Mechanical Systems*, pages 855 – 858, 2005.

[ADBC86] A. Ashkin, J. M. Dziedzic, J. E. Bjorkholm, and S. Chu. Observation of a single-beam gradient force optical trap for dielectric particles. *Optics Letters*, 11(5):288–290, May 1986.

[ADY87] A. Ashkin, J. M. Dziedzic, and T. Yamane. Optical trapping and manipulation of single cells using infrared-laser beams. *Nature*, 330(6150):769–771, Dec 1987.

[AE95] T. Abell and M. Erdmann. Stably supported rotations of a planar polygon with two frictionless contacts. In *Proceedings of the IEEE/RSJ International Conference on Intelligent Robots and Systems*, pages 411–418, 1995.

[AEM+07] F. Arai, T. Endo, H. Maruyama, T. Fukuda, T. Shimizu, and S. Kamiya. 3D manipulation of lipid nanotubes using laser trapped

functional gel microbeads. In *Proceedings of the IEEE/RSJ International Conference on Intelligent Robots and Systems*, pages 3125 –3130, Nov 2007.

[AF09] S. J. Annesley and P. R. Fisher. Dictyostelium discoideum-a model for many reasons. *Molecular and Cellular Biochemistry*, 329(1-2):73–91, Sep 2009.

[AII93] Y. Aiyama, M. Inaba, and H. Inoue. Pivoting: A new method of graspless manipulation of object by robot fingers. In *Proceedings of the IEEE/RSJ International Conference on Intelligent Robots and Systems*, volume 1, pages 136 –143, Jul 1993.

[AKS08] J. D. Adams, U. Kim, and H. T. Soh. Multitarget magnetic activated cell sorter. *Proceedings of the National Academy of Sciences*, 105(47):18165–18170, 2008.

[ALG+05] R. Alterovitz, A. Lim, K. Goldberg, G. S. Chirikjian, and A. M. Okamura. Steering flexible needles under markov motion uncertainty. In *Proceedings of the IEEE/RSJ International Conference on Intelligent Robots and Systems*, pages 1570 – 1575, 2005.

[AM92] S. Akella and M. T. Mason. Posing polygonal objects in the plane by pushing. In *Proceedings of the IEEE International Conference on Robotics and Automation (ICRA)*, volume 3, pages 2255–2262, 1992.

[AMS+03] F. Arai, H. Maruyama, T. Sakami, A. Ichikawa, and T. Fukuda. Pinpoint injection of microtools for minimally invasive micromanipulation of microbe by laser trap. *IEEE-ASME Transactions on Mechatronics*, 8(1):3–9, Mar 2003.

[ANBN07] J. J. Abbott, Z. Nagy, F. Beyeler, and B. J. Nelson. Robotics in the small, part i: Microbotics. *IEEE Robotics Automation Magazine*, 14(2):92 –103, jun 2007.

[ANM+05] F. Arai, C. Ng, H. Maruyama, A. Ichikawa, H. El-Shimy, and T. Fukuda. On chip single-cell separation and immobilization using optical tweezers and thermosensitive hydrogel. *Lab on a Chip*, 5:1399–1403, 2005.

[AOF+00] F. Arai, M. Ogawa, T. Fukuda, K. Horio, T. Sone, K. Itoigawa, and A. Maeda. High speed random separation of microobject in microchip by laser manipulator and dielectrophoresis. In *Proceedings of the Thirteenth Annual International Conference on Micro Electro Mechanical Systems*, pages 727–732, Jan 2000.

[AOIM09] F. Arai, K. Onda, R. Iitsuka, and H. Maruyama. Multi-beam laser micromanipulation of microtool by integrated optical tweezers. In *Proceedings of the IEEE International Conference on Robotics and Automation (ICRA)*, pages 1832 –1837, May 2009.

[AOM+99] F. Arai, M. Ogawa, T. Mizuno, T. Fukuda, K. Morishima, and K. Horio. Teleoperated laser manipulator with dielectrophoretic assistance for selective separation of a microbe. In *Proceedings of the IEEE/RSJ International Conference on Intelligent Robots and Systems*, volume 3, pages 1872 –1877, 1999.

[Ash92] A. Ashkin. Forces of a single-beam gradient laser trap on a dielectric sphere in the ray optics regime. *Biophysics Journal*, 61(2):569–582, Feb 1992.

[AT99] M. P. Allen and D. J. Tildesley. *Computer Simulation of Liquids*. Oxford University Press, 1999.

[AWYY06] S. Ayano, Y. Wakamoto, S. Yamashita, and K. Yasuda. Quantitative measurement of damage caused by 1064-nm wavelength optical trapping of escherichia coli cells using on-chip single cell cultivation system. *Biochemical and Biophysical Research Communications*, 350(3):678–684, Nov 2006.

[AYA+99] Y. Arai, R. Yasuda, K. Akashi, Y. Harada, H. Miyata, K. Kinosita, and H. Itoh. Tying a molecular knot with optical tweezers. *Nature*, 399(6735):446–448, Jun 1999.

[AYSF04] F. Arai, K. Yoshikawa, T. Sakami, and T. Fukuda. Synchronized manipulation and force measurement by optical tweezers using high-speed laser scanning. In *Proceedings of the IEEE/RSJ International*

Conference on Intelligent Robots and Systems, volume 1, pages 890–895, Apr 2004.

[AZ88] W. M. Arnold and U. Zimmermann. Electro-rotation - development of a technique for dielectric measurements on individual cells and particles. *Journal of Electrostatics*, 21(2-3):151–191, Sep 1988.

[Bal11] A. Balijepalli. *Modeling and experimental techniques to adapt optical tweezers for nanoscale prototyping*. PhD thesis, Department of Mechanical Engineering, University of Maryland, 2011.

[BB94] Z. Balorda and T. Bajd. Reducing positioning uncertainty of objects by robot pushing. *IEEE Transactions on Robotics and Automation*, 10(4):535 –541, Aug 1994.

[BBGL08] A. G. Banerjee, A. Balijepalli, S. K. Gupta, and T. W. LeBrun. Radial basis function based simplified trapping probability models for optical tweezers. In *Proceedings of the ASME 28th Computers and Information in Engineering Conference*, Brooklyn, NY, Aug 2008.

[BBGL09] A. G. Banerjee, A. Balijepalli, S. K. Gupta, and T. W. LeBrun. Generating Simplified Trapping Probability Models From Simulation of Optical Tweezers System. *Journal of Computing and Information Science in Engineering*, 9(2), Jun 2009.

[BCGV12] S. Bista, S. Chowdhury, S. K. Gupta, and A. Varshney. Using GPUs for realtime prediction of optical forces on microsphere ensembles. In

Proceedings of the ASME 32nd Computers and Information in Engineering Conference, Chicago, IL, Aug 2012.

[BCGV13] S. Bista, S. Chowdhury, S. K. Gupta, and A. Varshney. Using GPUs for realtime prediction of optical forces on microsphere ensembles. *Journal of Computing and Information Science in Engineering*, 13(3):031002, Apr 2013.

[BCLG11] A. G. Banerjee, S. Chowdhury, W. Losert, and S. K. Gupta. Survey on indirect optical manipulation of cells, nucleic acids, and motor proteins. *Journal of Biomedical Optics*, 16(5), May 2011.

[BCLG12] A. G. Banerjee, S. Chowdhury, W. Losert, and S. K. Gupta. Real-time path planning for coordinated transport of multiple particles using optical tweezers. *IEEE Transactions on Automation Science and Engineering*, 9(4):669 –678, Oct 2012.

[BG08] A. G. Banerjee and S. K. Gupta. Use of simulation in developing and characterizing motion planning approaches for automated particle transport using optical tweezers. In *Proceedings of the 2nd International Virtual Manufacturing Workshop (VIRMAN)*, Turin, Italy, Oct 2008.

[BG13] A. G. Banerjee and S. K. Gupta. Research in automated planning and control for micromanipulation. *IEEE Transactions on Automation Science and Engineering*, 10(3):485–495, 2013.

[BGGL12] A. Balijepalli, J. J. Gorman, S. K. Gupta, and T. W. LeBrun. Significantly improved trapping lifetime of nanoparticles in an optical trap using feedback control. *Nano letters*, 12(5):2347–2351, 2012.

[BGS90] S. M. Block, L. S. B. Goldstein, and B. J. Schnapp. Bead movement by single Kinesin molecules studied with optical tweezers. *Nature*, 348(6299):348–352, Nov 1990.

[Bic00] A. Bicchi. Hands for dexterous manipulation and robust grasping: A difficult road toward simplicity. *IEEE Transactions on Robotics and Automation*, 16(6):652–662, Dec 2000.

[BLG06] A. Balijepalli, T. LeBrun, and S. K. Gupta. A flexible system framework for a nanoassembly cell using optical tweezers. In *Proceedings of the ASME 26th Computers and information in engineering conference*, Philadelphia, PA, Sep 2006.

[BLG09] A. G. Banerjee, W. Losert, and S. K. Gupta. A decoupled and prioritized stochastic dynamic programming approach for automated transport of multiple particles using optical tweezers. In *Proceedings of the ASME 3rd International Conference on Micro and Nanosystems (MNS)*, San Diego, CA, Aug 30-Sep 2 2009.

[BLG10] A. Balijepalli, T. W. LeBrun, and S. K. Gupta. Stochastic simulations with graphics hardware: Characterization of accuracy and per-

formance. *Journal of Computing and Information Science in Engineering*, 10(1):011010, 2010.

[BLGG09] A. Balijepalli, T. LeBrun, J. J. Gorman, and S. K. Gupta. Evaluation of a trapping potential measurement technique for optical tweezers using simulations and experiments. In *Proceedings of the ASME 3rd International Conference on Micro- and Nanosystems*, San Diego, CA, Aug 30-Sep 2 2009.

[BLL+01] M. L. Bennink, S. H. Leuba, G. H. Leno, J. Zlatanova, B. G. de Grooth, and J. Greve. Unfolding individual nucleosomes by stretching single chromatin fibers with optical tweezers. *Nature Structural Biology*, 8(7):606–610, Jul 2001.

[BOvdS02] R. P. Berretty, M. H. Overmars, and A. F. van der Stappen. Orienting polyhedral parts by pushing. *Computational Geometry*, 21:21–38, Jan 2002.

[box] http://www.box2d.org/, Last checked date:Sep 13, 2013.

[BPLG10] A. G. Banerjee, A. Pomerance, W. Losert, and S. K. Gupta. Developing a Stochastic Dynamic Programming Framework for Optical Tweezer-Based Automated Particle Transport Operations. *IEEE Transactions on Automation Science and Engineering*, 7(2):218–227, Apr 2010.

[BSG+95] P.J. Bronkhorst, G.J. Streekstra, J. Grimbergen, E.J. Nijhof, J.J. Sixma, and G.J. Brakenhoff. A new method to study shape recovery of red blood cells using multiple optical trapping. *Biophysics Journal*, 69(5):1666 – 1673, 1995.

[BSK+99] M. L. Bennink, O. D. Scharer, R. Kanaar, K. Sakata-Sogawa, J. M. Schins, J. S. Kanger, B. G. de Grooth, and J. Greve. Single-molecule manipulation of double-stranded DNA using optical tweezers: Interaction studies of DNA with RecA and YOYO-1. *Cytometry*, 36(3):200–208, Jul 1999.

[BTER+02] U. Bockelmann, P. Thomen, B. Essevaz-Roulet, V. Viasnoff, and F. Heslot. Unzipping DNA with optical tweezers: high sequence sensitivity and force flips. *Biophysics Journal*, 82(3):1537–1553, Mar 2002.

[BVHS09] V. Bormuth, V. Varga, J. Howard, and E. Schaeffer. Protein Friction Limits Diffusive and Directed Movements of Kinesin Motors on Microtubules. *Science*, 325(5942):870–873, Aug 2009.

[Can86] J. Canny. A computational approach to edge detection. *IEEE Transactions on Pattern Analysis and Machine Intelligence*, PAMI-8(6):679 –698, Nov 1986.

[CATW+13] S. Chowdhury, P. Svec A. Thakur, C. Wang, W. Losert, and S. K. Gupta. Enhancing range of transport in optical tweezers assisted microfluidic chambers using auto- mated stage motion. In *Proceedings of*

the ASME 7th International Conference on Micro- and Nanosystems, Portland, Oregon, Aug 2013.

[CC05] N. J. Carter and R. A. Cross. Mechanics of the kinesin step. *Nature*, 435(7040):308–312, May 2005.

[CCS11] H. Chen, J. Chen, and D. Sun. A novel allocation-based formation algorithm for swarm of micro-scaled particles. In *Proceedings of the IEEE International Conference on Robotics and Automation (ICRA)*, pages 1664–1669, 2011.

[CCWS10] H. Chen, J. Chen, Y. Wu, and D. Sun. Flocking of micro-scale particles with robotics and optical tweezers technologies. In *Proceedings of the IEEE/RSJ International Conference on Intelligent Robots and Systems*, pages 6155–6160, 2010.

[CDS09] J. Castillo, M. Dimaki, and W. E. Svendsen. Manipulation of biological samples using micro and nano techniques. *Integrative Biology*, 1(1):30–42, Jan 2009.

[CFM+06] D. J. Cappelleri, J. Fink, B. Mukundakrishnan, V. Kumar, and J. C. Trinkle. Designing open-loop plans for planar micro-manipulation. In *Proceedings of the IEEE International Conference on Robotics and Automation*, pages 637 –642, May 2006.

[CG96] J. Crocker and D. G. Grier. Methods of digital video microscopy for colloidal studies. *Journal of Colloid and Interface Science*, 179(1):298–310, 1996.

[CGD06] S. C. Chapin, V. Germain, and E. R. Dufresne. Automated trapping, assembly, and sorting with holographic optical tweezers. *Optics express*, 14(26):13095, 2006.

[CKG02] J. E. Curtis, B. A. Koss, and D. Grier. Dynamic holographic optical tweezers. *Optics Communications*, 207(1-6):169–175, Jun 2002.

[CL05] N. Chronis and L. P. Lee. Electrothermally activated SU-8 microgripper for single cell manipulation in solution. *Journal of Microelectromechanical Systems*, 14(4):857–863, Aug 2005.

[CLH+05] H. Choset, K. Lynch, S. Hutchinson, G. Kantor, W. Burgard, L. Kavraki, and S. Thrun. *Principles of Robot Motion: Theory, Algorithms, and Implementations*. The MIT Press, Cambridge, MA, 2005.

[CPPM08] M. Castelain, F. Pignon, J. M. Piau, and A. Magnin. The initial single yeast cell adhesion on glass via optical trapping and Derjaguin-Landau-Verwey-Overbeek predictions. *Journal of Chemical Physics*, 128(13), Apr 2008.

[CQZ+06] K. Chen, Y. Qin, F. Zheng, M. Sun, and D. Shi. Diagnosis of colorectal cancer using raman spectroscopy of laser-trapped single living epithelial cells. *Optics Letters*, 31(13):2015–2017, Jul 2006.

[CS11] H. Chen and D. Sun. Pairing and moving swarm of micro particles into array with a robot-tweezer manipulation system. In *Proceedings of the IEEE/RSJ International Conference on Intelligent Robots and Systems*, San Francisco, CA, 2011.

[CS12] H. Chen and D. Sun. Moving groups of microparticles into array with a robot-tweezers manipulation system. *IEEE Transactions on Robotics*, 28(5):1069–1080, 2012.

[CSS05] K. Castelino, S. Satyanarayana, and M. Sitti. Manufacturing of two and three-dimensional micro/nanostructures by integrating optical tweezers with chemical assembly. *Robotica*, 23(Part 4):435–439, Jul 2005.

[CSW+11] S. Chowdhury, P. Svec, C. Wang, K. Seale, J. P. Wikswo, W. Losert, and S. K. Gupta. Investigation of automated cell manipulation in optical tweezers-assisted microfluidic chamber using simulations. In *Proceedings of the ASME 5th International Conference on Micro and Nanosystems (MNS)*, Washington DC, Aug 2011.

[CSW+12] S. Chowdhury, P. Svec, C. Wang, W. Losert, and S. K. Gupta. Robust gripper synthesis for indirect manipulation of cells using holographic

optical tweezers. In *Proceedings of the IEEE International Conference on Robotics and Automation (ICRA)*, St. Paul, MN, May 2012.

[CSW+13] S. Chowdhury, P. Svec, C. Wang, K. T. Seale, J. P. Wikswo, W. Losert, and S. K. Gupta. Automated cell transport in optical tweezers-assisted microfluidic chambers. *IEEE Transactions on Automation Science and Engineering*, 10(4):980–989, 2013.

[CTS11] B. Craig, L. D. Thomas, and H. Steve. Decision-theoretic planning: Structural assumptions and computational leverage. *CoRR*, abs/1105.5460, 2011.

[CTS+13] S. Chowdhury, A. Thakur, P. Svec, C. Wang, W. Losert, and S. K. Gupta. Automated manipulation of biological cells using gripper formations controlled by optical tweezers. *IEEE Transactions on Automation Science and Engineering*, 2013. Accepted for publication.

[CTW+12] S. Chowdhury, A. Thakur, C. Wang, P. Svec, W. Losert, and S. K. Gupta. Automated indirect transport of biological cells with optical tweezers using planar gripper formations. In *Proceedings of the IEEE International Conference on Automation Science and Engineering*, Seoul, Korea, Aug 2012.

[CTW+13] S. Chowdhury, A. Thakur, C. Wang, P. Svec, W. Losert, and S. K. Gupta. Automated indirect manipulation of irregular shaped cells with optical tweezers for studying collective cell migration. In *Pro-*

ceedings of the IEEE International Conference on Robotics and Automation (ICRA), Karlsruhe, Germany, May 2013.

[CVJ+05] A. E. M. Clemen, M. Vilfan, J. Jaud, J. S. Zhang, M. Barmann, and M. Rief. Force-dependent stepping kinetics of myosin-V. *Biophysics Journal*, 88(6):4402–4410, Jun 2005.

[CWL13] H. Chen, C. Wang, and Y. Lou. Flocking multiple microparticles with automatically controlled optical tweezers: Solutions and experiments. *IEEE Transactions on Biomedical Engineering*, 60(6):1518–1527, 2013.

[Deb01] K. Deb. *Multi-Objective Optimization using Evolutionary Algorithms*. John Wiley & Sons, 2001.

[DFL11] M. K. Driscoll, J. T. Fourkas, and W. Losert. Local and global measures of shape dynamics. *Physical Biology*, 8(5):055001, 2011.

[DG98] E. R. Dufresne and D. G. Grier. Optical tweezer arrays and optical substrates created with diffractive optics. *Review of Scientific Instruments*, 69(5):1974–1977, 1998.

[DGWW97] D. E. Dupuis, W. H. Guilford, J. Wu, and D. M. Warshaw. Actin filament mechanics in the laser trap. *Journal of Muscle Research and Cell Motility* , 18(1):17–30, Feb 1997.

[DKB99] A. Docoslis, N. Kalogerakis, and L. A. Behie. Dielectrophoretic forces can be safely used to retain viable cells in perfusion cultures of animal cells. *Cytotechnology*, 30(1-3):133–142, 1999.

[DKKN93] T. Dean, L. P. Kaelbling, J. Kirman, and A. Nicholson. Planning with deadlines in stochastic domains. In *Proceedings of the Eleventh National Conference on Artificial Intelligence*, pages 574–579, 1993.

[DLK+12] X. Ding, S. C. S. Lin, B. Kiraly, H. Yue, S. Li, I. K. Chiang, J. Shi, S. J. Benkovic, and T. J. Huang. On-chip manipulation of single microparticles, cells, and organisms using surface acoustic waves. *Proceedings of the National Academy of Sciences*, 2012.

[DLP+07] K. Dholakia, W. M. Lee, L. Paterson, M. P. MacDonald, R. McDonald, I. Andreev, P. Mthunzi, C. T. A. Brown, R. F. Marchington, and A. C. Riches. Optical separation of cells on potential energy landscapes: Enhancement with dielectric tagging. *IEEE Journal of Selected Topics in Quantum Electronics*, 13(6):1646–1654, Nov 2007.

[DMK+12] M. K. Driscoll, C. McCann, R. Kopace, T. Homan, J. T. Fourkas, C. Parent, and W. Losert. Cell shape dynamics: From waves to migration. *PLoS Computational Biology*, 8(3):e1002392, Mar 2012.

[DSD+01] E. R. Dufresne, G. C. Spalding, M. T. Dearing, S. A. Sheets, and D. G. Grier. Computer-generated holographic optical tweezer arrays. *Review of Scientific Instruments*, 72(3):1810–1816, 2001.

[dVKvDK05] A. H. B. de Vries, B. E. Krenn, R. van Driel, and J. S. Kanger. Micro magnetic tweezers for nanomanipulation inside live cells. *Biophysics Journal*, 88(3):2137–2144, Mar 2005.

[DWLB00] R. J. Davenport, G. J. L Wuite, R. Landick, and C. Bustamante. Single-molecule study of transcriptional pausing and arrest by E-coli RNA polymerase. *Science*, 287(5462):2497–2500, Mar 2000.

[EEN+07] E. Eriksson, J. Enger, B. Nordlander, N. Erjavec, K. Ramser, M. Goksor, S. Hohmann, T. Nystrom, and D. Hanstorp. A microfluidic system in combination with optical tweezers for analyzing rapid and reversible cytological alterations in single cells upon environmental changes. *Lab on a Chip*, 7:71–76, 2007.

[EGR+04] J. Enger, M. Goksor, K. Ramser, P. Hagberg, and D. Hanstorp. Optical tweezers applied to a microfluidic system. *Lab on a Chip*, 4:196–200, 2004.

[Erd98] M. Erdmann. An exploration of nonprehensile two-palm manipulation. *The International Journal of Robotics Research*, 17(5):485–503, 1998.

[ESL+10] E. Eriksson, K. Sott, F. Lundqvist, M. Sveningsson, J. Scrimgeour, D. Hanstorp, M. Goksör, and A. Granéli. A microfluidic device for reversible environmental changes around single cells using optical tweez-

ers for cell selection and positioning. *Lab on a Chip*, 10(5):617–625, 2010.

[FEC+05] E. Ferrari, V. Emiliani, D. Cojoc, V. Garbin, M. Zahid, C. Durieux, M. Coppey-Moisan, and E. Di Fabrizio. Biological samples micromanipulation by means of optical tweezers. *Microelectronic Engineering*, 78-79(Sp. Iss. SI):575–581, Mar 2005.

[FFDT+08] A. Fontes, H. P. Fernandes, A. A. De Thomaz, L. C. Barbosa, M. L. Barjas-Castro, and C. L. Cesar. Measuring electrical and mechanical properties of red blood cells with double optical tweezers. *Journal of Biomedical Optics*, 13(1), Jan 2008.

[FLS05] D. Ferguson, M. Likhachev, and A. T. Stentz. A guide to heuristic-based path planning. In *Proceedings of the International Workshop on Planning under Uncertainty for Autonomous Systems, International Conference on Automated Planning and Scheduling (ICAPS)*, Jun 2005.

[FSH+08] S. Faley, K. Seale, J. Hughey, D. K. Schaffer, S. VanCornpernolle, B. McKinney, F. Baudenbacher, D. Unutmaz, and J. P. Wikswo. Microfluidic platform for real-time signaling analysis of multiple single T cells in parallel. *Lab on a Chip*, 8(10):1700–1712, Oct 2008.

[FSJ+04] E. Fallman, S. Schedin, J. Jass, M. Andersson, B. E. Uhlin, and O. Axner. Optical tweezers based force measurement system for quan-

titating binding interactions: system design and application for the study of bacterial adhesion. *Biosensors & Bioelectronics*, 19(11):1429–1437, Jun 2004.

[FSL09] C. Fulgenzi, A. Spalazani, and C. Laugier. Probabilistic rapidly exploring random trees for autonomous navigation among moving obstacles. In *Workshop on Safe Navigation, Proceedings of the IEEE International Conference on Robotics and Automation (ICRA)*, 2009.

[FSS94] J. T. Finer, R. M. Simmons, and J. A. Spudich. Single Myosin molecule mechanics - piconewton forces and nanometer steps. *Nature*, 368(6467):113–119, Mar 1994.

[GBL12] J. J. Gorman, A. Balijepalli, and T. W. LeBrun. Feedback control of optically trapped particles. In Jason J. Gorman and Benjamin Shapiro, editors, *Feedback Control of MEMS to Atoms*, pages 141–177. Springer US, 2012.

[GHKR09] L. J. Guibas, D. Hsu, H. Kurniawati, and E. Rehman. Bounded uncertainty roadmaps for path planning. In GregoryS. Chirikjian, Howie Choset, Marco Morales, and Todd Murphey, editors, *Algorithmic Foundation of Robotics VIII*, volume 57 of *Springer Tracts in Advanced Robotics*, pages 199–215. Springer Berlin Heidelberg, 2009.

[GL04] M. Garber and M. Lin. Constraint-based motion planning using voronoi diagrams. *Algorithmic Foundations of Robotics V*, pages 541–

558, 2004.

[Gol93] K. Goldberg. Orienting polygonal parts without sensors. *Algorithmica, Special Issue on Computational Robotics*, 10:201–225, 1993.

[Gri03] D. G Grier. A revolution in optical manipulation. *Nature*, 424(6950):810–816, 2003.

[HBMM02] K. Hirano, Y. Baba, Y. Matsuzawa, and A. Mizuno. Manipulation of single coiled DNA molecules by laser clustering of microparticles. *Applied Physics Letters*, 80(3):515–517, Jan 2002.

[HJB+03] B. G. Hosu, K. Jakab, P. Banki, F. I. Toth, and G. Forgacs. Magnetic tweezers for intracellular applications. *Review of Scientific Instruments*, 74(9):4158–4163, Mar 2003.

[HLLK11] P. Honarmandi, H. Lee, M. J. Lang, and R. D. Kamm. A microfluidic system with optical laser tweezers to study mechanotransduction and focal adhesion recruitment. *Lab on a Chip*, 11:684–694, 2011.

[HLRG99] S. Henon, G. Lenormand, A. Richert, and F. Gallet. A new determination of the shear modulus of the human erythrocyte membrane using optical tweezers. *Biophysics Journal*, 76(2):1145–1151, Feb 1999.

[HNR68] P. E. Hart, N. J. Nilsson, and B. Raphael. A formal basis for the heuristic determination of minimum cost paths. *IEEE Transactions on Systems Science and Cybernetics*, 4(2):100 –107, Jul 1968.

[HS11] S. Hu and D. Sun. Automatic transportation of biological cells with a robot-tweezer manipulation system. *The International Journal of Robotics Research*, 30(14):1681–1694, December 2011.

[HWC+09] Y. Huang, J. Wan, M. C. Cheng, Z. Zhang, S. M. Jhiang, and C. H. Menq. Three-axis rapid steering of optically propelled micro/nanoparticles. *Review of Scientific Instruments*, 80(6), Jun 2009.

[HZM09] Y. Huang, Z. Zhang, and C. H. Menq. Minimum-variance brownian motion control of an optically trapped probe. *Applied Optics*, 48(30):5871–5880, Oct 2009.

[IAY+05] A. Ichikawa, F. Arai, K. Yoshikawa, T. Uchida, and T. Fukuda. In situ formation of a gel microbead for indirect laser micromanipulation of microorganisms. *Applied Physics Letters*, 87(19), Nov 2005.

[IF09] O. Ilina and P. Friedl. Mechanisms of collective cell migration at a glance. *Journal of Cell Science*, 122(18):3203–3208, Sep 2009.

[IHE+06] A. Ichikawa, A. Honda, M. Ejima, T. Tanikawa, F. Arai, and T. Fukuda. In-situ formation of a gel microbead for laser micromanipulation of microorganisms, dna and virus. In *Proceedings of the 2006 International Symposium on Micro-NanoMechatronics and Human Science*, pages 1–6, Nov 2006.

[JIL00] E. W. H. Jager, O. Inganas, and I. Lundstrom. Microrobots for micrometer-size objects in aqueous media: Potential tools for single-cell manipulation. *Science*, 288(5475):2335–2338, Jun 2000.

[JIP+02] E. W. H. Jager, C. Immerstrand, K. H. Peterson, K. E. Magnusson, I. Lundstrom, and O. Inganas. The cell clinic: Closable microvials for single cell studies. *Biomedical Microdevices*, 4(3):177–187, Jul 2002.

[JLYS11a] T. Ju, S. Liu, J. Yang, and D. Sun. Apply RRT-based path planning to robotic manipulation of biological cells with optical tweezer. In *Proceedings of the International Conference on Mechatronics and Automation (ICMA)*, Beijing, China, 2011.

[JLYS11b] T. Ju, S. Liu, J. Yang, and D. Sun. Path planning for 3D transportation of biological cells with optical tweezers. In *Proceedings of the IEEE International Conference on Automation and Logistics (ICAL)*, Chongqing, China, 2011.

[JSGF04] S. Jeney, E. H. K. Stelzer, H. Grubmuller, and E. L. Florin. Mechanical properties of single motor molecules studied by three-dimensional thermal force probing in optical tweezers. *ChemPhysChem*, 5(8):1150–1158, Aug 2004.

[KB97] M. S. Z. Kellermayer and C. Bustamante. Folding-unfolding transitions in single titin molecules characterized with laser tweezers (vol 276, pg 1112, 1997). *Science*, 277(5329):1117, Aug 1997.

[KCA+11] B. Koss, S. Chowdhury, T. Aabo, S. K. Gupta, and W. Losert. Indirect optical gripping with triplet traps. *Journal of Optical Society of America B*, 28(5):982–985, Apr 2011.

[KCL+03] B. Kim, D. Collard, M. Lagouge, F. Conseil, B. Legrand, and L. Buchaillot. Thermally actuated probe arrays for manipulation and characterization of individual bio-cell. In *Proceedings of the 12th International Conference on Transducers, Solid-State Sensors, Actuators and Microsystems*, volume 2, pages 1255 – 1258 vol.2, 8-12 2003.

[KDG11] Y. S. Kim, N. G. Dagalakis, and S. K. Gupta. A two degree of freedom nanopositioner with electrothermal actuator for decoupled motion. In *Proceedings of the ASME 5th International Conference on Micro- and Nanosystems (MNS)*, Washington DC, Aug 2011.

[KDG12a] Y. S. Kim, N. G. Dagalakis, and S. K. Gupta. Design and fabrication of a three-dof mems stage based on nested structures. In *Proceedings of the ASME 6th International Conference on Micro- and Nanosystems (MNS)*, Chicago, IL, Aug 2012.

[KDG12b] Y. S. Kim, N. G. Dagalakis, and S. K. Gupta. Design, fabrication and characterization of a single-layer out-of-plane electrothermal actuator for a mems xyz stage. In *Proceedings of the Performance Metrics for Intelligent Systems (PerMIS'12) Workshop*, College Park, MD, Mar 2012.

[KDG13] Y. S. Kim, N. G. Dagalakis, and S. K. Gupta. Creating large out-of-plane displacement electrothermal motion stage by incorporating beams with step features. *Journal of Micromechanics and Microengineering*, 23(5):055008, 2013.

[KL02] S. Koenig and M. Likhachev. D* lite. In *Proceedings of the AAAI Conference of Artificial Intelligence*, pages 476–483, 2002.

[KL05] S. Koenig and M. Likhachev. Fast replanning for navigation in unknown terrain. *IEEE Transactions on Robotics*, 21(3):354–363, Jun 2005.

[KLBT95] K. Konig, H. Liang, M. W. Berns, and B. J. Tromberg. Cell-damage by near-in microbeams. *Nature*, 377(6544):20–21, Sep 1995.

[KMHY97] H. Kojima, E. Muto, H. Higuchi, and T. Yanagida. Mechanics of single kinesin molecules measured by optical trapping nanometry. *Biophysics Journal*, 73(4):2012–2022, Oct 1997.

[KSGR05] H. Kress, E. H. K. Stelzer, G. Griffiths, and A. Rohrbach. Control of relative radiation pressure in optical traps: Application to phagocytic membrane binding studies. *Physical Review E*, 71(6, Part 1), Jun 2005.

[KSL+96] K. Konig, L. Svaasand, Y. G. Liu, G. Sonek, P. Patrizio, Y. Tadir, M. W. Berns, and B. J. Tromberg. Determination of motility forces

of human spermatozoa using an 800 nm optical trap. *Cellular and molecular biology (Noisy-le-Grand, France)*, 42(4):501–509, Jun 1996.

[KWLT08] M. C. Kim, Z. Wang, R. H. W. Lam, and T. Thorsen. Building a better cell trap: Applying lagrangian modeling to the design of microfluidic devices for cell biology. *Journal of applied physics*, 103(4):044701, 2008.

[KYI+01] S. Katsura, A. Yamaguchi, H. Inami, S. Matsuura, K. Hirano, and A. Mizuno. Indirect micromanipulation of single molecules in water-in-oil emulsion. *Electrophoresis*, 22(2):289–293, Jan 2001.

[KYY+12] Y. S. Kim, J. M. Yoo, S. H. Yang, Y. M. Choi, N. G. Dagalakis, and S. K. Gupta. Design, fabrication and testing of a serial kinematic mems xy stage for multifinger manipulation. *Journal of Micromechanics and Microengineering*, 22(8):085029, 2012.

[Lan12] B. Landenberger. Microfluidic sorting of arbitrary cells with dynamic optical tweezers. *Lab on a Chip*, 2012.

[Lar00] P. Laroche. Building efficient partial plans using markov decision processes. In *Proceedings of the IEEE International Conference on Tools with Artificial Intelligence (ICTAI)*, 2000.

[LaV06] S. M. LaValle. *Planning Algorithms*. Cambridge University Press, Cambridge, U.K., 2006.

[LBT07] P. T. X. Li, C. Bustamante, and I. Tinoco. Real-time control of the energy landscape by force directs the folding of RNA molecules. *Proceedings of the National Academy of Sciences*, 104(17):7039–7044, Apr 2007.

[LC12] X. Li and C. C. Cheah. Dynamic region control for robot-assisted cell manipulation using optical tweezers. In *Proceedings of the IEEE International Conference on Robotics and Automation (ICRA)*, pages 1057–1062, 2012.

[LCHS13] X. Li, C. C. Cheah, S. Hu, and D. Sun. Dynamic trapping and manipulation of biological cells with optical tweezers. *Automatica*, 49(6):1614 – 1625, 2013.

[Lee05] H. Lee. *Microelectronic/microfluidic hybrid system for the manipulation of biological cells*. PhD thesis, 2005.

[LHP+02] V. M. Laurent, S. Henon, E. Planus, R. Fodil, M. Balland, D. Isabey, and F. Gallet. Assessment of mechanical properties of adherent living cells by bead micromanipulation: Comparison of magnetic twisting cytometry vs optical tweezers. *Journal of Biomechanical Engineering-Transactions of The ASME*, 124(4):408–421, Aug 2002.

[LHW04] H. Lee, T. P. Hunt, and R. M. Westervelt. Magnetic and electric manipulation of a single cell in fluid. In *Proceedings of the Materials Research Society Symposium*, 2004.

[LLHW07] H. Lee, Y. Liu, D. Ham, and R. M. Westervelt. Integrated cell manipulation system - CMOS/microfluidic hybrid. *Lab on a Chip*, 7(3):331–337, 2007.

[LLLL08] C. Li, Y. P. Liu, K. K. Liu, and A. C. K. Lai. Correlations between the experimental and numerical investigations on the mechanical properties of erythrocyte by laser stretching. *IEEE Transactions on Nanobioscience*, 7(1):80–90, Mar 2008.

[LM95] K. Lynch and M. T. Mason. Stable pushing: Mechanics, controllability, and planning. In *Proceedings of the Workshop on Algorithmic Foundations of Robotics*, pages 239–262, Boston, MA, 1995.

[LM96] K. M. Lynch and M. T. Mason. Stable pushing: Mechanics, controllability, and planning. *The International Journal of Robotics Research*, 15(6):533–556, 1996.

[LOS+01] J. Liphardt, B. Onoa, S. B. Smith, I. Tinoco, and C. Bustamante. Reversible unfolding of single RNA molecules by mechanical force. *Science*, 292(5517):733–737, APR 27 2001.

[LP83] T. Lozano-Perez. Spatial planning: A configuration space approach. *IEEE Transactions on Computers*, C-32(2):108 –120, Feb. 1983.

[LSBT96] Y. Liu, G. J. Sonek, M. W. Berns, and B. J. Tromberg. Physiological monitoring of optically trapped cells: Assessing the effects of confine-

ment by 1064-nm laser tweezers using microfluorometry. *Biophysics Journal*, 71(4):2158–2167, Oct 1996.

[LVK+96] H. Liang, K. T. Vu, P. Krishnan, T. C. Trang, D. Shin, S. Kimel, and M. W. Berns. Wavelength dependence of cell cloning efficiency after optical trapping. *Biophysics Journal*, 70(3):1529–1533, Mar 1996.

[LWS13] X. Li, J. Wang, and D. Sun. Coalition transportation of cells with optical tweezers. In *Proceedings of the 8th IEEE International Conference on Nano/Micro Engineered and Molecular Systems (NEMS)*, pages 1151–1154, 2013.

[Mas01] M. T. Mason. *Mechanics of Robotic Manipulation*. The MIT Press, 2001.

[MCB+06] P. Mangeol, D. Cote, T. Bizebard, O. Legrand, and U. Bockelmann. Probing DNA and RNA single molecules with a double optical tweezer. *European Physical Journal E*, 19(3):311–317, MAR 2006.

[MDS10] S. Mannepalli, A. Dutta, and A. Saxena. A multi-objective ga based algorithm for 2d form and force closure grasp of prismatic objects. *International Journal on Robotics and Automation*, 25(2):142–154, 2010.

[MFA09] H. Maruyama, T. Fukuda, and F. Arai. Laser manipulation and optical adhesion control of functional gel-microtool for on-chip cell ma-

nipulation. In *Proceedings of the IEEE/RSJ International Conference on Intelligent Robots and Systems*, St. Louis, MO, 2009.

[MGEF02] M. Moll, K. Goldberg, M.A. Erdmann, and R. Fearing. Orienting micro-scale parts with squeeze and roll primitives. In *Proceedings of the IEEE International Conference on Robotics and Automation (ICRA)*, volume 2, pages 1931 – 1936, 2002.

[MR06] P. E. Missiuro and N. Roy. Adapting probabilistic roadmaps to handle uncertain maps. In *Proceedings of the IEEE International Conference on Robotics and Automation (ICRA)*, pages 1261 –1267, May 2006.

[MRB02] M. Miyata, W. S. Ryu, and H. C. Berg. Force and velocity of Mycoplasma mobile gliding. *Journal of Bacteriology*, 184(7):1827–1831, Apr 2002.

[MS07] N.A. Mechior and R. Simmons. Particle rrt for path planning with uncertainty. In *Proceedings of the IEEE International Conference on Robotics and Automation (ICRA)*, 2007.

[MSD03] M. P. MacDonald, G. C. Spalding, and K. Dholakia. Microfluidic sorting in an optical lattice. *Nature*, 426(6965):421–424, Nov 2003.

[MSS87] B. Mishra, J. T. Schwartz, and M. Sharir. On the existence and synthesis of multifinger positive grips. *Algorithmica*, 2(4):541–558, 1987.

[MTT+08] U. Mirsaidov, W. Timp, K. Timp, M. Mir, P. Matsudaira, and G. Timp. Optimal optical trap for bacterial viability. *Physical Review E*, 78, Mar 2008.

[MWL+07] M. Manosas, J. D. Wen, P. T. X. Li, S. B. Smith, C. Bustamante, I. Tinoco, Jr., and F. Ritort. Force unfolding kinetics of RNA using optical tweezers. II. Modeling experiments. *Biophysics Journal*, 92(9):3010–3021, MAY 1 2007.

[MYK96] H. Miyata, R. Yasuda, and K. Kinosita. Strength and lifetime of the bond between actin and skeletal muscle alpha-actinin studied with an optical trapping technique. *Biochimica Et Biophysica Acta-General Subjects*, 1290(1):83–88, May 1996.

[MYP+12] B. Ma, B. Yao, F. Peng, S. Yan, M. Lei, and R. Rupp. Optical sorting of particles by dual-channel line optical tweezers. *Journal of Optics*, 14(10):105702, 2012.

[NCL+99] K. C. Neuman, E. H. Chadd, G. F. Liou, K. Bergman, and S. M. Block. Characterization of photodamage to Escherichia coli in optical traps. *Biophysics Journal*, 77(5):2856–2863, Nov 1999.

[NF72] J. I. Neimark and Nikolaĭ A. Fufaev. *Dynamics of nonholonomic systems*, volume 33. American Mathematical Society, 1972.

[NKHM97] M. Nishioka, S. Katsura, K. Hirano, and A. Mizuno. Evaluation of cell characteristics by step-wise orientational rotation using optoelec-

trostatic micromanipulation. *IEEE Transactions on Industry Applications*, 33(5):1381 –1388, Sep 1997.

[NMY+95] T. Nishizaka, H. Miyata, H. Yoshikawa, S. Ishiwata, and K. Kinosita. Unbinding force of a single motor molecule of muscle measured using optical tweezers. *Nature*, 377(6546):251–254, Sep 1995.

[OA12] K. Onda and F. Arai. Parallel teleoperation of holographic optical tweezers using multi-touch user interface. In *Proceedings of the IEEE International Conference on Robotics and Automation (ICRA)*, pages 1069–1074, 2012.

[OCP+07] A. T. Ohta, P. Y. Chiou, H. L. Phan, S. W. Sherwood, J. M. Yang, A. N. K. Lau, H. Y. Hsu, A. Jamshidi, and M. C. Wu. Optically controlled cell discrimination and trapping using optoelectronic tweezers. *IEEE Journal of Selected Topics in Quantum Electronics*, 13(2):235–243, Mar 2007.

[OPS+03] M. Ozkan, T. Pisanic, J. Scheel, C. Barlow, S. Esener, and S. N. Bhatia. Electro-optical platform for the manipulation of live cells. *Langmuir*, 19(5):1532–1538, Mar 2003.

[OZDF08] S. E. Ong, S. Zhang, H. Du, and Y. Fu. Fundamental principles and applications of microfluidic systems. *Frontiers in Bioscience*, 13:2757–2773, Jan 2008.

[PBGL06] T. Peng, A. Balijepalli, S. K. Gupta, and T. LeBrun. Algorithms for on-line monitoring of components in an optical tweezers-based assembly cell. In *Proceedings of the ASME 26th Computers and Information in Engineering Conference*, Philadelphia, PA, Sep 2006.

[PBGL07a] T. Peng, A. Balijepalli, S .K. Gupta, and T. LeBrun. Algorithms for extraction of nanowires attributes from optical section microscopy images. In *Proceedings of the ASME 27th Computers and Information in Engineering Conference*, Las Vegas, NV, Sep 2007.

[PBGL07b] T. Peng, A. Balijepalli, S. K. Gupta, and T. LeBrun. Algorithms for on-line monitoring of micro spheres in an optical tweezers-based assembly cell. *Journal of Computing and Information Science in Engineering*, 7(4):330–338, 2007.

[PBGL09] T. Peng, A. Balijepalli, S. K. Gupta, and T. LeBrun. Algorithms for extraction of nanowire lengths and positions from optical section microscopy image sequence. *Journal of Computing and Information Science in Engineering*, 9(4):041007, 2009.

[PDB+12] R. Patro, J. P. Dickerson, S. Bista, S. K. Gupta, and A. Varshney. Speeding up particle trajectory simulations under moving force fields using gpus. *Journal of Computing and Information Science in Engineering*, 12(2):021006, May 2012.

[PFdT+09] L. Y. Pozzo, A. Fontes, A. A. de Thomaz, B. S. Santos, P. M. A. Farias, D. C. Ayres, S. Giorgio, and C. L. Cesar. Studying taxis in real time using optical tweezers: Applications for Leishmania amazonensis parasites. *Micron*, 40(5-6):617–620, Jul 2009.

[PPM+05] L. Paterson, E. Papagiakoumou, G. Milne, V. Garces-Chavez, S. A. Tatarkova, W. Sibbett, F. J. Gunn-Moore, P. E. Bryant, A. C. Riches, and K. Dholakia. Light-induced cell separation in a tailored optical landscape. *Applied Physics Letters*, 87(12), SEP 19 2005.

[PPM+07] L. Paterson, E. Papagiakoumou, G. Milne, V. Garces-Chavez, T. Briscoe, W. Sibbett, K. Dholakia, and A. C. Riches. Passive optical separation within a 'nondiffracting' light beam. *Journal of Biomedical Optics*, 12(5):054017, Oct. 2007.

[PQSC94] T. T. Perkins, S. R. Quake, D. E. Smith, and S. Chu. Relaxation of a single DNA molecule observed by optical microscopy. *Science*, 264(5160):822–826, May 1994.

[Qia03] H. Qiao. Two- and three-dimensional part orientation by sensor-less grasping and pushing actions: Use of the concept of 'attractive region in environment'. *International Journal of Production Research*, 41(14):3159–3184, 2003.

[Reu76] F. Reuleaux. *The Kinematics of Machinery.* Macmillan and CO., 1876.

[RG99] N. Rezzoug and P. Gorce. Dynamic control of pushing operations. *Robotica*, 17(06):613–620, 1999.

[RHX+04] J. Robert, S. Harlepp, A. Xayaphoumine, J. F. Leger, D. Chatenay, and H. Isambert. Probing complex RNA structures by mechanical force. *Biophysics Journal*, 86(1, Part 2 Suppl. S):189A, Jan 2004.

[ROS08] M. B. Rasmussen, L. B. Oddershede, and H. Siegumfeldt. Optical tweezers cause physiological damage to Escherichia coli and Listeria bacteria. *Applied and Environmental Microbiology*, 74:2441–2446, Mar 2008.

[RSC08] M. Roa, R. Suarez, and J. Cornella. Quality measures for object grasping. *Revista Iberoamericana De Automatica E Informatica Industrial*, 5(1):66+, 2008.

[RWG+10] R. Roy, C. Wenjin, L. A. Goodell, H. Jun, D. J. Foran, and J. P. Desai. Microarray-facilitated mechanical characterization of breast tissue pathology samples using contact-mode atomic force microscopy (afm). In *Proceedings of the 3rd IEEE RAS and EMBS International Conference on Biomedical Robotics and Biomechatronics (BioRob)*, pages 710 –715, Sep 2010.

[SA08] N. R. Sims and M. F. Anderson. Isolation of mitochondria from rat brain using percoll density gradient centrifugation. *Nature Protocols*, 3(7):1228–1239, Jul 2008.

[SB94] K. Svoboda and S. M. Block. Biological Applications of Optical Forces. *Annual Review of Biophysics and Biomolecular Structure*, 23:247–285, Mar 1994.

[SEPG08] K. Sott, E. Eriksson, E. Petelenz, and M. Goksr. Optical systems for single cell analyses. *Expert Opinion on Drug Discovery*, 3(11):1323–1344, 2008.

[SFCW10] K. T. Seale, S. L. Faley, J. Chamberlain, and J. P. Wikswo. Macro to nano: a simple method for transporting cultured cells from milliliter scale to nanoliter scale. *Experimental Biology and Medicine*, 235(6):777–783, Jun 2010.

[SHC+01] C. K. Sun, Y. C. Huang, P. C. Cheng, H. C. Liu, and B. L. Lin. Cell manipulation by use of diamond microparticles as handles of optical tweezers. *Journal of The Optical Society of Americal B- Optical Physics*, 18(10):1483–1489, Oct 2001.

[SHRS02] G. V. Soni, F. M. Hameed, T. Roopa, and G. V. Shivashankar. Development of an optical tweezer combined with micromanipulation for DNA and protein nanobioscience. *Current Science*, 83(12):1464–1470, Dec 2002.

[SL97] G. V. Shivashankar and A. Libchaber. Single DNA molecule grafting and manipulation using a combined atomic force microscope and an optical tweezer. *Applied Physics Letters*, 71(25):3727–3729, Dec 1997.

[SLB+10] M. Socol, C. Lefrou, F. Bruckert, D. Delabouglise, and M. Weidenhaupt. Synchronization of dictyostelium discoideum adhesion and spreading using electrostatic forces. *Bioelectrochem.*, 79(2):198 – 210, 2010.

[SSL98] G. V. Shivashankar, G. Stolovitzky, and A. Libchaber. Backscattering from a tethered bead as a probe of DNA flexibility. *Applied Physics Letters*, 73(3):291–293, Jul 1998.

[SSSB93] K. Svoboda, C. F. Schmidt, B. J. Schnapp, and S. M. Block. Direct observation of kinesin stepping by optical trapping interferometry. *Nature*, 365(6448):721–727, Oct 1993.

[ST01] B. E. A. Saleh and M. C. Teich. *Beam Optics in Fundamentals of Photonics*. John Wiley & Sons, Inc., New York, USA., 2001.

[STNS+05] L. Sacconi, I. M. Tolic-Norrelykke, C. Stringari, R. Antolini, and F. S. Pavone. Optical micromanipulations inside yeast cells. *Applied Optics*, 44(11):2001–2007, Apr 2005.

[SVC+08] R. C. Spero, L. Vicci, J. Cribb, D. Bober, V. Swaminathan, E. T. O'Brien, S. L. Rogers, and R. Superfine. High throughput system for magnetic manipulation of cells, polymers, and biomaterials. *Review of Scientific Instruments*, 79(8):083707, 2008.

[SWSG99] J. Sleep, D. Wilson, R. Simmons, and W. Gratzer. Elasticity of the red cell membrane and its relation to hemolytic disorders: An optical tweezers study. *Biophysics Journal*, 77(6):3085–3095, Dec 1999.

[SYEL07] B. S. Schmidt, A. H. Yang, D. Erickson, and M. Lipson. Optofluidic trapping and transport on solid core waveguides within a microfluidic device. *Optics Express*, 15(22):14322–14334, Oct 2007.

[TCW+12] A. Thakur, S. Chowdhury, C. Wang, P. Svec, W. Losert, and S. K. Gupta. Automated indirect optical micromanipulation of biological cells using indirect pushing to minimize photo-damage. In *Proceedings of the ASME 6th International Conference on Micro and Nanosystems,*, Chicago, IL, Aug 2012.

[TDANE12] M. Tavalaee, M. Deemeh, M. Arbabian, and M. Nasr-Esfahani. Density gradient centrifugation before or after magnetic-activated cell sorting: which technique is more useful for clinical sperm selection? *Journal of Assisted Reproduction and Genetics*, 29:31–38, 2012. 10.1007/s10815-011-9686-6.

[THM03] F. Takahashi, Y. Higashino, and H. Miyata. Probing the cell peripheral movements by optical trapping technique. *Biophysics Journal*, 84(4):2664–2670, Apr 2003.

[TZQ+12] S. Tottori, L. Zhang, F. Qiu, K. Krawczyk, A. Franco-Obregn, and B. J. Nelson. Magnetic helical micromachines: Fabrication, controlled

swimming, and cargo transport. *Advanced Materials*, 24(6):pp. 811–816, Feb 2012. highlighted as the front cover.

[UWIY03] Senkei Umehara, Yuichi Wakamoto, Ippei Inoue, and Kenji Yasuda. On-chip single-cell microcultivation assay for monitoring environmental effects on isolated cells. *Biochemical and biophysical research communications*, 305(3):534 – 540, 2003.

[VBW+98] C. Veigel, M. L. Bartoo, D. C. S. White, J. C. Sparrow, and J. E. Molloy. The stiffness of rabbit skeletal actomyosin cross-bridges determined with an optical tweezers transducer. *Biophysics Journal*, 75(3):1424–1438, Sep 1998.

[Ver67] L. Verlet. Computer experiments on classical fluids.I. thermodynamical properties of Lennard-Jones molecules. *Physical review*, 159(1):98–&, 1967.

[VGB96] K. Visscher, S.P. Gross, and S. M. Block. Construction of multiple-beam optical traps with nanometer-resolution position sensing. *IEEE Journal of Selected Topics in Quantum Electronics*, 2(4):1066–1076, 1996.

[Vol06] J. Voldman. Electrical forces for microscale cell manipulation. *Annual Review on Biomedical Engineering*, 8(1):425–454, 2006.

[VSB99] K. Visscher, M. J. Schnitzer, and S. M. Block. Single kinesin molecules studied with a molecular force clamp. *Nature*, 400(6740):184–189, Jul 1999.

[WBC03] B. H. Weigl, R. L. Bardell, and C. R. Cabrera. Lab-on-a-chip for drug development. *Advanced Drug Delivery Reviews*, 55(3):349–377, Feb 2003.

[WCGL13] C. Wang, S. Chowdhury, S. K. Gupta, and W. Losert. Optical micromanipulation of active cells with minimal perturbations: direct and indirect pushing. *Journal of Biomedical Optics*, 18(4):045001–045001, 2013.

[WCK+11] X. Wang, S. Chen, M. Kong, Z. Wang, K. D. Costa, R. A. Li, and D. Sun. Enhanced cell sorting and manipulation with combined optical tweezer and microfluidic chip technologies. *Lab on a Chip*, 11:3656–3662, 2011.

[WCMF95] J. S. Wolenski, R. E. Cheney, M. S. Mooseker, and P. Forscher. In-vitro motility of immunoadsorbed brain myosin-V using a limulus acrosomal process and optical tweezer-based assay. *Journal of Cell Science*, 108(Part 4):1489–1496, Apr 1995.

[Wei89] M. Weissbluth. *Photon-atom interactions*. Academic Press, Boston, MA, 1989.

[WGB03] C. Wilhelm, F. Gazeau, and J. C. Bacri. Magnetic micromanipulation. *Review of Scientific Instruments*, 74(9):4158–4163, Mar 2003.

[WKC+98] P. Wilding, L. J. Kricka, J. Cheng, G. Hvichia, M. A. Shoffner, and P. Fortina. Integrated cell isolation and polymerase chain reaction analysis using silicon microfilter chambers. *Analytical Biochemistry*, 257(2):95 – 100, 1998.

[WKI+93] M. Washizu, Y. Kurahashi, H. Iochi, O. Kurosawa, S. Aizawa, S. Kudo, Y. Magariyama, and H. Hotani. Dielectrophoretic measurement of bacterial motor characteristics. *IEEE Transactions on Industry Applications*, 29(2):286 –294, Mar 1993.

[WML+07] J. D. Wen, M. Manosas, P. T. X. Li, S. B. Smith, C. Bustamante, F. Ritort, and I. Tinoco, Jr. Force unfolding kinetics of RNA using optical tweezers. I. Effects of experimental variables on measured results. *Biophysics Journal*, 92(9):2996–3009, May 2007.

[WOHT08] A. E. Wallin, H. Ojala, E. Haeggstrom, and R. Tuma. Stiffer optical tweezers through real-time feedback control. *Applied Physics Letters*, 92(22), Jun 2008.

[WSH11] Y. Wu, D. Sun, and W. Huang. Force and motion analysis for automated cell transportation with optical tweezers. In *Proceedigns of the 9th World Congress on Intelligent Control and Automation (WCICA)*, pages 839–843, 2011.

[WSHX13] Y. Wu, D. Sun, W. Huang, and N. Xi. Dynamics analysis and motion planning for automated cell transportation with optical tweezers. *IEEE/ASME Transactions on Mechatronics*, 18(2):706–713, 2013.

[WSY+02] J. Wakayama, M. Shohara, C. Yagi, H. Ono, N. Miyake, Y. Kunioka, and T. Yamada. Zigzag motions of the myosin-coated beads actively sliding along actin filaments suspended between immobilized beads. *Biochimica Et Biophysica Acta-General Subjects*, 1573(1):93–99, Oct 2002.

[WTSH10] Y. Wu, Y. Tan, D. Sun, and W. Huang. Force analysis and path planning of the trapped cell in robotic manipulation with optical tweezers. In *Proceedings of the IEEE International Conference on Robotics and Automation (ICRA)*, pages 4119 –4124, May 2010.

[WUH04] P. K. Wong, U. Ulmanella, and C. M. Ho. Fabrication process of microsurgical tools for single-cell trapping and intracytoplasmic injection. *Journal of Microelectromechanical Systems*, 13(6):940–946, Dec 2004.

[WWS10] X. Wang, Z. Wang, and D. Sun. Cell sorting with combined optical tweezers and microfluidic chip technologies. In *Proceedings of the 11th IEEE International Conference on Control Automation Robotics & Vision (ICARCV)*, pages 201–206. IEEE, 2010.

[WYCS12] X. Wang, X. Yan, S. Chen, and D. Sun. Automated parallel cell isolation and deposition using microwell array and optical tweezers. In *Proceedings of the IEEE International Conference on Robotics and Automation (ICRA)*, pages 4571–4576, 2012.

[WYL+97] M.D. Wang, H. Yin, R. Landick, J. Gelles, and S.M. Block. Stretching dna with optical tweezers. *Biophysics Journal*, 72(3):1335 – 1346, 1997.

[WZY+08] M. T. Wei, A. Zaorski, H. C. Yalcin, J. Wang, M. Hallow, S. N. Ghadiali, A. Chiou, and H. D. Ou-Yang. A comparative study of living cell micromechanical properties by oscillatory optical tweezers. *Optics Express*, 16(12):8594–8603, Jun 2008.

[YLJY06] C. Q. Yi, C. W. Li, S. L. Ji, and M. S. Yang. Microfluidics technology for manipulation and analysis of biological cells. *Analytica Chimica Acta*, 560(1-2):1–23, Feb 2006.

[ZA12] Q. Zhang and R. H. Austin. Applications of microfluidics in stem cell biology. *BioNanoScience*, pages 1–10, 2012.

[ZD07] X. Zhu and H. Ding. An efficient algorithm for grasp synthesis and fixture layout design in discrete domain. *IEEE Transactions on Robotics*, 23(1):157 –163, Feb 2007.

[ZW03] X. Zhu and J. Wang. Synthesis of force-closure grasps on 3-d objects based on the q distance. *IEEE Transactions on Robotics and Automation*, 19(4):669 – 679, Aug 2003.